Hydrocarbon Measurements And Their Use As Atmospheric Tracers

Shalini Punjabi

Submitted in accordance with the registration for the degree of doctor of philosophy

PhD

University of York

Chemistry

January 2013

Abstract

Non-methane hydrocarbons (NMHCs) have been measured in the boundary layer and free troposphere to investigate their behaviour under different atmospheric chemical regimes. Ambient air samples were collected using the Whole Air Sampling (WAS) system aboard the UK atmospheric research aircraft - FAAM BAe 146 - and analysed using a dual-channel gas chromatograph coupled with the flame ionization detectors (FID). Hydrocarbon ratios were used to determine the presence of nitrate radicals in the atmosphere during summer, winter and autumn phases of the ROle of Nightime chemistry in controlling the Oxidizing Capacity of the AtmOsphere (RONOCO) campaign. The extensive data set showed that the pentane $n - iso$ isomer pair were particularly useful when diagnosing the presence of different oxidants during day, night, dusk and dawn. A hydrocarbon variability versus lifetime approach applied to the entire winter and summer datasets proved useful in determining the presence or absence of the nitrate radical. Free tropospheric NMHC measurements were made over the period January 2009 - January 2011 above the UK. These data provided a rare description of the seasonal variations in this region of the atmosphere. A comparison of this work with earlier UK free troposphere studies made twenty years ago, revealed a decline in the amplitude of the seasonal cycle by a factor of approximately two for acetylene, benzene and toluene. Airborne measurements of NMHCs have also been made in boreal forest fire plumes over Canada between 12th July 2010 and 2nd August 2010 as a part of the research project - Quantifying the impact of BORreal forest fires on Tropospheric oxidants over the Atlantic using Aircraft and Satellites (BORTAS). The fire emission ratios for 29 different organic species relative to emission of CO have been derived. The comparison between observationally derived emission ratios and the GEOS-Chem Chemical Transport Model highlighted the influence of biomass burning as a large contributor to benzene, toluene, ethene and propene levels in many global locations.

Contents

List of Figures

List of Tables

Acknowledgements

Declaration

The candidate confirms that the work submitted in this thesis is her own and that appropriate credit has been given where reference has been made to the work of others.

Chapter 6 in this thesis is derived from observations and analysis made during the course of this PhD, but also includes input from a variety of other collaborators who are acknowledged in the text. The chapter distils the combined work published in:

'The influence of boreal forest fires on the global distribution of non-methane hydrocarbons.' A.C.Lewis, M.J.Evans, J.R.Hopkins, S.Punjabi, K.A.Read, S.Andrews, S.J.Moller, L.J.Carpenter, J.D.Lee, A.R.Rickard, P.I.Palmer, and M.Parrington. *Atmos. Chem. Phys. Discuss.*, 12, 23433-23469, 2012. This is now accepted for ACP.

Chapter 1:

An overview of tropospheric trace gases

1.1   Introduction

The region of the Earth's atmosphere in which we live and breathe, classified as the troposphere, is composed of many different kind of gases. More than 99.9% of the molecules are nitrogen (78.1%), oxygen (20.9%), chemically inert noble gases and highly variable water vapour amounts. The percentage of water vapour ranges from near-zero to as much as 4% in the humid tropics. This 99.9% has been present and chemically stable at nearly constant levels for the past several hundred million years. However, the remaining 0.1% that is represented by atmospheric trace constituents termed as 'trace species', have influenced our lives on Earth in the form of smog formation, increased temperatures, destruction of the ozone hole, formation of acid rain and so on. It is astonishing that despite their presence at such low concentrations, the impact of trace gases on Earth's climate is so life threatening. In addition to the trace gases, suspension of particles in a gas (aerosols) contributes further towards air pollution problems and climate change.

The aim of this chapter is to highlight the importance of selected trace species in terms of sources, sinks and their impacts in the troposphere with special attention on 'volatile organic compounds' (VOCs), a set of vapour phase atmospheric organics, as this is the key topic on which this thesis is based. For the sake of convenience these trace gases are grouped in such a way that the compounds containing sulphur, nitrogen, halogen and carbon form separate groups. Before the discussion, it is important to understand the way of expressing the amounts of the gases in the atmosphere, conversion between units and the concept of lifetime.

1.1.1 Expressing the amount of gases in the atmosphere

There are broadly two ways to describe the amount of trace gases present in the atmosphere. First is the 'concentration' of a trace gas which is defined as the

amount of gas (or mass) per volume of air at a given temperature (Platt and Stutz, 2008)

$$c \quad = \quad \frac{\text{Amount of trace gas}}{\text{Volume of air}} \qquad 1.1$$

where c denotes the concentration of a trace gas.

The SI unit for the amount of a substance is the mole (mol). The number of atoms or molecules in one mol is Avogadro's number $N_A = 6.022 \times 10^{23} \text{ mol}^{-1}$. Examples for units of concentration are mol m^{-3}, µg m^{-3} or molecule cm^{-3}. Often particular units are used for different species, for example the concentration of OH radicals (typically 1×10^6 molecule cm^{-3}) is mostly expressed in the form of number density. The switching between units can sometimes make it difficult to draw direct comparisons between observations. The concentration of VOCs is generally expressed in µg m^{-3}.

The second way for expressing the amount is 'mixing ratio'. The mixing ratio in atmospheric chemistry is defined as the ratio of the amount (or mass) of the substance in a given volume to the total amount (or mass) of all constituents in that volume. In this definition for a gaseous substance the sum of all constituents includes all gaseous substances, including water vapour, but not including particulate matter or condensed phase water. Hence mixing ratio is just the fraction of the total amount (or mass) contributed by the substance of interest.

$$x \quad = \quad \frac{\text{Amount of trace gas}}{\text{Amount of air} + \text{Trace gas}} \qquad 1.2$$

where x is the mixing ratio of a trace gas.

The amount can be in volume (volume mixing ratio = x_v), number of moles (mole mixing ratio = x_M), number of molecules or mass (mass mixing ratio = x_m).

$$x_V \quad = \quad \frac{\text{Unit vol. of trace gas}}{10^6 \text{ unit vols. of (air} + \text{trace gas)}} = \text{ppmv} \qquad 1.3$$

where vol and vols represent volume and volumes respectively.

The most important carbon-containing species is carbon dioxide (CO_2), which plays a crucial role as a greenhouse gas and undergoes little chemistry in the atmosphere, is found in the atmosphere currently at the level of 392.81 parts per million (Nov, 2012) (ESRL, 2012). Its mixing ratio has continuously increased since 1960. **Figure 1.1** shows the recent monthly mean CO_2 at Mauna Loa Observatory. Data are reported as a dry air mole fraction defined as the number of molecules of CO_2 divided by the number of all molecules in air, including CO_2 itself, after water vapour has been removed. The mole fraction is expressed as parts per million (ppm).
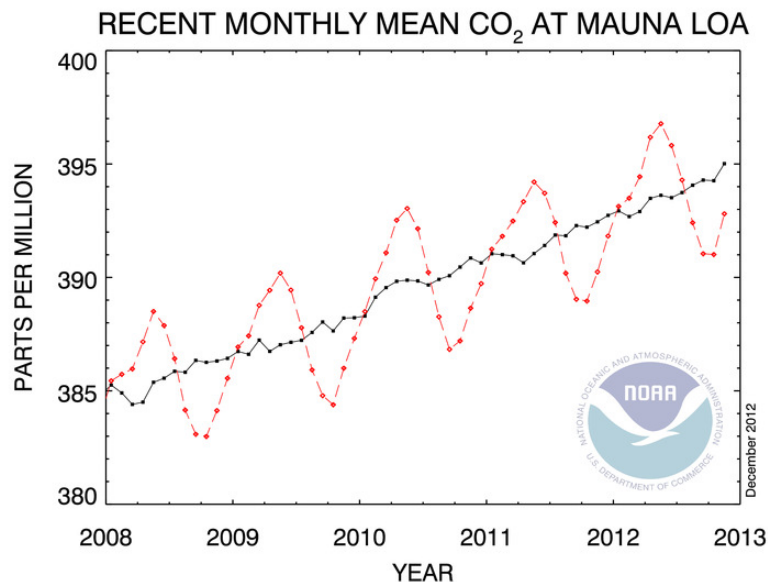
Figure 1.1: Recent monthly mean CO_2 measured at Mauna Loa Observatory, Hawaii. The mole fraction is expressed as parts per million (ppm). The dashed red line with diamonds symbols represent the monthly mean values centred on the middle of each month. The black line with square symbols represents the same, after correction for the average seasonal cycle (ESRL, 2012).

Of the chemically reactive compounds, methane (CH_4) is by far the most abundant, at a current Northern Hemisphere (NH) ground-level mixing ratio of about 1.7 parts per million by volume (ppmv). In other words, it can be said that 10^6 litres of air contains 1.7 litres of CH_4.

Smaller mixing ratios (as shown in equation 1.4 and 1.5) are represented by parts per billion (ppb) and parts per trillion (ppt) as shown in equation 1.4 and equation 1.5. It is important to mention here that throughout the chapters the terminology 'volume mixing ratio' (ppbv or pptv) as shown in following equations has been used for expressing the amount of VOCs in the atmosphere rather than concentration as both have entirely different interpretations.

$$x_V \quad = \quad \frac{\text{Unit vol of trace gas}}{10^9 \text{ unit vols of (air} + \text{trace gas)}} = \text{ppbv} \qquad 1.4$$

$$x_V \quad = \quad \frac{\text{Unit vol of trace gas}}{10^{12} \text{ unit vols of (air} + \text{trace gas)}} = \text{pptv} \qquad 1.5$$

Sometimes air monitoring results are reported in a form of parts per billion on a carbon basis (ppbC) rather than ppbv. The relation between the two is expressed by the following equation

$$\text{ppbC} \quad = \quad \text{ppbv x number of carbon atoms} \qquad 1.6$$

On the basis of above definition, the mixing ratio of benzene (6 carbon aromatic compound) in form of 6.0 ppbC is actually equal to 1.0 ppbv.

The mixing ratios in terms of mass are rarely used in atmospheric chemistry. The new SI unit for mixing ratios is expressed in terms of moles. Air under ambient conditions can be considered as an ideal gas, hence moles per mole is equivalent to volume mixing ratio.

$$x_M \quad = \quad \frac{\text{Moles of trace gas}}{\text{Moles of (air} + \text{trace gas)}} \qquad 1.7$$

where x_M = mole mixing ratio.

Hence the terms μmol mol^{-1} (micromole per mole), nmol mol^{-1} (nanomole per mole) and pmol mol^{-1} (picomole per mole) are essentially equivalent to ppmv, ppbv and pptv respectively. The use of SI units of mixing ratios is most popular in gas cylinders having multicomponent standard gas mixtures. For example a 30-component NPL gas cylinder used in this study has mixing ratios of all components in the range of approximately 4 nmol mol^{-1}.

It is equally important to understand the conversion of units of amount of trace gases. For example, the conversion between number density (c_n in molecule cm^{-3}) and mass concentration (c_m in gram cm^{-3}) for ozone (O_3) can be expressed as follows:

$$(c_m)_{O_3} \quad = \quad \frac{c_n . M_{O_3}}{N_A} \qquad 1.8$$

where M_{O3} denotes the molecular mass of O_3 in g mol^{-1} and N_A is Avogadro's number. Hence the conversion between number density and mass concentration is different for species with different molecular (or atomic) mass.

The conversion used in chapters include the conversion of number density c_n (in molecule cm^{-3}) into the corresponding volume mixing ratio or vice versa according to the following equation

$$x_V \quad = \quad c_n \frac{V}{N_A} \qquad 1.9$$

where V denotes the molar volume in cm^3 for the pressure p and temperature T at which the number density c_n was measured. For standard conditions (at 1 atmospheric pressure and at 273.15 K temperature, the molar volume V is 22414.00 cm^3 mol^{-1}. Hence

$$1\,\text{ppmv} \quad = \quad 2.46 \times 10^{13} \text{ molecule cm}^{-3}$$

$$1\,\text{ppbv} \quad = \quad 2.46 \times 10^{10} \text{ molecule cm}^{-3}$$

$$1\,\text{pptv} \quad = \quad 2.46 \times 10^{7} \text{ molecule cm}^{-3}$$

For arbitrary temperature T' and pressure conditions P', one has to take into account the new volume value V' at that temperature and pressure. In that case the conversion takes the following form

$$x_V \quad = \quad c_n \frac{1}{N_A} \cdot \frac{RT'}{P'} \qquad 1.10$$

Using the conversion between number density and mass concentration from equation 1.8 the above equation can be presented as

$$x_V \quad = \quad c_m \frac{1}{M_i} \cdot \frac{RT'}{P'} \qquad 1.11$$

where M_i is the molecular mass of the species i in g mol^{-1}.

This expression converts volume mixing ratio in mass concentration (g cm^{-3}). For example 1 ppbv O_3 (molecular mass= 48.0g mol^{-1}) is equivalent to 1.995 µg m^{-3} at 293 K and 1 atmosphere pressure.

The most important thing to keep in mind is that mixing ratios x_V and x_M are independent of temperature and pressure. Consequently, they are conserved during vertical transport in the atmosphere. In contrast the concentration depends on both parameters and change when air is transported (Harrison, 2001). The importance of trace gas concentrations is relevant while calculating the chemical reaction rates and radiative properties.

1.1.2 Lifetime and transport

Owing to the great variability of emission and chemical interactions of trace gases, the composition for a given volume of air is not fixed at any time. These trace gases are released to the atmosphere directly as a result of human activities or natural processes or formed by chemical transformations. Their removal processes are either by physical (dry or wet depositions) or chemical degradation methods. Dry deposition involves the transfer and removal of gases and particles at land and sea surfaces without the intervention of rain or snow whilst wet deposition involves scavenging by precipitation (rain, snow, hail etc) (Harrison, 2001). If the concentration of a species has reached a steady state value, that is its rate of production P is equal to its rate of destruction D, then a useful quantity in this context is steady state lifetime or residence time (the difference between the usage of lifetime and residence time is further explained in section 1.2.8.2) which can be defined as follows:

$$\tau \quad = \quad \frac{c}{D} \text{ or } \frac{c}{P} \qquad 1.12$$

where *c* is the concentration of a trace species and τ is the steady state lifetime.

Most of the species in the troposphere are removed by the OH radical according to the following reaction

$$OH + A \quad \xrightarrow{\ k\ } \quad \text{products} \qquad 1.13$$
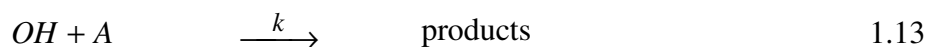
The parameter *k* is the rate constant for the reaction. The rate of the reaction R or loss rate of A can be expressed as presented in equation 1.14

$$R \quad = \quad k[OH][A] \qquad 1.14$$

The square brackets around these denote the concentration of a substance.

Substituting the concentration and loss rate in equation 1.12 gives the lifetime

$$\tau \quad = \quad \frac{1}{k[OH]} \qquad\qquad 1.15$$

where $[OH]$ is the globally averaged troposphere concentration of OH radicals.

Taking a typical average daytime OH concentration of 1×10^6 molecule cm^{-3} and using laboratory rate constants (Atkinson and Arey, 2003), the lifetime of CH$_4$ with respect to OH is approximately 4.9 years, whilst for propane it is 10.5 days. The comparison between the lifetimes of both species illustrates that CH$_4$ reacts so slowly in the troposphere and generally is not of concern from the point of view of O$_3$ formation over the time scale of hours to a few days in urban areas. It is also the reason that CH$_4$ is the only organic hydrocarbon molecule to survive long enough in the troposphere to cross the tropopause and enter the stratosphere in significant concentrations, whilst propane reacts sufficiently quickly that it can contribute to local and regional photochemical smog formation. In other words it can also be said that for least reactive species like CH$_4$, transport can redistribute them globally over their long lifetime whilst species that are highly reactive like propene may be born and die in effectively the same place.

Figure 1.2 shows the representative atmospheric trace gases and their lifetime. Accordingly these pollutants are transported on scales reaching from a few meters to several kilometres representing the global scale.

9
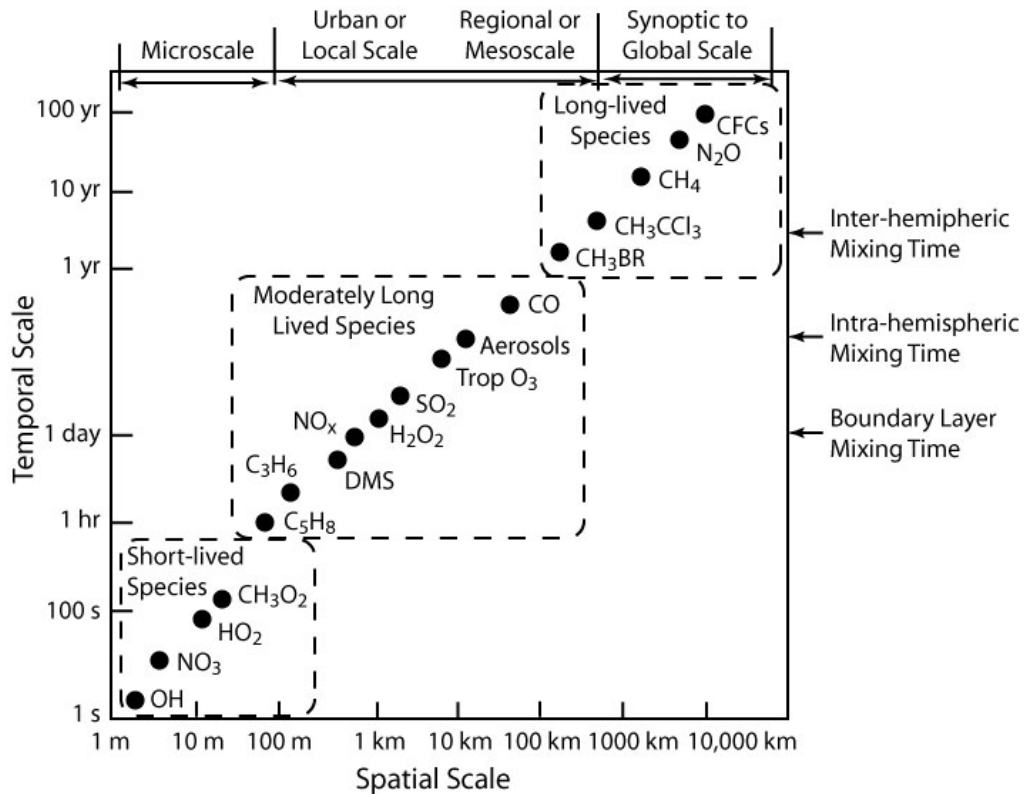
Figure 1.2: Trace gases with a range of lifetimes and their spatial distribution (Stewart, 2009)

Junge (Junge, 1974)) first described an inverse relationship between concentration variability and residence time for relatively long-lived tropospheric trace gases. This concept was further extended by Jobson et al (Jobson et al., 1998) to non-methane hydrocarbons (NMHCs). This is further discussed in detail in section 1.2.8.2.

When calculating the lifetime using above mentioned calculations, one has to take all competing loss processes into account, such as photolysis and reactions with oxidants other than the OH radical. For example, the lifetime of propene in a nighttime environment can be calculated by considering all three oxidants; the OH radical, the NO_3 radical and the O_3 molecule according to following expression:

$$\tau \quad = \quad \frac{1}{k_{OH}[OH] + k_{NO_3}[NO_3] + k_{O_3}[O_3]} \qquad 1.16$$

where k_{OH}, k_{NO3} and k_{O3} are the rate constants of propene with respect to OH, NO_3 and O_3, respectively.

The lifetime of a VOC is crucially dependant on the assumed concentration of OH radicals used in the calculation. The actual concentration of OH at various geographical locations and under a variety of conditions is highly variable; for example its concentration varies diurnally since it is produced primarily by photochemical processes. In addition to this, the concentration of OH varies with altitude so the VOC lifetime will depend on where in the troposphere the reaction occurs. Since OH radical concentrations vary with insolation, lifetimes of trace gases changes significantly with season and latitude. The uncertainty in OH concentration is a major source of uncertainty in the estimated lifetime of trace gases.

Once the trace gases are emitted into the atmosphere, their distribution depends on the meteorology at a particular location, dry and wet sink mechanisms and the atmospheric chemical removal rates during transport of the compound. To understand the vertical transport of trace compounds, it is necessary to understand the pressure and temperature structure of the atmosphere. If temperature were constant, the pressure would drop in a simple exponential manner with altitude; however, the temperature structure is more complex and hence these changes lead to a small deviation from pure exponential behaviour. The characteristic distance over which the pressure drops by a factor of *e* is known as the scale height and it varies from about 8.5 km for a temperature of 290 K (typical surface temperature) to 6 km at 210 K (typical of an altitude of 20 km).

Figure 1.3 shows the variation of temperature with altitude. Near the surface, temperature decreases with increasing altitude and colder air lies on top of the warm air. This region is termed as troposphere ('tropos' is Greek for 'turning') and is characterized by strong vertical mixing. In the troposphere the temperature decreases linearly with height due to the increase in distance from the sun-warmed Earth. For dry air the lapse rate is 9.7 K km^{-1}. The ordinary atmospheric wind and weather systems are set up within the troposphere. This region extends from the surface to about 8 km altitude at the poles and from the surface to about 18 km at the equator. The troposphere is further divided into the atmospheric boundary layer and free troposphere. These are discussed briefly afterwards.
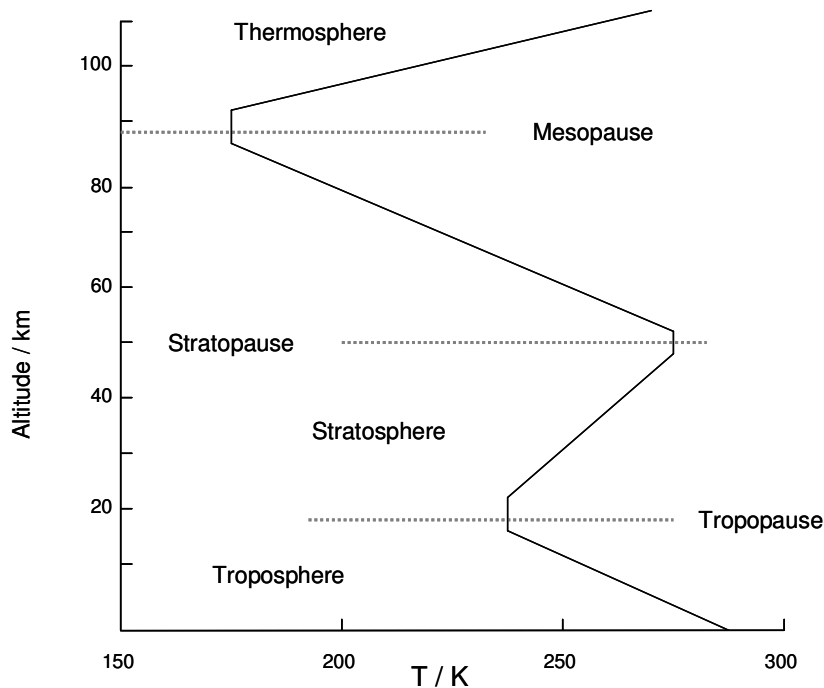
Figure 1.3: Layers of the atmosphere divided according to the change in temperature with respect to altitude.

Coming back to the second layer of the atmosphere, which is characterized by the rise in temperature with altitude and termed as stratosphere ('stratus' is Latin for 'layered'); in contrast to the troposphere, here the warmer layer lies on top of the cold air. This region extends up to 50 km. The stratosphere is stable and characterized by very limited vertical mixing. The hypothetical boundary

between the troposphere and the stratosphere is the tropopause. Above the stratosphere, the atmosphere heating becomes too weak to sustain the temperature inversion, and cooling is once again observed in the mesosphere, a region which extends up to 80 km. The region higher than mesosphere is characterized by an increase in temperature again and termed as thermosphere. The region relevant to the discussion in this thesis is the troposphere. The data from a campaign discussed in chapter 3 and 4 are from the nighttime boundary layer in both seasons (winter and summer) except few flight data from daytime boundary layer. Observations from chapter 5 are exclusively from free troposphere.

The boundary layer extends from the surface from a few meters to roughly 2 km. This is the region where pollutants emitted from the ground are accumulated. The fluctuations in the ground temperature are quickly reflected by the boundary layer air temperature, over a period of less than an hour. The response time is much longer for the free troposphere towards the changes in the ground temperature (Jacobson, 2002). **Figure 1.4a and Figure 1.4b** compare a typical temperature variation in the boundary layer over land between day and night.

During the day (**Figure 1.4a**), the boundary layer is characterized by a surface layer, a convective mixed layer, and an entrainment zone. The surface layer which comprises the bottom 10% of the boundary layer is a region of strong change of wind speed with height. The region above the surface layer is termed as the convective mixed layer. When the ground is warmed by sunlight during the day, the transfer of energy from ground to the air just above the ground takes place *via* conduction. The cold air lies above the warm layer and warm air rises buoyantly as a thermal. The warm air parcels rise and gain their maximum acceleration in the convective mixed layer. In the process of thermal formation, the colder air is being displaced by warm air parcels and move in the downward direction and finally this upward and downward movement renders the turbulence to the boundary layer.
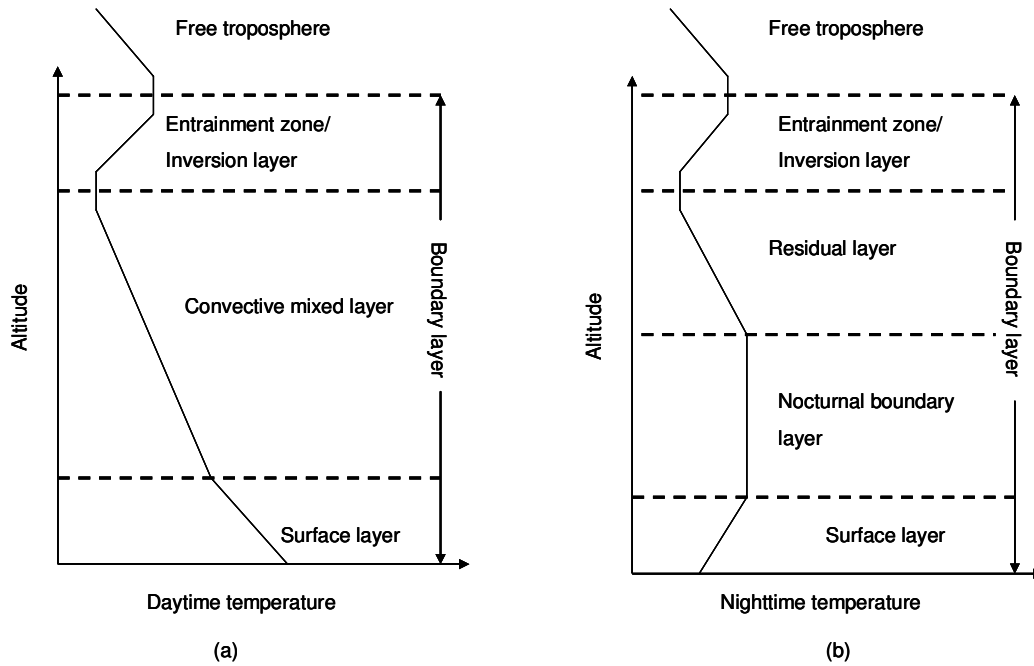
Figure 1.4: A comparison for variation of temperature with height between day and nighttime boundary layer adapted from (Jacobson, 2002).

This turbulent nature of the boundary layer means pollutants from the surface are mixed thoroughly throughout this layer. The top of the convective mixed layer is often bounded by a temperature inversion, which is an increase in temperature with increasing height. The thermals are inhibited by this inversion; however, some mixing (entrainment) between the inversion and mixed layer does occur; thus the inversion layer is also called an entrainment zone. Pollutants are generally trapped beneath or within an inversion; thus the closer the inversion is to the ground, the higher pollutant concentration becomes.

The temperature profile is different during the night as shown in **Figure 1.4b**; the ground cools radiatively causing air temperature to increase with increasing height from the ground, creating a surface inversion. Once the nighttime surface inversion forms, pollutants when emitted are confined to the surface layer. The effect of radiative cooling is a relatively cold temperature at the top of the surface layer which induces the cooling of the bottom of the convective mixed layer. Consequently the buoyancy and associated mixing at the base of the mixed layer

14

are reduced. The portion of the daytime mixed layer that loses its buoyancy at night is the nocturnal boundary layer (NBL) and the remaining portion of the mixed layer is the residual layer. Owing to the absence of thermals at night, the residual layer does not undergo much change at night except at its base. At night the NBL thickens, eroding the residual–layer base. Above the residual layer, the inversion remains. **Figure 1.5** shows the variation of temperature with height while the research aircraft, FAAM BAe-146, during one of the flights (B564), was descending to make a missed approach to assess the boundary layer structure at night. The boundary layer at night during this flight was roughly 1000 metres.
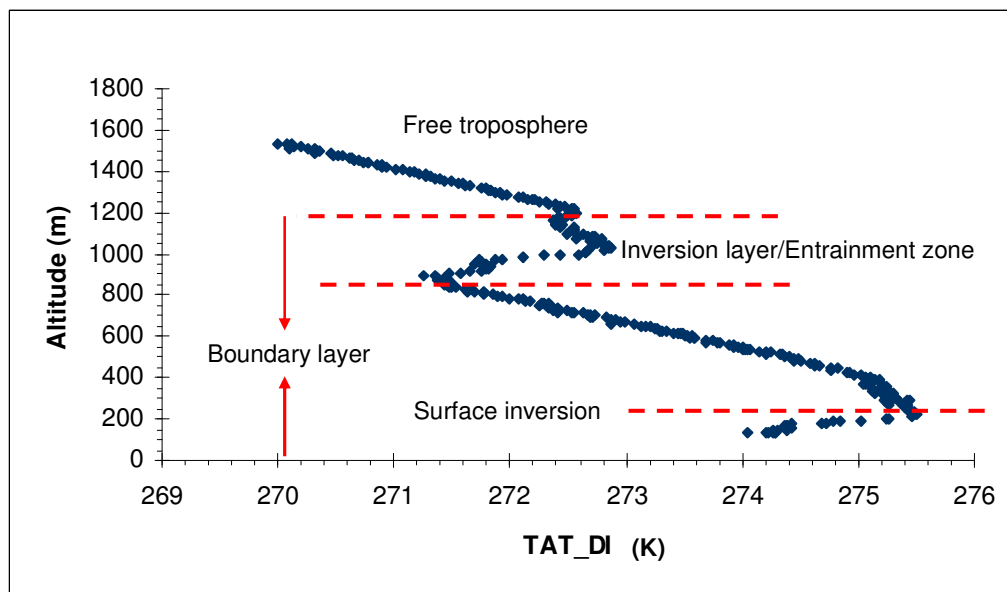
Figure 1.5: Descent profile (1500 m to 400 m) during flight B564 to assess the boundary layer (BL) structure. The parameter on the *x* axis is true air temperature from the Rosemount deiced temperature sensor (TAT_DI) in K. The flight was made on 11/01/2011 at night as a part of a research project - The ROle of Nighttime chemistry in controlling the Oxidizing Capacity of the AtmOsphere (RONOCO).

The free troposphere extends from the top of the BL to the tropopause. It is a region in which temperature decreases with increasing altitude. The highly reactive species tend to be confined to the boundary layer near source regions whilst the species with longer lifetime escape from the boundary layer to the free troposphere. Once in the free troposphere, the trace gases move over much larger distances than in the boundary layer. Consequently the free tropospheric air

contains the longer-lived atmospheric components, together with contributions from pollutants which have escaped the boundary layer, and from some downward mixing stratospheric air.

1.2 Trace constituents

1.2.1 Sulphur-containing compounds

The main sulphur compounds in the atmosphere are hydrogen sulphide (H_2S), dimethylsulphide or DMS (CH_3SCH_3), carbon disulphide (CS_2) carbonyl sulphide (COS) and SO_2. The London-type smog and acid rain problems are examples of industrialization and resulting increase in sulphur emissions. Natural activities through biological processes in the soil and the ocean emit sulphur in the form of H_2S, CH_3SCH_3, COS and through Volcanic eruptions, SO_2 is emitted. The combustion of coal in power stations is by far the most major single source of SO_2 for the United Kingdom (Harrison, 2001). Since the recognition of SO_2 as a major air pollutant, substantial progress has been made towards the fulfilment of air quality standards. In the background troposphere, SO_2 mixing ratios range from 10 pptv to 1 ppbv whilst in polluted air, it ranges from 1 to 30 pbbv (Jacobson, 2002). As we can see from **Figure 1.2** both SO_2 and DMS are moderately long-lived species with *e*-folding lifetimes of 4 and 2 days, respectively.

DMS is the dominant sulphur compound emitted from the world's oceans through phytoplankton activities. The average DMS mixing ratio in the marine boundary layer (MBL) is in the range of 80-110 ppt but can reach values as high as 1 ppb over entrophic (e.g. coastal, upwelling) waters (Seinfeld and Pandis, 1998). The mixing ratio of DMS decreases with altitude and its levels are up to few parts per trillion in the free troposphere. As a result of transfer of DMS across the air-sea interface into the atmosphere, it reacts predominantly with the OH radical and the NO_3 radical. The presence of DMS in the MBL presents the

substantial sink for the NO_3 radical (Seinfeld and Pandis, 1998). In addition to this, due to the important role of sulphur in the formation of aerosol particles and cloud condensation nuclei (CCN), DMS has received considerable attention. A substantial amount of DMS and methyl iodide (CH_3I) which originate in sea water can escape oxidation in the MBL and reach the upper troposphere where their oxidation products may form aerosols and CCN (Kley, 1997).

1.2.2 Halogen-containing compounds

A general term referring to halogen-containing organic compounds is halocarbons. Chlorofluorocarbons (CFCs) is the collective name given to a series of halocarbons containing carbon, chlorine, and fluorine atoms. Atmospheric lifetimes of these species range from months to decades and longer. Although these species are released into the troposphere, due to their longer lifetime their impacts are much significant in the stratosphere. The role of halogen radicals in tropospheric chemistry has received much attention since the discovery of halogen chemistry in stratosphere O_3 destruction and episodes of zero O_3 concentration in the lower troposphere during polar sunrise (Andreae and Crutzen, 1997). With notable exceptions (such as methyl chloride (CH_3Cl) methyl bromide (CH_3Br), and CH_3I) most halocarbons are predominantly anthropogenic in origin. CH_3Cl was assumed to be released into the atmosphere as a result of biological processes in the ocean prior to 1996; however, biomass burning, tropical terrestrial sources also contribute to this. The mean atmospheric mixing ratio of this compound is 500 ppt (Seinfeld and Pandis, 1998). CH_3Cl is used as a tracer for biomass burning. It supplies 0.5 ppb of chlorine to the stratosphere (Seinfeld and Pandis, 1998). CH_3Br is the most abundant atmospheric bromocarbon responsible for over half of the bromine reaching the stratosphere (Seinfeld and Pandis, 1998). Its sources are natural as well as manmade. The ocean acts as both a source and sink for CH_3Br. Because of its toxicity to a broad range of pests it is used industrially as a fumigant. The mean tropospheric mixing ratio of CH_3Br is 10 ppt and its lifetime is 0.8 yr (Seinfeld and Pandis, 1998).

1.2.3 Nitrogen-containing compounds

The important nitrogen-containing trace species emitted in the atmosphere are nitrous oxide (N_2O), nitric oxide (NO), nitrogen dioxide (NO_2), nitric acid (HNO_3) and ammonia (NH_3). N_2O is mainly emitted by biological sources in soils and water. A large number of other sources such as biomass burning, degassing of irrigation water, agricultural activities and industrial processes are also responsible for emission of N_2O in smaller quantities. Since preindustrial times there has been an approximately 15% increase in mixing ratio of N_2O. In comparison with CO_2 and water vapour, the mixing ratio of this gas is low (approximately 315 ppb); however, it plays an important role as a greenhouse gas. The reason for this is its long residence time (120 years) and its relatively large energy absorption capacity per molecule (Seinfeld and Pandis, 1998). Due to its inert nature and long residence time, 90% of its sink mechanism is *via* photodissociation in the stratosphere and about 10% sink processes involve the reaction with excited oxygen atoms O (^{1}D).

The most important nitrogen-containing traces species after nitrogen and N_2O is NH_3 due to its participation in aerosol formation. It is emitted predominantly by livestock waste, ammonification of humus material followed by emission from soils, losses of ammonia based fertilizers from soils and industrial emissions. The main removal mechanism for ammonia is wet and dry deposition. The ammonium ion (NH_4^+) is an important component of continental tropospheric aerosols. It is readily absorbed by surfaces such as water and soils; hence its residence time in the lower troposphere is approximately 10 days. Owing to its short residence time, the variability in mixing ratio of ammonia is significant. A typical continental ammonia mixing ratio is between 0.1 -10 ppb.

The oxides of nitrogen (NO + NO_2) are collectively called NO_x because interconversion between NO and NO_2 is rapid with a tropospheric time scale of approximately 5 minutes. NO_x is produced in a large number of natural and

anthropogenic processes. Sources where air is heated to high temperatures such as in combustion processes (in internal combustion engines), forest fires, or lightning are particularly important. The forest fires, lightning storms and emissions from soils are the largest natural source of NO_x whilst anthropogenic NO_x emission can be grouped mainly in three categories; combustion of fossil fuels (power station, industry, and home heating), automobile emissions and anthropogenic influence due to intentional forest fires and artificial fertilisation. Most of the direct emission of NO_x to the atmosphere is in the form of NO. NO_2 is formed in the atmosphere by conversion of NO. NO_x together with VOCs act as major precursors of O_3. The VOC-OH reaction initiates the oxidation sequence. There is a competition between VOCs and NO_x for the OH radical. At a high ratio VOC to NO_x mixing ratio, OH reacts mainly with VOCs; at a low ratio, the NO_x reaction can dominate and it will form the loss route of OH radical by forming HNO_3. NO_x mixing ratio ranges from 5 to 20 ppb or higher in urban areas, about 1 ppb in rural areas and from 10 to 100 ppt in the remote troposphere. The lifetime of NO_2 with regard to oxidation by OH to HNO_3 is roughly 1 day.

Another category of reactive nitrogen compounds is known as NO_y. It is defined as the sum of the two oxides of nitrogen ($NO_x = NO+NO_2$) and all compounds that are produced during the atmospheric oxidation of NO_x. These include HNO_3, nitrous acid (HONO), the nitrate radical (NO_3), dinitrogen pentoxide (N_2O_5), peroxynitric acid (HNO_4) peroxyacetylnitrate (PAN) ($CH_3C(O)OONO_2$) and its homologues, alkylnitrates ($RONO_2$), and peroxyalkylnitrates ($ROONO_2$). PAN acts as a reservoir species for NO_x and extends the lifetime of NO_x where it is absent (Wayne, 2000). PAN is in thermal equilibrium with its precursors as presented by equation 1.19. The equilibrium is shifted towards right hand side at lower temperatures, for example in the free troposphere, and hence this species is relatively stable; however as it is transferred from cooler to warmer regions, NO_2 is released. Over the Pacific Ocean where the NO_2 mixing ratio is less than roughly 30 ppt, a mixing ratio of PAN has been observed in the range of 10-400

ppt. In addition to acting as a reservoir to NO_x species, it is an eye irritant and has adverse effects on plants (Wayne, 2000).

The formation route is through the acetyl radical (CH_3CO) which is formed from a number of routes, mainly through acetaldehyde (CH_3CHO) oxidation as follows:

$$CH_3CHO + OH \quad\quad \rightarrow \quad\quad CH_3CO + H_2O \quad\quad\quad 1.17$$

$$CH_3CO + O_2 \quad\quad \rightarrow \quad\quad CH_3C(O)OO \quad\quad\quad 1.18$$

$$CH_3C(O)OO + NO_2 \quad\quad \rightleftarrows \quad\quad CH_3COO_2NO_2 \text{ (PAN)} \quad\quad\quad 1.19$$
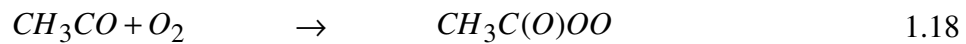
Another important compound from the NO_y family is HNO_3, which is the major oxidation product of NO_x in the atmosphere. Due to its water solubility properties, it is rapidly absorbed on surfaces and in water droplets. In presence of ammonia, HNO_3 can form ammonium nitrate (NH_4NO_3) aerosol. Here, particular attention is paid to the NO_3 radical, an important nighttime oxidant, as two chapters in this thesis are based on the diagnosing the presence of NO_3 radical through log-log plots and the influence of NO_3 radicals on hydrocarbon variability-lifetime relationships from a dataset acquired during the RONOCO campaign.

The NO_3 radical was first identified and measured in the polluted troposphere by Differential Optical Absorption Spectroscopy (DOAS) in the Los Angeles basin and in Colorado Mountain air with levels up to 355 ppt observed one hour after sunset (Platt et al., 1980;Noxon et al., 1980). Since the discovery of the NO_3 radical, the advancements in instrumentation techniques, particularly in terms of weight and energy requirements, have made it possible to measure NO_3 and other short lived radical species aboard aircraft in flight.

The property of absorbing light in the red region (620-670nm) of the visible spectrum makes NO_3 a candidate atmospheric gas species for measurement and detection by spectroscopic techniques (Finlayson-Pitts and Pitts, 2000). During the RONOCO field campaign, which is a central part of this thesis, the instruments measuring NO_3 and NO_2 were based on three channel Broadband Cavity Enhanced Absorption Spectroscopy (BBCEAS) and Laser Induced Fluorescence (LIF), respectively. In combination this gave atmospheric observations of NO_3, N_2O_5 and NO_2. This campaign presents a wealth of data including a wide range of gas phase radical species in a wide range of environments and underpins the work in this thesis.

1.2.3.1 Basic features of NO$_3$ radical chemistry

1.2.3.1.1 Production of NO$_3$ radical

The production of NO_3 radicals is mainly by slow reaction (equation 1.20) of NO_2 and O_3 in the same air mass (Heintz et al., 1996) . The rate constant for this reaction is k_1 = 1.2 x 10^{-13} exp(-2450/T) $cm^3 molecule^{-1}s^{-1}$ or $3.2x10^{-17}$ cm^3 $molecule^{-1} s^{-1}$ at 298 K (Sander et al., 2011). The production rate of the NO_3 radical can be calculated by measuring the concentration of NO_2 and O_3 in a given air mass using equation 1.21:

$$NO_2 + O_3 \qquad \xrightarrow{k_1} \qquad NO_3 + O_2 \qquad\qquad 1.20$$

$$d\frac{[NO_3]}{dt} \qquad = \qquad k_1[NO_2][O_3] \qquad\qquad 1.21$$

where k_1 is the rate constant for NO_3 formation. The NO_3 production rate during summer phase of the RONOCO campaign varied from 3.9 x 10^4 to 2.1 x 10^7 molecule cm^3 s^{-1} with a median value of 7.4 x 10^5 molecule cm^3 s^{-1} and during winter phase from 4.7 x 10^4 to 3.6 x 10^6 molecule cm^3 s^{-1} with a median value of 5.7 x 10^5 molecule cm^3 s^{-1}.

1.2.3.1.2 Loss Processes

There are three main (different) types of direct loss of the NO_3 radical: photolysis; reaction with NO; and reaction with VOCs (Heintz et al., 1996).

NO_3 is photolysed (maximum absorption 662 nm) mainly *via* reaction 1.22 during the daytime with a combined photolysis rate of reaction 1.22 and 1.23 of $\approx 0.2 \text{ s}^{-1}$ at noon. Hence, the lifetime of NO_3 is very short during the day (≈ 5 s) (Vrekoussis et al., 2003).

$$NO_3 + h\nu \qquad \rightarrow \qquad NO_2 + O(^3P) \qquad\qquad 1.22$$

$$NO_3 + h\nu \qquad \rightarrow \qquad NO + O_2 \qquad\qquad 1.23$$

However, during the night, using a lunar photolysis rate of NO_3 of $2 \times 10^{-7} \text{ s}^{-1}$ at full moon, the NO_3 lifetime is about 1400 hrs (Solomon et al., 1993). This allows concentrations to accumulate to significant levels.

Another loss process involves the reaction with NO. NO is mainly emitted as vehicular exhaust. In addition to combustion sources, NO is also formed during the day *via* photolysis of NO_2 (equation 1.24)

$$NO_2 + h\nu(\lambda \leq 400nm) \qquad \rightarrow \qquad NO + O \qquad\qquad 1.24$$

Reaction of NO_3 with NO is very fast ($k_{NO3\text{-}NO} = 1.5 \times 10^{-11} \exp(170/T)$ cm3 molecule^{-1} s^{-1} ; 2.6×10^{-11} cm^3 molecule^{-1} s^{-1} at 298 K) (Sander et al., 2011) reducing its lifetime (equation 1.25) during the day along with the photolysis loss pathway.

$$NO_3 + NO \qquad \xrightarrow{k_{NO_3-NO}} \qquad NO_2 + NO_2 \qquad\qquad 1.25$$

However, during nighttime due to an absence of NO_2 photolysis and in the presence of sufficient O_3 concentrations, NO levels drop very rapidly in the background atmosphere (k_{NO-O3} = 3.0 x 10^{-12} exp(-1500/T) cm^3 molecule^{-1} s^{-1} ; 1.9x10^{-14} cm^3 molecule^{-1} s^{-1} at 298 K (Sander et al., 2011).

$$NO + O_3 \qquad \xrightarrow{\quad k_{NO-O_3} \quad} \qquad NO_2 + O_2 \qquad\qquad 1.26$$
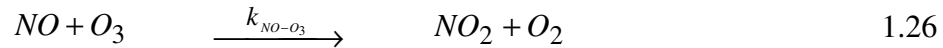
In certain conditions, however, O_3 is titrated by continued fresh NO emissions preventing NO_3 levels from building up to significant levels. These features make rural and urban nighttime chemistries distinct from one another - the latter having the potential for continued nighttime NO emissions in large quantities.

It is clear now that the members of the NO_x family behave differently at night than during daylight hours. Although NO_3 is not a member of NO_x family (NO and NO_2) (Brasseur et al., 1999) , due to its close coupling with NO_2 and its role in the regulation of NO_x , here NO_3 and NO_x form the central part of the two schematics (**Figure 1.6 and Figure 1.7**) for the ease of comparison of NO_x removal and VOC degradation between day and nighttime.

As can be seen from **Figure 1.6** the alkyl peroxy radicals (RO_2) generated by VOCs convert NO to NO_2 during daytime. NO_2 is then photolyzed to form NO and O. The reaction of atomic oxygen with molecular oxygen leads to the formation of O_3. NO reacts with O_3 to form NO_2 so there is no net loss or formation of O_3 during NO-NO_2 inter conversion cycle. In conditions of high $[NO_x]/[VOC]$ ratios, OH reacts with NO_2 to form HNO_3 which is finally removed from the atmosphere by dry and wet deposition and on the surfaces of aerosols. Thus the reaction of OH with NO_2 forms a major chemical removal route during daytime.
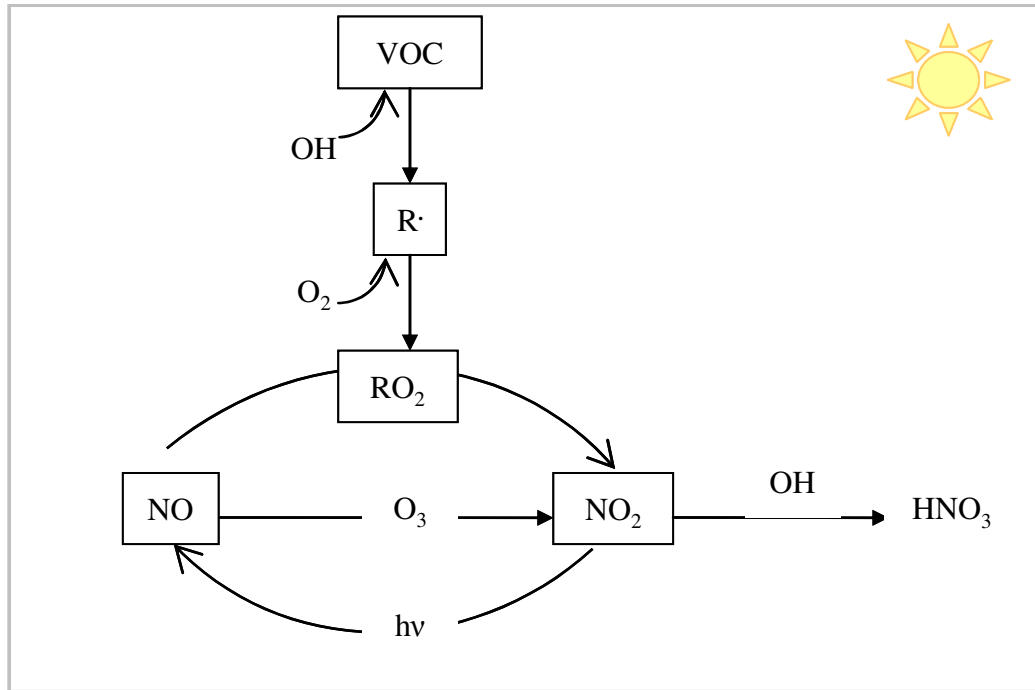
Figure 1.6: Schematic representation of the degradation of VOCs and removal of NO_X during daylight hours.

On the other hand, NO_2 and NO_3 do not photolyze during the night and any NO present during night reacts rapidly with O_3 so during night all NO_x is converted to NO_2. The presence of NO_2 and O_3 in a same air mass leads to the formation of NO_3.

As depicted in **Figure 1.7**, the source of alkyl peroxy radicals (RO_2) at night is reaction of VOC with NO_3 (equations 1.27 and.1.28). In the absence of NO, alkylperoxy radicals (RO_2) react with NO_3 (equation 1.29) to form alkoxy radicals (RO) followed by the formation of HO_2 radicals. The fate of HO_2 radical is either reaction with O_3 (equation 1.31) or with NO_3 (equation 1.32) to produce an OH radical. This depends on the ratio of $[NO_3]$ to $[O_3]$ which is in turn determined by the amount of NO_x present. (Wayne, 2000)
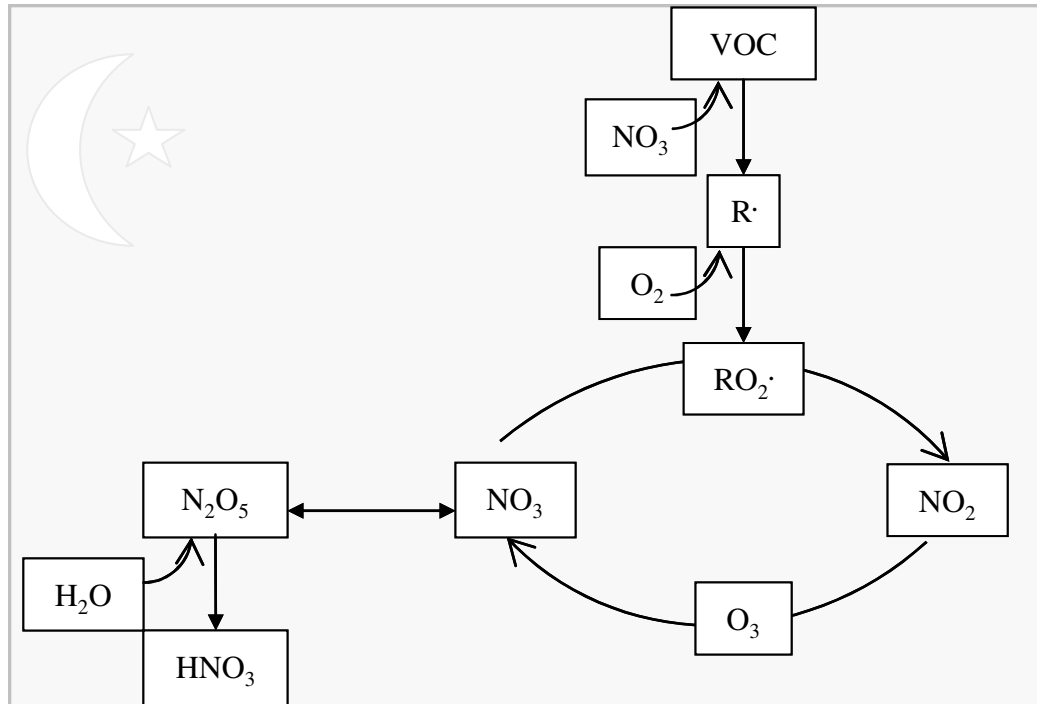
Figure 1.7: Schematic representation of the degradation of VOCs and removal of NO_x during nighttime.

$$NO_3 + VOC \quad \rightarrow \quad R + HNO_3 \quad\quad\quad 1.27$$

$$R + O_2 \quad \rightarrow \quad RO_2 \quad\quad\quad 1.28$$

$$RO_2 + NO_3 \quad \rightarrow \quad RO + NO_2 + O_2 \quad\quad\quad 1.29$$

$$RO + O_2 \quad \rightarrow \quad R'R''CO + HO_2 \quad\quad\quad 1.30$$

$$HO_2 + O_3 \quad \rightarrow \quad OH + 2O_2 \quad\quad\quad 1.31$$

$$HO_2 + NO_3 \quad \rightarrow \quad OH + O_2 + NO \quad\quad\quad 1.32$$
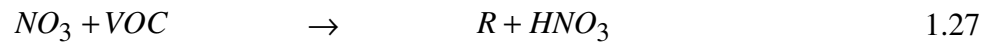
In addition to reaction with VOCs, the principal reaction of NO_3 at night is with NO_2 to form N_2O_5 in a reversible reaction (equation 1.33) with a strongly temperature dependent equilibrium constant (K_{eq}) 3.0x 10^{-27} exp(10990/T) cm^3molecule^{-1} (Sander et al., 2011). The lifetime of NO_3 with respect to this reaction is few seconds for an ambient NO_2 of 10 ppb. The decomposition of

thermally unstable N_2O_5 takes place on a similar timescale thereby causing equilibrium to be established rapidly.

$$NO_3 + NO_2 + M \qquad \rightleftharpoons \qquad N_2O_5 + M \qquad\qquad 1.33$$

Due to close coupling between NO_3 and N_2O_5, any direct loss of N_2O_5 forms an indirect loss for NO_3. N_2O_5 reacts heterogeneously with water on wet surfaces of aerosols and clouds to form HNO_3.as shown in equation 1.34. A significant anticorrelation has been observed in previous studies (Heintz et al., 1996) between relative humidity and NO_3 concentration. Eventually, HNO_3 is lost *via* multiple processes including dry deposition and formation of particulate ammonium nitrate (McLaren et al., 2004).

$$N_2O_5 + H_2O_{(aq)} \qquad \rightarrow \qquad 2HNO_3 \qquad\qquad 1.34$$
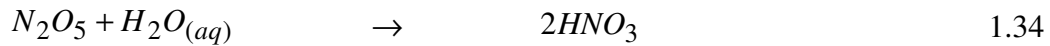
The rate at which VOCs are degraded during the night (equation 1.35) depends on the concentration and reactivity of the oxidant (equation 1.36) which in turn determines the lifetime of the different organic compounds (equation 1.37) (Warneke et al., 2004).

$$VOC + Oxidant(OH, NO_3, O_3) \quad \rightarrow \quad \text{Product} \qquad\qquad 1.35$$

$$-\frac{d[VOC]}{dt} \quad = \quad k_{VOC-Oxidant} \times [VOC] \times [Oxidant] \qquad 1.36$$

$$\tau_{VOC} \quad = \quad \frac{1}{(k_{OH} \times [OH]) + (k_{NO_3} \times [NO_3]) + (k_{O_3} \times [O_3])} \qquad 1.37$$

As far as reactivity comparisons between NO_3 and OH are concerned, NO_3 reacts with most volatile organic compounds at slower rates than VOCs react with OH.

(see **Table 3.1** on page 150). There are exceptions however; DMS, monoterpenes, isoprene, cresols, phenols and naphthalene react with NO_3 at comparable rates to OH. The loss of monoterpenes by NO_3 has been found to be more important than anthropogenic VOCs and oxygenated VOCs at night during a daytime and nighttime comparison of VOC loss rate in a previous study (Warneke et al., 2004). However, the reactivity comparisons among anthropogenic VOCs shown by (Penkett et al., 1993) using the ratio of rate constants (k_{OH} to k_{NO3}) of particular VOC with OH and NO_3, reveal that the alkenes followed by branched-chain alkanes and acetylene are the compounds which are removed most efficiently by the NO_3 radical.

The rate constants for reaction of alkanes with NO_3 radical are very small and the loss process can be considered insignificant; however, these reactions can contribute to HNO_3 formation (Wayne et al., 1991). Reactions of alkanes, phenols, alcohols, cresols, DMS, aldehydes and aromatics take place through H-atom abstraction (equation 1.38). The ease of H-atom abstraction is greater from the tertiary carbon in branched-chain isomers than primary carbon in straight chain analogue (Wayne et al., 1991).

$$NO_3 + RH \qquad \rightarrow \qquad R + HNO_3 \qquad\qquad 1.38$$
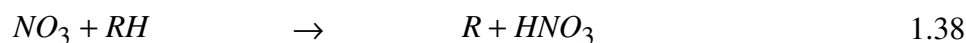
Reactions with alkenes take place *via* addition to C=C bond.

$$NO_3 + CH_2 = CH_2 \qquad \rightarrow \qquad CH_2(ONO_2)CH_2 \qquad\qquad 1.39$$

Previous studies (Wayne et al., 1991;Aliwell and Jones, 1998) have used empirical correlations between the log of two rate constants ($\log k_{NO3}$ *versus* $\log k_{OH}$) based on the principle of rate constants and Gibbs Free energy relation - termed as 'linear free energy relationship' - to compare the reactivity of the same compound with respect to OH and NO_3

$$\log(k_{NO_3}) \quad = \quad m \times \log(k_{OH}) + C \qquad 1.40$$

Figure 1.8 demonstrates a relationship between two rate constants for three categories of organic compounds namely saturated, unsaturated and aromatics, analyzed in course of this thesis. The rate constants are taken from (Atkinson and Arey, 2003). The correlation is quite significant ($R^2 = 0.93$) for unsaturated compounds (ethene, propene, butenes, isoprene and 1,3- butadiene) as compared to saturated (C_2 to C_8 alkanes) ($R^2 = 0.82$) and aromatic (benzene, toluene, ethylbenzene, xylenes, and isomers of trimethylbenzene) ($R^2 = 0.73$).
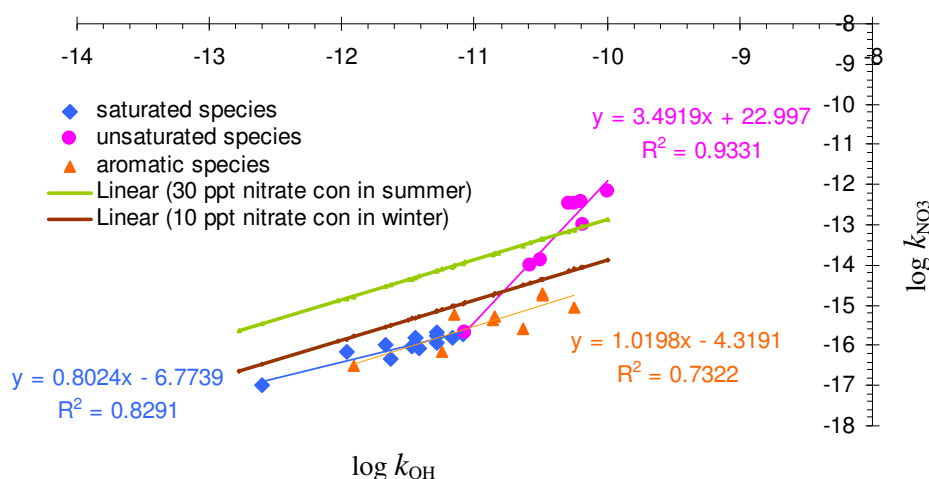
Figure 1.8: Plot of log k_{NO3} *versus* log k_{OH} for the same compound. The two lines, one at 30 ppt during summer and other at 10 ppt during winter, at a given OH concentration represents the same rate of reaction with NO_3 and OH. The correlation is quite significant ($R^2 = 0.93$) for unsaturated compounds (ethene, propene, butenes, isoprene and 1,3- butadiene) as compared to saturated (C_2 to C_8 alkanes) ($R^2 = 0.82$) and aromatic (benzene, toluene, ethylbenzene, xylenes, isomers of trimethylbenzene) ($R^2 = 0.73$). Data points above the lines (butenes) show a dominance of NO_3 as the principal oxidant, and below, OH.

In addition to these compounds, for a given concentration of NO_3 (average 30 ppt during summer campaign and average 10 ppt during winter campaign in terms of mixing ratio; these are converted into molecule cm^{-3}) and OH (1 x 10^6

molecule cm^{-3} during summer and 1 x 10^5 molecule cm^{-3} during winter), the rates constants for the reaction with OH and NO$_3$ with the same VOC are also compared by drawing two lines representing different NO$_3$ concentrations (in graph these lines represent unit in terms of mixing ratio; however, these are converted into molecule cm^{-3}). Data points above the lines show a dominance of NO$_3$ as the principal oxidant, and below, OH. It is clear from this plot that unsaturated compounds, especially butenes, (lying above 30 ppt and 10 ppt lines) are being removed effectively by NO$_3$ as compared to aromatics and alkanes (lying below both lines).

1.2.3.1.3   Lifetime of the NO$_3$ radicals

The lifetime of the NO$_3$ radical has been used to probe the nature of sinks in a particular field dataset in previous studies (Heintz et al., 1996;Geyer et al., 2001;Brown et al., 2003;Martinez et al., 2000).

The following four set of reactions can be used to derive the NO$_3$ lifetime. (Brown et al., 2003;Heintz et al., 1996)

$NO_2 + O_3$	$\xrightarrow{k_1}$	$NO_3 + O_2$	1.41
$NO_3 + NO_2 + M$	$\rightleftarrows$	$N_2O_5 + M$	1.42
$NO_3 + X$	$\xrightarrow{k_X}$	Product	1.43
$N_2O_5 + Y$	$\xrightarrow{k_Y}$	Product	1.44

where k_1 is the rate constant for NO$_3$ formation, *M* is a third body, *X* and *Y* are any sinks for NO$_3$ and N$_2$O$_5$ first order loss processes respectively, and k_X and k_Y are their corresponding rate constants. Any losses for N$_2$O$_5$ are indirect losses for NO$_3$.

Lifetimes can be calculated by assuming an approximation of steady state conditions with respect to NO$_3$:

$$\frac{d[NO_3]}{dt} \quad = \quad k_1 \times [NO_2] \times [O_3] - k_X \times [NO_3] \times [X] - k_Y \times [N_2O_5] \times [Y] = 0 \qquad 1.45$$

Assuming equilibrium is established between NO_3 and N_2O_5 with a strongly temperature dependent equilibrium constant, then the equilibrium concentration of N_2O_5 is given by equation 1.46:

$$[N_2O_5] \quad = \quad \frac{[NO_3][NO_2]}{K_{eq}(T)} \qquad 1.46$$

Substituting the N_2O_5 equilibrium concentration into equation 1.45, the steady state NO_3 concentration can be calculated by following equation 1.47:

$$[NO_3] \quad = \quad \frac{k_1 \times [NO_2] \times [O_3]}{k_X \times [X] + k_Y \times [Y] \times [NO_2] \times K_{eq}(T)} \qquad 1.47$$

Similarly a steady state concentration of N_2O_5 can be expressed as:

$$[N_2O_5] \quad = \quad \frac{k_1 \times K_{eq} \times [NO_2]^2 [O_3]}{k_X \times [X] + k_Y \times [Y] \times [NO_2] \times K_{eq}(T)} \qquad 1.48$$

The terms $k_X[X]$ and $k_Y[Y]$ are defined as loss frequencies of NO_3 and N_2O_5 respectively against any first order loss processes. As NO_3 and N_2O_5 are in rapidly established equilibrium, any losses for N_2O_5 are indirect losses for NO_3. The inverse of loss frequency is equal to 1/*e* lifetime of the radical.

$$\tau_{NO_3} \quad = \quad \frac{1}{k_X[X]} \qquad 1.49$$

30

$$\tau_{N_2O_5} \quad = \quad \frac{1}{k_Y[Y]} \qquad\qquad 1.50$$

Hence, the lifetime of NO_3 radical due to direct and indirect losses can be expressed as equation 1.51:

$$\tau_{NO_3} \quad = \quad \frac{1}{k_X[X]+k_Y[Y]} \qquad\qquad 1.51$$

Depending on the nature of the sinks, the steady-state lifetime can be further considered under three scenarios:

The first case is when N_2O_5 loss is negligible or $k_y[Y] = 0$

Substituting zero for N_2O_5 loss frequency in equation 1.47, the steady state life-time is expressed as:

$$\tau_{NO_3} \quad = \quad \frac{[NO_3]}{k_1[O_3][NO_2]} \qquad\qquad 1.52$$

The denominator in this equation represents the production rate of the NO_3 radical. Therefore, by measuring the NO_3 concentration and its production rate, the steady state NO_3 lifetime can be estimated. This is a useful procedure to calculate the steady state lifetime of the radical while carrying out field observations of NO_3. The reciprocal of this lifetime can be compared with that calculated from the sum of the first-order loss processes involving NO_3 and N_2O_5. In principle, all loss processes should be equal to the inverse of this lifetime and in this way it provides a test of whether all the processes that remove NO_3 have been accounted for ((Allan et al., 1999). The average steady state NO_3 lifetime during summer and winter phases of the RONOCO campaign was 1032 s and 573 s respectively.

Another case can be considered by assuming negligible sinks for NO_3 or $k_x[X] = 0$. Substituting zero for the NO_3 loss frequency in equation 1.48 the steady state lifetime for N_2O_5 can be expressed as:

$$\tau_{N_2O_5} \quad = \quad \frac{K_{eq}(T)[NO_3]}{[O_3] \times k_1} \qquad 1.53$$

Equation 1.53 can be rearranged in terms of NO_3 steady state lifetime

$$\tau_{NO_3} \quad = \quad \frac{\tau_{N_2O_5}}{K_{eq}(T) \times [NO_2]} \qquad 1.54$$

Putting the value for τ_{N2O5} from 1.53 in equation 1.54, the same expression is obtained as in case of negligible sinks for N_2O_5.

$$\tau_{NO_3} \quad = \quad \frac{[NO_3]}{k_1[O_3][NO_2]} \qquad 1.55 \equiv 1.52$$

Hence, regardless the nature of the sinks, the NO_3 lifetime can be expressed by the same expression but interpretation of this above equation suggests that if indirect sink processes dominate, then a plot of NO_3 lifetime should give an inverse relationship with NO_2 concentration.

The final and the more general situation when the sinks for both NO_3 and N_2O_5 are non zero or $k_X[X]$ and $k_Y[Y] \neq 0$

$$\tau_{NO_3} \quad = \quad (k_X[X] + k_Y[Y]K_{eq}[NO_2])^{-1} \qquad 1.56$$

Brown et al (Brown et al., 2003) showed the importance of equation 1.56 in extracting information quantitatively for both NO_3 and N_2O_5 sinks by plotting a graph of τ_{NO3} *versus* $K_{eq}(T)[NO_2]$ provided that steady state assumption is valid, and the sinks show constant behaviour relative to temperature and $[NO_2]$ variations. The slope and intercept of this equation gives information for N_2O_5 and NO_3 sinks, respectively. This concept has been used in chapter 4 to investigate whether direct loss processes (VOC loss) or indirect loss processes *(via* N_2O_5 loss) dominated in the RONOCO campaign dataset.

1.2.4 Carbon-containing compounds

A very large number of carbon-containing trace species are present in the atmosphere. The most important is CO_2, which plays a crucial role as the greenhouse gas that is responsible for much of the global warming that has occurred in the past century. It is a by-product of chemical reactions and produced during many biological processes and due to its non-reactivity towards other atmospheric agents, it is not considered as an important outdoor pollutant. Other sources of CO_2 include evaporation from the oceans, chemical oxidation of carbon monoxide and organic gases, volcanic outgassing, natural and anthropogenic biomass burning and fossil fuel combustion. CO_2 is removed from the air by oxygen-producing photosynthesis, dissolution into ocean water, transfer to soils and ice caps and chemical weathering. Its *e*-folding lifetime from emission to removal due to all loss processes ranges from 50 to 200 years. As shown in Figure 1.1, the mixing ratio of CO_2 has increased steadily since 1958 reaching the current level of approximately 393 ppm in November 2012 (ESRL, 2012).

The second most abundant carbon species is CH_4. CH_4 is a greenhouse gas that absorbs thermal IR radiation 25 times more efficiently in comparison with CO_2. It is difficult to distinguish natural and anthropogenic sources of CH_4 as the emissions predominantly stem from animals, including farm livestock, and wetlands, which includes rice paddies. To a lesser extent, the contribution from fossil fuels, biomass burning and atmospheric chemical reactions is also an emission source of CH_4. Its sinks include reaction with OH radical, transfer to soils, ice caps, the oceans, and consumption by methanotrophic bacteria. The *e*-folding lifetime of methane is about 4 to 10 years. The average mixing ratio of CH_4 in the troposphere is 1.7 ppmv, a factor of two increase (0.8 ppmv) in comparison with that of mid 1800s (Seinfeld and Pandis, 1998). Its tropospheric mixing ratio has increased steadily due to increased biomass burning, fossil-fuel combustion, fertiliser use, and landfill development.

Carbon monoxide (CO) is a product of incomplete combustion of fossil fuels and biomass burning. In addition, CO is a product of the chemical degradation of both CH_4 and VOCs. It is estimated that about two-thirds of the CO comes from anthropogenic activities, including oxidation of anthropogenically derived CH_4 (Jacobson, 2002). Hence CO is used often in studies as a tracer for anthropogenic activities. The use of CO in addition to other biomass burning tracers (furan and furfural) has been applied for airmass filtering of biomass burning data in chapter 6. In that chapter a mixing ratio greater than 200 ppb along with the presence of other tracers has been used as a filter threshold in identifying the biomass burning plume from anthropogenic and background plumes. Also, CO has been used as a reference compound (discussed in chapter 6) to normalize the excess mixing ratio of hydrocarbons species as presented in equation 1.57. The emission ratio is defined as excess mixing ratio of species X normalized to the excess mixing ratio of a reference species.

$$\text{Emission ratio} \quad = \quad \frac{\Delta X}{\Delta Y} \qquad\qquad 1.57$$

where $\Delta X = X_{plume} - X_{bkgd}$

and $\Delta Y = Y_{plume} - Y_{bkgd}$

where X_{plume} and X_{bkgd} are the mixing ratios of trace species X in the fresh smoke plume and the background air, respectively; Y_{plume} and Y_{bkgd} are the mixing ratio of trace species Y (It can be CO or CO_2 or ethane depending upon the availability of data/analyzer) in fresh smoke plumes and background air, respectively.

The major sink for CO is reaction with OH radicals, with soil uptake and diffusion into the stratosphere being minor routes. Its lifetime is about 30–90 days on the global scale of the troposphere. Due to its intermediate lifetime, its seasonal variations are quite apparent with a maximum mixing ratio during the local spring and the minimum during the late summer or early fall (Seinfeld and Pandis, 1998). As far as its role in formation of O_3 is concerned, it plays a small role in urban areas whilst in the background troposphere, it becomes an

important species. CO is not an important greenhouse gas, but its emission and oxidation to CO_2 affect global climate. The NH has more CO than in the Southern Hemisphere (SH). Tropospheric CO mixing ratios typically range from 40 to 200 ppb (Seinfeld and Pandis, 1998). Maximum mixing ratios are observed near the surface and decreases with respect to altitude reaching to a free troposphere average value of about 120 ppb near 45 °N. In the SH, CO tends to be more nearly uniformly mixed vertically with a mixing ratio of about 60 ppb near 45 °S(Seinfeld and Pandis, 1998).

1.2.4.1   Hydrocarbons

The word 'hydrocarbon' indicates a molecule containing only carbon and hydrogen atoms. Throughout the chapters, this is used as a synonym of VOC and non-methane hydrocarbon (NMHC); however, strictly speaking NMHCs includes all alkanes except CH_4 whilst VOCs include hydrocarbon species in addition to the organic compounds containing heteroatoms such as nitrogen, sulphur or oxygen. The measurement of VOCs has long been an important research area among atmospheric scientists due to their role in photochemical O_3 formation, influencing the oxidising capacity of the atmosphere and causing adverse health effects on human beings (Derwent et al., 1995).

VOCs are emitted into the atmosphere by a variety of anthropogenic and biogenic sources. The relative importance of anthropogenic and biogenic sources on a global scale depends on the geographic location and seasonal variations for e.g. NH (between 40 °N and 50 °N) is dominated by anthropogenic emissions whilst biogenics are mostly emitted in the tropics. The global distribution and source strength of anthropogenic NMHCs are usually taken from the Emission Databases for Global Atmospheric Research (EDGAR) database (Koppmann, 2007). The global emission of anthropogenic VOCs is estimated to amount to 186 Tg yr^{-1}. However, the majority of VOCs in the atmosphere are related to biogenic emissions including vegetation and small contributions from oceans and

soils with estimated totals between 377 TgC yr^{-1} (IPCC, 2001) and 1150 TgC yr^{-1} (Guenther et al., 1995). On a global average, the use of fossil fuel accounts for about 40% of emitted VOCs. About 25% of the emissions are due to biomass burning and rest is about equally divided between the use of biomass and industrial processes. According to (Andreae and Merlet, 2001) the global VOC emission due to biomass burning is 60 Tg yr^{-1}. The relative contributions of anthropogenic and biomass burning emissions to the background abundance of benzene, toluene, ethene and propene species has recently been examined (Lewis et al., 2012). This study not only highlights the influence of regional and transboundary biomass burning as the largest fractional contribution to observed benzene, toluene, ethene and propene levels in many global locations but also suggests to adopt a practical approach in setting air quality targets especially for heavily regulated species for example benzene, which is thought of in the background atmosphere primarily due to anthropogenic emissions.

Once these organic emissions from various sources are introduced into the atmosphere, their distribution is controlled by the atmospheric transport phenomena in addition to the various physical and chemical removal processes. Depending on the latitude, season, prevailing meteorology, location of the sources, and the reactivities of particular compounds, their spatial and temporal distribution varies from urban centres to global background. The major source of VOCs in the UK atmosphere is primarily emissions from road transport (37.77%) followed by solvent usage (27.89%) (Harrison, 2001). In the UK, the Hydrocarbon Network has been making automated hourly measurements of speciated hydrocarbons since 1991. This measurement programme is focused on assessing ambient concentrations of a range of VOCs with significant photochemical oxidant forming potential, measuring benzene for comparison with the ambient air quality objectives and 1,3-butadiene for comparison with UK objectives. A comparative study between free tropospheric VOC observations made above the UK between January 2009 and January 2011 with previous UK free tropospheric study in chapter 5 clearly indicates that benzene,

acetylene, toluene, butanes and pentanes emissions have declined up to 50% since the early 1990s emission levels.

Chemical removal processes include three main oxidants; these are the OH radical, NO_3 radical, and O_3. The concentration of the OH radical is abundant during daytime because it is primarily formed by the photolysis of O_3 in presence of sunlight. Although the precursors for formation of NO_3 are available during the day, owing to its light absorbing properties in visible region, this leads to its photodissociation, such that NO_3 is mainly a night-time oxidant. The oxidant O_3 is essentially available all the time although its concentration varies widely and can be reduced to zero when NO concentrations are high (Wayne et al., 1991). The rate of emissions of VOCs and the removal processes of these trace gases in determining air quality is equally important during the night (Vrekoussis et al., 2003) but is less well studied compared to day time OH chemistry.

The reactive halogen species also participate in the removal of VOCs to a lesser extent especially in certain marine environments (Jobson et al., 1994;Hopkins et al., 2002); however, reactive bromine (Br and BrO) and perhaps iodine species, can act as an NO_3 scavenger in certain conditions (Platt and Janssen, 1995). Thus the presence of reactive bromine species and NO_3 together during night cannot be interpreted to enhance the oxidation rate of organic compounds in a synergistic way. Previous studies have shown that degradation of VOCs by NO_3 radicals is associated with the production of peroxy radical (Fleming et al., 2006) and OH radical (Atkinson and Aschmann, 1993). The presence of NO_3 together with O_3 and OH act in an additive way to increase the self-cleansing capacity of the atmosphere during the night (Wayne et al., 1991).

The rate constants of most VOCs with NO_3 radicals are less than that with OH radicals (see Table 3.1). Despite this lower reactivity with VOCs, the significant concentration of NO_3 during night (10 -100 times higher) as compared to OH can

make nighttime chemistry as important as OH chemistry during the day (Wayne, 2000). The relative contribution of NO_3, OH and O_3 to total VOC degradation processes was found to be 28%, 55% and 17% on a 24-hour average basis during the BERLIOZ campaign (Geyer et al., 2001); however the involvement of NO_3 was slightly higher (31%) when oxidation of only olefinic VOCs was compared. During the RONOCO campaign, a comparison between two chief nighttime oxidants , the NO_3 radical and the O_3 molecule, towards VOC loss rates indicate that in summer the contribution of the NO_3 radical is more than double than that of O_3 whilst an equal participation of both oxidants to VOC loss rate is seen in winter.

One of the important differences between the degradation processes of VOCs taking place during day and night is that the OH radical catalyzes the degradation process by regenerating itself and photochemical O_3 is formed, whilst NO_3 radicals initiates the degradation procedure without forming O_3 (Monks, 2005). These differences between day time and nighttime processes enhance the importance of exploring the role of nighttime chemistry in the degradation of VOCs, which in turn has a role determining their availability for the following day to participate in photochemical O_3 formation.

1.2.5 Atmospheric O_3

O_3 is a key compound in the chemistry of the atmosphere. In addition to being an important greenhouse gas, it is a component of smog, poisonous to humans, animals and plants as well as precursor to cleansing agent (such as OH radical). O_3 also acts as a continuously available oxidant. Most of the Earth's atmospheric O_3 (90%) is found in the stratosphere where it plays a critical role in absorbing ultraviolet radiation of wavelengths between 240 and 290 nm emitted by the sun. Such radiation is harmful to unicellular organisms and to surface cells of higher plants and animals. That is the reason of referring to stratospheric O_3 as "good" O_3. In addition, ultraviolet radiation in the wavelength range 290-320 nm, so-

called UV-B is biologically active. It has been well established that anthropogenically emitted substances, such as halocarbons with a longer lifetimes, as discussed in the previous section, have the potential to escape from the troposphere and seriously deplete the natural levels of O_3 in the stratosphere. A decrease in stratosphere O_3 level allows UV-B radiation to enter into the Earth stroposphere and which can lead to increased incidence of skin cancer (Wayne, 2000).

As far as Earth's tropospheric O_3 levels are concerned, these are generally small - roughly 10-40 ppb at sea level in contrast to 10 ppm in stratosphere. Recent evidence suggests that background NH tropospheric O_3 concentrations have approximately doubled since the turn of the century (Harrison, 2001;Air quality expert group, 2009). The reason for increased tropospheric O_3 is increased formation from the oxidation cycles of CH_4 and enhanced anthropogenic emissions including VOC, NO_x and CO. O_3 at ground level at elevated concentrations can lead to respiratory effects in humans and hence tropospheric O_3 at elevated mixing ratios has been considered as "bad" O_3. In clean environments, O_3 mixing ratios are in the range of 10-40 ppb with somewhat higher mixing ratios in the upper troposphere. Tropospheric loss processes for O_3 include photolysis in the visible and ultraviolet regions, and reaction with species such as NO_2, HO_2 and unsaturated hydrocarbons. The tropospheric abundance of O_3 is critically important in determining the oxidizing capacity of the troposphere; because O_3 is the primary source of OH radicals as well as itself acting as an oxidant.

1.2.6 Aerosols

In addition to the mixture of gases, particulate matter commonly referred to as aerosols is also an important part of the atmosphere. The technical definition of aerosol is a suspension of fine solid or liquid particles in a gas, whilst common usage refers to aerosol as liquid droplets in air and particulates solids in air.

(Seinfeld and Pandis, 1998). Primary aerosols are emitted directly, whilst secondary aerosols are formed in the atmosphere by gas-to-particle conversion processes. Their size varies from a few nanometres (nm) to tens of micrometres (μm) in diameter. Their role in climate and atmospheric chemistry has well been established as they scatter sunlight, provide condensation nuclei for cloud droplets and participate in heterogeneous chemical reactions. Sulphate aerosol is a very effective cloud condensation nucleus and hence much research has been focused on DMS and its oxidation products. In cities, organic aerosols and soot are also emitted directly, particularly from diesel exhausts. Particles smaller than 10 μm (PM10) can be effectively inhaled by humans and create several health-related problems.

1.2.7 Observations *versus* models

Models provide a link between atmospheric measurements and laboratory studies and provide a numerical simulation of the chemistry and physics of the real atmosphere. A large number of observational experiments using surface, aircraft, balloon and satellite platforms and ranging from short-term campaigns to long-term networks not only provide a large dataset for exploring the chemical processes but also are used as an input to modellers. The comparison between observations and models is a useful approach to test our knowledge of atmospheric oxidation processes. During comparison if there is a good agreement between the two then it points out the good understanding of chemical atmospheric processes and if some discrepancies exist then these indicate towards the need for development of improved representations. An example is three-dimensional (3D) chemical transport models (CTMs) which include the latest understanding of homogenous and heterogeneous fast photochemistry. The observations from a project focused on boreal forest fires have been compared with the output from the GEOS-Chem global 3-D chemical transport model (CTM) in chapter 6 to highlight the influence of biomass burning on the global distributions of benzene, toluene, ethene and propene (Lewis et al., 2012).

1.2.8 Approaches used for data analysis

1.2.8.1 Hydrocarbon ratio: a useful approach

The mixing ratio of hydrocarbons between source and sampling point varies by the combined effects of dilution and chemical loss processes. In order to deal with these intricate and combined effects, two or more species are correlated in terms of ratio so as to remove the effects of dilution by clean air; dilution will act equally on any pair of hydrocarbons with a common source. In such a case the hydrocarbon ratio of two compounds, having different lifetimes and similar sources, gives an insight of the nature of the chemical decay processes.

The example of [acetylene]/[CO] ratio and [propane]/ [ethane] ratio falls into this category. However, the use of both ratios as a marker of photochemical processing should be done with caution (McKeen et al., 1996) as mixing and dilution effects play a major role in atmospheric processing of these compounds as compared to photochemistry (Smyth et al., 1996;McKeen et al., 1996). This study uses acetylene mixing ratio as a tracer to track changes in the hydrocarbon ratio from less processed to more processed air. The [acetylene]/[CO] ratio also has been used to compare the range of air masses encountered during this campaign. However, the ratios of two species having similar lifetimes (e.g. [propane]/[acetylene], [benzene]/[acetylene], and [propane]/[benzene]) but different sources, may reveal characteristics of the source profile (Russo et al., 2010)

The change in mixing ratio due to dilution and chemical loss processes (McKeen et al., 1996) can be expressed as:

$$\frac{d[X]}{dt} \quad = \quad -F_x[X] - A \times ([X] - [X]^B) \qquad 1.58$$

$$= \quad -k_x[OH][X] - A \times ([X] - [X]^B) \qquad 1.59$$

where $[X]$ is the mixing ratio of hydrocarbon species, t is the elapsed time between source and sampling point, $[X]^B$ is the assigned mixing ratio of X in the background air, F_x is the degradation frequency of species X with oxidant OH ,assuming that VOC only reacts with OH radical, $(F_x = k_x[OH])$, k_x is the bimolecular rate constant, $[OH]$ is the time averaged concentration and A is a mixing coefficient.

By making assumptions that A and $k_x[OH]$ are constant during the transport time and not taking into account the background mixing ratios other than $[X]^B$ gives solution of above equation as presented in equation1.60:

$$[X] \quad = \quad \frac{A[X]^B}{A+F_X} + \left([X]^0 - \frac{A[X]^B}{A+F_X} \right) e^{(-A+F_x)t} \qquad 1.60$$

where $[X]^0$ is the initial mixing ratio of X upon emission.

In addition to these assumptions, the removal of hydrocarbons is considered here as a pseudo first order loss process and multiple sources or fresh injections of hydrocarbons from source to sampling point are completely ignored. Although this is an idealised approach, the following examples illustrate the applicability and utility of this approach in extracting information in a qualitative to semi quantitative way.

For the sake of simplicity, the above equation is further discussed by making assumptions under different scenarios. The First scenario assumes the chemical decay processes are much faster than mixing effects (F_x>>A). Applying this assumption in equation 1.60 gives the following expression:

$$[X] \quad = \quad [X]^0 e^{-k_x[OH]t} \qquad 1.61$$

$$\ln \frac{[X]}{[X]^0} \quad = \quad -k_x[OH]t \qquad 1.62$$

Using equation 1.62 for two hydrocarbon species in a ratio form, an expression 1.64 can be derived to calculate the product [OH]t termed as photochemical age, provided that initial ratio of mixing ratio is known.

$$\ln\frac{[X]}{[Y]} \qquad = \qquad \ln\frac{[X]^0}{[Y]^0} - (k_x - k_y)[OH]t \qquad\qquad 1.63$$

$$\ln\frac{[X]/[Y]}{[X]^0/[Y]^0} \qquad = \qquad -(k_x - k_y)[OH]t \qquad\qquad 1.64$$

$$t \qquad = \qquad \frac{\ln[X]^0/[Y]^0 - \ln[X]/[Y]}{(k_x - k_y)\times[OH]} \qquad\qquad 1.65$$

The photochemical age is defined as the time integrated exposure of a trace species to the OH radical between injection and sampling time. By using an arbitrary starting point, the relative age of different air masses can be calculated using equation 1.65. The concept of photochemical age appears to be simple; however, the impact of mixing on observed ratios stops this equation from being used to deduce an accurate photochemical age.

In order to avoid the uncertainties in OH radical concentration, the expression 1.65 can be interpreted in terms of *n*-butane lifetime (τ_{butane}) (Rudolph and Johnen, 1990) as shown in equation 1.66 provided that the ratio of initial mixing ratios is known.

$$\frac{t}{\tau_{n-butane}} \qquad = \qquad k_{n-butane-OH} \times \left(\frac{\dfrac{\ln[X]/[Y]}{\ln[X]^0/[Y]^0}}{k_{Y-OH} - k_{X-OH}} \right) \qquad\qquad 1.66$$

where $\tau_{n\text{-butane}}$ is *n*-butane lifetime as presented in equation 1.67:

$$\tau_{n-butane} \qquad = \qquad \frac{1}{k_{n-butane-OH}[OH]} \qquad\qquad 1.67$$

Comparing expression 1.66 for three ratios ([propane]/[ethane], [*n*-butane]/[ethane] and [*iso*-butane]/[ethane]) and getting a good agreement among these for t/τ_{butane} (Rudolph and Johnen, 1990) gives us confidence in following the simple, yet ideal approach .

The difference in the photochemical age can be estimated by measuring ratios in two air parcels having the same initial injection, in the case when the ratio of initial concentrations is not known.

$$t'-t \qquad = \qquad \frac{\ln[X]/[Y] - \ln[X']/[Y']}{(k_x - k_y)[OH]} \qquad\qquad 1.68$$

So hydrocarbon ratios in this way act as a clock that measures the exposure of [OH] in an air parcel since emission. The expression 1.64 has been used by (Blake et al., 1993) to infer OH concentration by taking acetylene as a relatively inert species to cancel out the dilution effects during experiment time in a Lagrangian fashion. The Lagrangian framework involves the tracking of same air mass by an observer with the wind and takes into account only physical and chemical changes associated with the air parcel rather than air motions.

It is interesting to compare the results obtained for derived OH from two different ratios or clocks defined by more reactive and less reactive hydrocarbon ratios. It has been shown by (Parrish et al., 1992) qualitatively how the age of newly mixed air parcels is affected if the original air parcel is mixed with fresh or aged air parcels having the same initial injection of hydrocarbons. The mixing with fresh air parcels readjusts the clock in such a way that new mixed air parcel appears to be younger. In other words the clock runs slow and the derived OH value is small. Conversely, the mixing with processed background air will transform the new air mass into an air parcel of older age and use of this faster clock will in turn give higher OH concentrations. In each mixing scenario, the derived age of new mixed air parcel will depend considerably on the use of more reactive and less reactive hydrocarbons.

Another application of equation 1.64 is that ratios of oxidants $[NO_3]/[OH]$ (Penkett et al., 2007) and $[Cl]/[OH]$ (Rudolph et al., 1997) can be derived by taking two different pairs and assuming that both hydrocarbon pairs are processed exclusively by a specific but different oxidant. This approach is dealt in chapter 4.

The use of two ratios defined by three species having the same and least reactive denominator gives an expression which eliminates the product [OH]t and establishes a log-log linear relationship (equation 1.69).

$$\ln \frac{[X]}{[Z]} \qquad = \qquad m \times \left\{ \ln \frac{[Y]}{[Z]} \right\} + C \qquad\qquad 1.69$$

where slope m and intercept C are defined as:

$$m \qquad = \qquad \frac{(k_x - k_z)}{(k_y - k_z)} \qquad\qquad 1.70$$

$$C \qquad = \qquad \ln \frac{[X]^0}{[Z]^0} - m \ln \frac{[Y]^0}{[Z]_0} \qquad\qquad 1.71$$

The expression 1.69 has been used by (Parrish et al., 1992) on wide variety of air masses (**Figure 1.9**) of different age by plotting ln [*n*-butane]/[ethane] versus ln [propane]/[ethane]. The correlation between two ratios is often quite good, although the slope from a linear least square fit rather different (1.47) from the expected kinetic slope (2.77 at 280K).(McKeen et al., 1996). This deviation may be explained by varying the background mixing ratio of ethane, the least reactive species used in the denominator.
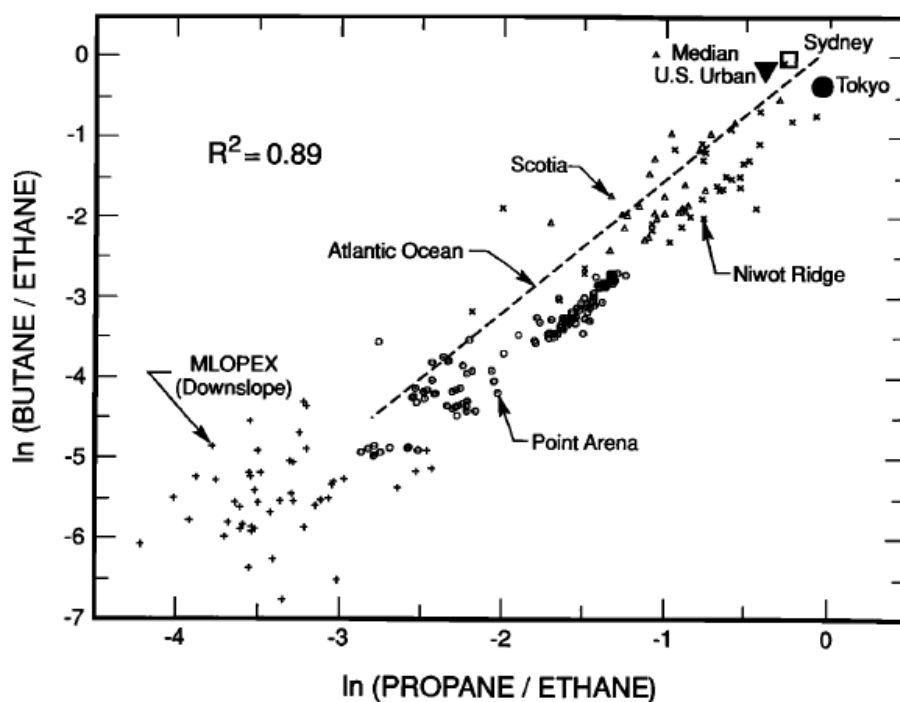
Figure 1.9: Correlation of the natural logarithms of ln [*n*-butane]/[ethane] *versus*
ln [propane]/[ethane] from wide variety of air masses (Parrish et al., 1992). Included are
the data from downslope periods of the Mauna Loa Observatory Photochemistry
Experiment (MLOPEX) study in Hawaii (Greenberg et al., 1992); Niwot Ridge,
Colorado (H.H Westberg et al, unpublished data ,1987); Scotia, Pennsylvania
(H.H.Westberg et al unpublished data 1988); the Atlantic ocean (Rudolph and Johnen,
1990); and Point arena (Singh and Kasting, 1988). The three large symbols are from the
urban study: United states (Seinfeld, 1989), Sydney (Nelson and Quigley, 1982) and
Tokyo(Uno et al., 1985).

Swanson et al (Swanson et al., 2003) argued that alkanes having different
emission ratios could also be the reason for deviation in slope from the expected
behaviour. The data points influenced from fresh biomass burning or petroleum
or natural gas field emissions could lie on the middle of the line or near the line
appearing to be indistinguishable from urban aged emissions. Evidence of a
changing photochemical environment of temperate North Pacific troposphere
was demonstrated by Parrish et al (Parrish et al., 2004) This was done by
correlating net O_3 production or loss with hydrocarbon processing from fresh to
aged air masses by using ln [propane]/[ethane] ratio as an indicator of extent of
photochemical processing. Another robust indicator, ln[propane]/[ethane] *versus*

46

ln [propane], was used to check the influence of divergent emission ratios in their data set.

By dividing equation 1.64 by 1.62 we get following relationship similar to previous study (Gong and Demerjian, 1997):

$$\ln \frac{[X]}{[Y]} \quad = \quad m \times \ln[X] + C \tag{1.72}$$

$$\ln \frac{[\text{propane}]}{[\text{ethane}]} \quad = \quad m \times \ln[\text{propane}] + C \tag{1.73}$$

where slope *m* and intercept *C* are defined as:

$$m \quad = \quad \frac{k_x - k_y}{k_x} \tag{1.74}$$

$$C \quad = \quad \ln \frac{[X]^0}{[Y]^0} - \frac{k_x - k_y}{k_x} \ln[X]^0 \tag{1.75}$$

Using this indicator the influence of different emissions other than urban anthropogenic emissions can be traced out as discussed in chapter 5; however, it is important to note that deviation in slope is not related to divergent emission patterns, rather it is the intercept of this plot which is affected by change in source profile (Rudolph and Johnen, 1990). An explanation for slopes less than expected values was given by (McKeen and Liu, 1993) by visualizing photochemistry and mixing together as a combined process rather than considering only OH chemistry to affect ratios. Further work from this research group (McKeen et al., 1996) explored the relationship between significant backgrounds and changing slopes. A significant background of the least reactive species not only alters the steepness of any slope but also the rate of change of the ratio-ratio relationship (McKeen et al., 1996). By assuming zero background for numerator species and prescribed background values $[Z^B]$ for denominator, an expression (1.76) having both an A and F term can be derived.

$$\frac{[X]}{[Z]-\left(\dfrac{[Z]^B A}{A+F_Y}\right)} \quad = \quad m \times \left[\frac{[Y]}{[Z]-\left(\dfrac{[Z]^B A}{A+F_Y}\right)}\right]^{\frac{F_x - F_z}{F_{Y-}F_z}} \qquad 1.76$$

The larger the background value, the lower the slope and the slower the rate of change of ratio-ratio relationship. The concept of background mixing ratio is not well defined; however; the background mixing ratio term is one of the major uncertainties in inferring OH concentration by using equation 1.60. The preferred way of using background values are either use of median mixing ratio of species at a desired altitude (Price et al., 2004), or sampling air masses from relatively clean air (McKeen et al., 1996) or rural sites (Dillon et al., 2002). Parrish et al. could show a reasonable agreement between model-measurement comparisons by using only emission ratios without using an assumed background concentration (Parrish et al., 2007). It is easy to use the concept of emission ratios instead of initial mixing ratios.

To deal with the mixing coefficient (A) quantitatively, a log-log plot for species *versus* species relationships can be derived by assuming zero background. The second scenario assumes zero background mixing ratio of species (A and F both terms are included in following equation)

$$[X] \qquad = \qquad X^0 e^{-(A+F_x)t} \qquad 1.77$$

This expression, if applied for three species, gives the same as equation 1.69 describing log-log plots of ratio *versus* ratio relationship, defined as a 'photochemical line'.

The advantage of using equation 1.77 is that if it is applied on two species (species *versus* species relationship) then a plot of log [X] versus log [butane] (equation 1.79) gives a slope which can be further derived in getting expression in terms of A/F_{butane} and the number gives an idea of relative contribution of mixing (A) in comparison to the loss frequency of butane F_X (McKeen et al., 1996).

$$[X] \quad = \quad [X]^0 \times \left(\frac{[Y]}{[Y]^0} \right)^m \qquad\qquad 1.78$$

$$\ln[X] \quad = \quad m \times \ln[Y] + C \qquad\qquad 1.79$$

where slope *m* and intercept *C* are defined as:

$$m \quad = \quad \frac{A + F_X}{A + F_Y} \qquad\qquad 1.80$$

$$C \quad = \quad \ln \frac{[X^0]}{[Y^0]^{\frac{A+F_x}{A+F_y}}} \qquad\qquad 1.81$$

Another way to deal with the mixing coefficient A in a quantitative manner is by assuming inert hydrocarbons under a third scenario ($F_x \ll A$)

$$[X] \quad = \quad [X^B] + ([X^0] - [X^B])e^{-At} \qquad\qquad 1.82$$

Applying expression 1.82 for three species and assuming zero background for X and Y and non-zero background for Z gives an equation 1.83 which is termed as the 'dilution line' X^B, $Y^B = 0$ but Z^B is not zero:

$$\ln \frac{[X]}{[Z]} \quad = \quad m \times \ln \frac{[Y]}{[Z]} + C \qquad\qquad 1.83$$

where slope *m* and intercept *C* are:

$$m \qquad = \qquad 1 \qquad\qquad\qquad 1.84$$

$$C \qquad = \qquad \ln \frac{[X]^0}{[Y]^0} \qquad\qquad\qquad 1.85$$

Throughout chapter 3, the ratio *versus* ratio relationships have been used with reference to the theoretical photochemical line (equation 1.69) and the dilution line (equation 1.83) to examine the changing pattern of log-log plots in the presence of different oxidants during different periods of time.

To derive the dilution coefficient A, the expression 1.82 has been applied on very slow reacting hydrocarbons (ethane), and trace species (CO) having well defined background mixing ratios (equation 1.86), which during the observed experimental time frame show variation in mixing ratio due exclusively to dilution (Price et al., 2004;Dillon et al., 2002).

$$[A] \qquad = \qquad \frac{1}{t} \ln \frac{(X^0 - X^B)}{(X^t - X^B)} \qquad\qquad\qquad 1.86$$

Or alternatively by plotting log of mixing ratio of species over its background mixing ratio ln $[X^t\text{-}X^b]$ versus *t* using equation 1.86 gives a slope which is equal to mixing coefficient A (McKeen et al., 1996).

Once the mixing coefficient 'A', background mixing ratio $[X]^B$ and initial mixing ratio X^0 are known, then equation 1.60 can be used to infer the OH concentration by using laboratory determined rate constants.

Another way to infer OH concentration is the use of expression 1.87 (Dillon et al., 2002) for very reactive species, for example toluene, and assuming zero background, a plot of decay rate of species *versus t* gives a slope which is equal

to sum of A and F$_x$. By subtracting A from the slope and dividing by the rate constant gives an OH determination (McKeen et al., 1996).

$$\ln[X] \qquad = \qquad m \times t + C \qquad\qquad 1.87$$

where slope *m* and intercept *C* are defined as

$$m \qquad = \qquad -(A + F_X) \qquad\qquad 1.88$$

$$c \qquad = \qquad \ln[X]^0 \qquad\qquad 1.89$$

A good agreement between the two methods to determine OH, the one without using mixing coefficient A, and using two species having different lifetime and the same source (Parrish et al., 1992) and the other by determining A using the least reactive species and using background and initial mixing ratio (Dillon et al., 2002) for a particular event gives confidence in applying this approach.

The idea of planning some Lagrangian flight frameworks during the RONOCO campaign was to compare this indirect approach to derive radical with direct measurement techniques.

1.2.8.2   Variability-lifetime relationship: another useful tool

The observed mixing ratio of an organic trace gas in the atmosphere at a given sampling time is a result of the balance between its production and removal rates. The removal mechanism of VOCs is primarily through OH radical chemistry. The wide variety of hydrocarbon species in the atmosphere have a similar level of diversity in their reactivities with respect to the OH radical; these lead to lifetimes of 2 months, for example ethane, down to 2 hours for isoprene. Depending upon the distance between sources and sampling, the variability in the mixing ratios can be due to changes in any single source emission rate, variation in different nearby contributing sources or due to transport and chemical removal

processes. It is anticipated therefore that a species with long lifetime should display less variation in the mixing ratio with respect to time and space as compared to the species with short lifetime. The atmosphere provides a 'smoothing' of these various signal forcings. On the basis of this theoretical concept, Junge (Junge, 1974) first established a link between the variability of tropospheric gases and their residence times by giving an empirical formula (equation 1.90) in which the relative standard deviation is inversely proportional to residence time provided that the distribution of sources and sinks is similar.

$$R.S.D \qquad = \qquad \frac{0.14}{\tau} \qquad\qquad 1.90$$

Here *R.S.D* is the relative standard deviation (standard deviation divided by the mean mixing ratio) and τ is the residence time in years. Before continuing this discussion, the difference between the usage of words 'residence time' and 'lifetime' should be understood. Basically, the word 'residence time' is used for trace gases that are removed exclusively by fluxes or non-chemical removal methods, whilst the word 'lifetime' is used for species that are destroyed by chemical degradation methods. Junge (Junge, 1974) used the variability-lifetime relationship on long-lived gases with troposphere with residence times measured in years - hence these gases can be considered in steady state. These gases are removed either by chemical degradation within the troposphere with a particular $1/e$ lifetime or by non-chemical removal that *via* flux from the troposphere boundaries into upper atmospheric layers. Removal by a combination of both schemes is of course possible and indeed highly likely and this combination defines the overall residence time. The gases included in the Junge (Junge, 1974) study were indeed removed by both processes so the word residence time has been generally used by authors throughout their discussions. In the present context, where hydrocarbons have much shorter lifetimes and are mainly removed by the chemical degradation process within the troposphere, this means that these gases are not likely to be considered in the steady state. Hence it is clear that when species are mainly removed by chemical processes then the

phrase 1/e lifetime is used and when it is mainly removed by flux through boundaries then the appropriate word to use is the residence time.

Returning to the variability-lifetime relationship, Jobson et al (Jobson et al., 1998) first applied this relationship to a dataset including NMHCs for which the variability is much higher, or sometimes with a dataset for reactive compounds, becomes equal to the mean mixing ratio - very different to long-lived trace gases such as CO_2. In order to make the variability in a dataset comprising of short-lived hydrocarbons comparable to the relative standard deviation in a data set that also includes long-lived trace gases, Jobson et al (Jobson et al., 1998) transformed hydrocarbon mixing ratios by taking the natural log and reformulated the relationship by relating standard deviation of the natural log of mixing ratio with lifetime (equation1.91)

$$Sln[X] \qquad = \qquad A\tau^{-b} \qquad\qquad 1.91$$

taking log of both sides of above equation.

$$\log Sln[X] \qquad = \qquad -b\log\tau + \log A \qquad\qquad 1.92$$

where X is the mixing ratio of the hydrocarbon species, Sln[X] is the standard deviation of the natural logarithms of all measurements, *A* and *b* are the fitting parameters (explained further in more detail in this section) and τ is the lifetime in days.

While using this relationship throughout the following chapters, the lifetime in days has been estimated by using an OH concentration of 1×10^5 molecule cm^{-3} in winter and 1×10^6 molecule cm^{-3} in summer seasons (Williams et al., 2001). The chosen value of OH concentration does not affect the *b* value, which is the slope of the plot between log Sln[X] *versus* log τ according to the equation 1.92,

though the value of *A* depends on the OH concentration. By changing the OH concentration, the absolute lifetime of a species varies and all data points are affected to similar extent leaving *b* unaffected; however, when it comes to making comparison between lifetime, and mixing and transport times then varying the concentration of OH does affect these comparisons. The purpose of equation 1.92 is primarily to check the relationship of different species' lifetime with their variability rather than performing a mixing and transport timescales comparison; therefore, the assumption of OH concentration is a workable approach for this discussion.

A is a proportionality constant and is a measure of the spread in the range of air mass ages in the sampled data. Aged air masses are a result of longer processing time during longer transport times whilst shorter transport time results in a less processed air mass. Hence, the standard deviation in the transit time distribution is conveyed by *A* in the above expression. The higher the standard deviation among the transport times in sampled air masses, the greater is the value of *A* and vice versa. Generally, the greatest standard deviation among transit times of air masses has been observed in stratospheric data sets where widely different air masses exist. When relatively young air masses from the troposphere enter into a stratospheric layer that is already several years older then this far greater spread of transit times results the higher value of *A* (Jobson et al., 1999) . However, when air masses with narrow range of ages are sampled, for example fresh continental emissions, then a low value of *A* is expected - as observed in a Harvard Forest data set (Goldstein et al., 1995b) with a value of *A* = 0.99 which is comparable with an *A* value of 1.1 in the nighttime boundary layer data set during RONOCO field campaign discussed in chapter 4. From this discussion, it should not be assumed that lower values of *A* are always expected in a tropospheric dataset. Although the troposphere is well mixed; the spread in time distribution among air masses entirely depends on the location of the sampling site and the distribution of transport times among air masses sampled; a smaller fraction of air masses influenced with nearby continental sources can lower the value of *A* in a dataset acquired from remote locations (Williams et al., 2000).

The *A* value equal to 3.5 in summer and 3.3 in winter data has been observed in UK free troposphere hydrocarbon dataset in chapter 5.

The exponent *b* is the slope in the logarithmic correlation plot between log Sln[X] *versus* log of estimated OH lifetime in days for different hydrocarbon species, and gives information on the sink term. It takes a value from 0 to 1 and is indicative of source-receptor distance at a first glance. A value close to zero has been observed over source regions, mostly in urban data set (*b* = 0.28, Boulder, Colorodo dataset, (Jobson et al., 1998) indicating a weaker dependence on lifetime or greater influence of mixing, or in other words, the observation is made near source where continuous local emissions are suppressing the variability provided that there is no other instrument artefact responsible for the reduced variability. A value equal to 0.5 is mostly exhibited in datasets from the well-mixed free troposphere and more remote troposphere locations, for example in three field experiments – The Arctic boundary Layer Expedition 3B (ABLE3B *b* =0.46) , the Transport and Atmospheric Chemistry Near the Equator-Atlantic (TRACE- A, *b*=0. 52) and the Pacific Exploratory Mission in the Western Pacific Ocean Phase B (PEM-West B, *b*=0.53) (Jobson et al., 1999). These values all range from 0.46 to 0.53 and can be interpreted in a way that mixing and chemistry both are responsible for the observed variability trends. Finally, the value of *b* close to 1 indicates that sampling site is distant from the sources for example in stratospheric datasets, and samples collected during Polar Sunrise Experiment (PSE) 1992 data from a site on the sea ice north of Alert, Canada (**Figure 1.10**) exhibit a greater influence of chemistry (*b* =0.92) on depleted mixing ratios over mixing (Jobson et al., 1999).
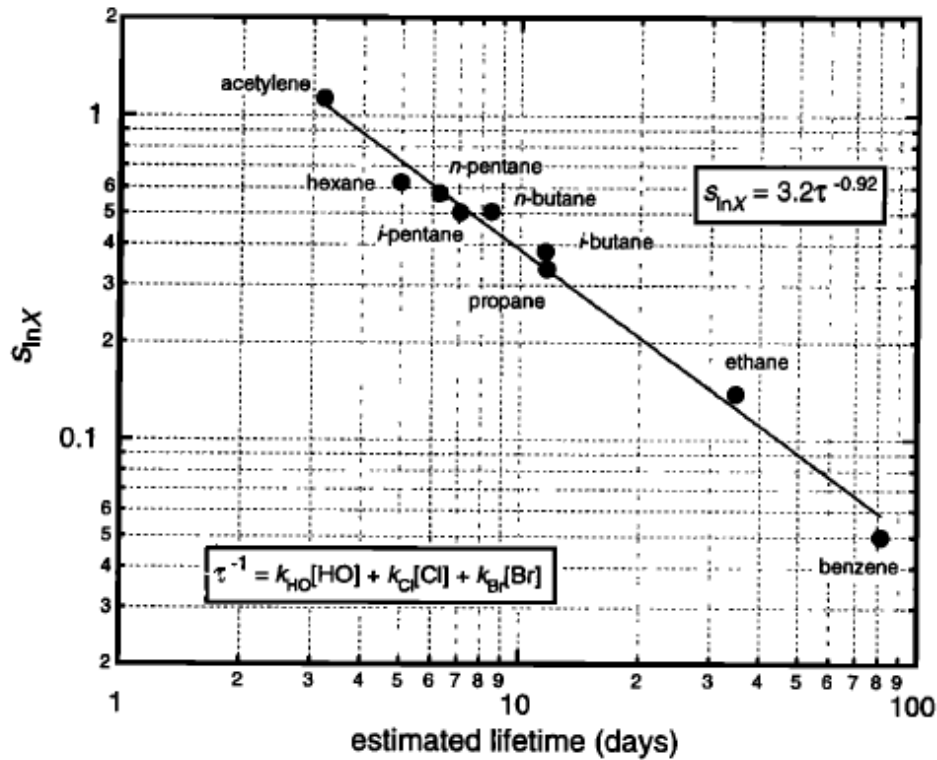
Figure 1.10: Sln[X] *versus* estimated lifetime (days) for the Polar Sunrise Experiment (PSE) 1992 data from a site on the sea ice north of Alert, Canada (Jobson et al., 1999). The lifetime is assumed by taking oxidants Cl and Br atoms as well as OH radical.

It is clear from the above discussion that close to source the value of *b* is zero and at distant locations the value approaches one; however, the comparison of extratropical stratospheric data for two field campaigns - the Airborne Southern Hemisphere Ozone Experiment (ASHOE) and the Airborne Arctic Stratosphere Expedition II (AASE II), both exhibiting greater τ dependence (*b* = 0.97 and *b* = 0.90 respectively) with another stratosphere dataset for field campaign- the Stratospheric Photochemistry Aerosols and Dynamics Expedition (SPADE) displaying weaker τ dependence *b* = 0.68 gave a new perspective to interpret *b* in a more meaningful way by relating it to mixing influences rather than the source-receptor distance.

The weaker τ dependence in SPADE data, in spite of having a remote extratropical stratosphere site, was attributed to the mixing amongst the air

parcels of different ages. Basically, the underlying principle behind source-receptor distance is related to mixing influences. When the sampling site is near source then there is a clear distinction between fresh and aged background air and mixing between widely different air masses weaken the τ dependence; as we move further away from the source this distinction gradually vanishes and now variability among different air masses exist primarily due to photochemical processing. Given the example of SPADE data, where mixing of the Vortex air with mid-latitude air, changes the concept of viewing b as an indicator of distance between the source and the sampling site. It is clear that the interpretation of b is more meaningful in terms of mixing influences rather than the source-receptor distance.

These variability-lifetime relationship trends find important applications in assessing the quality of a dataset, identifying outliers or any instrumental artefact, for example i) co-elution, contamination or integration problems, ii) influence of mixing or chemical processing on data, iii) identifying the presence of oxidants other than OH, iv) examining the local source influence ((Jobson et al., 1998;Jobson et al., 1999;Williams et al., 2000) calculating the OH concentration (Ehhalt et al., 1998;Williams et al., 2000;Williams et al., 2001;Karl et al., 2001;Bartenbach et al., 2007). In this thesis, the data set from a two-year study of VOCs in free troposphere above the UK is discussed in chapter 5 and from the RONOCO field campaign data set collected in the UK boundary layer at night in summer and winter months discussed in chapter 4, provide a unique opportunity to test this approach with different objectives. In addition to checking the consistency and quality of data and precision of the instrument involved (in study) in both datasets, the focus of the free tropospheric study is to compare the variability and influence of mixing between summer and winter seasons whilst the RONOCO field campaign data presents an opportunity to examine the influence of the NO_3 radical on the variability of branched-chain isomers.

1.2.9 Thesis outline

The aim of this thesis is to make hydrocarbon observations in the atmosphere and relate composition to seasonal behaviour, geographic distribution and variability in a range of different environments, using hydrocarbons as sensitive atmospheric tracers.

Chapter 2 covers the analytical procedures involved at each stage of the instrumentation, measurement techniques and quality assurance/quality control procedures adopted in this study. In addition to these, new alternatives to the current technique have been tested including trial experiments using an Entech 7150 headspace preconcentrator on an Agilent 6890 gas chromatograph.

Chapter 3 is dedicated to the application of hydrocarbon ratio approaches on data from an aircraft-based field campaign over UK -The ROle of Nighttime chemistry in controlling the Oxidizing Capacity of the AtmOsphere (RONOCO). The work described in this chapter uses ratios to test the ability of pentane isomer pairs and other branched chain isomer pairs to diagnose NO_3 radicals in different seasons and different periods of the day.

Chapter 4 extends the discussion further using data from the RONOCO field campaign dataset and applying an analysis using variability-lifetime relationships to examine the influence of the NO_3 radical on hydrocarbon variability trends. Two approaches, the hydrocarbon ratio approach and the variability-lifetime relationship, have been compared with respect to the pentane isomer pair for typical flights. In addition to this, the impact of NO_3 at night on the loss of anthropogenic VOCs in UK urban boundary layer has been investigated.

Chapter 5 concerns the true free tropospheric VOC measurements above the UK during a study period between January 2009 and January 2011. This study presents an opportunity to make a comparison in terms of hydrocarbon composition, seasonal trends, source profile and oxidation chemistry with the previous UK free tropospheric studies made approximately 20 years ago. In addition to this, the hydrocarbon ratio approach to data analysis has been used to investigate the influence of air masses with different source signatures on the composition of the UK free troposphere.

Chapter 6 examines the hydrocarbon data collected from a research project-Quantifying the impact of BOReal forest fires on Tropospheric oxidants over the Atlantic using Aircraft and Satellites (BORTAS). This campaign took place between 12th July 2010 and 2nd August 2010. The emission ratios from observations and the GEOS-Chem global 3-D chemical transport model (CTM) have been compared to highlight the influence of biomass burning on the global distribution of selected non-methane organic compounds.

Chapter 2:

On the use of the dual channel gas chromatograph for measurements of Volatile Organic Compounds and field deployments

2.1   Introduction

The presence of trace gases, organic aerosols and particles render the air a complex heterogeneous mixture. The work described in this thesis focuses on the analysis of gaseous volatile organic compounds (VOCs) from different environments. These compounds are introduced into the atmosphere as a result of fossil fuel use, emissions from vegetation on land and in the ocean, biomass burning and geochemical processes; these are typically present in the atmosphere at nmol mol^{-1} (parts per billion) amount fractions down to pmol mol^{-1} (parts per trillion) amount fractions (Apel et al., 1994). The contribution of VOCs to the pollution burden of the atmosphere, their influence on the cleansing capacity of the atmosphere, their role as a precursor of O_3 and secondary organic aerosols, as a major source of CO and oxygenated volatile organic compounds (oVOCs) and their adverse human health effects are the main reasons for monitoring of the ambient levels of these compounds.

In addition to the above concerns, on the basis of differential reactivity with respect to OH radical and hence different atmospheric lifetimes, the ratios of suitable pairs give an insight into photochemical aging, transport and mixing processes. Moreover, the variability in lifetime and reactivity differences have been exploited to identify and quantify the presence of oxidants such as the NO_3 radical and the OH radical as discussed in chapter 4. The reaction of several key oxidants during different periods of the day, for example the OH radical mainly during daytime, the NO_3 radical chiefly at night, and O_3 which is available all the time, with trace gases involve several complex reactions which eventually lead to the formation of CO_2 and water vapour. The burden of mixing ratios of trace gases determines the extent of the oxidising capacity of the atmosphere. These trace gases constantly move in a dynamic matrix depending on the particular meteorological conditions at the sampling site and make it difficult to capture a sample representative of the boundary layer or free troposphere (Dettmer and Engewald, 2003). Furthermore, the separation and identification of a variety of hydrocarbons and a vast number of compounds at varying concentration levels in

different environments is also highly challenging; for example, high concentrations of VOCs exist in complex mixtures in the urban air matrix, whilst a relatively smaller variety of VOCs are found in the remote environment and upper free troposphere; between these two extremes, intermediate mixtures in terms of both concentration and complexity are found in rural environments. Instrumental methods must be able to cope with this wide variety of conditions and this makes the analysis a challenging task (Apel et al., 1994). Measurement instruments clearly make a key contribution to improving our knowledge as does appropriate design of experiments, for example flight planning, a prerequisite step to aircraft-based campaigns and sampling strategies. For all measurements, both long and short term in nature, analytical techniques and methods need to be combined with quality assurance and quality control procedures.

One of the most important selection parameters for a sampling strategy and detection method for VOC measurement is the atmospheric lifetime, which determines the range of transport from the source region (Heard, 2007). The *e*-folding lifetime is defined as the time required for the concentration of a gas to decrease to $1/e$ (37%) of its initial concentration. The range of lifetime of VOCs varies from a few hours (e.g. isoprene) to many days (e.g. ethane) due to different reaction rates with the OH radical. The species with relatively long lifetimes, for example ethane, acetylene, propane and benzene, are carried away from the source regions either by horizontal or vertical transport mechanisms, affecting the photochemistry of remote regions. The reactive species such as alkenes participate in regional photochemistry and produce O_3 near source regions. However, the reactive species with short lifetimes can also on occasion be uplifted to the free troposphere by vertical convections at shorter time scales (Purvis et al., 2003). In order to capture the features related to latitudinal, longitudinal and vertical distribution, sources, sinks and seasonal behaviour of these compounds over a wide range of spatial and temporal scales, the deployment of field instrumentation on various platforms has become a necessity for atmospheric researchers. These field observations are further used by atmospheric modellers to predict the future trends, in addition to testing the

theoretical models. The field observations, laboratory studies coupled with the computer modelling allow us to give a three dimensional picture of the various aspects of atmospheric chemistry.

The Global Atmosphere Watch (GAW) project of the World Meteorological Organization (WMO) coordinates the measurement of VOCs in remote locations across the globe on various platforms (GAW Report No 171, 2006)). The data from these platforms have provided insight into the seasonal behaviour, long-term trends and the distribution of VOCs in the background atmosphere and helped to address the plethora of issues related to the aging, mixing and transport phenomena. The recommended sample collection methods, analytical procedures and potential target compounds (depending on the ease of measurements in the remote atmosphere and their importance to provide useful information on various aspects of atmospheric composition) are presented in the GAW reports. These reports also place emphasis on the quality assurance and quality control procedures (GAW Report No 111, 1995;GAW Report No 171, 2006) that should be used. The configuration of instruments and chromatographic methods vary from laboratory to laboratory depending upon the type (anthropogenic or biogenic or both) and the number of the compounds of interest to be reported with adequate identification and quantification. Despite the use of the common techniques and instrumentation within different laboratories, there are often differences between datasets which can be attributed to variety of analytical differences; one of the most significant which is the use of different calibration standards and scales. A previous study (Swanson et al., 2003) and reference therein highlight that the deviation from the NIST and NCAR calibrated values for VOCs ranged from 10-50% between independent laboratories, which yields large uncertainties in the intercomparison of published data from different labs.

By far the most widely used methods of VOC monitoring include a combination of 1) efficient water removal stage, 2) enrichment or preconcentration step (a stage of sample preparation prior to injection to column), 3) gas chromatography

separation and 4) subsequent detection with the flame ionization detector (FID) (Helmig, 1999;Dewulf et al., 2002). The configuration of the instrument used in this current work is based on a dual-bed charcoal trap cooled at – 23 °C as an enrichment stage, and a combination of two capillary columns (for analysing hydrocarbons and oxygenates) at the separation stage of the sample analysis methods with subsequent detection by two FIDs. This instrument is provided and maintained by the Facility for Ground-based Atmospheric Measurements (FGAM) at York (FGAM-York) for the UK atmospheric science community, hence named as the York-FGAM dual channel gas chromatograph (Hopkins et al., 2003;Hopkins et al., 2011).

2.1.1 Field measurements: importance and challenges

Given the importance of atmospheric chemistry and resulting effects on the Earth's climate, the field measurements of atmospheric composition over a wide range of temporal and spatial scales from ground-based platforms, including vehicle-based mobile laboratories to satellite and other space borne platforms are gaining importance day by day. The VOC data analysis and results from three field campaigns are presented in following chapters which all use data collected from the dual channel gas chromatograph. The ambient air samples are collected by deploying the Whole Air Sampling (WAS) system aboard the research aircraft, FAAM BAe 146-301, during all three field campaigns. The FAAM BAe 146-301 aircraft, a facility provided by the UK Met office and Natural Environment Research Council (NERC) for the UK atmospheric research community, has a ceiling altitude of 35000 feet and a maximum endurance of about 6 hours (indicated air speed around 200 knots or 100 ms^{-1}). It is typically involved in variety of different overseas detachments and UK-based campaigns throughout the year.

Depending on the type, location and accessibility of the field sites, the GC instruments are tailored to the measurement challenges. For example an

observatory located at 2225 m elevation on the summit caldera of an inactive volcano on the island of Pico, Azores uses a GC system with maximum power consumption, approximately less than 700 W, *in situ* prepared consumable gases, cryogen free, automated, unattended and remotely controlled operation (Tanner et al., 2006) The York-FGAM instrument used in this study also avoids the use of cryogens at the preconcentration stage by using a dual-bed adsorbent trap cooled by the use of Peltier plates suitable for field use. The main challenges associated with fieldwork in real air monitoring are the availability of gases, cryogen and power at the field work site; weight is a further major issue with the aircraft field campaigns. During field campaigns using FAAM BAe 146-301 research aircraft, the deployment of WAS system aboard the aircraft puts a maximum limit of 64 samples collection per flight. In order to fulfil the criteria of minimum weight, continuous advancements are going on to develop on board GC system by using a cooled adsorbent trap followed by GC with Helium Ionisation Detector (HID) (Whalley et al., 2004) and micro fabricated portable comprehensive GC system (Halliday et al., 2010).

The major limitation while using a conventional GC system as an on-line technique on the ground is the long term provision of gas cylinders. From aircraft the issues are different – rather it is the speed on analysis that is key problem, and the relative instability of the FID in flight. The proton transfer reaction mass spectrometer (PTR-MS) is gaining popularity for aircraft use since high frequency observations are possible. They require no gases for normal operation and are available commercially. However, the PTR-MS is not a separation technique and compounds are detected and identified primarily only by their molecular weight. Owing to the variety of compounds with potentially the same mass fragments, this technique is only suitable for the speciation of a selected group of compounds and hence should be considered to be complimentary to the GC techniques rather than an effective alternative. There are also several key VOCs such as ethane, acetylene and propane which are not ionised or detected by PTR-MS. In order to overcome the limitations of on-line techniques from

aircraft, offline techniques are an interesting and commonly used alternative because only the sampling system goes on–board (Bechara et al., 2008).

The campaigns that are conducted typically on short scales at different field sites, rely on moving the instrument from laboratory to the field site; such a methodology benefits from the use of well-equipped mobile laboratories in vans and converted shipping containers, which allow often complex GC instruments to be shipped from one place to another with the advantage of rapid installation. The York-FGAM dual channel gas chromatograph instrument is housed in a shipping container at the University of York, York, UK. This instrument was shipped to Halifax, Canada as a part of the three-week BORTAS campaign and the instrument was deployed near Halifax airport, Canada to analyze the whole air samples immediately after captures. However, during the RONOCO campaign, a UK detachment project and a two-year study of VOC monitoring over UK free troposphere, the canister samples were transported back to the University of York, after the conclusion of the flights for subsequent analysis. **Figure 2.1** shows the laboratory-container at a field site and the GC system housed within it.

Figure 2.1 Shipping container at a field site in Borneo; The inset shows the inside of the shipping container, showing the instrument.

2.1.2 Aims

In order to make field observations, the first step is to develop a suitable analytical technique to fulfil the needs of campaign's objectives. The York-FGAM instrument has been designed for either *in situ* or off-line sampling and to cover a range of VOCs including C_2 to C_9 non-methane hydrocarbons (NMHCs), C_2 to C_6 oxygenated volatile organic compounds (oVOCs), selected monoterpenes and dimethylsulphide (DMS) and their analysis at trace levels present in the atmosphere (Hopkins et al., 2003;Hopkins et al., 2011). This instrument has been deployed in several campaigns (NAMBLEX, OP3, AMMA, ITOP, BORTAS, ClearfLo) over the last ten years and has continued to be developed within that time. The major aim of this chapter is to describe in detail the analytical procedures involved at each stage of the instrumentation in addition to describing the fundamental principles of the measurement technique. The individual chapters within this thesis contain instrumentation details relevant and specific to the particular field campaigns and focus more on the data analysis. In addition to describing the finer details of instrumentation in section 2.3-2.7, the quality assurance and quality control procedures are discussed in section 2.9 to demonstrate that the data from this GC-laboratory are reliable, reproducible and up to the set standards adopted by GAW World Calibration Centre for VOCs (GAW-WCC-VOC).

Progress in VOC measurements has been made with advances in each stage of the instrumentation, from sampling through enrichment and separation to detection, enabling the detection of greater numbers of compounds with better accuracy and precision. The York-FGAM GC system has also passed through phases of continuous improvements and advances with the passage of time, including the addition of selected monoterpenes and DMS in the list of the resolvable compounds (Hopkins et al., 2003;Hopkins et al., 2011). In addition to using the current instrument configuration, new alternatives to the current technique have been tested including trial experiments using the Entech 7150 headspace preconcentrator on an Agilent 6890 gas chromatograph. This

preconcentrator is thought to be capable of recovering C_2-C_{25} species at parts per million (ppm) to sub parts per billion (ppb) levels with potentially better water management with the thermal desorption stages. Selected results from this new three-stage preconcentration technique and a comparison with the existing single-stage enrichment technique are presented in section 2.10. This section demonstrates the strengths and weaknesses of new preconcentration system and its use for field measurements.

2.2   Measurement technique

2.2.1 Gas chromatography

The term chromatography (Greek for colour–chroma and write –graphein) was first used by the Russian Chemist Tswett to describe his work on the separation of coloured plant pigments into bands on a column of chalk. A rapid rise in the routine use of chromatography as a universal technique particularly in chemistry, biology and medicine began in 1960s. In spite of being recognised as a flexible and the powerful analytical procedure, it has primarily remained as a separation technique (Braithwaite and Smith, 1985). According to the International Union of Pure and Applied Chemistry (IUPAC), chromatography is defined as: '*A method used primarily for the separation of the components of a sample, in which the components are distributed between two phases, one of which is stationary while the other moves. The stationary phase may be a solid, or a liquid supported on a solid, or a gel. The stationary phase may be packed in a column, spread as a layer, or distributed as a film, etc.; in these definitions 'chromatographic bed' is used as a general term to denote any of the different forms in which the stationary phase may be used. The mobile phase may be gaseous or liquid*' (IUPAC, 1974).

In the process of separating a complex mixture into its components or analytes, the sample is transported through a packed bed of material (the stationary phase)

under the influence of a fluid (mobile phase) and on the basis of different rate of reaction of sample components with the stationary phase, the analytes start eluting one by one. According to the physical state of the mobile phase, the chromatography is further split into gas, liquid or supercritical. The other features of this technique that forms the basis of classification are: (i) the nature of stationary phase, whether it is liquid or solid or bonded liquid; (ii) the mechanism of separation which depends on the type of interaction e.g. partition, adsorption, ion exchange or exclusion; and (iii) the technique employed, for example, the stationary phase may be in the form of a flat bed of material consisting of an adsorbed layer spread evenly over a sheet of glass, plastic or aluminium (called thin-layer or planer chromatography), or a sheet of cellulose material (paper chromatography) or the stationary phase may be packed into a glass or metal column (column chromatography). The instrumentation involved in present work uses the gas chromatography variant in which silica capillary columns are used.

Column chromatography may be further sub divided according to the nature and dimensions of the column. If the stationary phase is coated or bonded onto an inert solid support and then packed into the column then the column is referred to as packed column. However, an alternative means to hold the stationary phase in the column is to spread it as a thin film onto the internal wall of a length of narrow bore tubing. These columns are called capillary columns. The term capillary columns usually refer to columns with a very small internal diameter (less than 0.5 mm i.d.). Inside the column there is a well characterized, immobilized and a highly viscous liquid coating onto the inner walls of the column known as the stationary phase.

The technique used in the present instrumentation is based on the use of Porous Layer Open Tubular (PLOT) capillary columns where the stationary phase is based on an adsorbent or a porous polymer suitable for analyzing a wide range of gases of different volatility. A carrier gas acts as a mobile phase flowing through

the capillary and over the stationary film surface through the column. Helium and hydrogen are the two primary carrier gases used in gas chromatography. Although nitrogen is also usable, it does not find many applications in atmospheric separation due to relatively slow optimal flow rates and poorer theoretical plate height minima. In gas chromatography the mobile phase is non-interactive or inert in that it does not affect the distribution of the sample molecules between two phases; the distribution depends only on the molecular interactions between the sample and the stationary phase.

The criteria for choosing a carrier gas are the gas with lowest density and high diffusion coefficient so as to achieve the maximum diffusivity and hence separation efficiency over a wide gas velocity range. On this scale, hydrogen is the best choice but due to the explosion risks associated with this gas, helium offers the safer environment over the use of hydrogen. For certain hydrocarbon species there is also a risk of hydrogenation of double bonds on column. The choice of carrier gas in the present technique is helium. To quantify the trace level analytes, this technique calls for very high purity gases as the presence of organic impurities in the carrier gas or in a mixture of hydrogen and air, a fuel for FID, may give rise to a significant base current response which may reduce the sensitivity of the detector; hence the gases are further purified by using the combination of oxygen, moisture and hydrocarbon traps (Hamilton and Lewis, 2007).

In gas chromatography the capillary columns are most commonly housed in a temperature programmed oven. Temperature programming is a technique in which the column temperature is gradually increased so as to speed up the elution of the higher boiling point compounds. The analytes from air, after sample enrichment and refocusing steps, are thermally desorbed and injected in to the carrier gas stream onto the column, where on the basis of different reaction rates with the stationary phase, sample components start eluting from the column one by one. They then reach the detection system in a short band with a degree of

70

band broadening (caused by longitudinal diffusion) to produce a Gaussian-shaped peak as depicted in **Figure 2.2**.

The peak area under the peak or peak height is a quantitative measure of its concentration. The maximum number of component peaks that can be resolved on a given column is defined as the peak capacity, which in turn is a measure of the overall resolving power of a chromatographic column. The complexity of air mixtures demands efficient enrichment steps, high peak capacities coupled with the use of selective detectors (Hamilton and Lewis, 2007).
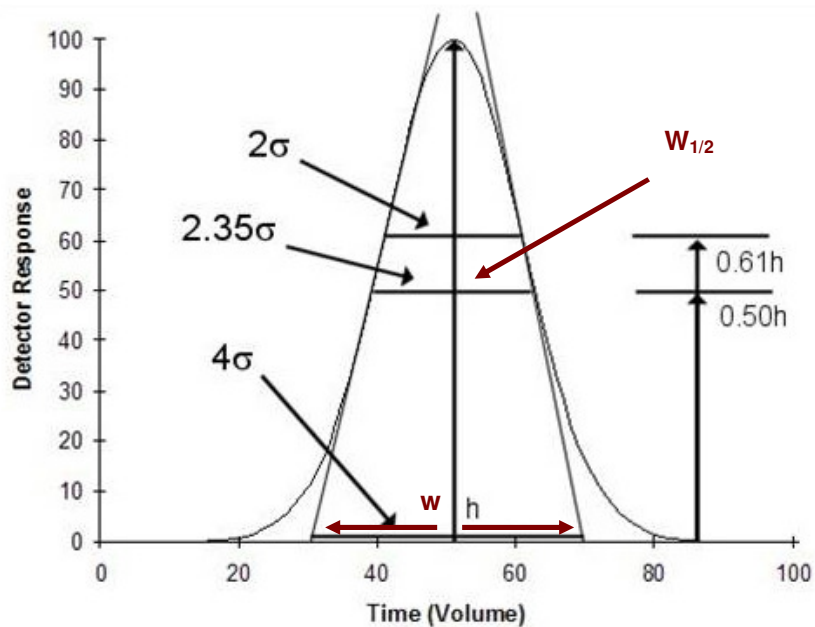
Figure 2.2: A typical Gaussian shape peak with peak height *h* and peak width *w*. The tangents intersect the baseline and cut off the distance *w* known as peak width at the base, which is equal to 4σ ($\pm 2\sigma$) and σ, the standard deviation is also called the quarter peak width at the base. The width at 60.7% of the peak height is 2σ ($\pm 1\sigma$) and at the 50% of the peak height it is 2.354σ and called the peak width at half height, $w_{1/2}$ (www.scientistsolutions.com, 2009).

71

2.2.1.1 Interpretation of chromatograms

2.2.1.1.1 Identification and quantification

The purpose of the chromatographic analysis is the identification and quantification of the sample components. As mentioned in the previous section, this technique has a tremendous capacity to resolve the mixtures; however, it provides only limited information on the chemical nature of the separated components when an FID is used as the detector. In addition, it is not necessarily the case that the number of peaks on the chromatogram is a representative of the total number of compounds present in the complex mixture, rather only the compounds able to be resolved above the detection limit by any particular method. It is fairly simple to interpret the chromatogram with available background information and only a few components; however, when a mixture is multicomponent and background information is limited then the interpretation becomes a challenging task (Domingo, 2012).

Broadly, the retention time and peak size (either peak area or peak height) are used to extract information on qualitative and quantitative aspect of the analysis. The peak size corresponds to the amount of the sample, the greater the peak area or peak height the higher the amount of the component, whilst the retention time helps in identifying a component. The time a compound takes to be eluted from the column is known as the retention time. If the column and all operating conditions are kept constant, then a given compound will always have the same retention time. The shift in retention time not only indicates a drift in the system but also causes delay in data processing. In order to deal with the data processing in a quick and on routine basis, the factors that affect the retention times of the hydrocarbons must be strictly controlled. For example, the laboratory room where GC is housed should be maintained at approximately 18 ± 2 °C, also the lower lab temperature is an efficient way to cool a GC system faster, whilst other instrumental factors that may contribute to drift of system response should also be taken into account. Flow meters, flow controllers, pressure transducers, valves, frits etc should be housed in a temperature controlled box at

approximately 38 ± 0.3 °C (Goldstein et al., 1995a). Most importantly for PLOT columns the amount of water in the sample must be controlled very tightly.

By introducing a known amount of pure sample components, in the present case a multi-component standard gas mixture having all compounds of interest that are expected to be quantified in an unknown ambient air sample, the peak size and retention time are determined. By using area under peak or peak height of a known concentration compound, the response factor (R.F) is calculated by using the following equation:

$$\text{R.F} \quad = \quad \frac{\text{Peak area}}{\text{Cal. con.}} \text{ or } \frac{\text{peak height}}{\text{cal. con.}} \qquad 2.1$$

where Cal. con. denotes the concentration of compounds in a standard cylinder.

These response factors of individual components are further used in quantifying the compounds present in an unknown air sample by using the following formula:

$$\text{Concentration} \quad = \quad \frac{\text{Peak area}}{\text{R.F}} \text{ or } \frac{\text{peak height}}{\text{R.F}} \qquad 2.2$$

The discussion under the following headings touches on the important features of the separation parameters; though this is a broad topic, here a few selected features that are relevant in the present context to interpret various features of the chromatogram are presented.

2.2.1.2   Separation parameters

2.2.1.2.1   Retention mechanism

In addition to having an idea of the general features of column chromatography discussed in previous section, it is also important to understand the specific

mechanism taking place inside the column when a sample is introduced onto it. The mechanism is based on the distribution of components between stationary phase and mobile phase (Swell and Clarke, 1987). Before the mechanism is described, let us remind ourselves a common laboratory technique solvent or liquid-liquid extraction that is used for the purification and separation of chemical compounds. The technique is based on the distribution of a solute between two essentially immiscible liquids, one usually being an organic solvent and the other aqueous. At equilibrium, a solute which is soluble in both phases will distribute between the two phases in a fixed proportion according to the distribution coefficient K_D which is defined according to the following equation

$$K_D \quad = \quad \frac{C_{org.}}{C_{aq.}} \qquad\qquad 2.3$$

where $C_{org.}$ and $C_{aq.}$ are the concentration of a solute in organic solvent and in aqueous solvent, respectively.

The idea of introducing this basic concept in the present context follows that of A.J.P Martin and R.L.M Synge, the 1952 Nobel Prize winners for their work in the development of modern chromatography. The chromatographic column can be considered analogues to a series of separating funnels containing two phases, one stationary and the other mobile. Hence redefining the distribution partition coefficient K_D as:

$$K_D \quad = \quad \frac{C_s}{C_m} \qquad\qquad 2.4$$

where C_s is the concentration of a component in the stationary phase and C_m is the concentration of the same component in the mobile phase.

The distribution coefficient is a physicochemical constant and only depends on the type of analyte, the type of stationary phase and the temperature. It does not depend on the volume of phases. A component with a low distribution coefficient

will have fewer of its particles in the stationary phase at any given time compared with another component with a higher distribution coefficient. Thus the rate of migration of a component down the column is inversely proportional to its distribution coefficient.

When a sample is introduced onto a column in the mobile phase then according to the value of its distribution coefficient, it distributes between the two phases and the equilibrium is thought to be achieved instantaneously. This can be considered as the separation in the first "separating funnel" as shown in **Figure 2.3**a. For the sake of simplicity, here it is assumed that one half of the column is occupied by the stationary phase S and the other half is occupied by the mobile phase M whilst in reality the stationary phase is dispersed throughout the column. Furthermore, to explain the process of retention in a column in a more simple way, the column is divided into three sections, the upper, the middle and the lower. Having been distributed between the two phases, the sample remaining in the mobile phase will move further down the column where it will meet fresh stationary phase. The sample will again move from the mobile phase into the stationary phase achieving equilibrium and this process is called sorption as presented in the middle section of the **Figure 2.3**b. Since the concentration of the sample in the mobile phase in the upper section has been reduced, sample will move from the stationary phase back into the mobile phase as depicted in the upper section of the **Figure 2.3**b (this is called desorption), so as to maintain the constant value of distribution coefficient. In a very short time, all the samples will have desorbed from the stationary phase in the upper section of the column and will be swept into the middle section of the column by the mobile phase. Eventually, equilibrium will again be established and the sample will be found completely in the middle section of the column as illustrated in **Figure 2.3**c. This process of sorption and desorption continues as shown in **Figure 2.3**d until the sample reaches at the end of the column or is eluted from the column.
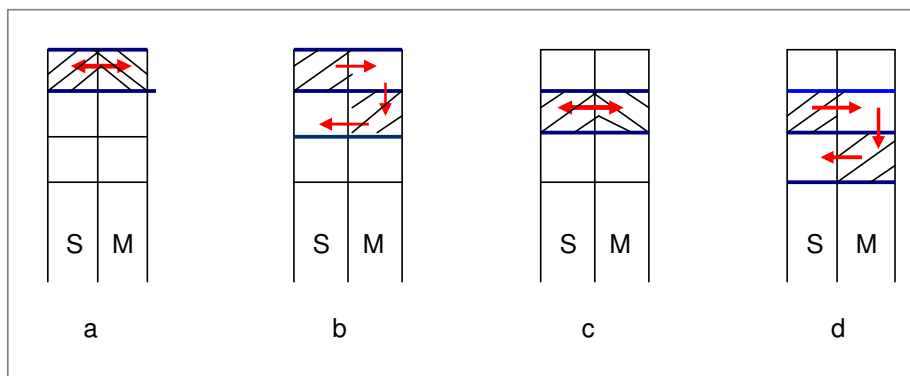
Figure 2.3: The various stages of retention in column chromatography. For the sake of simplicity the column is divided in two halves, the left half portion is occupied by stationary phase denoted by S and right half portion is occupied by the mobile phase denoted by M and also the mechanism of retention is exhibited in three sections, the upper, the middle and the lower one, which is a representative of the phenomena taking place along the entire length of the column. A perfect equilibrium between stationary and mobile phases is illustrated in figure a and c whilst in figure b and d, the process of sorption and desorption are depicted. The process of moving sample from mobile phase to stationary phase is called sorption whilst the reverse is desorption. In all diagrams there is no movement directly down the column in the stationary phase. The particles move only across the boundary between the stationary phase and the mobile phase and down the column during the time spent in the mobile phase. In the mobile phase all particles will move at the same speed so that the amount of time spent in the mobile phase is the same for all particles (Swell and Clarke, 1987).

2.2.1.2.2   Theoretical plates and column efficiency

Rather than referring or imagining sorption and desorption process as occurring in a series of discrete steps as with the separating funnel or speaking in terms of sections of the columns, the appropriate terminology commonly used is termed as 'theoretical plate'. The theoretical plate is a hypothetical zone or stage in which a perfect equilibrium is established between the two phases. This plate model successfully accounts for the Gaussian shape of chromatographic peaks as well as for factors that influence the differences in solute migration rates. However, this model doesn't adequately account for zone broadening because of its basic assumption that equilibrium conditions prevail throughout a column during elution. While considering sorption and desorption process, it has been

assumed that this process is a series of static processes whilst the chromatography is a dynamic process; at the same time this is also true that by making these steps or theoretical plates extremely small the static and dynamic process becomes equivalent. The assumption of equilibrium can never be valid in the dynamic state that exists in a chromatographic column, where mobile phase is moving quickly such that there is insufficient time to establish equilibrium. Hence, the plate model is not a very good representation of a chromatography column and it should be visualized in terms of assessment of column efficiency rather than having any physical significance (Miller, 1987;Skoog, 2004).

The column efficiency may be defined by considering a narrowness of a peak relative to the time spent in the column. A narrowness of a peak is a result of when all molecules of the same compound are eluted within a narrow time window. The higher the number of equilibrium steps or theoretical plates the better the performance of the column. Theoretical plates or column efficiency (N) can be measured from the peak profile in several different ways. Two of the most commonly used expressions are represented by the following equations:

$$N \quad = \quad 5.545 \left(\frac{t_r}{w_{1/2}} \right)^2 \qquad\qquad 2.5$$

$$N \quad = \quad 16 \left(\frac{t_r}{w} \right)^2 \qquad\qquad 2.6$$

where t_r is the retention time $w_{1/2}$ and w are the peak width in time units at half peak height and peak width in time units at the base line respectively, as shown in **Figure 2.2**.

A column with a high number of theoretical plates will have a narrower peak at a given retention time than a column with a lower N number. The broadness of the peak reflects the poor efficiency and resolving power of the column, which then results in the potential identification of fewer distinct peaks within affixed time period. Column efficiency is a function of the column dimensions (internal

diameter i.d., length L and film thickness d_f), the type of the carrier gas and its flow rate or linear average velocity and the compound and its retention. For column comparison purposes, the number of theoretical plates per meter (N/m) is often used (Agilent technologies, 2007). Theoretical plate numbers are only valid for a specific set of conditions; notionally isothermal temperature conditions are required. The combination of two columns of different polarities have been used in the present instrumentation: a Na_2SO_4 deactivated aluminium oxide (Al_2O_3) PLOT column (L x i.d. x d_f =50 m, 0.53 mm ,10 μm) for analysis of less polar NMHCs and a LOWOX columns in series (10 m, 0.53 mm, 10 μm , Varian Netherlands) for more polar VOC analysis.

Another measure of column efficiency is the length of the column corresponding to a theoretical plate, called the Height Equivalent to a Theoretical Plate (or HETP or simply H), and it is usually reported in millimetres. The shorter each theoretical plate, the more plates are contained in any length of column. This of course translates to more plates per meter and higher column efficiency.

$$H \qquad = \qquad \frac{L}{N} \qquad\qquad 2.7$$

where *L* is the length of column in mm and *N* is the number of theoretical plates.

The smaller the value of H, the more equilibration steps there are in a column or in other words the column is efficient and shows only limited band broadening. Efficiency can also be considered as '*how much the peak has broadened, compared to how long it has been travelling through the column*'. Thus, for a given travel time (or retention time) if a peak is broadened less then the system is more efficient. This concept is really only valid for isothermal operation and for the more commonly used temperature programmed operation. **Figure 2.4** shows a section of chromatogram from a typical air sample in which towards the end of the run the peaks of heavier weight compounds (isomers of trimethylbenzene peaks 9, 10 and 11) are relatively broad as compared to the lighter weight compound which are sharp; however, the extent of broadness in comparison with

the time spent in column for these compounds is not unreasonable. The broadening of peaks reflect that large number of molecules of the same compound are eluting in a broad time window due to diffusion along the axis of the column and slow mass transfer in the stationary phase.
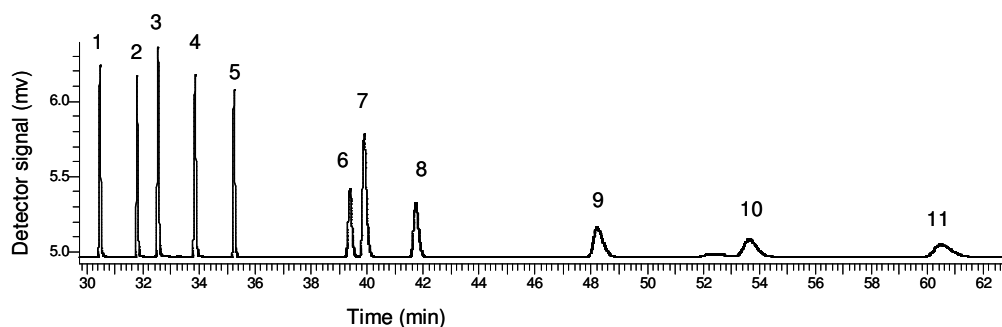
Figure 2.4: A section of chromatogram from analysis of a typical air sample. The peaks towards the end of the run labelled as 9, 10 and 11are broader in comparison with the peaks in the earlier section. The extent of broadness for these peaks in comparison with the time spent in the column is reasonable. The flow of carrier gas is increased to 40 ml min^{-1} through each column at 33.5 minutes, which is reflected by the sloppy baseline at that time due to the pressure differences, to speed up the elution of heavier weight compounds so as to avoid the build-up of these compounds within the system. The peaks in the chromatogram are labelled as (1) *n*-heptane, (2) benzene, (3) 2,2,4-trimethylpentane, (4) *n*-octane, (5) toluene,(6) ethylbenzene,(7) *m+p*-xylene , (8) *o*-xylene, (9) 1,3,5-trimethylbenzene, (10) 1,2,4-trimethylbenzene and (11) 1,2,3-trimethylbenzene.

The carrier gas flow rate is 20 ml min^{-1} through each column until 33.5 minutes and then after that time, it is increased to 40 ml min^{-1} to speed up the elution of heavier weight compounds so as to improve the separation of some of these compounds and avoid the build-up of particularly heavy weight compounds within the system. The increase in column flow results in a sloping baseline in middle section of the chromatogram at that particular time (33.5-35.2 min).

79

2.2.1.2.3 Retention time

Referring back to the mechanism of retention in **Figure 2.3**, in all diagrams there is no movement directly down the column in the stationary phase. The particles move only across the boundary between the stationary phase and the mobile phase and down the column during the time spent in the mobile phase. In the mobile phase all particles will move at the same speed so that the amount of time spent in the mobile phase is the same for all particles. This time is called the hold-up time or column dead time (t_m). It is the time spent in the stationary phase t_r which is different for different components and thereby causes a differential rate of migration and hence different retention time t_r of an individual component. The stronger the interaction is, the longer it takes for a component to elute from the column. The time a compound takes to be eluted from the column is known as the retention time t_r. In present instrumentation technique the methane is the unretained compound (**Figure 2.5**), which means that molecules of this compound do not interact with the stationary phase and they travel down the column at the same rate as carrier gas. The retention time of methane t_m is essentially independent of temperature.
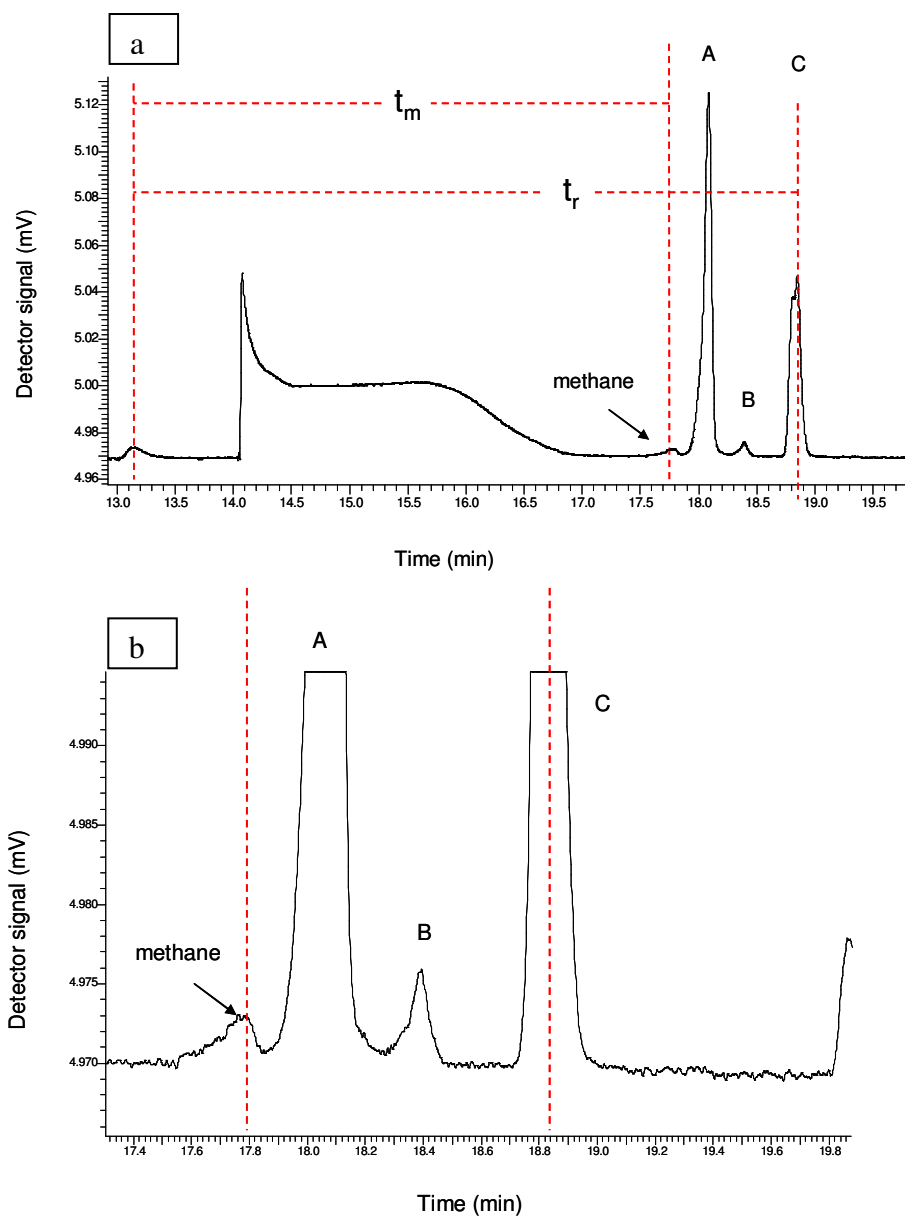
Figure 2.5: A section of chromatogram showing methane as an unretained peak in upper panel and ethane (A),ethene (B), and propane (C) as retained peaks in lower panel The peaks in lower panel are in zoom mode to highlight the unretained peak to illustrate the hold-up time t_m and retention time t_r . The molecules of methane have minimal interaction with the stationary phase and they travel down the column at the same rate as carrier gas. The retention time of methane t_m is essentially independent of temperature whilst the other compounds for example ethane, ethene and propane shown in the figure interacts with the stationary phase to varying degree of extent and thus exhibiting different retention times.

81

For a column of length L, the velocity of mobile phase is given by the following equation:

$$\mu_m = \frac{L}{t_m} \qquad 2.8$$

where μ_m is the mobile phase velocity, L is the length of the column and t_m is hold-up time or column dead time.

The overall retention time of a component is given by the sum of the times spent in a mobile (t_m) and stationary phases ($t_{r'}$) such that

$$t_r = t_{r'} + t_m \qquad 2.9$$

t_r is the time between injection and elution of a retained component and $t_{r'}$ is the amount of time spent in stationary phase.

t_r and t_m are related as shown in following equation:

$$t_r = t_m \left(1 + K \frac{V_s}{V_m} \right) \qquad 2.10$$

Substituting the value of t_m from equation 2.8 into equation 2.10

$$t_r = \frac{L}{\mu_m} \left(1 + K \frac{V_s}{V_m} \right) \qquad 2.11$$

where K is the distribution coefficient and V_s and V_m are the volumes of the stationary and mobile phase.

The distribution coefficient which is a ratio of solute's concentration in the stationary and mobile phases is fixed for the same stationary phase, column temperature and solute. The column in a GC is contained in an oven, the temperature of which is precisely controlled electronically. The rate at which a

sample passes through the column is directly proportional to the temperature of the column. The higher the column temperature the faster the sample moves through the column. However, the faster a sample moves through a column the less it interacts with the stationary phase and the less the analytes are separated. In general the column temperature is selected to compromise between the length of the analysis and the level of the separation. The GC oven (Perkin Elmer) in the present instrumentation has been programmed to achieve the separation of compounds of interest in a reasonable length of analysis time as follows: 40 °C for 3.5 minutes then heated at a rate of 13 °C min^{-1} to 110 °C and finally the ramp rate is 8 °C min^{-1} until the temp 200 °C is achieved which is maintained until the end of the run. It takes an hour to finish a single GC run. In addition to oven programming, the carrier gas flow rate has also been optimised with an initial flow of 20 ml min^{-1} through each column up to 33.5 minutes and then it is increased to 40 ml min^{-1} after 33.5 minutes to speed up the elution of heavier weight compounds which also reduces the length of analysis as it is obvious from the relationship of retention time with carrier gas flow rate in equation 2.11.

2.2.1.2.4   Retention factor

Another parameter of interest in equation 2.11 is retention factor (k) which has been defined as :

$$k \qquad = \qquad K \frac{V_s}{V_m} \qquad\qquad 2.12$$

Before the importance of the whole term is realised and compared with the retention time, let us first break up the above equation in two parts - the first is K and the other one is $1/\beta$ as V_m/V_s is termed as phase volume ratio β as shown in equation 2.13:

$$\beta \qquad = \qquad \frac{V_m}{V_s} \qquad\qquad 2.13$$

A column's phase ratio is a dimensionless value and calculated by following equation

$$\beta \qquad = \qquad \frac{r}{2d_f} \qquad\qquad 2.14$$

where r is column radius in micrometer (μm) and d_f is the film thickness in micrometer (μm).

In our case the phase ratio for PLOT and LOWOX columns (r=265μm and film thickness is 10 μm) is 13.25. The phase ratio decreases with the decrease in column diameter or increase in film thickness. Either of these column changes results in an increase in solute retention. The phase ratio increases with the increase in column diameter or decrease in film thickness. Either of these column changes results in a decrease in solute retention (Agilent technologies, 2007). If the same stationary phase and the column temperature are maintained, the change in the phase ratio can be used to calculate the change in the solute's retention, expressed by the following equation:

$$K \qquad = \qquad \beta.k \qquad\qquad 2.15$$

Substituting the value of β from equation 2.14 into equation 2.15

$$K \qquad = \qquad k\frac{r}{2d_f} \qquad\qquad 2.16$$

As the distribution coefficient is constant for same stationary phase, column temperature and solute, any change in phase ratio will result a corresponding change in retention factor or in other words, an increase in phase ratio will result in a decrease in retention factor as distribution coefficient is constant. Actually, the distribution coefficient describes the distribution equilibrium of sample components in terms of their concentration, whilst the retention factor k describes the distribution of sample components in terms of their mass amounts

in both phases rather than concentration terms as presented in following equation.

$$k = \frac{\text{Total amount of component in stationary phase}}{\text{Total amount of component in mobile phase}} \qquad 2.17$$

$$k = \frac{C_s V_s}{C_m V_m} \qquad 2.18$$

$$\text{since } K_D = \frac{C_s}{C_m}$$

$$\text{Hence } k = K\frac{V_s}{V_m}$$

The retention factor is another measure of retention. It is a variable indicating how much time a component spends in the stationary phase compared to a non-retained inert component.

$$k = \frac{t_r - t_m}{t_m} \qquad 2.19$$

The retention factor is also known as the partition ratio or capacity factor. Since all solutes spend the same amount of time in the mobile phase, the retention factor is a measure of retention by the stationary phase. For example o-xylene with a k value of 1.34 (t_r=41.73 min , t_m= 17.78) is roughly 1.4 times as retained by the stationary phase as a solute toluene with a k value of 0.98 (t_r=35.24 min , t_m= 17.78) as shown in **Figure 2.6**.

The retention factor does not provide absolute retention information, it provides relative retention information. An unretained compound has retention factor = 0. The advantage of using retention factor rather than the retention time is the fact

that it is independent of the column length and the flow rate of the mobile phase whist the retention time depends on both of these factors. The retention factor for a sample component is directly related to the temperature. It is for this reason that the retention factor is only defined in isothermal GC. It should not be used in temperature programmed separations. Figure 2.7 shows a comparison between retention factor for a section of a chromatogram with heaver weight compounds when the column temp is at 200 °C.
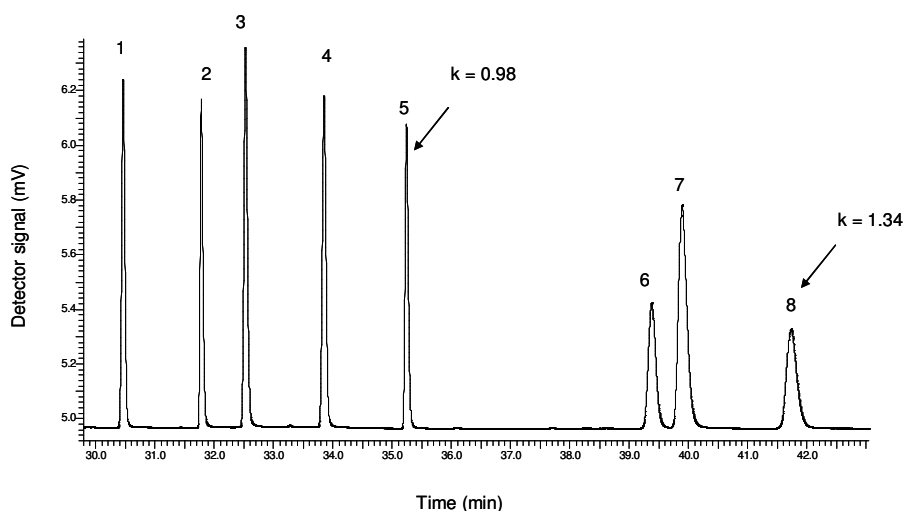
Figure 2.6: Comparison of retention factor for toluene (label 5) and *o*-xylene (label 8) compounds when column temperature is at 200 °C.

2.2.1.2.5   Separation factor

This is another important feature of the chromatogram which tells that the compounds in the mixture are selectively retained on column or not. The selectivity is measured by the separation factor which is defined as the time or distance between the maxima of two peaks. It is calculated using the following equation.

$$\alpha \quad = \quad \frac{k_2}{k_1} \qquad\qquad 2.20$$

86

where k_1 =retention factor of first peak and k_2 is the retention factor of second peak.

If α =1 the two peaks have the same retention time and co elute.

Figure 2.7 illustrates that isomers of pentanes (*iso*-pentane labelled as 1 with t_r= 23.611 min and *n*-pentane labelled as 2, t_r=23.295 min) are very well resolved and give a value for α for *iso*-pentane/*n*-pentane pair of 0.94 and *n*-pentane/*iso*-pentane pair of 1.06, whilst the 2- and 3-methyl pentane (3 and 4 respectively) with retention times (2-methyl pentane , t_r= 26.4945 min and 3-methyl pentane t_r =26.544 min) are not very well resolved (α =1) and although they can be seen as two separate peaks (number C and D) they are shown to overlap, with 3-methyl pentane (label 4) appearing as a "*shoulder*" of the larger 2-methyl pentane peak(label 3). The hold-up time t_m is 17.78 min for these calculations.
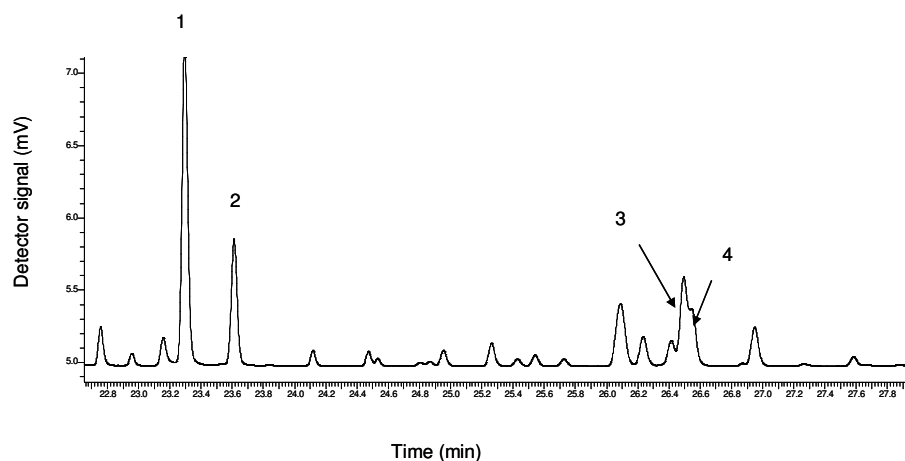
Figure 2.7 Comparison of separation factor for isomer of pentanes labelled as: *iso*-pentane (1), *n*-pentane (2), 2-methylpentane (3), and 3-methylpentane (4).

2.2.1.2.6   Resolution

The efficiency of chromatographic column is better measured by the term 'resolution' which is a measure of the degree of separation between the two peaks. The higher the degree of separation is between the successive peaks the less is the overlap between two adjacent peaks. Resolution takes into consideration both the separation factor α and the width of the peaks w. It is

calculated by using following equation which is a ratio of distance between successive peaks to their mean peak width:

$$R_s \quad = \quad \frac{t_{r2} - t_{r1}}{\frac{1}{2}(w_1 + w_2)} \qquad 2.21$$

where t_{r2} and t_{r1} are the retention times of peak 2 and peak 1 and w_1 and w_2 are the basal peak widths of the peaks 1 and 2.

As the numerator in above equation is the distance d between the peak maxima, this can be simplified by the following equation:

$$R_s \quad = \quad \frac{2d}{w_1 + w_2} \qquad 2.22$$

If the width of the two peaks is same then this equation is reduced to d/w. As shown in **Figure 2.2** that basal peak width is equal to 4σ for each peak therefore, the distance between two peaks should also be equal to 4σ (2 σ from peak 1 and 2 σ form peak 2) and in this way the value of resolution is 1.0 which means 98% resolution.

For simplicity this equation is often reduced to $R_s = d/w_b$ since the peak widths are usually the same. A resolution of about 1.5 is necessary for complete separation and value less than 1.0 represents poorer separation. The above equation is strictly valid when both peaks have same peak height. It is not always easy to get good chromatography with good resolution, efficiency and selectivity for compounds of similar volatility and retention characteristics. We saw in the previous section that resolution for 2+3-methylpentane and *m+p*-xylene is poor; however, for the majority of species there is good separation when using optimal conditions of carrier gas flow rate and oven temperature programming.
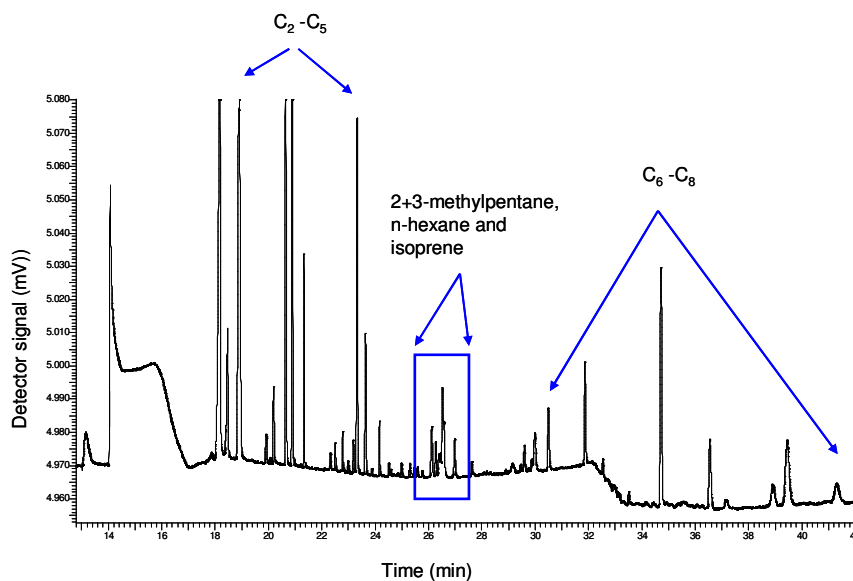
Figure 2.8: A typical chromatogram of an ambient air sample.

2.3   Sampling techniques

The first and most important step in the process of ambient air sample analysis is to choose a suitable sampling technique. The procedures adopted during the sampling step are important to minimise the chances of error introduction at this stage, which cannot be corrected later during the analysis (Kumar and Viden, 2007). There are two broad sampling approaches: (1) *in situ* and (2) grab sampling with subsequent analysis. For *in situ* sampling the length and material of the manifold and height of the inlet are important considerations to avoid surface losses and contamination risks and obtain a characteristic sample during sampling. The main advantage of *in situ* sampling is the production of real-time data which may be required where a rapid response to changing conditions is needed.

The grab sampling approach uses collection of either whole air samples by using stainless steel canisters, glass flasks, plastic bags (such as Tedlar, Teflon or aluminized Tedlar) or a fraction of VOC collection onto solid adsorbents known as sorbent sampling, with subsequent removal of the collected samples either by

89

thermal desorption or solvent desorption process. The air sampling by both *in situ* and flask sampling at the same time is an interesting comparison activity between two different sampling approaches among GAW atmospheric observatories. The purpose of collection of air nearly simultaneously is a part of quality control exercise. The NOAA (U.S National Oceanic and Atmospheric Administration) glass flask sampling network, the European EMEP (Co-operative Programme for Monitoring and Evaluation of the Long-range Transmission of Air) and the Canadian flask sampling network are the examples of flask sampling network which coordinate their activities with *in situ* sampling networks (Pollmann et al., 2008;GAW Report No 171, 2006).

Given the availability of various types of sampling methods, a few important points are worth considering before choosing a method (i) the composition and concentration range of the compounds of interest (ii) sampling methods and possibilities of reaction of sample with the material of sampling device (iii) the cleanliness of sampling device and (iv) stability of sample during storage and transportation in the sampling device (Kumar and Viden, 2007). A brief discussion of main sampling approaches with their advantages and disadvantages has been given under following headings.

2.3.1 Adsorbent sampling

In contrast to *in situ* sampling, adsorbent sampling is not a real-time sampling technique. A fraction of VOCs is trapped on solid sorbents (adsorbent material) rather than collected as a gas in a whole air samples. Depending on the type and amount of the sorbent, a typical sorbent tube is 70-150 mm long and 4-10 mm in diameter (Harper, 2000). The first thing is to select the appropriate sorbent material which depends on the sample matrix and on the suite of VOCs of interest. The compounds which are less polar and strongly retained on sorbents are difficult to recover at later stages of the analysis whilst very volatile organic compounds tend to pass through the sorbent without being trapped which is

known as breakthrough (Kumar and Viden, 2007). Therefore, to sample a wide range of VOCs by using this approach, a careful selection of adsorbent material is required. There exists a wide variety of adsorbent materials for example porous polymers (Tenax, Hayesep, Porpak, Chromosorb etc) and activated carbon (charcoal, Carbopack, Carboxen), silica gel, Alumina and Florisil. Some sorbent materials for example Carbosieve, have a high breakthrough volume but at the same time also retains appreciable quantities of water vapour, which is not desirable. The presence of water vapour poses detrimental effects at the analysis stage by causing degradation of the chromatographic column and changing retention times. The criteria for selecting an ideal sorbent are (i) large breakthrough volume (BTV) for the compound to be sampled, (ii) smooth recovery of trapped compounds, (iii) no affinity towards water vapour and (iv) minimised contamination, degradation, modification or any artefact generation. No single adsorbent has all of these qualities; therefore, to cover a wide VOC range multiple sorbents are often used. Another important thing is the type of sampling method used with this approach.

There are two modes of sampling (i) active sampling in which sampling pump is required to control sampling rate and sampling time and (ii) passive tube sampling or diffusive sampling in which analytes are collected on the basis of concentration gradients. Active sampling offers high sampling volume in comparison with passive sampling; though, passive sampling is a low cost technique as no bulky or expensive pump is required. Finally, the recovery of trapped analytes can be achieved by thermal desorption process or solvent extraction process. Thermal desorption is most useful for compounds with boiling points of less than 150°C and solvent extraction is very useful for compounds with boiling point above 300°C. (Wang and Austin, 2006)). In current work the sorbents are used in the pre-concentration of canister samples prior to separation step.

91

The problems associated with the sorbent sampling techniques (breakthrough problems with more volatile compounds, sample recovery, no possibility of replicate analysis, artefact, storage) are mostly overcome by the use of stainless steel canisters; however, sorbent sampling, due to its easy handling and suitability for less volatile and polar compounds, still receives extensive attention for further improvements. The recent improvement in this technique has been achieved (Bechara et al., 2008) by focusing on multisorbent tube composition, breakthrough volume, moisture removal, two stage desorption and cyrotrap temperature. This technique has been successfully used by deploying multisorbent tubes as an automatic sampler AMOVOC (Airborne Measurements of Volatile Organic Compounds) to measure C_5-C_9 NMHCs on-board French research aircraft during the African Monsoon Multidisciplinary Analysis (AMMA) aircraft field campaign. During this campaign, 200 tubes were collected and most of the data were validated. The handling of this sampler is comparatively easy and it needs limited manpower in addition to the minimal power requirements to use this unit aboard the research aircraft. It is worth also considering that the majority of VOC measurements now made for air quality purposes in the UK are also made now using adsorbent tubes. These only provide data on 1,3-butadiene and benzene, and have replaced the more expensive to operate online GC systems that operated between 1997 and 2005.

2.3.2 Whole air sampling

2.3.2.1　　Plastic bags

Collection of samples within plastic or polymer bags (such as Tedlar, Teflon or aluminized Tedlar) can also be used and is a simple and cost-effective alternative to canisters and adsorbent tubes. These bags are available in various sizes 500 ml to 100 litre of volume and can be filled using a clean pumping device. The major issue with this sampling device is that samples are not stable more than 24-48 hours because of the permeability of bag material to certain chemicals. Overall, despite the low cost of these bags and easy handling, the stability of samples is

one of the main disadvantages in comparison with canister sampling (Wang and Austin, 2006).

2.3.2.2 Stainless steel canisters

The most commonly used containers for air samples are made of stainless steel canisters. The canisters are available commercially in varying size and shape. The internal layer of stainless steel canisters can be further coated by using electro polishing, silica, or Teflon coatings to make the inner walls of the canister passive. In 1965 R.A Rasmusssen developed a SUMMA™ (SUMMA is a trademark) electro-polishing technique in which the interior surface of grade 316 stainless steel containers were coated with a pure chrome-nickel oxide layer in order to passivate the surface of inner wall of stainless steel (Wang and Austin, 2006). This is the principal reason for the high cost associated with the canister sampling. This passivation procedure resolves many issues associated with wall adsorption. Another recent popular coating is fused silica, in which a thin fused silica layer is chemically bonded to the interior stainless steel surfaces to reduce surface reactivity. The canisters used for sampling in current work are based on fused-silica coating. Fused-silica-lined canisters (FSL) are found to be more inert than SUMMA canisters (Kumar and Viden, 2007) though there have been some reports of FSL canister lining which are degraded with the passage of time (Wang and Austin, 2006). Such canisters are available from a number of manufacturers and suppliers including Entech Instruments Inc (Silonite canisters) and Restek Corporation (Bellefonte, PA, USA; SilocCan). Overall the coating techniques combined with the sophisticated sampling and cleaning procedures have broadened the range of VOCs of varying polarity to be covered and analyzed by this method without being lost on walls of the container.

The collection of the whole air matrix in a pre cleaned evacuated stainless steel canister can be done either at sub-atmospheric pressure (passive sampling) or by pressurising with ambient air to 40 psig using an all-stainless steel assembly

double headed bellows pump (active sampling). Filling samples at high pressure ensures the stability for the sample for unknown reasons (GAW Report No 111, 1995;GAW Report No 171, 2006). Double valve canisters allow for flushing the canister prior to pressurization hence these are expensive; though, accurate results are thought to be achieved with or without flushing the canisters prior to pressurization. The purpose of canister pressurization is to increase sample volume while subsequent analysis of samples occurs at ambient pressure. The increased sampling volume offers replicate analysis of samples which is an advantage of canister sampling over adsorbent sampling. The data from replicate analysis further helps to monitor the stability of air samples between sampling and analysis time. The presence of humidity in air plays an important role while collecting samples in canisters. It may be beneficial or detrimental depending upon its amount. To some extent the presence of moisture is beneficial because it occupies the active sites which reduce the adsorption losses or chemical interactions on the inner walls of the canisters. Polar VOCs are more prone to be lost on inner surfaces of canisters in comparison with non-polar VOCs, hence to cover a wide range of VOCs including oxygenates VOCs, the presence of water is an added advantage; however, the high moisture contents offer the dissolution of target compounds in condensed water which might be a major loss mechanism (Hamilton and Lewis, 2007).

Depending on the type of canisters, there are various conditioning processes to remove the memory effects of previous samples. The evacuation procedure in current work involves the use of a scroll vacuum pump (Edwards XDS10) to achieve a vacuum of the order of 1×10^{-2} mbar recorded by a Pirani gauge. Before deploying these canisters on-board, a leak check is an essential activity. In addition to adopting evacuation procedures, the canisters are checked for any contamination or memory effects by using ultra pure nitrogen gas once in a year.

Mostly stainless steel canisters are deployed aboard the aircraft; however, the research group involved in the CARIBIC (Civil Aircraft for the Regular

94

Investigation of the atmosphere Based on an Instrument Container) project prefers the use of glass sampling flasks over stainless steel canisters to include alkyl nitrate, CO_2 isotopologues in addition to NMHCs. The sample collection is fully automatic and consists of two TRAC (Triggered Reterospective Air Collector) sampling units each of which contains 14 glass sampling flasks of 2.67 l. A HIgh REsolution whole air Sampling system (HIRES) has been added since autumn 2009 by this research group and used during CARIBIC volcano flights. This sampling unit consist of 88 stainless steel sampling cylinders, each of 1 litre internal volume. The internal surfaces have been passivated by the use of laser polishing (Rauthe-Schoch et al., 2012).

Overall for most active research groups, the preferred method of sampling is canister sampling due to the universal means of collection without any breakthrough, and possibility of replicate analysis; however, the high initial cost, requirement of complex sampling apparatus and sophisticated cleaning procedures remain reasons for choosing sorbent sampling over canister sampling. The current work discussed in the thesis is based on the use of the WAS system consisting of stainless steel canisters for sample collection as shown in **Figure 2.9**; the WAS system has been deployed aboard the FAAM BAe146 research aircraft throughout the all three field campaigns. There are three identical sets of WAS system available for the UK atmospheric research community. Each set of WAS consists of 64 silica passivated single valve stainless steel canisters (Thames Rested ,UK) of three litre internal volume. This sampling unit is fitted to the rear hold of the aircraft. The system is connected to an all-stainless steel assembly double-headed bellows pump (Senior Aerospace USA) which draws air from the main sampling manifold of the aircraft, situated at the forward of the engine; after initial flushing with ambient air for few seconds, the outlet valve is closed and air is pressurised into the canisters to a maximum pressure of 40 psi ($\approx$ 3 bar). The final pressure in the canisters is measured by the pressure sensor fitted between the outlet of the pumping system and inlet of the sampling system; once the required pressure is achieved the inlet valve is closed and a pressure release valve opens to direct the excess pressure to the exhaust line. Since the

atmospheric pressure decreases with the increase in altitude, the time required to fill the sample varies between 10 sec and 60 sec depending on the sampling location (boundary layer or lower or upper free troposphere). Depending on the speed of the aircraft (215 knt), an air mass sampled between these filling time is representative of the spatial resolution between 1.09 km to 6.54 km.

Figure 2.9: A case of Whole Air Sampling (WAS) system consisting of 15 double valve (manual inlet and pneumatic controlled inlet) stainless steel canisters. Compressed gas is used to open the metal bellows solenoid valve which let sample pass through into or out of the canister. The manual valves are typically left open unless in storage. Once the whole case is attached to GC system through a sample inlet line a canister controller box (controlled by Lab view software, National Instruments) controls the opening of each canister for a sampling time of 10 minutes. All canisters in a case are analysed one by one in an automatic way. The flows of gas extracted from the canisters are logged in order to reject data with insufficient sample flow.

Sample acquisition is controlled by software which is operated either in an automatic or manual mode. After the conclusion of flights, the samples are either analysed immediately in a laboratory set up temporarily near the campaign area or transported back to the University of York, for analysis within a week time in a GC laboratory housed in shipping container. One of the most important considerations while carrying out VOCs measurements is the time between the sample collection and analysis that should be minimum so as to avoid any

contamination or storage artefact. The samples from all campaigns were analyzed within a week or at the most two weeks after sample collection. The stability tests have been performed during this period at the interval of two weeks. Two WAS cases filled with samples from boundary layer, high altitude and mid-tropospheric layer have been selected. **Figure 2.10** shows the chromatogram from high altitude samples. These chromatograms overlay perfectly well indicating no sign of decay or growth during this period.
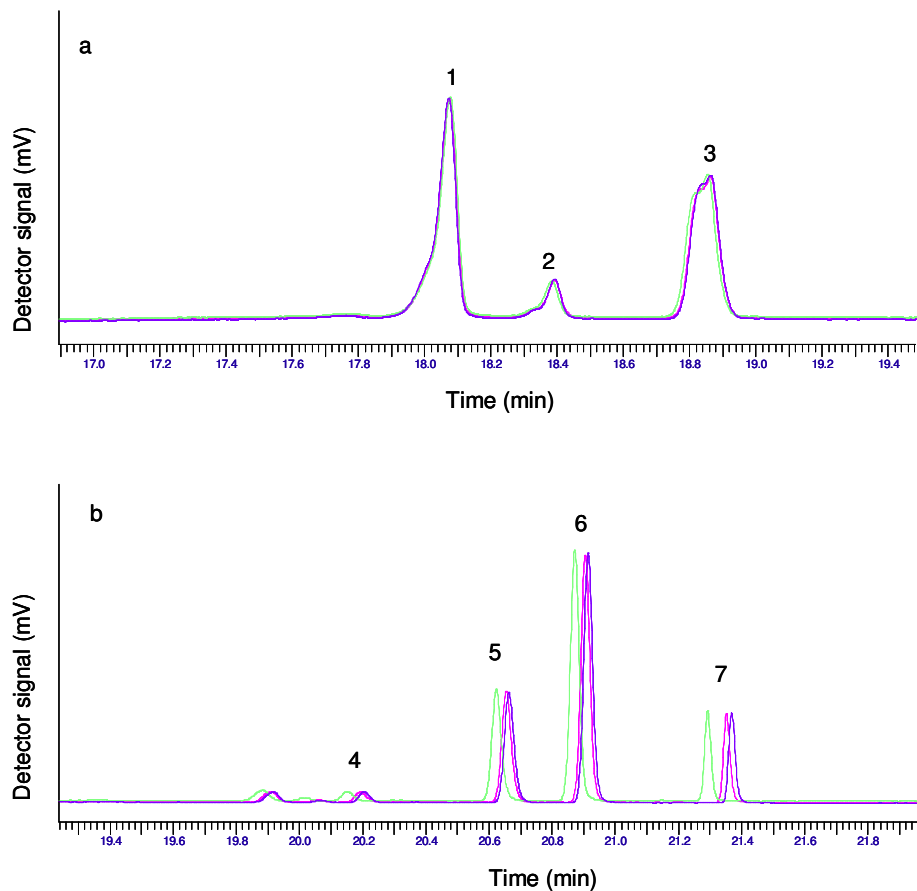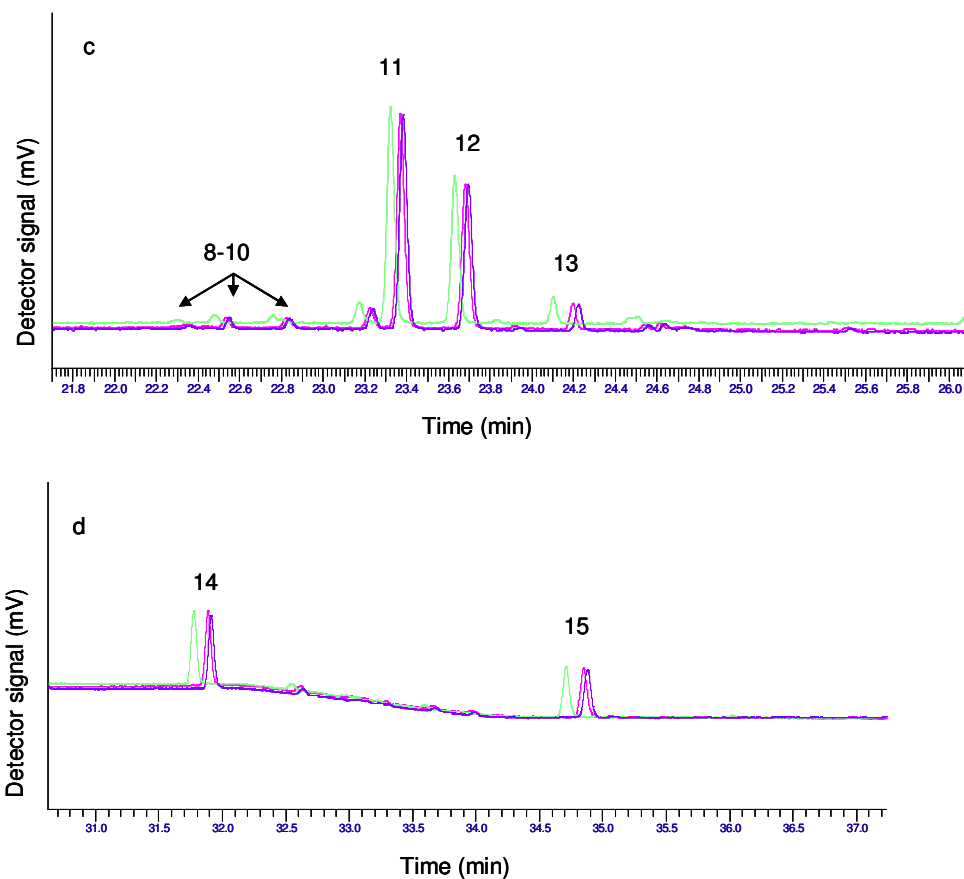
Figure 2.10: Comparison of results from analysis of high-altitude whole air samples from same canisters. The chromatograms in an overlaid mode represent original run (green), first repeat (pink) and second repeat (blue). The time interval between the original run, the first repeat, and the second repeat is two weeks each. The peaks are labelled as follows: (1) ethane,(2) ethene,(3) propane,(4) propene,(5) *iso*-butane,(6) *n*-butane(7) acetylene,(8-10) butenes,(11) *iso*-pentane,(12) *n*-pentane,(13) 1,2-butadiene,(14) benzene and (15) toluene.

2.4 Sample preparation

2.4.1 Moisture management

The presence of water in ambient air samples is much higher (mg L^{-1}) than the presence of VOC levels (pg L^{-1}- ng L^{-1}). Moisture in samples is removed prior to the preconcentration step; the preconcentration step is carried out at low temperatures so the presence of any trace amount of water vapour is sufficient to interfere with the analysis. The introduction of water into the columns, especially

Alumina PLOT columns, induces a large change in stationary phase affinity which in turn shifts the retention time and reproducibility of the separation. The water eluting from the column can also extinguish the flame of the FID causing an interruption in an automatic analysis. Over multiple analyses, water residuals in the adsorbent trap can end up blocking the flow path with ice.

To minimise the negative influence of water on analysis and to obtain a uniform water content for all samples to improve reproducibility, there are several ways to eliminate water before sample is passed to the next stage. These include the use of a condensation trap immersed at low temperature, inorganic adsorbents (such as magnesium pechlorate and potassium carbonate as a drying agent) and Nafion dryers. Nafion is an ionic copolymer of tetrafluoroethylene (Teflon) and a flurosulfonic acid group. Each sulfonic acid group can co-ordinate up to 13 molecules of water causing the selective permeability for water (Dettmer and Engewald, 2003) and this forms the basis of the Nafion dryer operation, based on the principle of a steep concentration gradient across a membrane that is permeable only to highly polar material such as water. This water is carried away by a counter-current of dry gas that is passed around the outside of the membrane as a sheath gas. However, in this present case the approach is not suitable because polar VOCs are also a part of the suite of VOCs to be quantified. Nafion driers produce only a differential reduction in moisture content, rather than reduction of moisture to a fixed dew point. Aircraft samples come from a wide range of humidity environments and this means that there is a lack of uniformity in moisture in the samples introduced on column. This reduces run to run reproducibility in retention times.

A condensation trap, immersed in a 50:50 water: ethylene glycol mix held at -30 °C, has been used in present configuration to remove water. Many research groups prefer the use of inorganic adsorbents in combination with the use of condensation trap as an initial stage (Slemr et al., 2004); however, the use of inorganic adsorbents by itself has limited capacity and requires frequent

regeneration and replacement. Depending on the water content, the use of inorganic adsorbents alone is enough for water elimination for example, the focus of the CARIBIC research group is on the study of free troposphere and extra-tropical upper troposphere as well as the lower stratosphere which means that samples collected from these altitudes have low water content so a drying tube containing magnesium perchlorate as a drying agent is used. The drying tube is at 55 °C while sample flows through this and is regenerated by heating at 80 °C for 25 min while flushing with hydrogen. The heating step serves as a regeneration of drying agent but has also been shown to significantly reduce any loss of larger (C≥8) NMHCs. (Baker et al., 2010). Similar drying agents were initially used by the research group at GAW Hohenpeisenberg observatory (Plass-Dulmer et al., 2002) but significant losses of isoprene and losses of C_7-C_9 led this research group to replace it by the Nafion dryer.

O_3 management is also important because the presence of O_3 in the air to be sampled can cause some loss of analytes, especially reactive unsaturated compounds. The O_3 scrubbers (thiosulphate impregnated sorbent traps, potassium-iodised traps etc) are most commonly used but analytes losses are also observed with these scrubbers (Dettmer and Engewald, 2003)). The alternative to scrubbers is the use of the heated stainless steel lines. In the present configuration, the sample line up to the inlet and the tubing of the sample leading to the cold trap are maintained at 70 °C. In addition to this, the individual valve heaters are used to heat the GC injector and switching valves up to 60 °C.

2.4.2 Sample enrichment

Since NMHCs in ambient air are usually at ppt or sub-ppb range, a quantitative sample enrichment combined with desorption step becomes an important stage prior to injection onto the GC columns for separation and to achieve common detection limits. There are mainly two sample enrichment techniques: cryogenic and adsorptive enrichment. The cryogenic method involves a U-piece stainless

steel sampling loop of appropriate dimension either empty or packed with glass beads or Tenax[TM] TA immersed in liquid nitrogen (-195.8 °C) or liquid argon (-186 °C). The use of liquid argon is preferred over liquid nitrogen since it may reduce the amount of oxygen retained in the refocusing stage (Hamilton and Lewis, 2007) as oxygen is harmful to most capillary GC columns. Since the preconcentration stage is carried out at such a low temperature hence the sample should be free of water vapour before passing through this stage so as to avoid the blockage of lines with ice. The compounds with a freezing point higher than the temperature of the liquid nitrogen or liquid argon are frozen in the section of tubing and the compounds with freezing point below this temperature, mainly nitrogen and oxygen, pass through this tubing. Once a sufficient volume has been acquired on the sampling loop, the U piece tube is lifted from the liquid nitrogen container and is generally flash heated either electrically or using hot water. This step introduces a very sharp band of compound to the head of the analytical column.

Another sample enrichment method is adsorptive enrichment by using a Peltier cooling device used as an alternative to cryogenic cooling; this makes an instrument easier to use in the field. The adsorbent trap used in present work is prepared from a glass liner (4 mm I.D., 6 mm O.D.) and packed with approximately 90 mg in total of Carboxen 1000 and Carbotrap B (Supelco) in order of increasing sorbent strength to cover a broad range of VOCs. The trapping efficiency of these materials depends on their surface areas and on the analyte volatility. A stronger sorbent (Carboxen 1000) is needed to trap the highly volatile compounds, however its ineffective desorption of heavier weight compounds, means a weaker sorbent (Carbotrap B) must be used in combination to covering a broad and diverse range of volatility and polarity without breakthrough and desorption problems. During active sampling, when the sample is pumped onto the adsorbent trap, the compounds start adsorbing onto its surfaces and depending on the length of sampling time and flow rate, the compounds slowly migrate from the front end of the trap to the rear. The amount of the sample that can be successfully trapped without being lost from the far end

of the trap is called the breakthrough volume. The breakthrough volume (BTV) tests were carried out by increasing sampling volume of a multi-component standard gas mixture Apel Reimer 54 (AR54) component mix manufactured in 2006 (reference number (CC236306) at a trapping temperature (-23 $^{\circ}$C). As can be seen from **Figure 2.11**, ethane the most volatile organic compound was retained on the trap up to at least 1500 ml sampling volume whilst for ethene, linearity is up to 1200 ml and then plot begins to curve. On the basis of smaller breakthrough volume for ethene, the sampling volume of a litre was established for the combination of trapping material used in enrichment step. The sample flow of 100 ml min^{-1} is controlled by mass flow controllers (MKS Instruments), with a trapping time of 10 minutes, a litre of sample is processed.
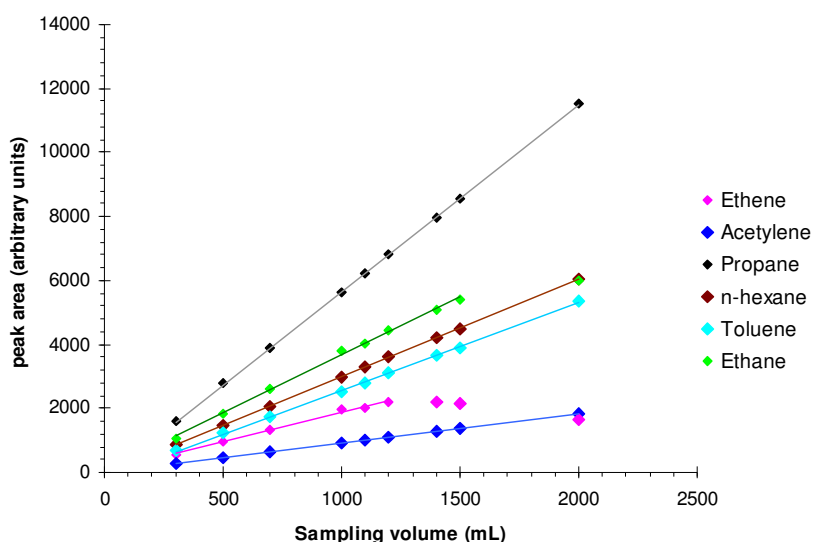
Figure 2.11: Peak area versus sample volume for C_2-C_7 hydrocarbons at -23 °C. The multicomponent AR 54 standard sample was drawn through a dual-bed charcoal trap (Carbotrap B and Carboxen 1000) at a flow rate of 100 ml min^{-1} maintained by mass flow controllers for a period corresponding to the required sample volumes. During the analysis, the column was maintained at 40 °C for 3.5 minutes after injection; then ramped at 13 °C min^{-1} to 110 °C and then finally ramped at 8 °C min^{-1} to 200 °C where it is remained for 20 minutes.

The adsorbent trap is contained within an optic injector unit (ATAS international B.V) and is sandwiched between two brass blocks (dimension of a brass block is l x w x h =5.2 x 4.4 x 6.3 cm) that are cooled by two dual-stage Peltier elements

(39.7 W, Supercool Inc.) The trapping temperature of -23 °C was set (7 °C above the water trap temperature -30 °C) to minimize the retention of water vapour. The high temperature sides of the two Peltier coolers are attached to cooling cells through which a water/ethylene glycol mix (12 °C) is continually passed to dissipate the excess heat. Since this cooling unit is maintained at low temperature during sample trapping stage, the whole brass block with Peltiers and cooling cells are housed in a sealed box in order to minimise the condensation which in turn can lead to inefficient heating and cooling of the trap by forming ice.
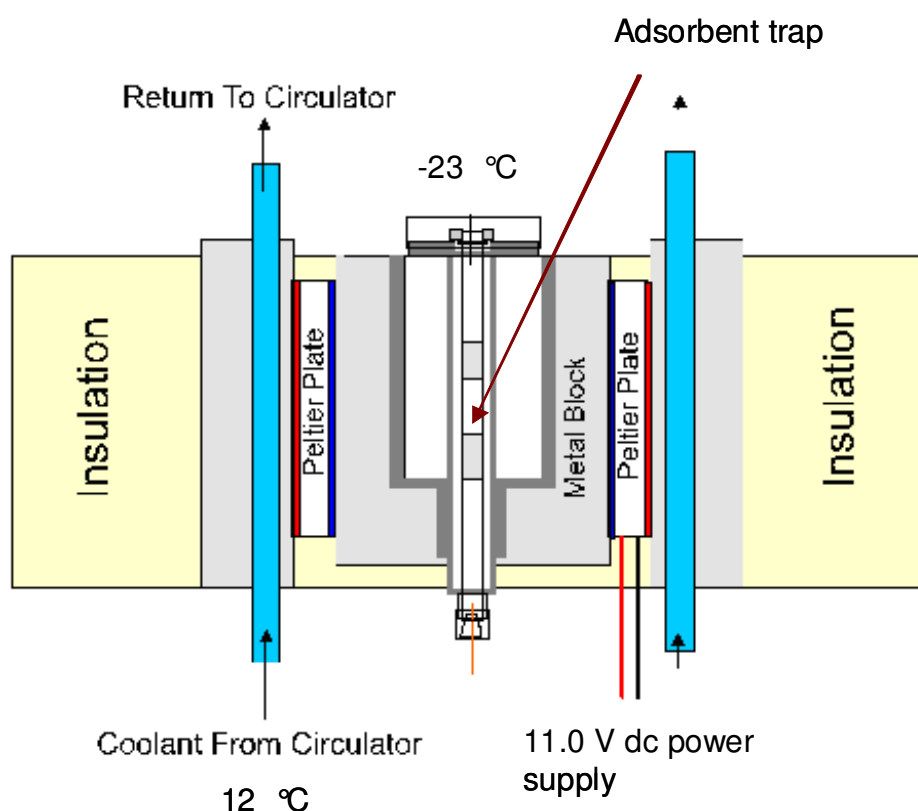
Figure 2.12: Schematic of adsorbent trap assembly. The adsorbent trap is sandwiched between two brass blocks that are cooled by two double-stage Peltier plates. The trapping temperature is maintained at -23 °C. The high temperature side of the Peltier elements are cooled by the circulation of ethylene glycol/water mix maintained at 12 °C. In order to prevent water condensation on cold elements, the adsorbent trap and Peltier elements are sealed in an air-tight box. Courtesy: (Hopkins, 2001)

The adsorbent trap is heated resistively to 325 °C at the rate of 16 °C sec^{-1} during desorption. A fast response low thermal mass sensor, type K thermocouple, is

positioned in the centre of the adsorbent trap in such a way that the thermal mass or electrical conductivity of the trap is unaltered during the monitoring of the trap temperature. Once the sample enrichment step is finished, the analytes are thermally desorbed in a flow of carrier gas which further splits in a 50:50 ratio between the two columns, using a T-piece union in–line between the injector and the columns, where an optimized separation begins.

2.5 Separation

The gas chromatography separation is achieved by the use of column of appropriate length, internal diameter (i.d.) and stationary phase (Supelco, 2010). The current method for the separation of VOCs uses capillary columns, mainly alumina-based Porous Layer Open Tubular (PLOT) columns. Depending on the application, there are primarily four parameters for column selection: stationary phase, column internal diameter (i.d.), film thickness and column length. As discussed in section 2.2.1.1 that the retention in chromatography depends on the extent of interaction of analyte with the stationary phase. The differences in the chemical and physical properties of VOCs and their interaction with stationary phase are the basis of the separation process. The ability of column to separate sample components depend on the phase polarity; the polar phase is suitable for separating polar compounds whilst the non polar phase is effective for the separation of nonpolar compounds or in other words, this is based on the general chemical principle of 'like dissolves like'. Nonpolar compounds are generally composed of only of carbon and hydrogen atoms and contain carbon-carbon single bonds, For example *n*-alkanes, the type of interaction between nonpolar compounds and the stationary phase is intermolecular attraction that increases with the size of the compound hence larger compounds with higher boiling points have long retention and thus elute towards the end of the run in comparison with the compounds with lower boiling point. However, the polar compounds are composed of carbon and hydrogen atoms in addition to one or more atoms of oxygen, nitrogen, sulphur, phosphorus or halogen atoms for example, alcohols, carboxylic acids, esters, ketones are typical polar compounds.

The type of interaction between polar compounds and the stationary phase include π-π and or acid–base interactions. The separation of polar compounds is based on the differences in the extent of these interactions; the higher the polarity the greater the retention time. The compounds with double bond (alkenes), triple bonds (alkynes) and benzene-ring (aromatic) containing compounds are categorized under polarisable compounds; these are also separated on polar columns. The PLOT columns are suitable for the separation of very volatile organic compounds without the need of cryogenic or sub-ambient cooling of the oven (Agilent technologies, 2007).

PLOT column stationary phases are small porous adsorbent particles. These solid adsorbent particles are attached to the inner walls of the capillary silica tubing using a binder or similar means. The separation occurs on the basis of different adsorption properties of different analytes. The most commonly used stationary phase is deactivated alumina (Al_2O_3). The nature of alumina is highly retentive hence in order to avoid peak tailing, the surfaces are deactivated by using inorganic salts such as sodium sulfate (Na_2SO_4) or potassium chloride (KCl) to control retention. KCl deactivation produces a relatively less polar column while Na_2SO_4 produces columns exhibiting increased retention of unsaturated hydrocarbons. In the present configuration, a Na_2SO_4 deactivated alumina PLOT column is used for C_2-C_9 NMHCs in conjunction with a CP-LOWOX column for analysis of the more polar VOCs including oxygenated species to perform parallel simultaneous GC separations. The CP-LOWOX column is an example of the use of mixed phase porous layer capillary columns, a recent advancement for the analysis of low-molecular weight oxygenated compounds. The CP-LOWOX column has unique properties of separating carbonyl compounds in the presence of hydrocarbons (Dettmer et al., 2000).

The thickness of the stationary phase is equally important in determining resolution and retention characteristics. Thick film columns i.e. 1 to 5 μm are best suited for analytes with low boiling points such as VOCs. The benefits of

thick film columns are increased sample capacity and higher retention for very volatile solutes but at the same time increased peak width (which may reduce resolution), and increased column bleed are the major drawbacks. The thickness of stationary phase in the present column is 10 μm. Thinner film columns i.e. 0.10- 0.25 μm are best for high boiling point (b.p>300°C) compounds and semivolatile trace analysis. The benefits of thin film columns are sharper peaks (which may increase resolution) and decreased column bleed whilst the drawback is decreased sample capacity and retention.

The third factor is column internal diameter (i.d.,) which balances the efficiency of column and the sample capacity. The column efficiency increases as the i.d. of the column decreases. It is best to choose narrow i.d. capillary columns when the sample has many analytes or analytes that elute closely. The sample capacity is the amount of any one sample component that can be applied to the column without causing the overloading. Exceeding the sample capacity of a column will result in skewed peaks and decreased resolution. The sample capacity increases with column i.d. ; tweaking the i.d. of column to optimize both factors depends on the analytical need. Columns with 0.23 to 0.53 mm i.d. are mostly used. The interfacing to the injection system and the detector is one of important criteria for selection of column diameter (Helmig, 1999). The diameter for both columns in present instrumentation is 0.53 mm which is suitable for high flow rates and the direct transfer from a preconcentration trap during thermal desorption step onto the columns.

The column length is also an important factor as it influences three parameters: efficiency, retention and carrier gas pressure. The efficiency of the column is proportional to the column length. It should be kept in mind that doubling the column length will not double the resolution because resolution increases according the square root of the column length. A longer column will provide greater resolution than a shorter column. Shorter columns such as those less than 15 m are generally used when great resolution is not required such for analysis

simple samples with components dissimilar in chemical nature. As clear from equation 2.11, the retention time is directly proportional to the column length which means the long analysis time. There are practical limits to increasing the column length. The column head pressure is also proportional to column length. Long and small diameter column requires extremely high head pressures whilst short and wide diameter column require very low pressure, both situations are not practical. Generally a best balance of resolution, analysis time and required column head pressure is achieved by using a 30 m column; however, the complex samples having volatile analytes require higher resolution and are generally analyzed on a 60 m column. The length of column in the present instrumentation is 50 m for PLOT and 10 m for CP-LOWOX.

Overall, to take advantage of the unique features of PLOT columns for getting an optimized separation and enhance their lifetime, careful maintenance and correct operation are a must. The practical precautions for maintenance of PLOT columns are adequate conditioning, proper connection to GC, not exceeding upper temperature operating limits and proper sampling technique. Actually PLOT columns are only good for 'clean' samples of which atmospheric samples are one (Ji et al., 1999).

2.6 Detection

So far we have seen the importance of selection parameters at preconcentraion and separation stages to achieve the best performance. The selectivity in detection is equally important to have successful gas chromatography. The purpose of the detector is to monitor the analytes eluting from the column and respond by measuring the variations in its composition accordingly. A number of detectors have been used with gas chromatographic separations, e.g the flame ionization detector (FID), the electron capture detector (ECD), the thermal conductivity detector (TCD) the mass spectrometer (MS), the photo ionization detector (PID), the helium ionisation detector (HID) and the nitrogen

phosphorous detector (NPD). The most popular detectors are FID, MS and ECD in their decreasing order of percent usage (Helmig, 1999). The choice of FID is predominant for hydrocarbons whilst the ECD is a method of choice for halogenated compounds. By using multi detectors, the hydrocarbons and halogens can be analysed in a one sample run by splitting and directing the column flow to specific detectors. Although MS detectors are the most powerful and GC-MS configuration is commonly considered to be of highest standard in term of qualitative as well as quantitative analysis, their complexity and cost may rule them out for being chosen on a regular basis. The FID is considered a universal detector since it responds to a wide variety of organic compounds; however, carbon dioxide, carbon monoxide, nitrogen, oxygen, carbon disulfide and inert gases are not responsive to FID. Formaldehyde, formic acid and heavily halogenated compounds produce a low or non-linear response because of the few carbon hydrogen bonds present. In the present instrument configuration, the eluents from two columns are fed to two FIDs placed in a parallel arrangement to analyse hydrocarbons and oxygenated VOCs.

Basically detectors are classified on the basis of the signal's proportionality with respect to concentration (mass/volume, gram ml^{-1}), i.e., concentration sensitive detectors (TCD, ECD etc) or mass flow rate (mass/time, gram sec^{-1}), i.e, mass sensitive detectors. (Miller, 1987). The FID comes under the mass sensitive type detector, that is it produces signal that is proportional to the rate of mass flow or in other words its signal depends only on the actual mass of analyte or number of the carbon atoms in the organic analyte passing through per unit time; if the mobile phase flow stops, the signal stops. When we use word 'signal' we generally mean height of the peak. By reducing the flow rate to half, a mass sensitive detector is expected to produce a signal that is half of the original peak height but unchanged peak area whilst the concentration sensitive detectors will produce a signal of same peak height, because concentration is same in case of original and reduced flow, but peak area would be double of original peak area. By demonstrating this example, it is clear that if during a GC run there is a slight change in flow then mass sensitive detectors could produce erroneous peak

heights and concentration sensitive detectors could produce erroneous peak areas; which one is a better measure of quantitative analysis is further discussed in section 2.8.

It is also important to understand the difference between the sensitivity and the minimum detectable quantity (MDQ) as these two terms are often misunderstood and used incorrectly. Sensitivity is a measure of the amount of signal generated by the detector for a given amount of analyte or it is actually a slope of the calibration curve plotted between response and concentration (for concentration sensitive detector) or response and mass (for mass sensitive detector) and according to definition, the sensitivity should be a constant. The signal can have variety of units like millivolts (mV) or amperes (A). The unit used to express sensitivity for FID which is a mass sensitive detector, is mVsec/g or ampere.sec/g or C/g (as a coulomb is an ampere-second). One of the characteristics for choosing the FID as an ideal detector is adequate sensitivity $(0.015$ coulombs $g^{-1})$ (Braithwaite and Smith, 1985). Adequate sensitivity implies fast response and low background noise.

Noise is the signal produced by a detector in the absence of a sample. It is caused by the electronic components from which the detector is made. It is important to establish the mean noise level in order to determine the MDQ. A more meaningful term is signal-to-noise ratio rather than noise. In most chromatographic work the smallest signal that can be attributed to an analyte is when the detector signal is at least twice the mean noise signal level or in other words it is the MDQ. A high background signal or noise will limit the sensitivity of the detector and this will be manifested in an increased MDQ. The units for MDQ $(g \ s^{-1})$ can be obtained by dividing the minimum detectable signal (mV) by the sensitivity (mV sec g^{-1}). In present case the MDQ for most of the compounds is 1 pg sec^{-1}.

Once the two terms are understood, it can be used to establish the linearity of a detector. The linearity is the sample concentration range over which the detector response is linear from the MDQ to the upper concentration limit. When sensitivity is plotted against the concentration then there comes a point when sensitivity corresponding to some value of high concentration falls off. According to the American Society for Testing and Materials (ASTM) recommendation, the upper limit is the concentration corresponding to sensitivity equal to 95% of the maximum sensitivity. Hence linearity can be calculated by dividing the upper limit by the MDQ and it is dimensionless. The FID can have a linear range of 10^7 ,i.e., it can be used over a concentration range of about 10^{-12} to 10^{-5} g per cm of sample (Braithwaite and Smith, 1985). Hence the wide linear dynamic range, adequate sensitivity which implies a rapid response, no or little response to water, carbon dioxide, the common carrier gas impurities hence a zero signal in absence of sample, stable baseline (mass sensitive so it is not significantly affected by fluctuations in temperature or carrier gas flow rate or pressure), good stability and reproducibility, long-term reliability and ease of operation and ruggedness, are the outstanding features which make FID an ideal detector.

A schematic diagram of a typical FID is shown in **Figure 2.13**. The effluents from the column are directed to the base of the detector where it is heated and mixed with hydrogen thoroughly before emerging at the jet into the air stream. The reason for the heated base is to avoid condensation of water generated by the flame and to prevent any hold-up of solutes as they pass from the column to the flame. The combustion is supported by the air supply to detector and hydrogen-air flame burns at a metal jet. A cylindrical collector electrode is located above the flame. The assembly is contained in a stainless steel or aluminium body to which are fitted a flame ignition coil and electrical connections to the collector electrode and a polarising voltage to the detector jet. When eluents burn in the flame, ions are generated and due to the potential difference between the jet and the collector electrode, the ions and electrons are collected at collector electrode and a flow of current is generated (approximately 10^{-12} A) which is then

measured with a picoammeter. The ionisation of carbon compounds in a flame is a complex process. The organic molecules undergo a series of reactions including thermal fragmentation, chemi-ionization ion molecules and free radical reactions to produce charged species (Braithwaite and Smith, 1985). The amount of current produced is proportional to the number of carbon atoms present and hence the number of molecules. As said previously, the FID is a mass-sensitive detector so any change in mobile phase flow or pressure will not affect the response of the detector which is an advantage. As eluents are burnt in the flame the process is destructive; this is the only disadvantage of the FID.
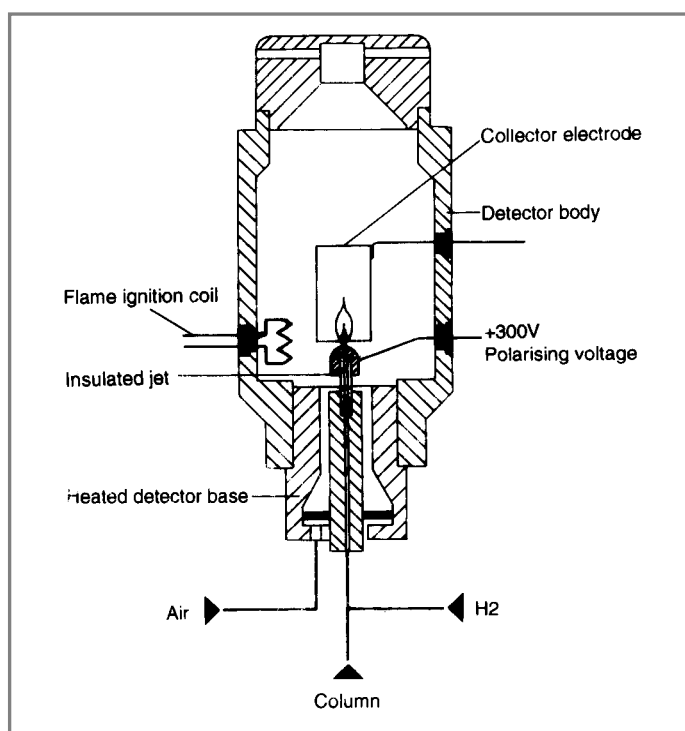
Figure 2.13: Schematic of FID. Courtesy (Hopkins, 2001)

2.7   The York FGAM dual channel gas chromatograph
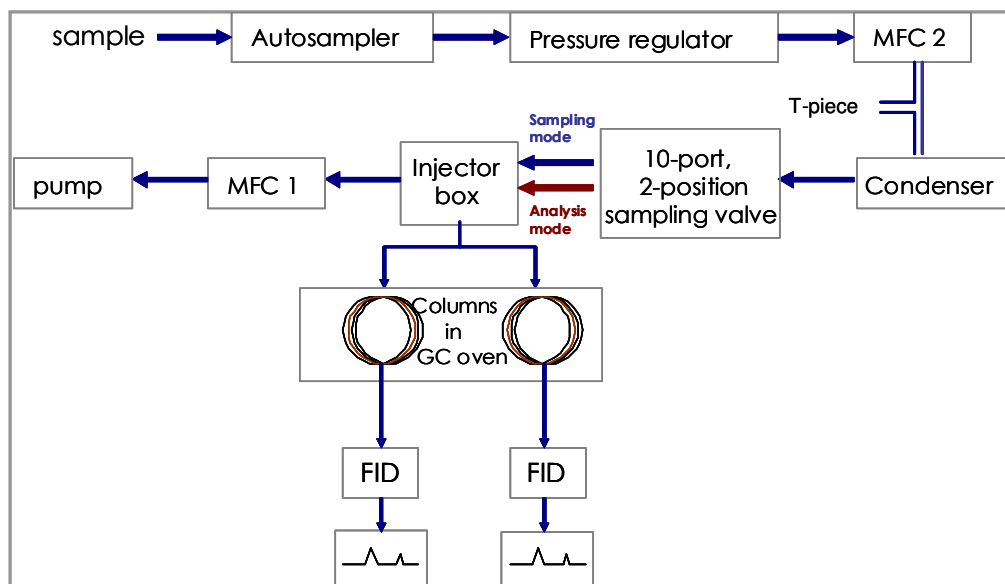
Figure 2.14: Schematic of the analytical system for measurement of C_2-C_9 NMHCs and selected oxygenates. The mass flow controllers are represented by MFC 1 (100 ml min^{-1}) and MFC 2 (120 ml min^{-1}). A T-piece between MFC 2 and cold trap acts as an overflow, bringing higher and changing pressure from canister samples to ambient pressure and to achieve a uniform response from multiple analyses of the same canister sample.

The dual channel GC-FID system for the measurement of C_2–C_9 hydrocarbons and selected oxygenated VOCs in ambient air samples is shown in **Figure 2.14**. The whole air samples in canisters are supplied at an initial pressure of 20-40 psi. It was observed that replicate analysis of the same canister at decreased inlet pressures affected the signal response slightly. The reason for a differing response for multiple samples from same canister was inadequate sample volume control at different inlet pressures, despite the use of mass flow controllers within the system. In order to maintain the uniformity in sample delivery pressure, a T-piece is included as an overflow valve between the first mass flow controller shown in figure as MFC 2 maintained at 120 ml/min and the condenser or cold trap. The utility of this overflow valve allows an excess pressure in the system to vent, such that multiple samples from the same canister were subsequently

sampled at atmospheric pressure after passing through MFC 2. The high pressure sample passes from autosampler, pressure regulator through MFC 2 and a T-piece to a cold trap immersed in a 50:50 water : ethylene glycol mix maintained at -30 °C for water removal. The 2-position 10 port valve sampling position allows the sample to pass through a dual-bed adsorbent trap (Carbotrap B and Carboxen 1000) held at -23 °C with the use of two dual-stage Peltier coolers. The high temperature side of the Peltiers are attached to a metal block with cooling cells (12 °C) through which a circulation of ethylene glycol and water (10:90) dissipates the excess heat. The flow rate is controlled by mass flow controller MFC 1 at 100 ml min^{-1} and during a 10 minute sampling time, a litre of sample is acquired. After 10 minutes sampling time, the trap is flushed with helium as a carrier gas for 3.5 minutes whilst the trap is cold. This lets methane pass out through the system as it can not be trapped quantitatively.

Once the methane is flushed out, the adsorbent trap is resistively heated to 325 °C (16 °C sec^{-1}) and the compounds are thermally desorbed in a constant flow of helium maintained at 40 ml min^{-1} (20 ml min^{-1} through each column) and flushed into the GC system. The two columns (a 50 m, 0.53 mm i.d. Al$_2$O$_3$ PLOT column for NMHCs analysis and a 10 m, 0.53 mm i.d. CP-LOWOX column for polar compounds) are placed in a GC oven. The sample flow from injector is further split in a 50:50 ratio *via* a T-piece union (in-line between the injector and the columns) and directed to the respective columns. The carrier gas flow is programmed by maintaining 40 ml min^{-1} until 33.5 minutes (20 ml min^{-1} through each column) and then after 33.5 minutes the flow is 80 ml min^{-1} (40 ml min^{-1} through each column) to speed up the elution of heavier weight compounds so that these shouldn't interfere with the next run. The GC oven is programmed using an initial temp of 40 °C for 3.5 minute after the injection of the sample to allow for some focusing of heavier weight species (which are generally desorbed from the trap less rapidly than those of more volatile nature) and then heated at a rate of 13 °C min^{-1} to 110 °C and is ramped at the rate of 8 °C min^{-1} till the final temp 200 °C is achieved where it is maintained for 20 minutes before cooling back to 40 °C and ready for the next injection. The eluents from each column are

analyzed using two flame ionization detectors (FID). Each run takes one hour to complete. The detection limit for most of the compounds for 1 litre sample is between 2-9 pptv.

2.8 Data processing

As described in **section 2.6** that response of the detector is proportional to number of C-H bonds therefore identical amounts of ethane, propane and butane would not give equal area count response. There are two main methods of determining quantitation (i) peak area and (ii) peak height as shown in **Figure 2.15**.
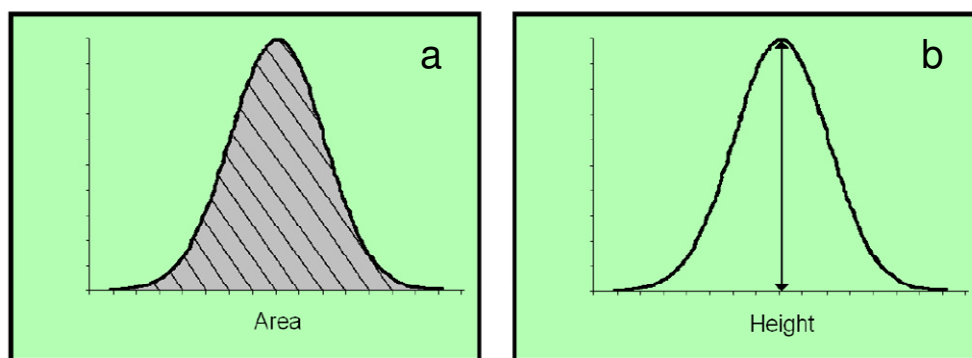
Figure 2.15: Representation of (a) peak area and (b) peak height (McShane, 2011).

Which is a better representation of quantity of analyte- peak area or peak height? This question has got a considerable attention (Miller, 1987). The first question is which one can be more accurately determined? In general terms manually, there are more chances of errors in making area measurements manually as compared to peak height measurements. With the development of electronic methods and good computer software, area measurements are now however as accurate as height measurements. The type of detector (concentration sensitive or mass sensitive) used for particular application is equally important in choosing one of the methods of quantitation. As discussed in earlier section, FID is a mass sensitive detector so any change in mobile phase flow will produce an error in peak height; therefore peak area measurements are preferred over peak height. A study among fifty laboratories found that the choice depends on the quality of the

chromatographic separation (Miller, 1987) for good separations, peak areas were as good as or better than peak heights, but for poorer separations (overlapped peak) peak heights were better. In summary, peak area is the preferred measurement especially if there are any changes in chromatographic conditions that can cause changes in peak height or peak width but not area. However, peak height measurements are less affected by overlapping peaks, noise, and sloping baselines (Miller, 1987).

In order to determine peak area or peak height, the crucial boundary is baseline. The process of measuring peak areas consists of integrating the area under the peaks. The integration can be performed automatically or manually. The error associated with manual integration is at least 2% (Miller, 1987). By using electronic or computer methods, not only the peaks with poor chromatography are handled quantitatively but also the error associated with it is reduced to 1%. At the same time the operator needs to review the integration done by the electronic integrator thoroughly and correct poor integrations manually by using integration events. In addition to software sold with GC systems, there are various commercially available chromatography software packages, for example GCWerks software (GCWerks, 2011).

The peak detection algorithm in automatic integration software is based on two parameters (i) peak width (PW) and (ii) peak threshold (PT). The PW setting control distinguishes peaks for baseline chromatographic noise. The PW is set to the approximate width at half height of peaks in the chromatogram. Small peaks much narrower than PW are smoothed out as noise. The best setting for the PW should be chosen in such a way that noise is not mistaken as a peak when peaks are very small. The other important parameter in peak detection is the PT. It is a noise rejection parameter. Peak detection based on the monitoring of the slope of the changing signal if slope is positive and equal to or greater than the threshold value then integration starts as it is shown by S (Braithwaite and Smith, 1985)

whilst negative slope equal to or less than the threshold indicate peak termination mark shown by E in **Figure 2.16**.

A higher threshold value usually results in fewer accepted peaks than a lower threshold value or selecting too low threshold results integration of background noise or simply speaking the peaks that do not rise above the threshold value are not integrated. The optimum setting will be low enough to trigger the start of the peak when the signal just barely exceeds the noise but high enough to prevent the noise from being mistaken for a peak. That is the threshold value should be low for small, wide peaks and higher for large, sharp peaks.
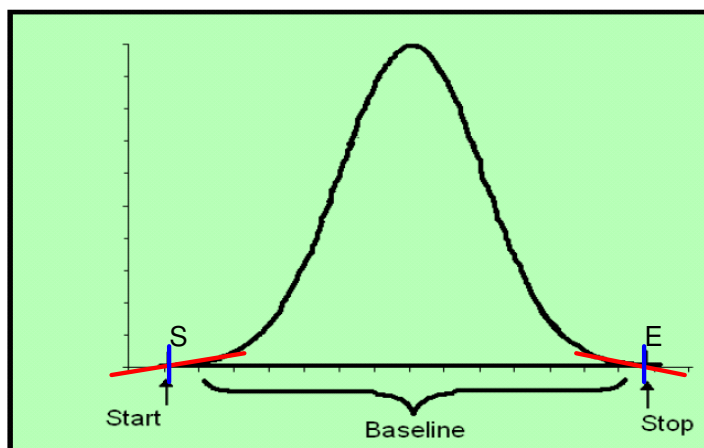
Figure 2.16: Peak detection based on slope monitoring. if slope is positive and equal to or greater than the threshold value then integration starts shown by S whilst negative slope equal to or less than the threshold indicate peak termination mark shown by E .

Despite the commercially available chromatography software, most of the research groups (Plass-Dulmer et al., 2002)) still prefer to use manual integration as overlapping or relatively small peaks cannot be handled automatically. Each peak in current work is manually processed throughout all campaign data. The error associated with integration has been discussed in next section.

2.9   Standards and calibration

During the study period, a gravimetrically prepared standard of 30 hydrocarbon species in nitrogen was used as a primary calibration. This was supplied by the National Physical Laboratory (NPL Teddington, United Kingdom, purchased in 2009, NPL'09 cylinder number D641613) having mixing ratios in the range of approximately 4 ppb with a quoted uncertainty of 0.08 ppbv for each compound (app 2%). It was used for peak identification, establishing response factors and finally quantifying the ambient air samples.

The response factor (RF) for each compound in a particular standard is calculated by dividing the detector response (peak area=A) by the mixing ratio (MR) of that particular compound in the gas standard (RF=A/MR). These response factors are further used to calculate the mixing ratio for each gas in the ambient air samples. The system was regularly calibrated by running standards before and after ambient air sample runs. The precision of analysis was determined by running 5 consecutive standards and it was less than 1% up to toluene and within 3% for compounds having carbon number higher than C_7.

While dealing with a long-term data set (as discussed in chapter 5) and reporting mixing ratios according to appropriate data quality requirements, it becomes a necessity to check the consistency of response factors for each compound present in the standard throughout the study period. This work also takes into account the flow through each column to precisely calculate a value for the peak area/ppb/ml, a useful check on the system to identify changing efficiency of the trapping material. The flow through each column was deduced by observing the amount of benzene eluting through each column in order to calculate the split ratio between columns.

117

Figure 2.17 illustrates the area/ppb/ml for each calibration data point for selected compounds.
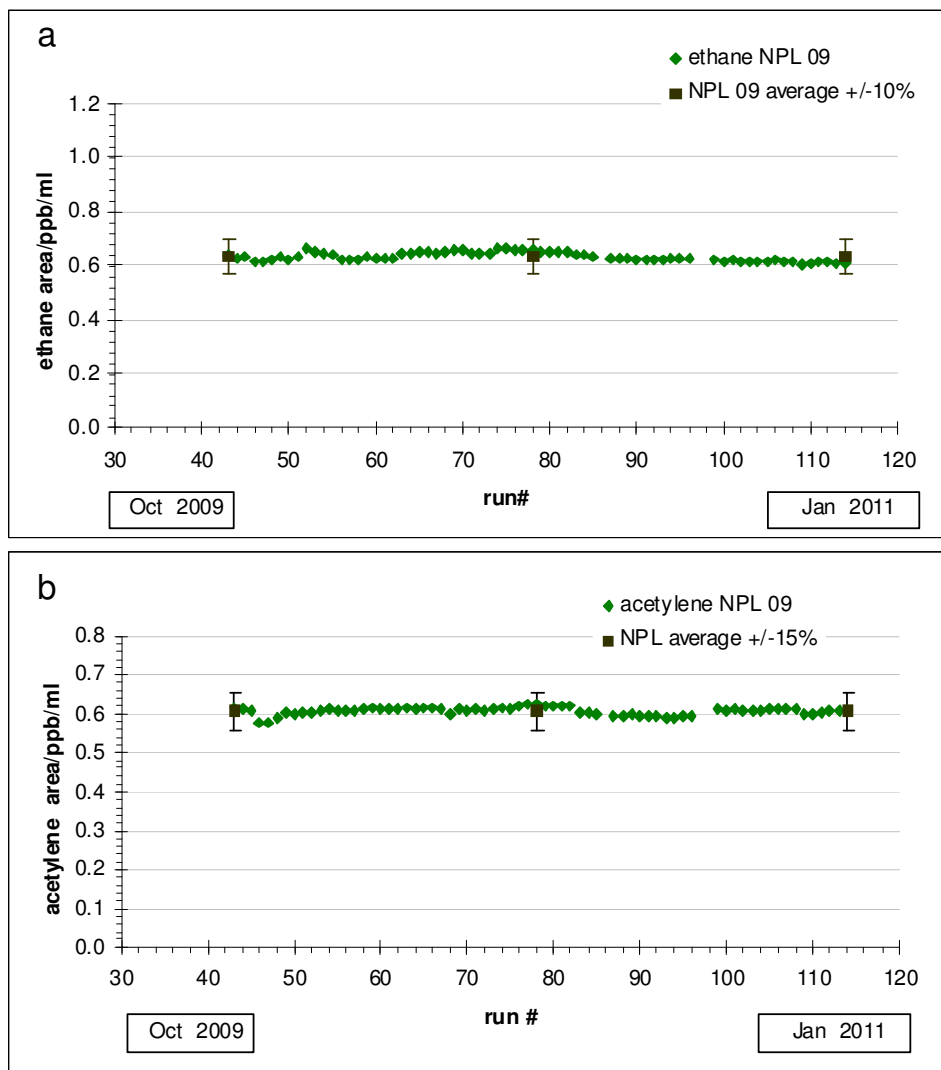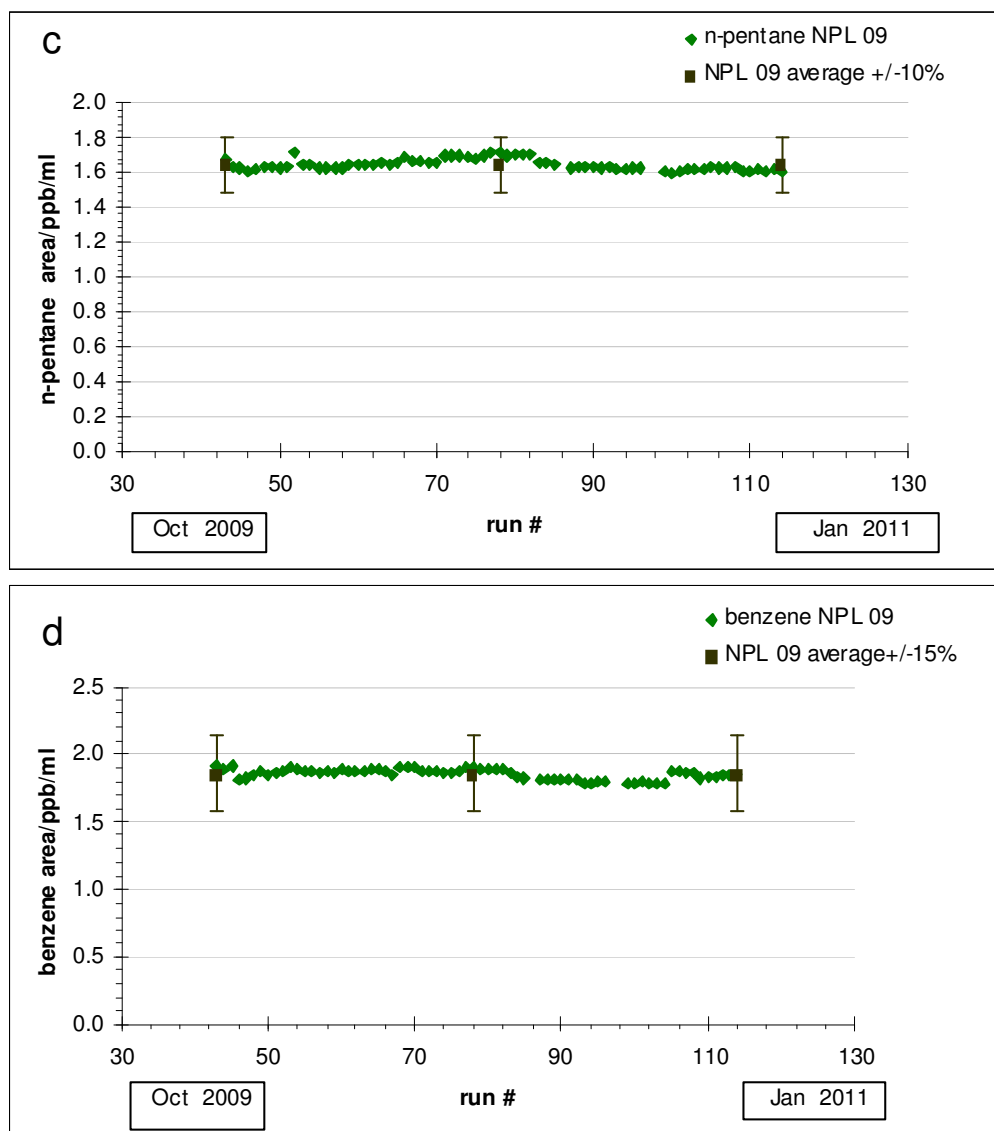
Figure 2.17: Area/ppb/ml for (a) ethane (b) acetylene(c) *n*-pentane and (d) benzene calculated from laboratory standard NPL 09 analyzed during the study period (2009-2011). The error bars, depending on the type of compound, around the average response factor are also shown according to the WMO GAW data quality objectives (DQOs) guidelines for acceptable uncertainties for each compound(DQOs are as follows :ethane and n-pentane: accuracy 10%, precision 5%; acetylene: accuracy 15%, precision 5%; benzene: accuracy 15%, precision 10%). These plots are plotted from the data analyzed by the York FGAM dual channel gas chromatograph.

The consistency among the data points confirms the nearly constant response factor of these compounds expressed per ml of sample gas on column

119

irrespective of the total flow passing through the each column over this period. The error bars around the average responses represent the acceptable limits of precision as defined by the WMO GAW World Calibration Centre for VOCs (WCC-VOC) and vary depending on the type of the compounds. The limits for uncertainty for GAW-VOC target compounds have been defined by the WMO GAW World Calibration Centre for VOCs (WCC-VOC) and are available in report number (GAW Report No 111, 1995). The measurements for NPL 09 are within these limits throughout the study period as illustrated in the figure.

In addition to the area/ppb/ml check, the per carbon response factors (PCRF=RF/ number of carbon atoms) (Baker et al., 2010) provide an additional check to monitor the changes in the detector sensitivity, instrument overall performance and stability of the compounds in the calibration standards over this time period. These are shown for all of the compounds in **Figure 2.18**. As a part of the quality assurance (QA) procedures involving exchanging calibration cylinders and inter comparison with GAW analytical laboratories, **Figure 2.18** also includes the PCRF from the official audit gas standard (NPL-GAW 28 components mixture) and NPL gas standard from Cape Verde (CV) Atmospheric Observatory supplied in 2008 (NPL08 CV, 30 component mixture) in addition to the PCRF from the laboratory standard (NPL09). The data points corresponding to the PCRF for NPL09 in this plot is an average for duration of eight months (Sep 2009 to April 2010) and nine months (May 2010 to Jan 2011). The consistency between averaged PCRF for each period further confirms the stability of the standard as well as the instrument performance. The WMO Audit gas standard (NPL GAW 28 components) also compares well with the laboratory gas standard (NPL 09, 30 components). The difference between NPL 2008 CV standard and NPL 09 is approximately 5% despite the nearly identical operating conditions. Whilst a greater difference than one would hope to see, this falls within the 5% gravimetric uncertainty quoted by NPL. Since the offset exists for nearly all VOC species deviation arising from gravimetric preparation would seem plausible.
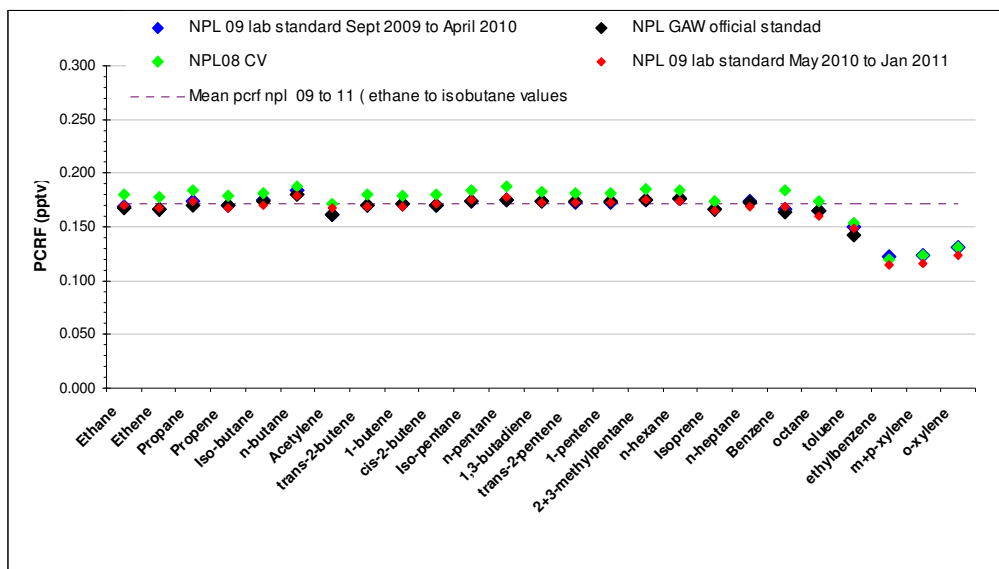
Figure 2.18: Comparison of per carbon response factor (PCRF) for laboratory standard 30 component NPL 09 with audit standard 28 component NPL GAW and NPL 30 component from Cape Verde Atmospheric Observatory. The data points corresponding to the PCRF for NPL 09 in this plot are an average for certain durations of eight months (Sep 2009 to April 2010) and nine months (May 2010 to Jan 2011). The dashed reference line is drawn for a guide by taking mean of PCRF for compounds from ethane to octane over the two year study period. This plot is from the data analyzed by the York FGAM dual channel gas chromatograph.

The most noticeable feature of this plot is that in all gas standards, the PCRF is nearly same up to benzene and then onwards it starts declining. The decreasing responses of heavier weight species point to potential losses through the transfer lines within the system, or non-linear carbon responses for aromatic compounds in an FID. Thorough flushing of transfer lines and regulators to ensure equilibration of gas mixtures with surfaces is known to be of utmost importance in order to achieve reproducible results. A recent intercomparison exercise within Aerosols, Clouds, and Trace gases Research Infrastructure Network (ACTRIS VOC network) adopted new Standard Operating Procedures (SOPs) for flushing the regulator and keeping transfer lines and pressure regulator pressurised with the standard for at leas a 24 hours equilibration period. This was thought to be an important advance, especially for heavier weight species and will be adopted in all future calibration analysis.

An anomalously high response for acetylene has been an issue among various research laboratories (Apel et al., 1994;Baker et al., 2010). However, as demonstrated from our results, the PCRF for acetylene in above figure is 5% lower in all gas standards than that of ethane and ethene compounds having same carbon numbers. It is regarded as the most potentially unstable compound in the standard in addition to isoprene, 1,3-butadiene and isomers of trimethylbenzene (Plass-Dulmer et al., 2002). It can be seen from **Figure 2.11** that breakthrough volume for acetylene is much higher than the sampling volume for this study which rules out the cause of lower response. This lower response can be explained in terms of the effective carbon number concept (ECN) (Sternberg et al., 1962;Dietz, 1967), according to which the response (peak area) of the FID is proportional to the number of molecules times the effective number of carbon atoms per analyte molecule; for example 2 ppb of propane has the same integrated response as 1 ppb of hexane in a same sample volume. If other than hydrogen or carbon bonds occur, the response of the respective carbon atom is adjusted to yield an effective carbon number. On this basis the adjustments in acetylenic bond in acetylene yields effective carbon number equal to 1.6 as compared to effective carbon number equal to 2 in ethane. The ECN for acetylene for present results is higher by 0.3 than reported by previous study (1.3) (Sternberg et al., 1962).

The above figure (**Figure 2.18**) presents a simple and crude picture of PCRF to give an idea of how different species, having different number of carbon atoms, behave on this scale with respect to each other. In order to get the finer details of PCRF variation on a monthly basis and to verify the uniformity of response for hydrocarbons containing the same number of carbon atoms but different class of compounds (Russo et al., 2010), the PCRF of C_2 to C_4 has been compared with their corresponding unsaturated compounds as shown in **Figure 2.19**.
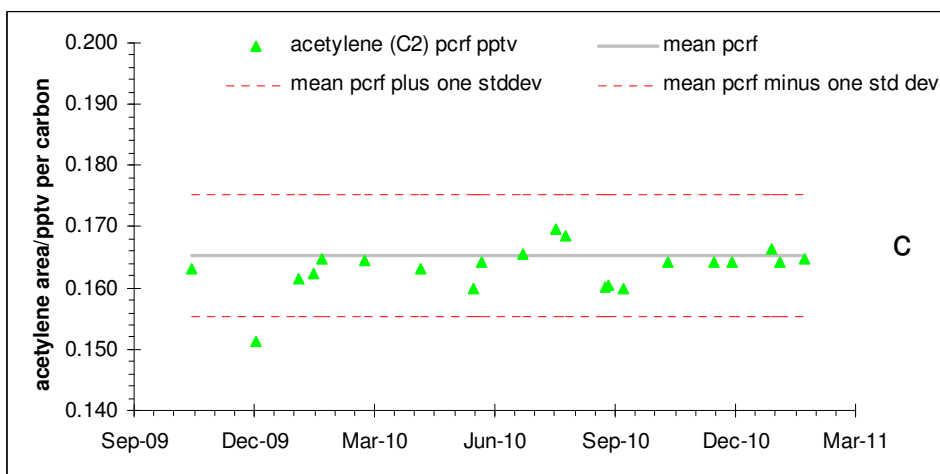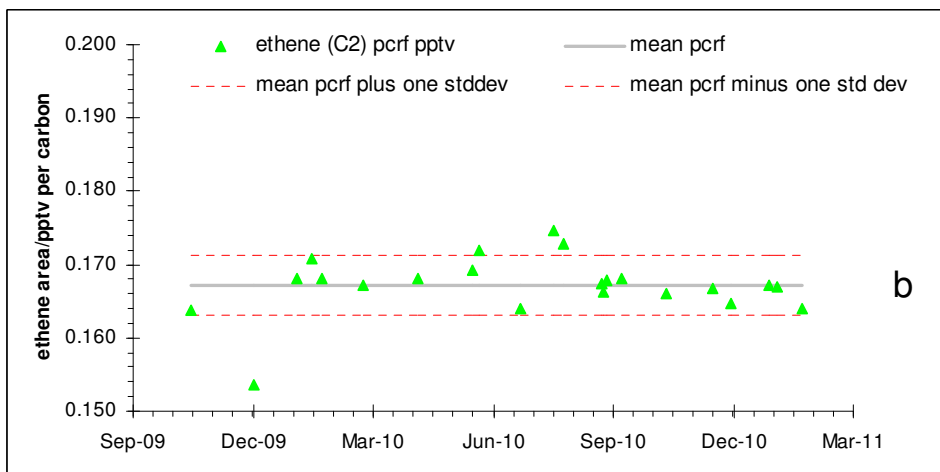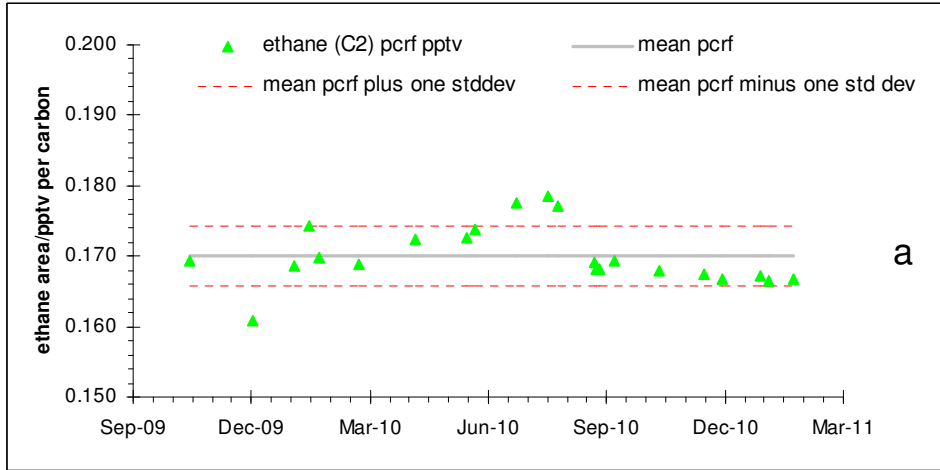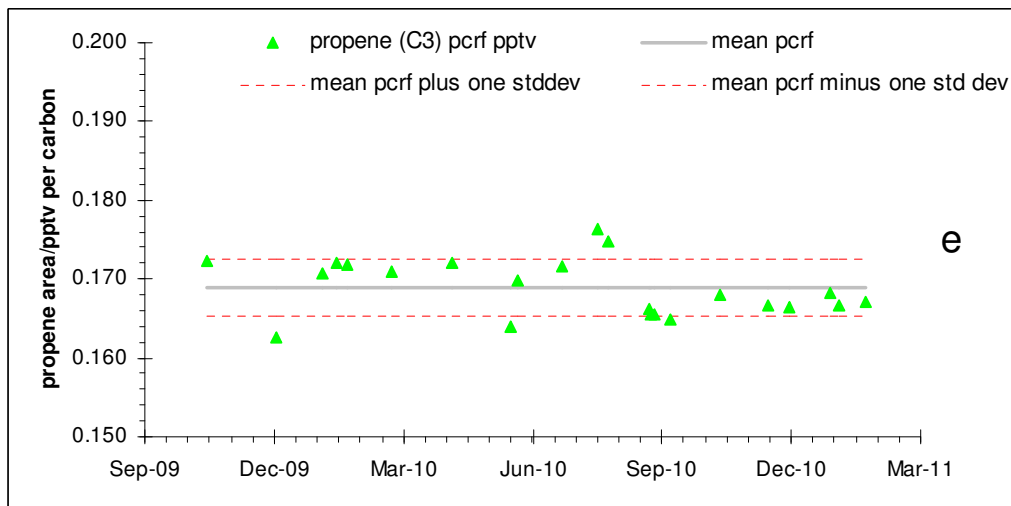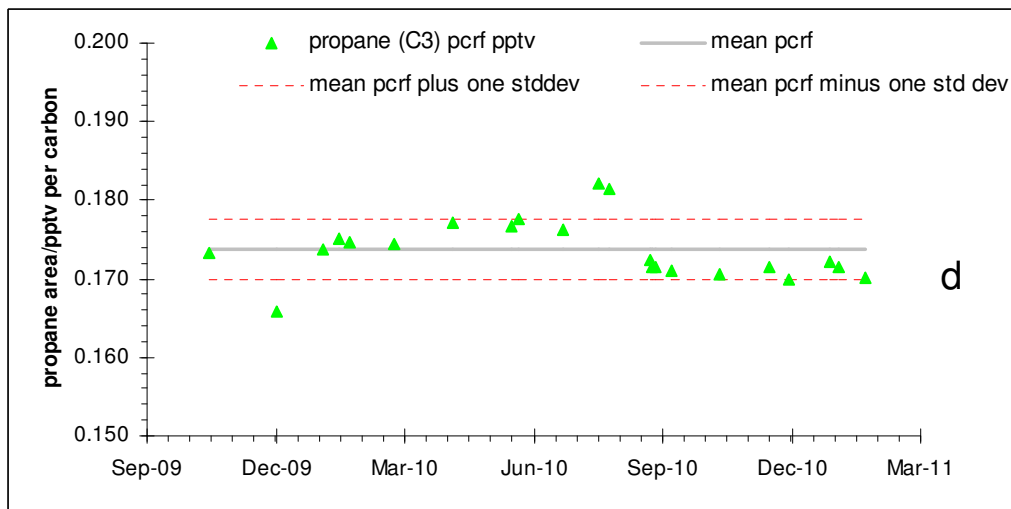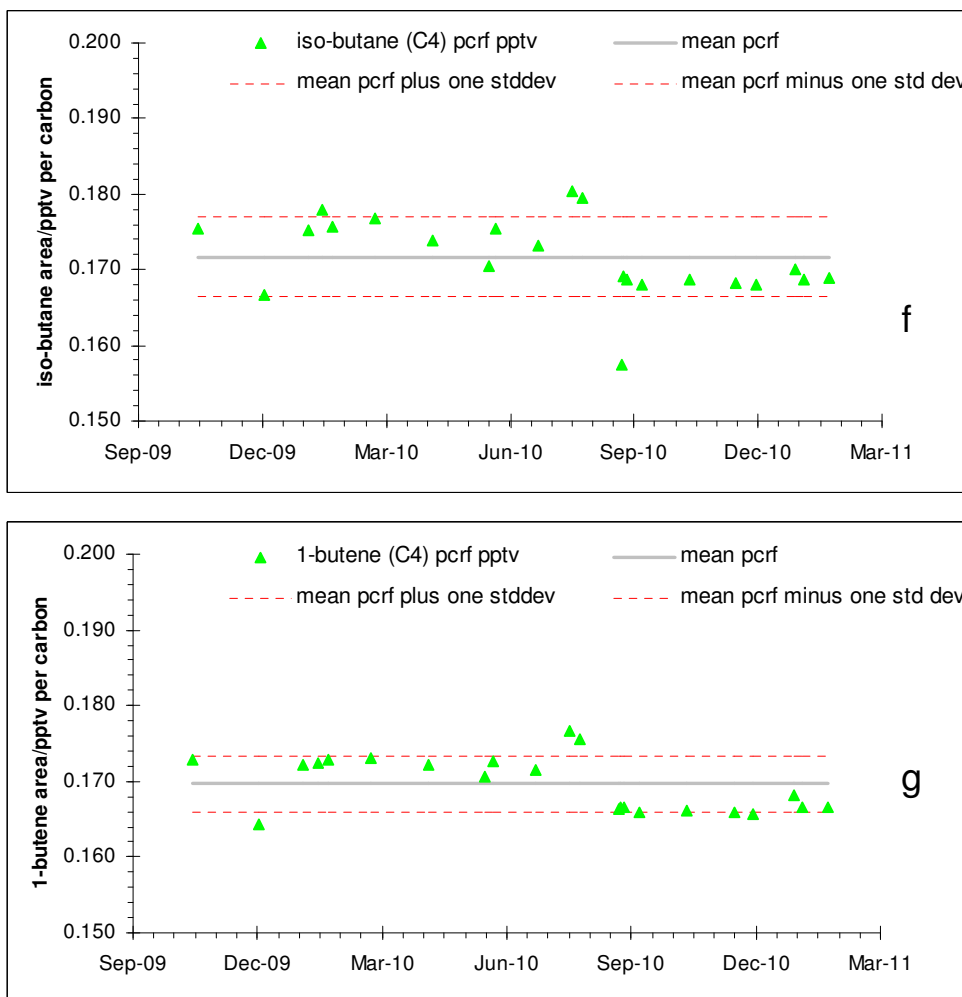
Figure 2.19: Per Carbon Response Factor (PCRF) monthly for (a) ethane, (b) ethene, (c) acetylene, (d) propane, (e) propene, (f) *iso*-butane, and (g) 1-butene in laboratory standard 30 component NPL 09 gas standard analysed during study period Jan 2009 – Jan 2011. The solid and dashed lines passing through the individual points represent mean PCRF and mean PCRF ±1 standard deviation of the PCRF included in each plot respectively. These plots are plotted from the data analyzed by using the York FGAM dual channel gas chromatograph.

Figure 2.19 shows that there is some scatter about the mean PCRF, which is consistent for all compounds over this period. The response for ethene (mean + std deviation = 0.167 + 0.004) and acetylene (0.165 + 0.010) is 2% less than that of ethane (0.170 + 0.004). Likewise is the behaviour of propene (0.169 + 0.003)

and butenes (0.170 + 0.003) in comparison with their respective saturates propane (0.174+0.004) and butanes (0.172 + 0.005). Overall the responses of unsaturates are 2% less than their corresponding saturates but the consistency among compounds within saturates and unsaturates is very good.

In all these plots, the one observation with a low PCRF, corresponding to a December month, shows immediately an analytical problem during that period which could be due to changes in the detector sensitivity. Given the picture of generally very stable responses of each compound over the study period, it was decided to use an average response factor to quantify the mixing ratio of compounds present in ambient air samples, following suitable systems checks with standards. The measurement uncertainties in the VOC observations have been calculated by considering the integration uncertainties (2% to 60%) in addition to fixed uncertainties associated with the certified standard mixture (approximately 2%) and sampling volume measured by mass flow controller (5 %) (Hopkins et al., 2011).

Figure 2.20 shows few examples of real air chromatograms from a range of different environments (clean through moderate to polluted environment) analysed by dual channel gas chromatograph.
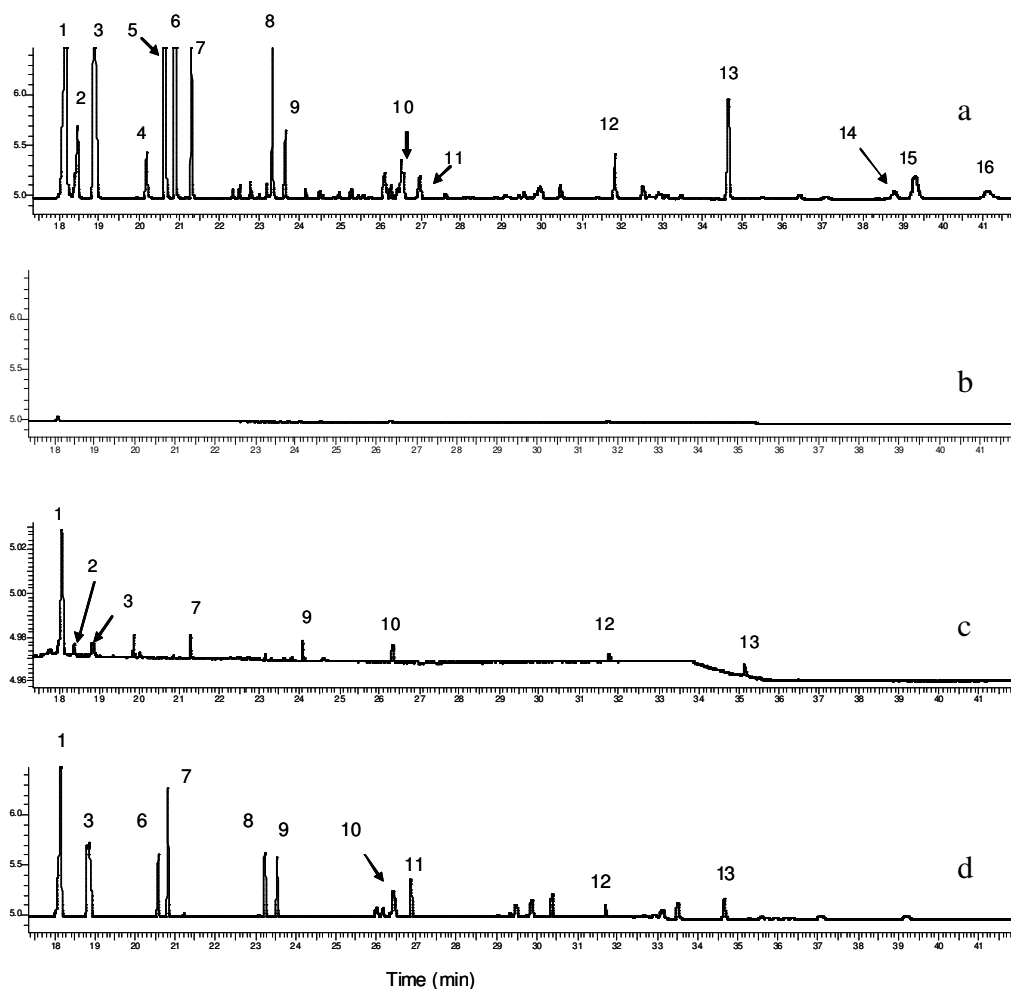
Figure 2.20: Example of real air chromatograms from different environments (a) very polluted sample from Elgin leaks. The Elgin platform is a gas/oil platform located in the North Sea at 240 km east of Aberdeen (Scotland) which provides the processing and control facilities to the Elgin-Franklin fields. The Elgin platform started leaking natural gas in March 2012, (b) background sample from the RONOCO campaign, (c) background sample chromatogram in zoom mode, and (d) moderately polluted sample from ClearFlo campaign. These chromatograms are taken from the data analyzed by using the York FGAM dual channel gas chromatograph. The peaks are labelled as follows: (1) ethane, (2) ethene, (3) propane, (4) propene, (5) *iso*-butane, (6) *n*-butane (7) acetylene, (8) *iso*-petane, (9) *n*-pentane, (10) 2+3-methylpentane, (11) *n*-hexane, (12) benzene, (13) toluene, (14) ethylbenzene,(15) *m+p*-xylene and (16) *o*-xylene.

2.10 Feasibility study: The Entech preconcentrator

2.10.1   Introduction

The current instrument (Perkin-Elmer) configuration discussed so far is a result of the improvements over many years to be able to cover a wide range of C_2 –C_9 hydrocarbons and selected oxygenates; however, the outdated components which have no direct replacement parts were a major motivation to update the system. The Entech preconcentrator system (7150) with auto sampler (7500A) was coupled with an existing Agilent 6890 gas chromatograph with the same column-set as the existing dual channel GC system. The ability of the Entech preconcentrator system to recover heavier weight (C_{12} to C_{25}) VOCs quantitatively and the use of an on-line water removal trap, instead of a large cold standalone trap used prior to preconcentration, were other reasons for testing this system.

The Entech preconcentrator involves three stages to trap heavier weight compounds along with the lighter weight compounds in addition to including on-line water removal system. The first stage uses an Active Solid Phase Micro Extraction (Active SPME) trap 1 to allow compounds from C_{12} to C_{25} to be trapped and recovered quantitatively without exposure to adsorbents or water removal steps as shown in **Figure 2.21**a solid-phase microextraction is a technique in which a fused silica fibre coated with a non-volatile polymer is used to extract organic analytes directly from the headspace above the samples. The analytes partition between the fibre and the headspace compounds. The classical SPME utilizes passive diffusion to collect or partition headspace compounds onto a coated filament and depending on the varying diffusion rates of compounds and coating affinities, the time required for each analyte to come to equilibrium with a SPME filament is different which leads to the SPME method being considered only a qualitative approach. However, the Active SPME utilizes a polydimethysiloxane (PDMS) coating that is similar to most SPME filaments, but places this coating into a precise actively swept flow path allowing

a known volume to be collected for quantitative measurements. As this stage comes before the water eliminating (second stage) and adsorbent steps (third stage) this means that these heavier weight compounds are not exposed to the cold trap (trap 2) and adsorbent trap (trap 3) and hence their recovery is quantitative. Moisture and lighter analytes are not trapped in this stage and pass through a CO_2 cooled water trap maintained at -30 °C, where water is removed by a direct vapour/solid transition which prevents the loss of water soluble compounds. Finally, the fraction of light weight VOCs is collected onto a CO_2 cooled Tenax trap at -40 °C.

Once the trapping and water elimination steps are completed, the water trap is baked out above the boiling point of water and flushed to the vent as shown in **Figure 2.21**b. Trap 1 and Trap 3 are maintained at their trapping temperatures during this process, allowing compounds of interest to remain intact while water is being eliminated. The next step involves the cooling of SPME to -50 °C to allow VOCs to refocus as they are transferred back from trap 3 to trap 1 (**Figure 2.21**c). Once the VOCs are refocused onto the active SPME trap along with the heavier weight compounds, they are injected onto the GC column at high temperature (**Figure 2.21**d).

(a)
Trapping

First stage

Active SPME trap

Second stage
Cold water trap

Third stage
Cold Tenax trap

Volume measurements
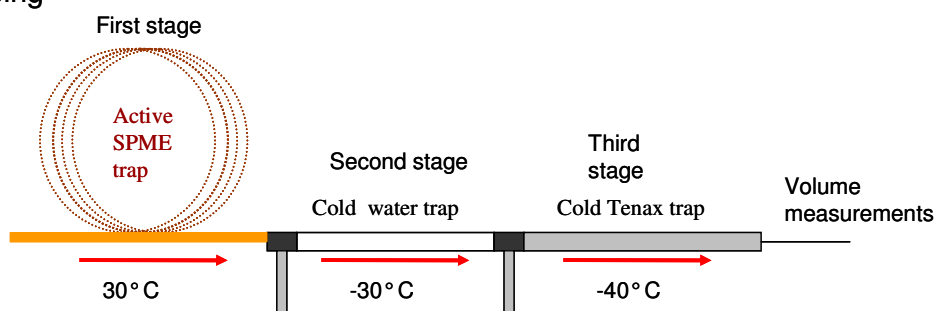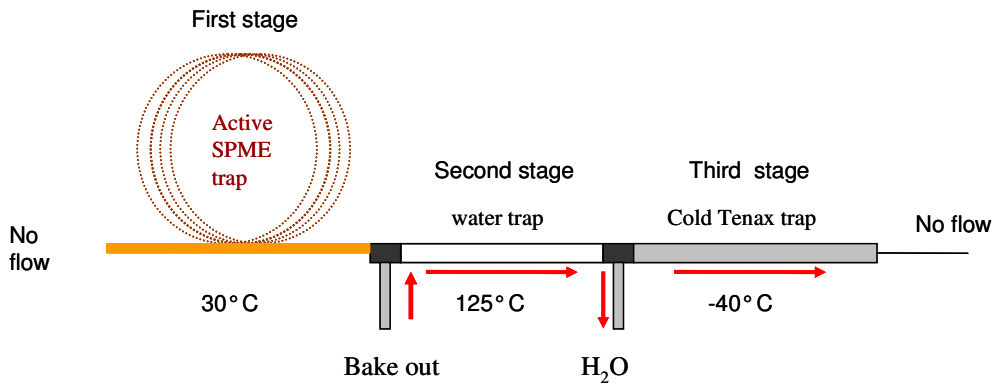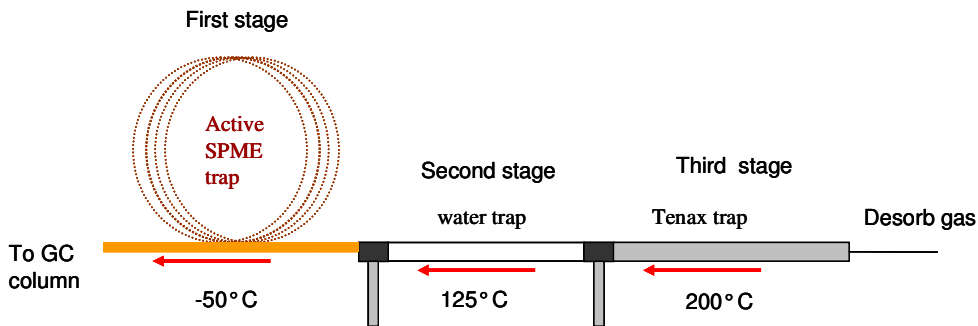
30° C   -30° C   -40° C
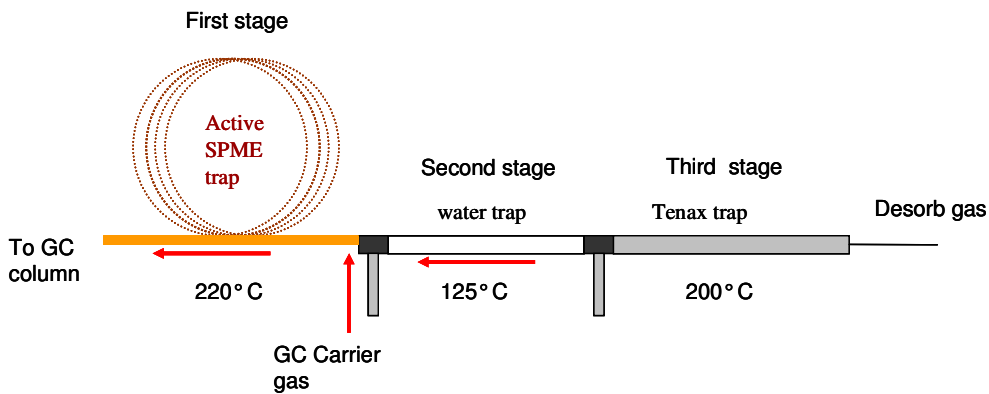
Figure 2.21: Three stage preconcentration by using three traps: Active SPME trap (trap 1), water trap (trap 2) and Tenax trap (trap 3) (a) Initial trapping of C_{12} to C_{25} heavier weight compounds on trap 1, water vapour/solid transition on an empty silonite coated trap 2 and trapping of C_2 to C_{10} compounds on trap 3. (b) Trap 2 is baked out while trap 1 and trap 3 are their trapping temperatures (c) Trap 1 is cooled to -50 °C to refocus VOC compounds as they are transferred back from trap 3 to trap 1. (d) Sample injection to the GC column.

2.10.2   Experimental

2.10.2.1   The current Perkin-Elmer GC-FID system and reference chromatogram

In order to compare the chromatograms obtained during different developing stages of method on the Entech preconcentrator system, here a reference chromatogram obtained from an NPL standard analyzed on the Perkin-Elmer system is shown in **Figure 2.22**.
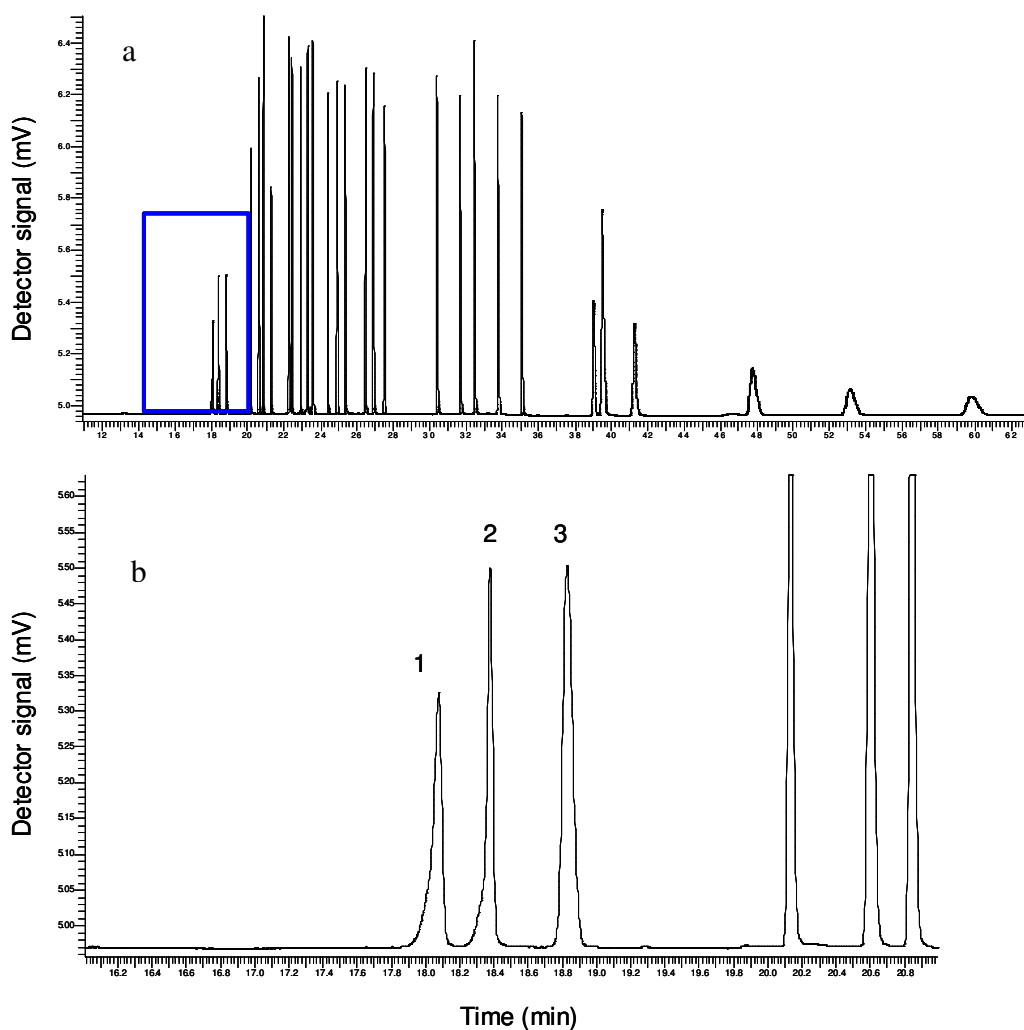
Figure 2.22: A chromatogram obtained as a result of separation of C_2 –C_9 compounds on an alumina - PLOT column by using an NPL standard on the Perkin-Elmer GC-FID system (a) full chromatogram, ethane (1), ethane (2) and propane (3) peaks are highlighted and further zoomed and shown in lower panel (b) the lighter weight compounds are zoomed to have an idea of the separation on the existing system.

For the sake of convenience while comparing the parameters between the two systems, a brief summary of measurement procedures adopted on the Perkin-Elmer system is as follows: after water removal step, the sample is collected onto a dual-bed adsorption trap (containing Carboxen 1000 and Carbotrap B), held at -23 °C, at a flow rate of 100 ml min^{-1} for 10 min (sampling volume 1000 ml). After sampling the trap is left cold and flushed with helium for 3.5 min before being heated to 350 °C during desorption onto the columns (50 m alumina-PLOT column and 10 m CP-LOWOX column). The oven is programmed as follows: 40 °C for 3.5 minutes and then heats at 13 °C min^{-1} to 110 °C followed by 8 °C min^{-1} to 200 °C. The carrier gas helium flow is 20 ml min^{-1} through each column until 33.5 minute and then after this time it is increased to 40 ml min^{-1} to let the heavier weight compound elute from the system rapidly.

2.10.2.2   The Entech preconcentrator and method development

Since the Entech preconcentrator involves three stages for trapping, it is a little more complex than a single stage trapping system in terms of changing parameters to develop a suitable method. It was also recommended in the manual (Entech Instruments Inc, March 2010) not to change more than 1-2 parameters at one time while trying to develop or improve upon the method. The following table (**Table 2.1**) summarises the list of parameters that were changed in order to improve the separation and resolution of compounds of interest. The 'T1 desorb time' in table indicates the time to transfer the samples onto the column when T1 is rapidly heated at 200 °C, whilst the T3 to T1 transfer time indicates the time to transfer the light weight compounds from trap T3 to T1 during refocusing step. The experimental work discussed under the following headings includes the use of an NPL multi-component gas standard.

Table 2.1: A list of parameters used during method development stages. The T1 desorbtion time indicates the time to transfer the samples onto the column while T1 trap is rapidly heated at 200 °C. The T3 to T1 transfer time indicates the time to transfer the lighter fraction of VOCs from T3 to T1 during refocusing step.

file name	T1 desorb time (min)	GC carrier flow (ml min^{-1})	T3 – T1 transfer time (min)	oven isothermal time (min) (40 °C at start of run)
"ANATUNE" .030	1.5	20	3	3.5
"ANATUNE" .031	1.0	20	3	3.5
"ANATUNE" .036	0.5	20	3	3.5
"ANATUNE" .037	1.0	10	3	3.5
"ANATUNE" .038	1.5	10	1.5	3.5
"ANATUNE" .039	1.5	15	3	3.5
"ANATUNE" .040	1.5	15	3	2

2.10.3   Chromatographic separation

2.10.3.1   The effect of reduced desorption time

It can be seen from **Table 2.1** that for the files 30, 31 and, 36, the T1 desorption time is being reduced by 0.5 minute keeping all parameters constant**.** The chromatogram from file 30 (desorption time 1.5) has unresolved ethane and ethene peaks with a rise in the baseline at the start of the run which is indicative of changing carrier gas flow as the system stabilise after injection.
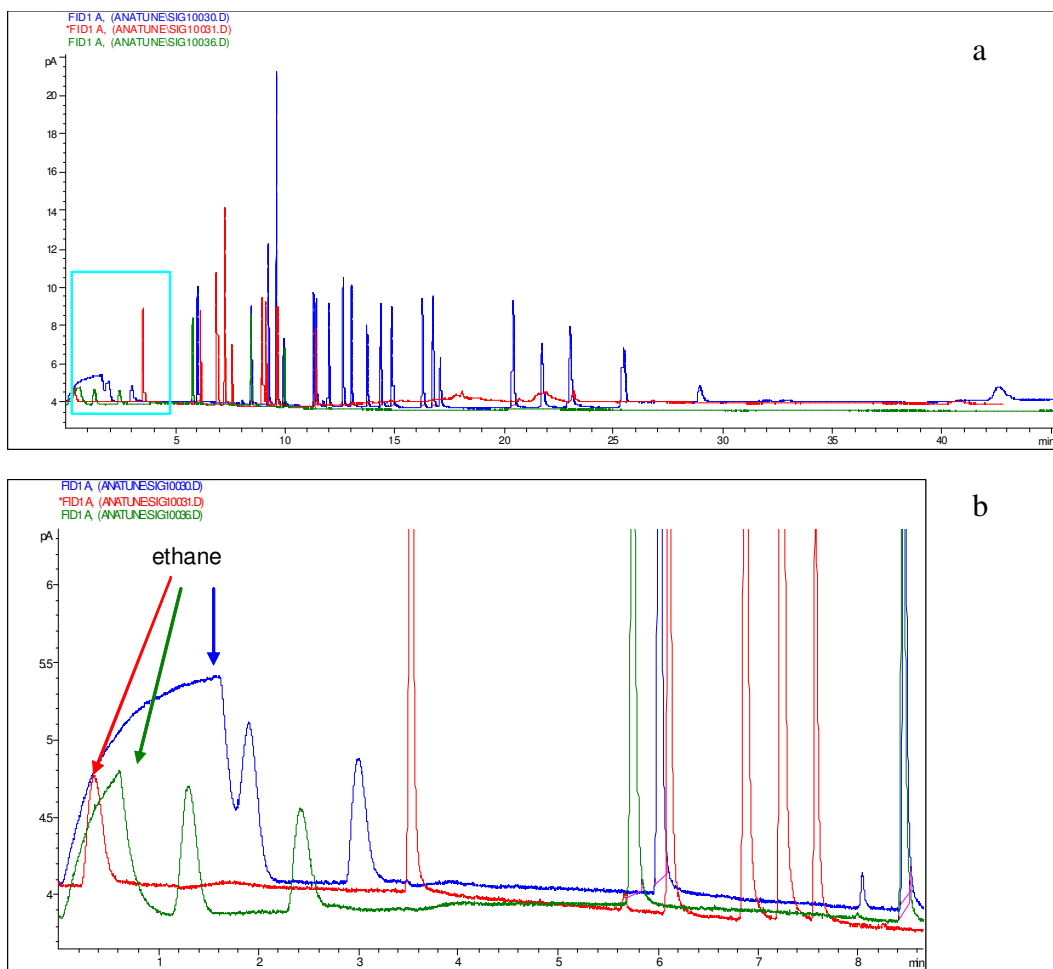
Figure 2.23: The effect of reduced desorption time. The chromatograms obtained from the analysis of a reference standard are from files 30 (blue), 31(red) and 36 (green). (a) Full scan (b) the lighter weight compounds in zoom mode. T1 desorption time for 30, 31 and 36 files is 1.5, 1.0 and 0.5 respectively. By reducing T1 desorption time from 1.5 to 1.0, the ethane peak was better resolved along with other lightweight compounds; however, some of the heavier weight compounds were lost.

As T1 time is reduced to 1.0 in file 31, the ethane peak is better resolved with other lightweight compounds; however, some of the heavier weight compounds were lost. The reason for missing heavier weight compounds seems to be the reduction in T1 desorb time which means that compounds are not fully desorbed from T1 trap to GC columns during injection. As the transfer time from T3 to T1 is same in all three cases which rules out the insufficient desorption of heavier weight compounds while transferring from T3 to T1 stage. This led us to change

the parameter related to reducing the T3 to T1 transfer time, keeping T1 desorption time unchanged as shown under the next heading.

2.10.3.2 Change in T3 to T1 transfer time
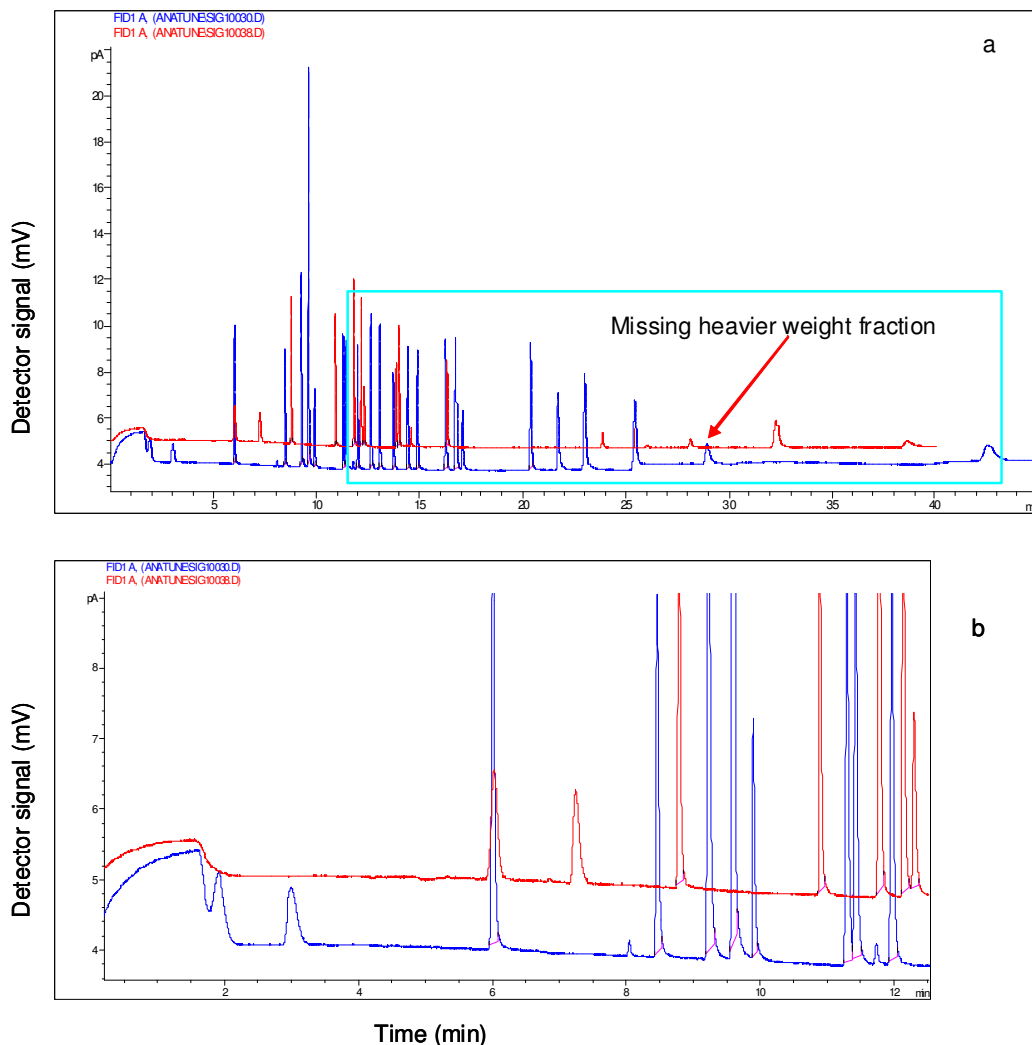
Figure 2.24: The effect of reduced T3 to T1 transfer time. The chromatograms obtained from the analysis of a reference standard are overlaid and are from files 30 (blue) and 38(red). (a) Full chromatogram showing the missing heavier weight fraction in chromatogram obtained from the analysis of file 38, (b) the lighter weight compounds in zoom mode indicate that reduced transfer time is not helpful in getting desired separation.

As it can be seen from the **Figure 2.24**, that keeping T1 desorption time the same (1.5 minute) and reducing T3 to T1 transfer time from 3.0 to 1.5 did not help in getting heavy weight compounds onto the column. The chromatograms obtained from the analysis of a reference standard are overlaid in following figure and are from files 30 and 38. The T3 to T1 transfer time for files 30 and 38 is 3.0 and 1.5 minutes respectively.

2.10.3.3   Effect of reduced carrier gas flow rate

Both parameters discussed above were primarily focused to improve the refocusing stage prior to injecting the sample onto the GC column. By altering both parameters (T1 desorption time and T3 to T1 transfer time), it was difficult to achieve a whole range of compounds with a good separation. In order to get a better separation of light weight compounds along with the presence of heavier weight fraction, the next focus was to increase the retention time either by changing the carrier gas flow or by changing the column temperature as discussed under the next heading. By reducing the carrier gas flow from 20 ml min^{-1} to 10 ml min$^{-1,}$ keeping all the parameters constant, the retention time was increased. This helped in getting improved resolution of ethane, ethene and propane peaks, but again the heavier weight compounds were missing. As it can be seen from **Figure 2.25** illustrating the overlaid chromatograms obtained from the analysis of files 31 and 37. The column flow for files 31 and 37 is 20 ml min^{-1} and 10 ml min^{-1}, respectively.
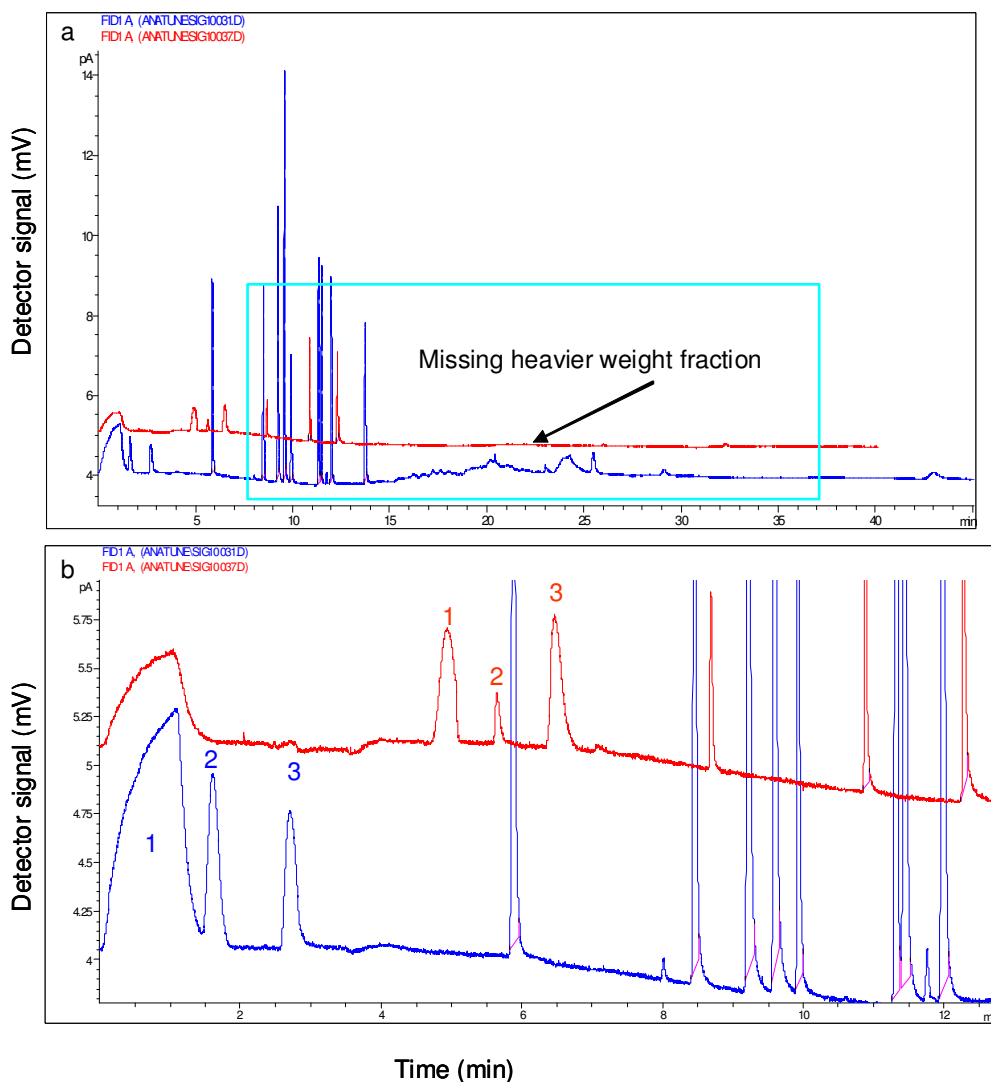
Figure 2.25: The effect of reduced carrier gas flow rate. The overlaid chromatograms are obtained from the analysis of a reference standard and are from files 31 (blue) and 37 (red) (a) Full scan (b) The carrier gas flow rate for 31 and 37 files is 20.0 ml min^{-1} and 10.0 ml min^{-1}, respectively. The ethane, ethene and propane peaks are now better resolved with longer retention time but again heavier weight compounds are missing.

2.10.3.4   Change in oven programming

The temperature of the column is another way of controlling the retention times. By changing the T1 desorption time and T3 to T1 transfer time parameters, it was clear that the optimum setting was to keep T1 desorption time to 1.5 minute and T3 to T1 transfer time of 3.0 minute to achieve the separation of heavier weight compounds. The following **Figure 2.26** shows the overlaid

137

chromatograms obtained from the analysis of a reference standard and are from files 39 and 40.
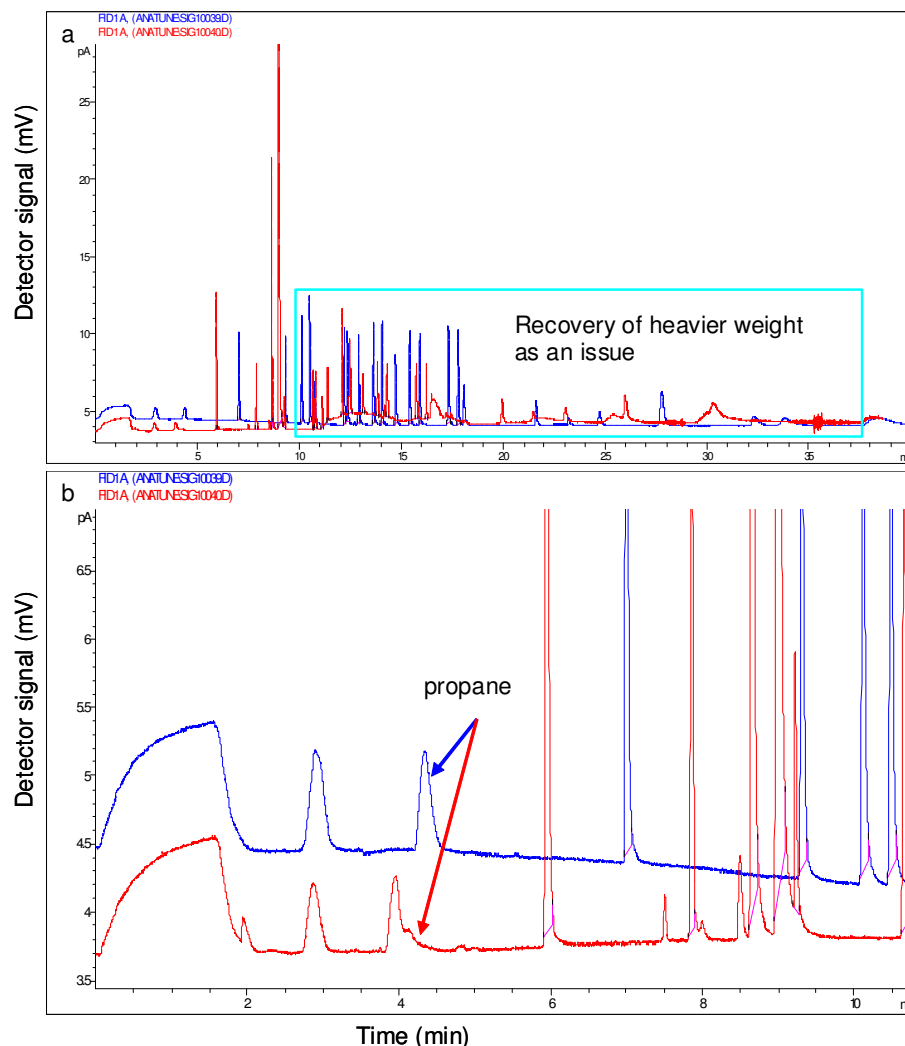
Figure 2.26: The effect of change in oven programming. The overlaid chromatograms are obtained from the analysis of a reference standard and are from files 39 (blue) and 40(red) (a) Full chromatogram (b) The initial isothermal temperature of 40 °C is maintained for 3.5 minutes after the injection of the sample to allow for some focussing of the heavier molecular weight species (file39) whilst in chromatogram obtained from the analysis of file 40 has an initial isothermal temperature of 40 °C maintained for 2.0 minutes. As a result of reducing time for the initial isothermal temperature, the retention time is lessened; however, the recovery of heavier weight fraction is still an issue.

Both chromatograms are a result of similar T1 desorption time and T3 to T1 transfer time but a slight change in an oven programming. In chromatogram 39,

the temperature of column after injection is 40 °C for 3.5 minute and then ramping starts whilst for the file 40 the initial temperature of 40 °C is maintained only for 2.0 minutes. As a result of reducing the time of initial isothermal temperature, the peaks in chromatogram for file 40 are shifted towards shorter retention times; however, the recovery of heavier weight compounds is still an issue.

2.10.3.5   Tenax trap and breakthrough volume

To this point it was clear that with the change in a number of parameters, it was not possible to get a whole range of compounds (C_2-C_9) with a desired separation with the use of a Tenax trap. Either the Tenax trap was not suitable for trapping lighter weight compounds or there is a problem during refocusing stage when light weight compounds were transferred from T3 to T1 as C_2 compounds are not refocused. As the water trap, positioned in between trap T1 and T3, is an empty silonite coated tube, so the possibility of VOC loss during their transfer from trap T3 to trap T1 is minimised. To work out the efficiency of the trapping material, the Tenax trap was replaced with a dual-bed adsorbent trap (the same trap which was being used for the Perkin-Elmer system). To work out the problem at the refocusing step, some further tests were done by immersing the front section of column in a Dewar flask filled with liquid nitrogen. Although Tenax is the most widely used adsorbent due to its high temperature limit (350 °C) and high hydrophobicity (Dettmer and Engewald, 2003), its low specific surface area (30 m^2 g^{-1}) means that it is only suitable for trapping medium to high boiling compounds.

The breakthrough volume of the Tenax trap was found to be between 200 ml and 400 ml for ethane and acetylene as shown in **Figure 2.27** which is not suitable for samples with low atmospheric concentrations. Consequently the Trap 3 was replaced with a dual- bed (Carboxen 1000 and Carbotrap B) adsorbent trap in order to improve the breakthrough volume for C_2 species.
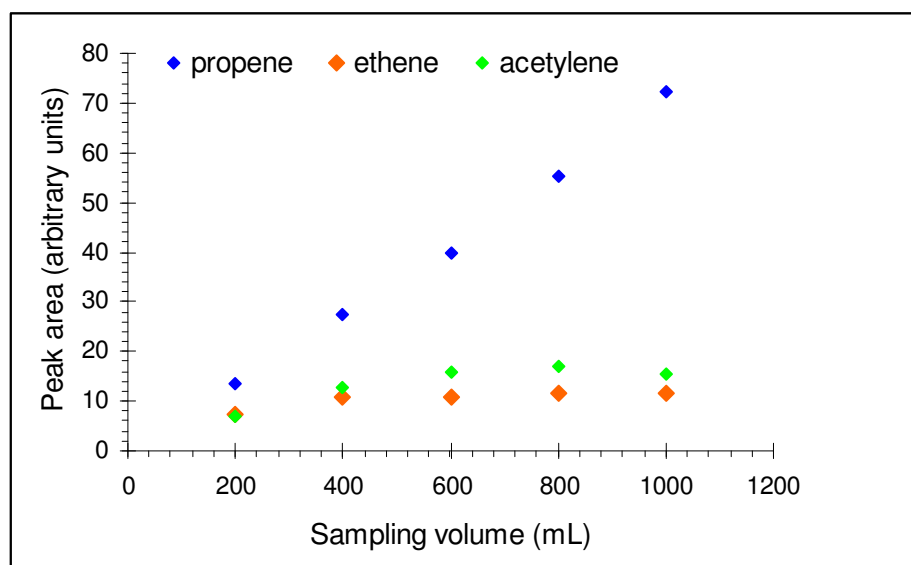
Figure 2.27: Peak area *versus* sample volume for C_2-C_3 hydrocarbons at -23 °C. The NPL 30 component standard sample was drawn through a Tenax at a flow rate of 100 ml min^{-1} maintained by mass flow controllers for a period corresponding to the required sample volumes.

2.10.3.6   Charcoal trap and method development

2.10.3.6.1   Use of liquid nitrogen to submerge front-end of column for 4 minutes

Although during the refocusing step the temperature of SPME trap is maintained at -50 °C whilst the compounds are being transferred from trap T3 to T1 during the refocusing step, to further improve the refocusing step, the front end of the column was submerged in a Dewar flask filled with liquid nitrogen for 4 min. **Figure 2.28** shows the overlaid chromatograms (file of date 2010/08/17 (blue) and 2010/08/19 (red)) obtained from the analysis of an NPL standard with the same transfer time from T3 to T1 but with a doubling of sample volume for file 2010/08/19. As can be seen from the figure, the separation for ethane and ethene is far from an ideal chromatogram and poor reproducibility is also obvious. This test suggested that the refocusing is not an issue with C_2 compounds.
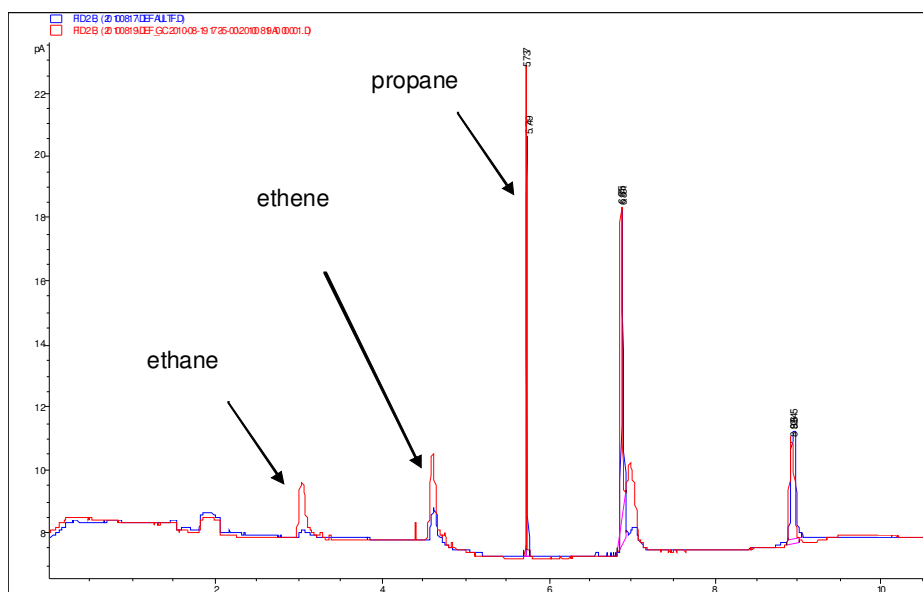
Figure 2.28: The effect of front section of column cooling in liquid nitrogen. The overlaid chromatograms are obtained from the analysis of an NPL standard from files 2010/08/17 (blue) and 2010/08/19 (red). The transfer time from T3 to T1 is same (2.0 min) for both case but the volume of sample is doubled for the file 2010/08/19. Despite the improvements with refocusing stage, the separation of ethane, ethene and propane peaks was not adequate and reproducibility was also poor.

2.10.3.6.2   Reducing T3 to T1 transfer time

As we saw in the previous section with Tenax trap, the reduction in transfer time did not help with the separation of light weight compounds; however, with a charcoal trap and by reducing the transfer time, a better separation for ethane, ethene and propane was achieved.

A comparison of chromatograms (10,11 and 19) obtained by reducing T3 to T1 transfer time from 2.0 to 0.5 minute on system analyzing the same reference standard cylinder is shown in **Figure 2.29**. The transfer time from T3 to T1 is 2.0 min for file 19, whilst for files 10 and 11, it is 0.5 minute. The sample volume for files 10 and 19 is 200 ml whilst for file 11 it is 400 ml.

141
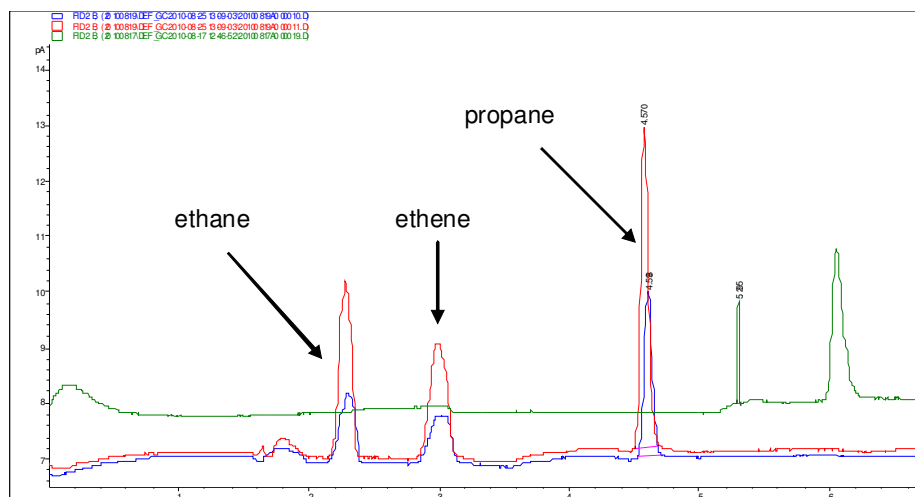
Figure 2.29: The effect of reducing the transfer time from T3 to T1 trap. The overlaid chromatograms are obtained from the analysis of an NPL standard from files 10 (blue) and 11 (red) and 19 (green). The transfer time fromT3 to T1 is same (2.0 min) for file 19 whilst for files 10 and 11 it is 0.5 minute. The sample volume for files 10 and 19 is 200 ml whilst for file 11 it is 400 ml. The reduction in transfer time helped in getting a proper separation of ethane, ethene and propane peaks. The intensity of the signal for files 10 and 11 is in accordance with the increased sample volume.

2.10.3.6.3   Validation of method

2.10.3.6.3.1   Reproducibility

In order to check the precision of the method, three consecutive samples from the same reference standard were analyzed. As it can be seen from the **Figure 2.30**, there is a good reproducibility among all three consecutive runs
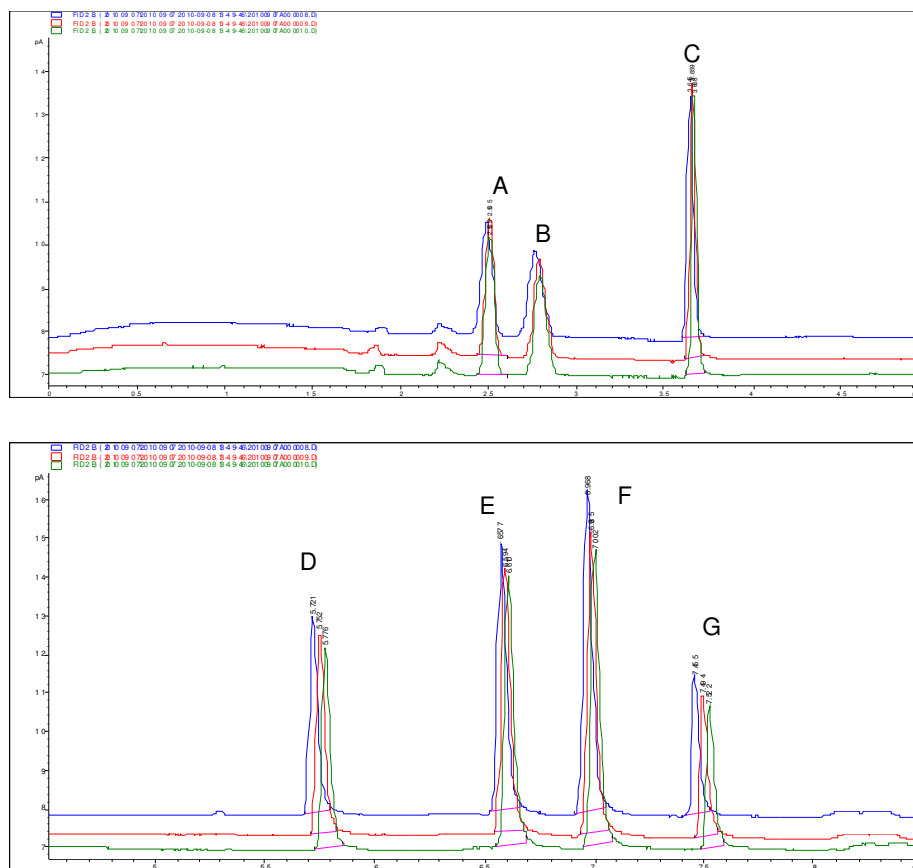
Figure 2.30: Reproducibility of three consecutive standard runs. The overlaid chromatograms are obtained from the files 8 (blue), 9 (red) and 10 (green). The peaks in upper panel are labelled as follows: ethane (A), ethane (B) and propane (C) peaks and in lower panel are labelled as: propene (D), *iso*-butane (E*), n*-butane (F) and acetylene (G).

2.10.3.6.3.2   Intercomparison

The ultimate test of the performance is to compare the same sample analyzed simultaneously on two different instruments. One litre of outdoor air was sampled simultaneously on the Agilent with preconcentrator and on the Perkin Elmer instrument; some small differences are expected due to differences in sampling times and lengths as shown in **Figure 2.31**.
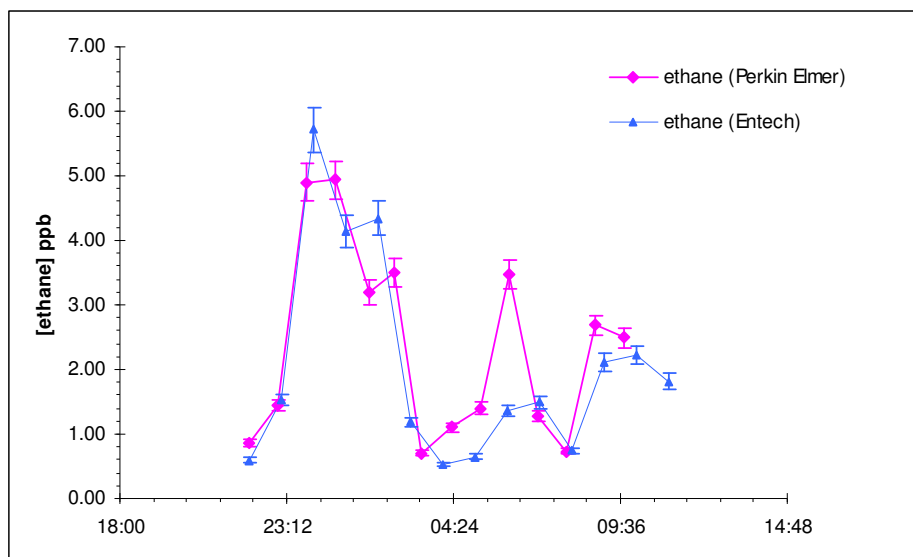
Figure 2.31: Intercomparison between the Agilent system installed with the Entech preconcentrator and the Perkin-Elmer system. One litre outdoor air was sampled simultaneously on both instruments. A reasonable correlation exists between the two instrument measurements; however, the differences in the length of sampling time may cause some deviation from correlation. The error bars on both time series data represent the uncertainties in the measurements on both instrument.

2.10.4 The Entech preconcentrator and its applicability for field use

Comparison of the results obtained with the Entech preconcentrator with the existing Perkin–Elmer system demonstrates the suitability of a carbon based trap (rather than Tenax) in obtaining the recovery of the desired range of VOC compounds and good breakthrough volumes. The on-line water trap seems to offers a replacement of the big external cold trap; however, the use of liquid CO_2 to achieve cooling is not suitable for field purposes, especially at the high usage rate of at least one cylinder per week during continual use. Another drawback is the poor temperature control during the trapping stage. This system uses Dean switching (for balancing and diverting flow in a proper direction) consequently helium consumption is exceptionally high. In addition to this, the maximum sampling capacity is 1300 ml and the flow rate during sampling is not constant. Overall, the Entech system was found to be adequate for the analysis of

144

lightweight VOCs by replacing Tenax trap with a dual bed charcoal trap, however, the use of carbon dioxide as a coolant and the increased helium consumption makes it less appropriate for field deployments.

2.11 Summary

The work discussed in this thesis is focused on the use of a dual channel gas chromatograph to analyze data from three field campaigns. Keeping the dual purpose (for field and laboratory use) of the instrument in mind, the instrument has been designed to cope with the measurement challenges faced from a variety of atmospheric sample types. The measurement technique used for instrumentation is based on gas chromatography coupled with FID. As far as the use of this instrument for research aircraft is concerned, the instrument is used as an offline technique by deploying only the WAS system on board due to the limitations of time and weight. The configuration of instrument, design of experiment, sampling strategy and the use of widely acceptable analytical technique and method combined with the quality assurance and quality control procedures adopted throughout all stages demonstrate that the data from this GC-laboratory are reliable, reproducible and upto the set standards adopted by the GAW World Calibration Centre for VOCs (GAW-WCC-VOC).

In addition to using current instrument configuration, as a part of our commitment to improve present analytical methods and find new alternatives to current technique, few trial experiments were made by installing the Entech 7150 headspace preconcentrator on an existing Agilent 6890 gas chromatograph. The Entech system was found to be adequate for the analysis of lightweight VOCs by replacing the Tenax trap with a dual bed charcoal trap, however, the use of carbon dioxide as a coolant and the increased helium consumption makes it less appropriate for field deployments.

Chapter 3:
Hydrocarbon ratios during the
RONOCO campaign

3.1 Introduction

3.1.1 The RONOCO field campaign

The ROle of Nightime chemistry in controlling the Oxidizing Capacity of the AtmOsphere (RONOCO), an aircraft-based field campaign over UK, took place between December 2009 and January 2011. The campaign started with two test flights (B494 on 8th Dec 2009 and B495 on 9th Dec 2009) using the Facility for Airborne Atmospheric Measurements (FAAM) atmospheric research aircraft (FAAM BAe-146-301). The initial test flights had the aims of mapping pollutant gradients and exploring operational requirements during night in the planetary boundary layer (PBL) for further intensive summer (July 2010), autumn (September 2010) and winter (January 2011) phases of the campaign.

A series of nine flights (B534-B542 from 12th July - 30th July 2010) in summer months, three flights (B549-B551 from 3rd September - 7th September 2010) in autumn and eight flights (B564-B571 from 10th January – 28th January 2011) in winter months were made from East Midlands Airport. The measurements were conducted in a range of gas phase and aerosol environments and with different meteorological conditions in UK boundary layer during the night. Flight planning and design of aircraft sorties were a crucial part throughout this campaign aiming to sample a spectrum of air mass types from less processed fresh pollution to more processed air samples (**Figure 3.1**). The experiments also aimed to capture important diurnal features using daytime, dusk, and dawn flights along with nighttime observations.

The main objectives of RONOCO campaign were:

- To measure the spatial distribution of NO_3 in different meteorological conditions and seasons in order to quantify the key processes and pathways of oxidized nitrogen chemistry at night in the troposphere.

- To assess the role and importance of NO_3 radical in nighttime chemical processes for UK regional and Western European air quality.

In addition to direct measurements of a wide variety of gas phase radical species and key trace gas species (discussed in section 3.2.1), whole air samples were collected in pressurized stainless steel canisters aboard the research aircraft and analyzed for volatile organic compounds (VOCs).
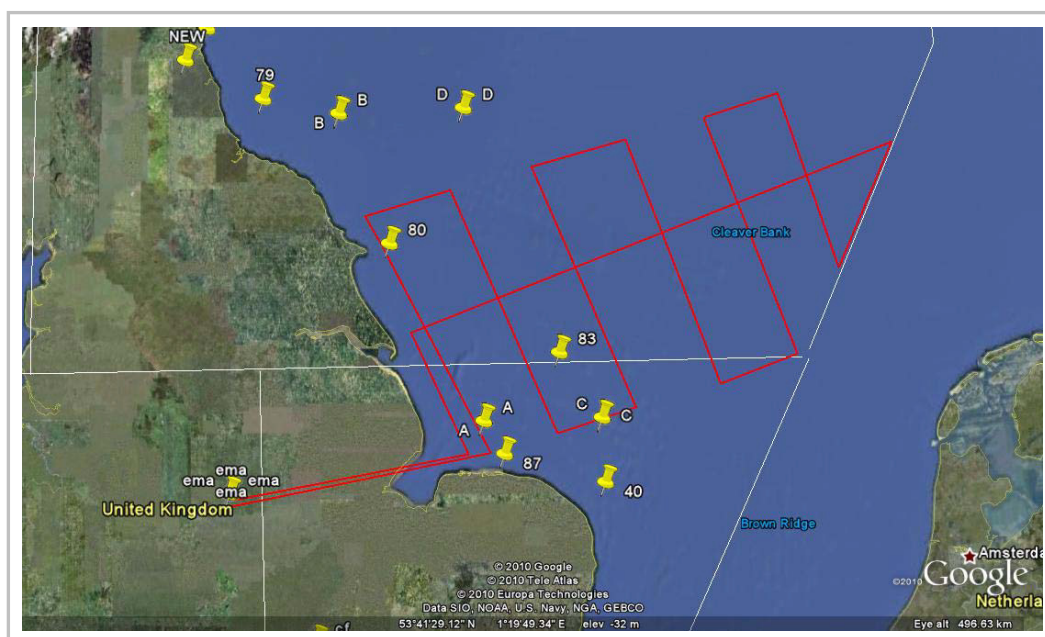
Figure 3.1: Typical RONOCO experimental flight track example for B565 along the East Coast/North Sea, January 2011.

One of the important applications of VOC measurements is to use these species as tracers for atmospheric processing (either of OH, NO_3, O_3 or halogen atoms), (McKeen et al., 1996) and to aid in the deconvolution of source distributions (Blake and Blake, 2002). This chapter focuses on the use of VOC ratios as an indirect approach to diagnose atmospheric radicals and their changing role from day to night and dusk to dawn throughout this campaign.

148

3.1.2 Campaign goals and hydrocarbon measurements

Hydrocarbon ratios have proved useful in previous studies (McKeen et al., 1996;Rudolph et al., 1997;Blake et al., 1993;Penkett et al., 2007) in investigating chemical processes, mixing and transport effects. The discovery of the NO_3 radical and its importance in nighttime chemistry provides further opportunity to use VOC ratios to trace chemical processes, since certain reactions amongst the hydrocarbon class have unique NO_3 sensitivities. One of the earliest uses of hydrocarbon ratios in the study of NO_3 was made by a previous study (Penkett et al., 1993). The role of OH radicals in shaping the seasonal cycle of free tropospheric hydrocarbons can be observed using winter maxima background mixing ratio/summer minima background mixing ratios. This study (Penkett et al., 1993) adopted an alternative ratio approach by examining winter background mixing ratios of various linear and branched-chain hydrocarbons over the North Atlantic and in the London urban plume.

The purpose of using this additional and alternative ratio approach with pairs of similar NMHCs was to avoid the disproportionate influence of summer values of more reactive hydrocarbons. The changing ratios in various hydrocarbons as a function of atmospheric processing time showed notable deviation from that expected with OH acting as an oxidant alone. The analysis indicated a systematically low abundance for branched-chain isomers (iso-pentane, iso-hexane and iso-octane) except for the butane isomer pair. The interpretation of differing-isomer ratios in the case of branched-chain hydrocarbons required the presence of oxidants other than OH radicals and that were selective to the tertiary methyl grouping. One explanation for this behaviour was given by suggesting the possible involvement of NO_3 radicals in removing *iso*-isomers at greater rates to the straight-chain isomers (see **Table 3.1**).

Table 3.1: Room-temperature (298K) rate constants k (cm^3 molecule^{-1} sec^{-1}) for selected compounds with OH radical, NO$_3$ radical and Cl atom. (x denotes no data reported). The asterisk symbol (*) on *iso*-octane represents 2,2,4-trimethylpentane.The superscript symbols on rate constants are as follows: a = (Atkinson and Arey, 2003),b = (Atkinson and Aschmann, 1993), c = (Geyer et al., 2001) and d = (Shi and Bernhard, 1997).

Compound	$k_{OH} \times 10^{12}$ (298K)[a]	$k_{NO_3} \times 10^{17}$ (298K)[a]	$k_{Cl} \times 10^{11}$ (296±2K)[b]
ethane	0.248	0.14[c]	6.29 ± 0.18
propane	1.09	1.7[c]	13.2 ± 0.5
n-butane	2.36	4.59	19.4
iso-butane	2.12	10.6	13.5 ± 0.2
n-pentane	3.80	8.7	24.8 ± 1.2
iso-pentane	3.60	16.2	20.0 ± 0.8
n-hexane	5.20	11.0	29.9 ± 0.6
2-methylpentane	5.2	18.0	25.0 ± 0.8
3-methylpentane	5.2	22.0	24.8 ± 0.6
n-heptane	6.76	15	33.6 ± 1.2
n-octane	8.11	19	40.5 ± 1.2
iso-octane*	3.34	9	23.1 ± 0.8
benzene	1.22	3.0[c]	0.00013[d]
toluene	5.63	7.0	5.9[d]
ethylbenzene	7.0	70[c]	x

The preferential removal of *iso*-pentane over *n*-pentane in air masses reaching Mace Head, Ireland was also observed by (Lewis et al., 1997) and was consistent with low level but persistent NO$_3$-initiated chemistry. To further confirm the evidence of NO$_3$ radicals, Penkett et al compared the atmospheric processing of two different hydrocarbon pairs (n-pentane/iso-pentane *versus* benzene/toluene) (Penkett et al., 2007) for a large dataset arising from the HANSA monitoring network. This study provided further evidence of NO$_3$ radicals and also derived an expression based on the ratio approach to infer an integrated NO$_3$ radical concentration over Europe.

Up to now, it has primarily been the pentane isomer pair which was shown the most consistent behaviour and almost universal additional depletion in processed polluted air. In principle, all isomer pairs with a branched and linear form should show a consistent behaviour; however, there has been little reported use of the ratio approach or derived NO_3 evidence by using isomer pairs higher than C_5. This is somewhat surprising, and may be attributed to somewhat selective reporting of data or that higher pairs of isomers simply have not been measured. This study focuses on examining changing pentane isomers behaviour using log-log plots, and testing their behaviour in different seasons (summer, autumn and winter) and different parts of the day (day, night, dusk and dawn) in accordance with the presence of oxidants. The same tests are then applied to isomers of carbon numbers greater than C_5.

The main objectives of hydrocarbon measurements towards achieving the campaign's goals were:

- To check the usefulness of the ratio approach in diagnosing averaged radicals by comparing changing patterns in different seasons and different periods of the day. This was to be achieved using log-log plots of pentane and other isomer pairs.

- To test the competency and consistency of isomer pairs other than pentane isomer in diagnosing radical abundance.

- To examine the atmospheric variability of C_2–C_8 VOCs in summer and winter seasons, and compare the trends for branched-chain isomers between day and night dataset with reference to the presence of NO_3 radicals.

- To compare the inferred $[NO_3]/[OH]$ ratio with the direct measurements and also with the historical HANSA data set.

- To investigate the impact of NO_3 at night on the loss of anthropogenic VOCs in UK urban boundary layer.

This chapter focuses on first two objectives; the later goals are discussed in chapter 4.

3.2 Experimental

3.2.1 Data coverage

A comprehensive suite of measurements were made during the RONOCO field campaign. A brief summary of species and corresponding analytical techniques are given in **Table 3.2**.

In addition to the trace gas species, 3-d wind components, wind speed, temperature, relative humidity, solar zenith angle, positional data including latitude, longitude and altitude were made available by FAAM.

3.2.2 Sampling procedures and operating area

Approximately 800 whole air samples were collected throughout the different phases of the campaign. An assembly of eight, nine or fifteen silica passivated interconnected stainless steel canisters (supplied by Thames Restek, UK), each having three litre internal volumes, forms a case of the WAS system. Before commencement of the campaign, the stainless steel canisters from all three sets of WAS were tested for any leaks and evacuated to a pressure of 1.2×10^{-2} mbar.A total of sixty four canisters were fitted to the rear hold of the aircraft per flight. The air sample pipe inlet was situated on the aircraft roof, forward of the engines, from which ambient air was drawn by double headed bellows pump (Senior Aerospace, USA) through a stainless steel manifold and directed to the canisters fitted to the rear hold of the aircraft. The inlet lines and canisters were flushed continuously before pressuring to 40 psig to fill the canisters.

Table 3.2: Species measured during the RONOCO field campaign, UK, December 2009 - January 2011.

Species measured	Analytical technique	Research group
$NO_3+N_2O_5,NO_2,H_2O$, Aerosol extinction	Broadband Cavity Enhanced Absorption Spectroscopy (BBCEAS)	Cambridge
$RONO_2,NO_2$,	Laser Induced Fluorescence (LIF)	University of L'Aquila,Italy
Peroxy Acetyl Nitrate (PAN)	Gas Chromatography/Electron Capture Detection	York
HNO_3	Chemical Ionization Mass Spectrometry (CIMS)	Manchester
OH,HO_2	Fluorescence Assay by Gas Expansion (FAGE)	Leeds
$\sum RO_2+HO_2$	Peroxy Radical Chemical Amplifier (PERCA)	Leicester
HCHO	Fluorometric detection (Hantzsch reaction)	East Anglia
H_2O_2	Fluorimetric detection	East Anglia
Aerosols	Aerosols Mass Spectrometry (AMS)	Manchester
O_3	Uv absorption detector Thermo Environmental , Model 49C	Facility for Airborne Atmospheric Measurements (FAAM)
NOx	Chemiluminscence NO-NO_2-NOx analyzer (Thermo Environmental, Model UK)	Facility for Airborne Atmospheric Measurements (FAAM)
CO	Fast Response fluorescence Instrument AL5002 (Aero-Laser GmbH	Facility for Airborne Atmospheric Measurements (FAAM)
Biogenic , aromatic, olefinic and oxygenated VOCs	Proton Transfer Reaction Mass Spectrometry (PTR-MS)	East Anglia
C_2-C_8 NMHCs and selected oxygenates	Whole Air Sampling System (WAS) with subsequent GC-FID	York
C_6-C_{12} Volatile Organic Compounds	WAS with subsequent comprehensive two dimensional gas chromatography (GC x GC)	York

Once the canister was filled to the desired pressure, the pressure relief valve was opened to let the air vent through exhaust pipes. Filling canisters at high pressures gave a usable volume of 9 litres sample gas at STP. Sample acquisition was controlled by software and depending upon the altitude, the time required to fill each canister was between 20 and 30 seconds. Therefore, depending on the aircraft speed (approx 215 knots), an air mass sampled during these filling times is representative of the spatial resolution between 2.19 and 3.29 km.

The flights were operated from a temporary base station at East Midlands Airport, UK during all phases of the campaign. The operational area is shown in **Figure 3.2** and covered from the North Sea to the English Channel, the East Coast to the South West Coast and included circuits around London (M25 motorway).
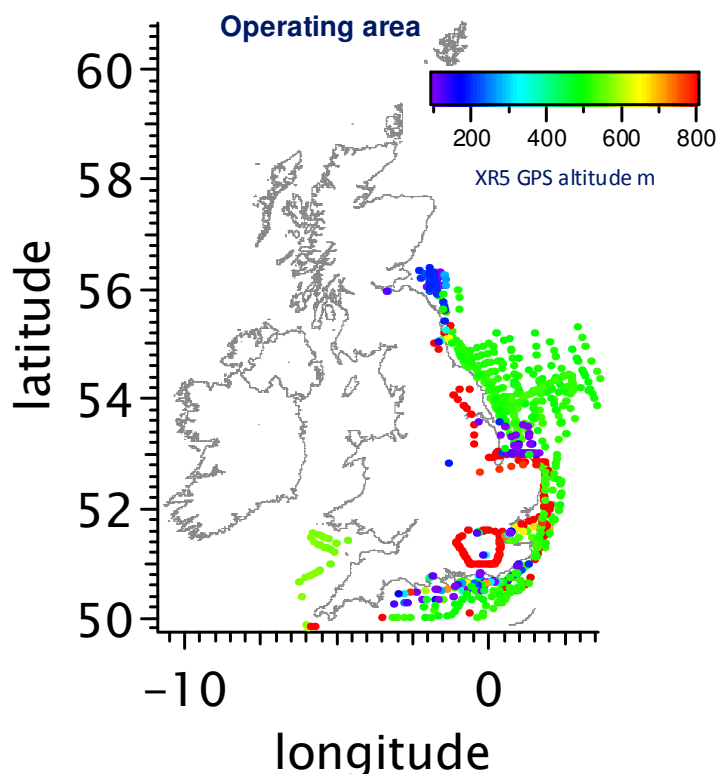
Figure 3.2: The operating area during the RONOCO field campaign (flights B534-B542 in July 2010 and B564-B571 in January 2011) where data points represent collection of whole air samples within the boundary layer.

154

The range of altitudes was below 2 km during summer and below 1 km during winter and was dependant on the nocturnal boundary layer (NBL) height. After the conclusion of flights, canister samples were brought back to the University of York to be analysed by the dual channel Gas Chromatograph coupled with Flame Ionisation Detectors (GC-FID). These air samples were also analysed for compounds higher than five carbons by Comprehensive Two-Dimensional Gas Chromatograph (2D GC) (Lidster et al., 2011).

3.2.3 Dual channel GC-FID system and measurement procedures

The whole air samples were analysed for C_2 to C_8 hydrocarbons and selected oxygenated VOCs using a GC-FID system (Perkin Elmer). A more detailed description of the system and procedures are presented by (Hopkins et al., 2003;Hopkins et al., 2011), a brief outline of which is as follows:

In order to control and automate the canister opening and shutting procedures during the sample transfer operation from canisters to GC, Lab view software, (home-written software La Vespa, National instruments) was used.

The first step requires flushing of the entire sampling lines followed by water removal by using a cold glass finger immersed in a 50:50 ethylene glycol : water mix maintained at -30 ^{o}C. The preconcentration stage involved trapping of samples at the flow rate of 100 ml min^{-1} for 10 minutes onto the dual-bed charcoal trap (Carboxen 1000 and Carbotrap B, Supelco), cooled by Peltier coolers to -23 ^{o}C . Once the sampling volume of 1 litre was attained, the trap was flushed with ultra pure helium (99.9999%), used as a carrier gas, for 3.5 minutes whilst cold in order to allow methane and oxygen elute from the system. The trap was then thermally heated at a rate of 16 ^{o}C s^{-1} to 325 ^{o}C to desorb the organic compounds. The analytes were then flushed with a flow of 40 ml min^{-1} helium

carrier gas into the GC oven and split in a 50:50 ratio between the two PLOT columns.

C_2 to C_8 hydrocarbons were separated on a Porous Layer Open Tubular Column (PLOT, Al_2O_3/Na_2SO_4, 50 m x 0.53 mm i.d, Varian Inc), on the basis of increasing boiling point and a CP-LOWOX column (mixed phase porous layer tubular column, 10 m x 0.53 mm i.d, Varian Inc) on the basis of increasing polarity. The columns were initially held at a temperature of 40 ^oC for 3 minutes before heating at a rate of 13 ^oC min^{-1} to 110 ^oC and finally at a rate of 8 ^oC min^{-1} to 200 ^oC. The final temperature stage remained constant for 15 minutes. The analytes from both columns were detected by two FIDs. The time for one complete GC run cycle was 54 minutes. The detector signals were analysed using the Total Chrom software and chromatograms were each manually processed for peak integration. Detection limits for a 1 litre sample were between 1 and 10 parts per trillion (pptv) for NMHCs and between 10 and 40 pptv for oxygenated VOCs.

The identification of peaks was made by using comparison with the retention time of the known gas standards. The gas standard used during this campaign was a gravimetrically prepared 30 hydrocarbons mix in a passivated aluminium cylinder with mixing ratios in the 4 nmol mol^{-1} range supplied by National Physical Laboratory (NPL, Teddington, United Kingdom,) with a quoted uncertainty of 0.08 ppbv for each compound (2%). The system was calibrated at regular intervals. The individual compound response factors were used to quantify the mixing ratios of hydrocarbons.

The analysis procedure by GC-FID was repeated thrice after every two weeks for selected canister samples from varying altitudes to test the integrity of samples in canisters. The results indicated no loss or increase in concentration. After the analysis of air samples, the canisters were vented and then evacuated to a pressure of 1.2 x 10^{-2} mbar to remove the memory effects of previous samples and ready for installation aboard the aircraft for further sample collection.

3.3 Results and Discussion

3.3.1 Evidence of NO$_3$ radical

The *n*-pentane/*iso*-pentane ratio was found to vary with acetylene mixing ratio (a marker for atmospheric processing) as indicated in **Figure 3.3**. The range of acetylene mixing ratios between 255 to 50 pptv indicated a reasonable variety of less processed to highly processed air masses. As the air mass becomes more processed, the *n*-pentane/*iso*-pentane ratio increases from 0.4 (which is the ratio at point of emissions) to 1.2. The *n*/*iso*-pentane ratio is relatively constant over a 100 to 250 pptv range of acetylene mixing ratios implying a degree of uniformity in the source. As the acetylene mixing ratio decreases from 100 pptv to 50 pptv, indicative of a transition to well processed air, the *n*-pentane/*iso*-pentane ratio increases suggesting an impact of NO$_3$ radicals. As shown in **Table 3.1**, the NO$_3$ radical reacts with *iso*-pentane at almost double the rate of *n*-pentane; the rate of oxidation with OH radical is almost same (difference less than 15%) for both isomers.
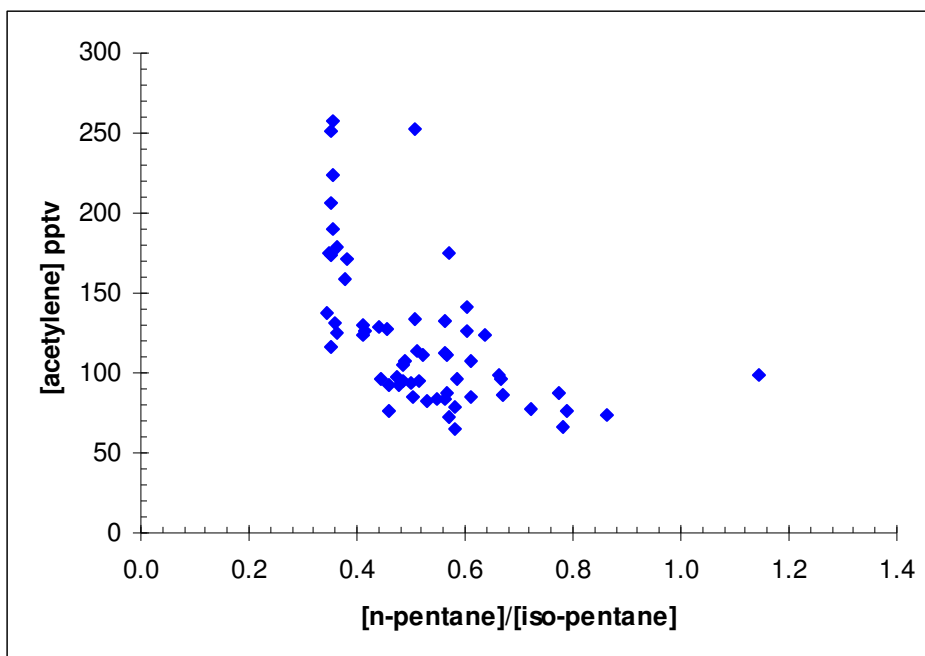
Figure 3.3: Variation of *n*-pentane to *iso*-pentane ratio with acetylene for a summer night B542 flight. The *n*-pentane/*iso*-pentane mixing ratio increases as acetylene mixing ratio decreases from 100 pptv to 50 pptv (an indicative of well processed air masses) suggesting an impact of NO$_3$ radical.

To further investigate the variation in ratios of pentane isomer pairs and by extension the dominant oxidants involved throughout this campaign, a linear log-log relationship between [*iso*-pentane]/[ethane] *versus* [*n*-pentane]/[ethane] has been used. This analysis is then applied to data collected during daytime, dusk, dawn and night time in summer, winter and autumn seasons.

3.3.2 Log-Log plot and pentane isomer behaviour

The linear relationship between the natural log of two ratios having the same denominator contrasts observed data against two extreme cases of atmospheric removal - namely the photochemical decay and dilution/mixing only. The photochemical decay line assumes that ratios change and evolve solely due to OH chemistry whilst the dilution line takes pure dilution into account assuming all hydrocarbons are inert in nature. In practice, an isomer pair following OH reaction chemistry in the atmosphere should lie somewhere between these two limits (since dilution cannot be avoided). Any data points outside these boundaries and having slopes greater than theoretical kinetic slope, would indicate the involvement of a further oxidant other than OH.

The OH photochemical line for a pentane isomer is expressed (according to equation 1.69 discussed in chapter 1) by following equation:

$$\ln \frac{[\text{iso} - \text{pentane}]}{[\text{ethane}]} \quad = \quad m \times \left\{ \ln \frac{[\text{n - pentane}]}{[\text{ethane}]} \right\} + C \qquad \qquad 3.1$$

where *m* is slope and *C* is intercept

$$m \quad = \quad \frac{k_{\text{iso}-\text{pentane}} - k_{\text{ethane}}}{k_{\text{n}-\text{pentane}} - k_{\text{ethane}}} \qquad \qquad 3.2$$

$$C \quad = \quad \ln \frac{[\text{iso} - \text{pentane}]^0}{[\text{ethane}]^0} - m \times \ln \frac{[\text{n} - \text{pentane}]^0}{[\text{ethane}]^0} \qquad \qquad 3.3$$

The equation for the dilution line (according to equation 1.83 as discussed in chapter 1) is expressed as follows:

$$\ln\frac{[\text{iso - pentane}]}{[\text{ethane}]} = 1\times\left\{\ln\frac{[\text{n}-\text{pentane}]}{[\text{ethane}]}\right\}+C \qquad 3.4$$

where *m* is the slope and *C* is intercept

$$m = 1 \qquad 3.5$$

$$C = \ln\frac{[\text{iso}-\text{pentane}]^0}{[\text{n}-\text{pentane}]^0} \qquad 3.6$$

The intercept for the photochemical line and the dilution lines have been set using observed data close to source data. The photochemical slope is calculated by using rate constants from (Atkinson and Arey, 2003) (see **Table 3.1**).

One of the noticeable points in these plots is that both numerators (*iso*-pentane and *n*-pentane) in the equation have very similar rate constants towards OH radical producing kinetic slopes similar to the dilution slopes. In order to compare the plots from various flights made at different times of the day, a plot (**Figure 3.4**) from day flight B550 made in month of September has been chosen as a starting and reference point for this discussion. An additional photochemical line having a theoretical slope of 1.85, which is the ratio-ratio variation due to exclusive NO_3 chemistry, has also been plotted to help in visualising the relative extents of different chemistries involved. The agreement between observed slope 0.90 and theoretical kinetic slope for OH chemistry 0.94 in **Figure 3.4** demonstrates the impact of a combination of OH radical chemistry and mixing during daytime in defining the changing in ratios. These two processes cannot be disentangled using this isomer pair combination.
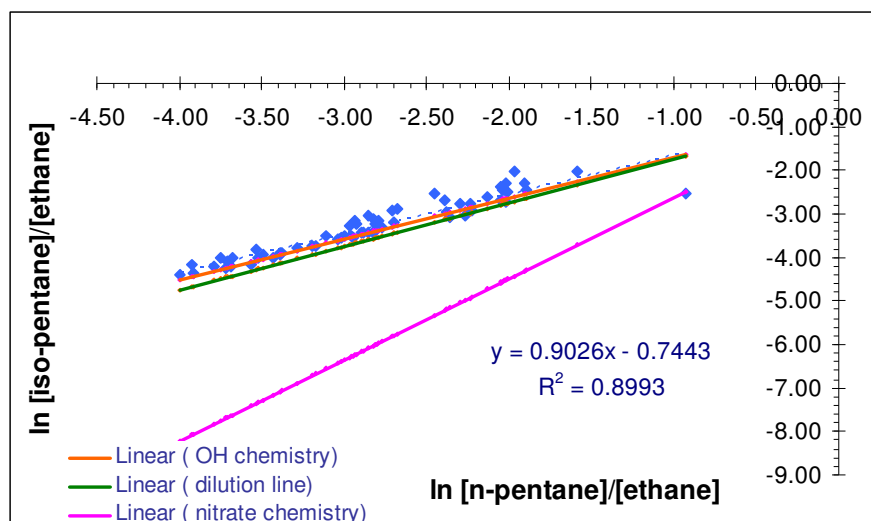
Figure 3.4: Plot of ln [*iso*-pentane]/[ethane] *versus* ln [*n*-pentane]/[ethane] for daytime B550 flight data (September 2010). The observed slope 0.90 is in agreement of theoretical OH chemistry slope 0.94 suggesting an impact of a combination of OH chemistry and dilution during daytime. Using the intercept value, the emission ratio ([*iso*-pentane]^0/[*n*-pentane]^0) comes out to be 0.47 for this flight.

Plotting the same relationship for night flight data from two flights from the summer period (July 2010) B542 and B536, shown in **Figure 3.5**, gives observed slopes (1.04 and 1.18) respectively, greater than the OH chemistry theoretical slope (0.94) indicating a substantial deviation from OH chemistry. This may be inferred as indicating the influence of NO_3 reactions.
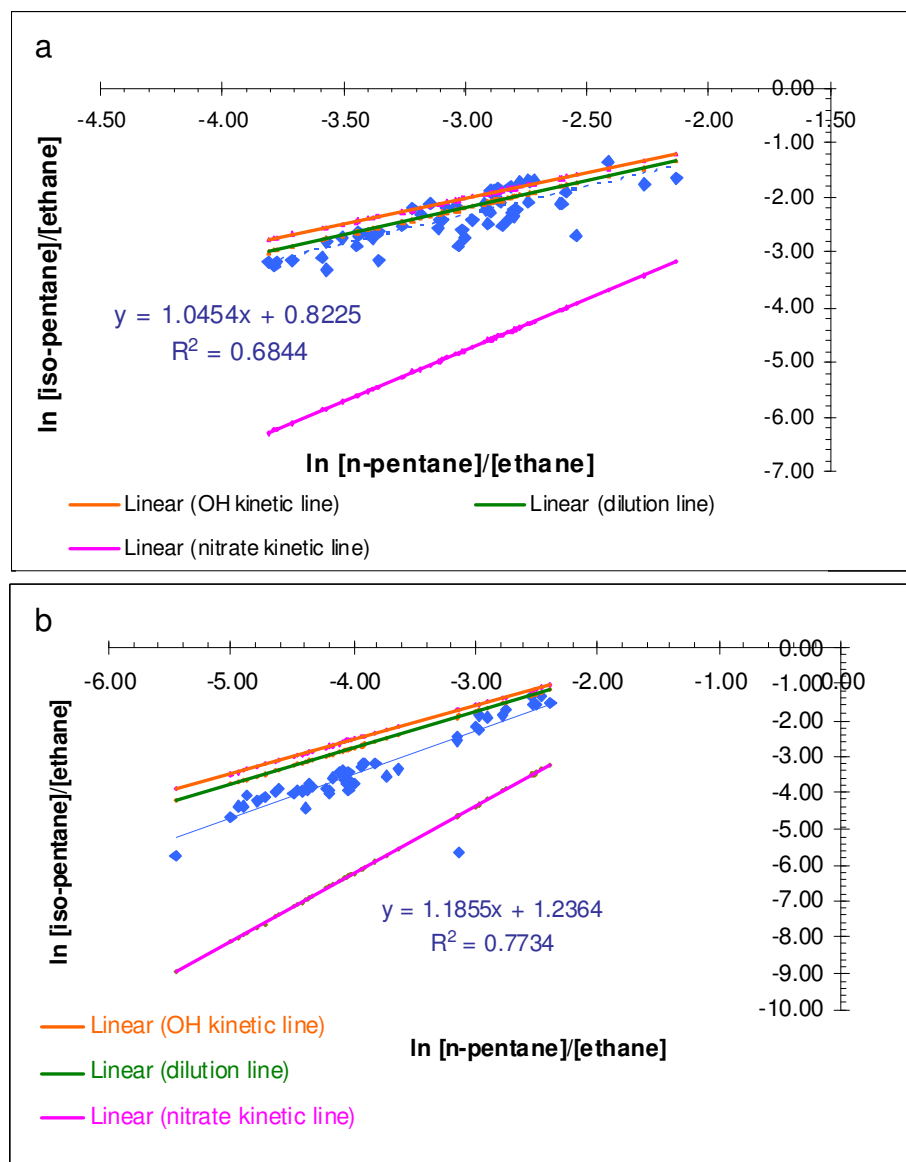
Figure 3.5: Plot of ln [*iso*-pentane]/[ethane] *versus* ln [*n*-pentane]/[ethane] for a summer night-time B542 flight (upper panel) and B536 flight (lower panel) (July 2010). The observed slope for B542 (1.04) and B536 (1.18) is higher than theoretical OH kinetic slope (0.94) indicating a substantial deviation from OH chemistry and a greater influence of NO_3 chemistry. Using the intercept value, the emission ratio ([*iso*-pentane]^0/[*n*-pentane]^0) comes out to be 2.27 and 3.3 for B542 and B536 flights, respectively.

The behaviour of pentane isomer pairs for summer data was therefore encouraging in terms of indications of NO_3 chemistry. Analysis using the same

technique for winter nighttime data, e.g. for flight B564 (as shown in **Figure 3.6**), clearly shows the relationship here is very different to the summer.
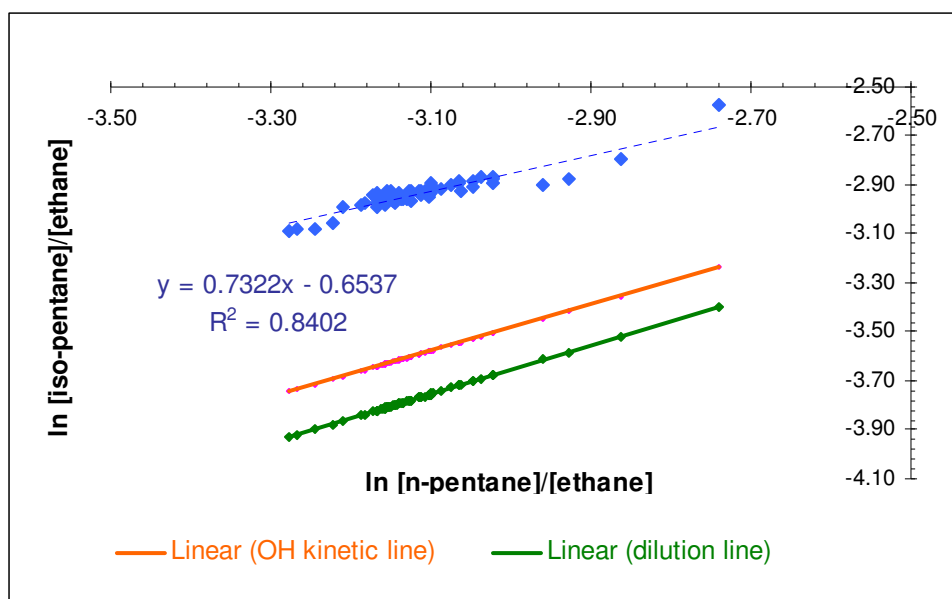
Figure 3.6: Plot of ln [*iso*-pentane]/[ethane] *versus* ln [*n*-pentane]/[ethane] for winter night B564 flight data (January 2011). The observed slope is significantly lower (0.73) than theoretical OH chemistry slope (0.94) suggesting the absence of NO_3 radical. In fact, the observed slope is close to theoretical Cl atom chemistry slope (0.74). Using the intercept value, the emission ratio ([*iso*-pentane]^0/[*n*-pentane]^0) comes out to be 0.52 for this flight

Firstly it should be noted that the variability in the ratios observed is very much less than that seen in the summer: -2.7 to -3.3 as compared to summer plots (-2.5 to -5.5) in **Figure 3.5**. The slope in winter data was also significantly lower (0.73) than theoretical OH chemistry slope suggesting the absence of NO_3 radical. This was the case for all three winter night flights (B564, B565 and B566). A slope less steep than the OH photochemistry line would however be in agreement with the presence of Cl atom chemistry. Using rate constants (**Table 3.1**) for the gas phase reactions of n-pentane, iso-pentane and ethane with Cl atoms at 296 ± 2 K (Aschmann and Atkinson, 1995), the kinetic slope for Cl atom reaction would be 0.74.

To examine further the potential presence of Cl atom chemistry, the butane isomer pair along with propane were used (Jobson et al., 1994). It is the *n*-butane isomer which reacts at faster rate with chlorine atom than *iso*-butane. The reactivity difference towards the OH radical is less than 10%.
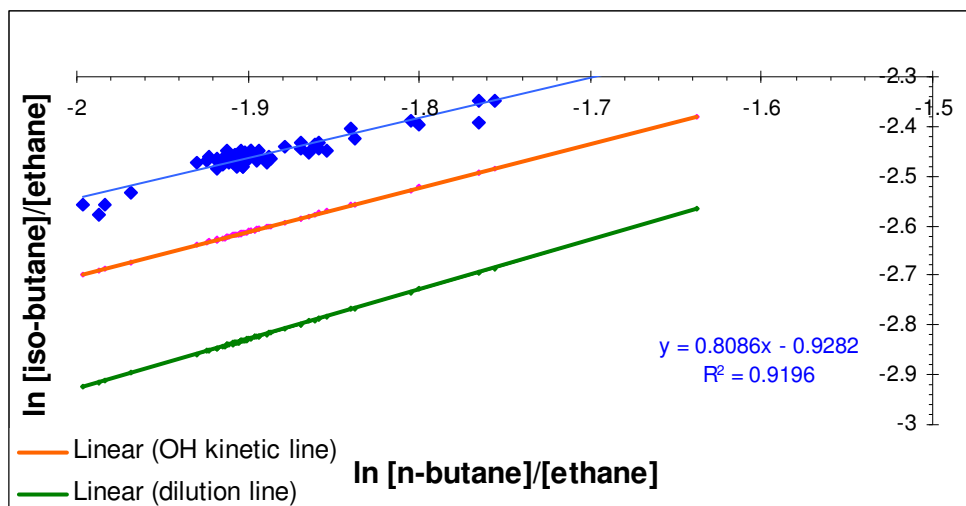
Figure 3.7: Plot of ln [*iso*-butane]/[ethane] versus ln [*n*-butane]/[ethane] for winter night B564 flight data (January 2011).The observed slope (0.81) is somewhat between the theoretical OH chemistry (0.88) and the Cl atom chemistry (0.73) slopes suggesting a further check to test the Cl atom chemistry involvement. Using the intercept value, the emission ratio ([*iso*-butane]^0/[*n*-butane]^0) comes out to be 0.39 for this flight.

The observed slope (0.80) in **Figure 3.7** is between the OH chemistry slope (0.88) and the Cl atom chemistry (0.73) making this somewhat inconclusive. To test further whether chlorine atoms were impacting in winter, further pair of hydrocarbons were used having the same OH reactivity but differing chlorine reactivity. The pairs [benzene]/[*n*-butane] *versus* [propane]/[*n*-butane] (observed slope of log-log plot is 1.55) and [hexane]/[benzene] *versus* [toluene]/[benzene] (observed slope of log-log plot is 0.48) (Rudolph et al., 1997) were also tested (not shown here). The value of theoretical kinetic Cl atom chemistry slope for both pairs ([benzene]/[*n*-butane] *versus* [propane]/[*n*-butane] and [hexane]/[benzene] *versus* [toluene]/[benzene]) is 3.12 and 5.06 respectively which is much higher than the observed slopes emphasizing the influence of OH chemistry on the data.

Having established very limited apparent chlorine atom chemistry impact on the winter nighttime data, it was interesting to then examine the variation of [*n*-pentane]/[*iso*-pentane] ratio with acetylene for the same winter B564 night flight. The range of acetylene mixing ratio (380-520 pptv) as indicated in **Figure 3.8** showed a rather narrow range of essentially less processed air masses with no clear trend of increasing ratio from less processed to high processed air masses. This analysis of winter highlights that very limited processing appears to be occurring and that even though the aircraft sampled over a wide spatial area, the composition was rather homogeneous. This was in clear contrast to the summer data where a wide range of differing isomer ratios and absolute mixing ratios were observed.

To further compare between air masses sampled during summer and winter, the acetylene/CO ratio was plotted for both seasons. **Figure 3.9** illustrates that in summer, well photochemically aged air masses (ratios between 0.8-1.2) have been captured as compared to winter (3.0-3.2).
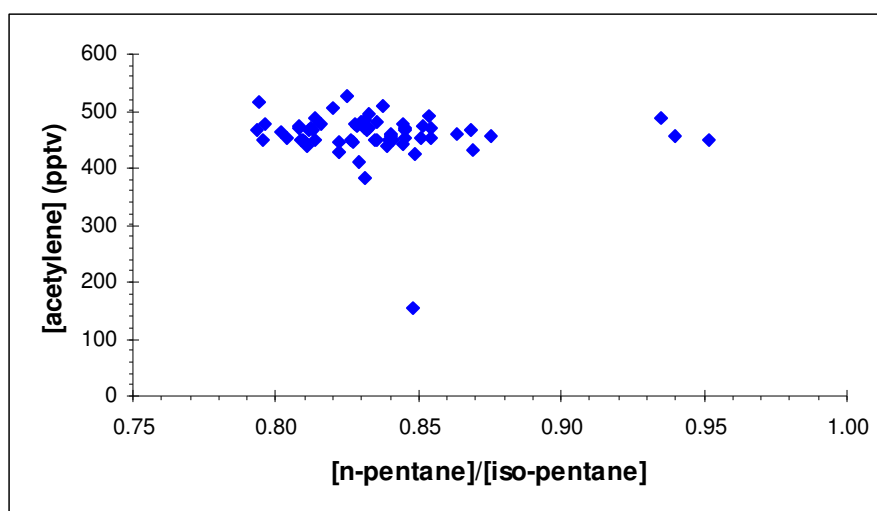
Figure 3.8: Variation of [*n*-pentane]/[*iso*-pentane] ratio with [acetylene] for winter night B564 flight data (January 2011). The range of acetylene mixing ratio is very narrow (380-520 pptv) indicating a lack of wide variety of air masses captured despite sampling over a wide spatial area; the [*n*-pentane]/[*iso*-pentane] ratio is expected to be constant within this narrow range of less processed air masses.
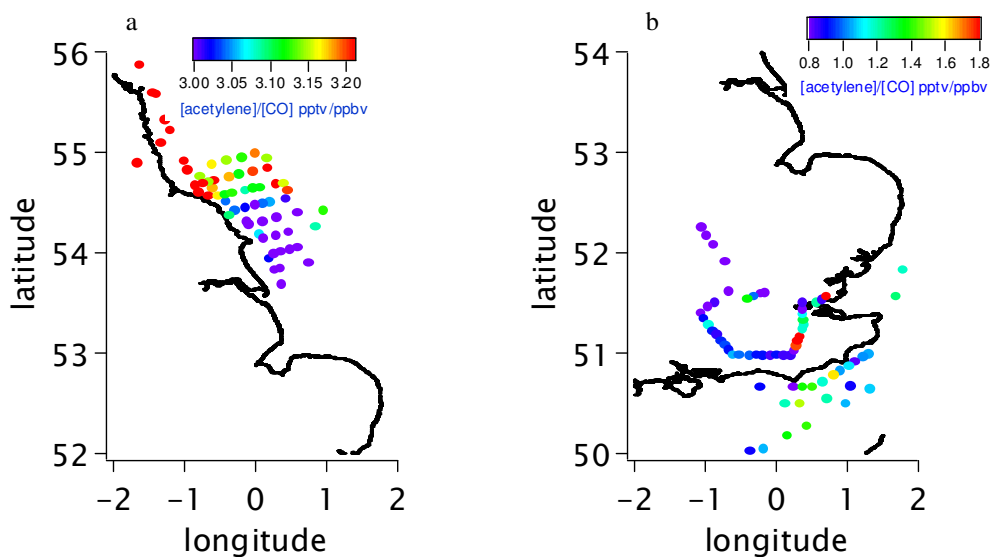
Figure 3.9: Comparison of [acetylene]/[CO] (pptv/ppb) ratio between (a) winter night B564 flight data and (b) summer night B542 flight data.

In winter owing to less OH processing, hydrocarbon mixing ratios are elevated and mixing between a similar and narrow range of air masses causes only small changes in mixing ratio. This is supported by **Figure 3.10** plotted for *n*-pentane, *iso*-pentane and ethane. This flight aimed to sample a distinct pollution plume passing out over the North Sea. It is clear that in terms of hydrocarbons, the background mixing ratios of hydrocarbons species and the plume mixing ratio are rather similar. McKeen et al. showed the impact of increasing background mixing ratio on hydrocarbon ratio slopes (McKeen et al., 1996). Three different ethane background values were used and a systematic decrease in slope was observed with respect to the pure photochemical line, which assumes zero background. During winter flights lower OH combined with the high background ethane mixing ratio seems to be suggestive of decreased slope for winter ln [*iso*-pentane]/[ethane] *versus* ln [*n*-pentane]/[ethane] plot.
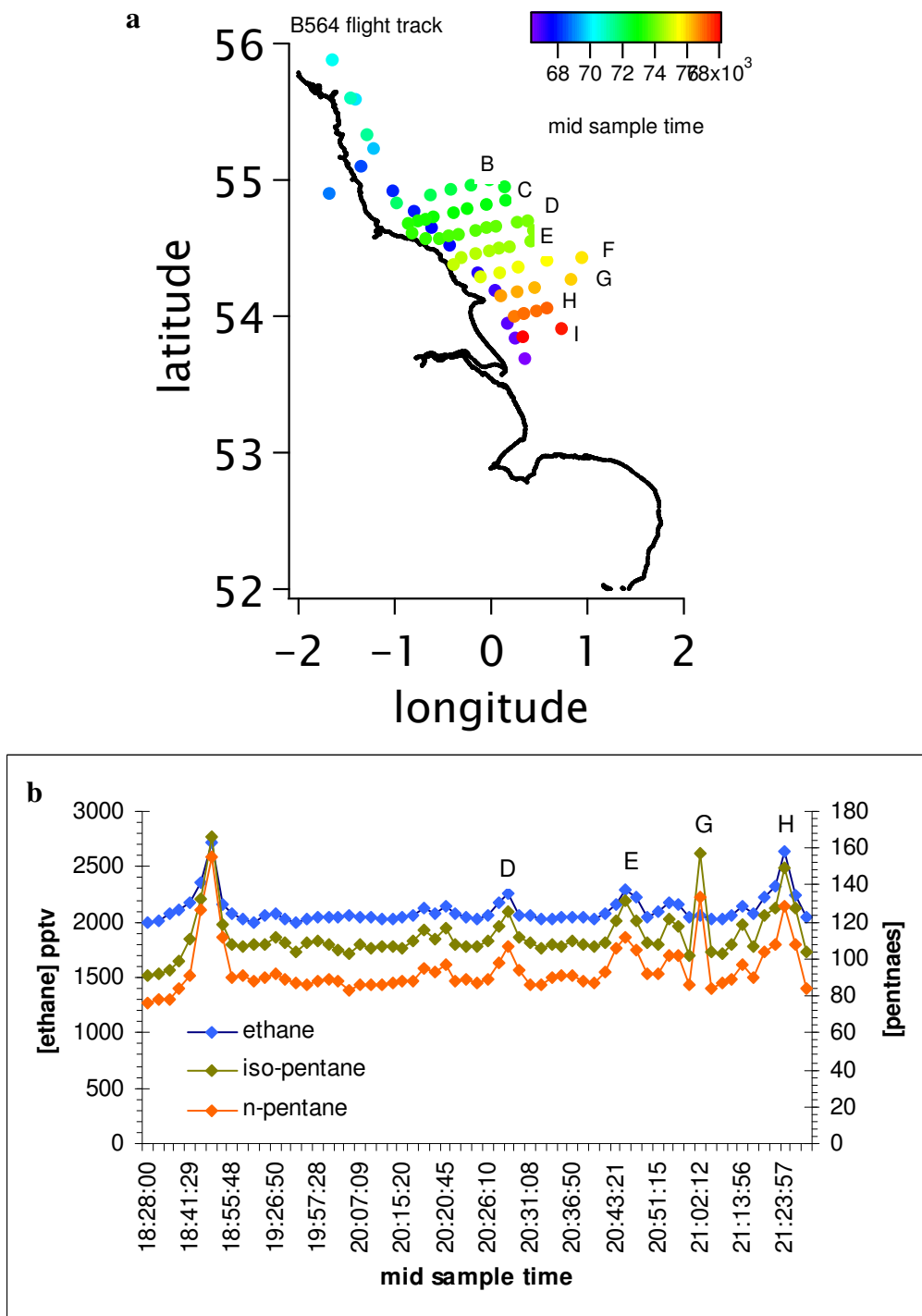
Figure 3.10: (a) The flight track for B564 along the East Coast indicating the plume interception points (B to I); the data points represent collection of whole air samples. (b) Variation of hydrocarbon mixing ratio during sampling time for winter night flight B564. The plume interception points are shown by D, E, G and H notation. The background mixing ratios of hydrocarbons species and the plume mixing ratio are rather similar. Therefore, high background ethane mixing ratio coupled with lower OH seems to be suggestive of decreased slope for all winter night flights made in January 2011.

However, during the sampling times for this flight (B564), a range of NO_3 mixing ratios between 2.0-11.0 ppt was observed and 75% of data were less than 7.7 ppt. By using 7.0 ppt NO_3 mixing ratio, the lifetime of [*n*-pentane]/[*iso*-pentane] ratio according to the following equation comes out to be 896 days.

$$\tau_{\frac{\text{n-pentane}}{\text{iso-pentane}}} = \frac{1}{(k_{\text{n-pentane}} - k_{\text{iso-pentane}})[NO_3]} \qquad 3.7$$

At this point there arise three main questions: first, is it possible to actually see a deviation from OH chemistry through log-log plots at such low radical mixing ratios? Second, are there any rate constant inaccuracies or measurement issues that may create an artefact radical abundance? If there are rate constant inaccuracies and measurement issues then actually it is information about OH being extracted from these plots instead of NO_3? Third, if a wide range of air masses had been captured then would it have been possible to observe the ratio change in accordance with NO_3 chemistry?

To find the solution for the first problem, an analysis of log-log relationships for dusk and dawn flights has been used as these are the periods of daytime when concentrations of both oxidants are at their minimum. In addition to this, the *in situ* levels of NO_3 observed during dusk and dawn flights were similar to night flights made in winter months. The dusk flight B549 was made in the month of September. The flight take-off and landing timings were 16:20:09 – 20:32:12. The sunrise and sunset time during this month was 06:14 and 19:46 which means that dusk flight covered 75% period before sunset and 25% period after sunset. On this basis, one should expect greater influence of OH chemistry rather than NO_3 chemistry on the data. The slope is slightly higher (0.99) than the theoretical OH kinetic slope (0.94) indicating (**Figure 3.11**a) that deviation from OH chemistry has started and the presence of NO_3 is possible. However, the data from the dawn flight B551 (shown in **Figure 3.11**b) made in the same month and between 03:45:49 – 07:25:17 shows only a small presence of NO_3 chemistry.

The flight take-off and landing time indicated that sampling time covered 75% period before sunrise and 25% after sunrise.
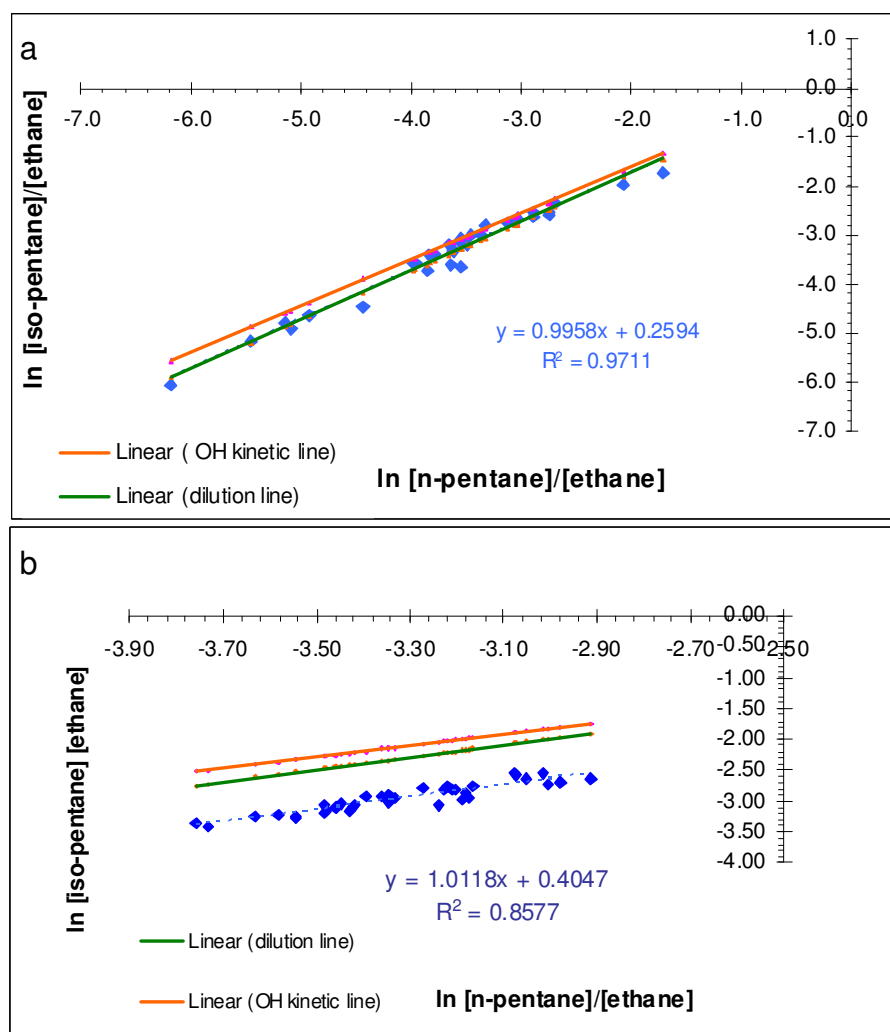
Figure 3.11 Plot of ln [*iso*-pentane]/[ethane] *versus* ln [*n*-pentane]/[ethane] for comparison of (a) autumn dusk B549 and (b) autumn dawn B551 flight data (September 2010). The observed slope is slightly higher (0.99) than theoretical kinetic slope (0.94) for dusk data indicating that deviation from OH chemistry has started and the presence of NO_3 is possible. Similarly, for dawn data the moderate increase in slope (1.01) also indicates the influence from nighttime chemistry. Using the intercept value, the emission ratio ([*iso*-pentane]^0/[*n*-pentane]^0) comes out to be 1.28 and 1.49 for B549 and B551 flights respectively.

The moderate increase in slope (1.01) in (**Figure 3.11**b) indicates the influence from nighttime chemistry. Unfortunately, during both flights, direct NO_3

measurement instruments were not installed so it was not possible to make a comparison with *in situ* data.

However, the difference in slopes is very small and it is not clear that the extent of deviation from OH chemistry during autumn dusk and dawn flights depended on the length of time covered before and after transition period. This was examined further using data from dusk and dawn flights made in month of January. During this month, the sunrise and sunset timings were 08:00 and 16:02 respectively.

In contrast to the autumn dusk flight B549, the take off and landing timings for winter dusk B568 (14:53:40-19:50:24) were such that the period covered was 25% before sunset and 75% after sunset. A slope of 1.17, greater than the kinetic OH slope (0.94) (**Figure 3.12**a) suggests the presence of NO_3 in accordance with the period covered before and after sunset. The directly observed NO_3 levels were 2.8-8.8 ppt with a upper 75th percentile value of 5.9 ppt.

Similarly the experiment for winter dawn flights was the opposite to the autumn dawn flight in terms of period covered before and after sunrise. The winter dawn flight B567 was made between 05:50:15-10:49:44 and covered 43% period before sunrise and 57% after sunrise suggesting more instantaneous influence from OH chemistry. The observed slope of 0.86 (**Figure 3.12**b) is less than theoretical kinetic slope (0.94) and suggestive of OH chemistry impact. However, the observed NO_3 levels were only slightly lower at 1.8 to 7.6 ppt with the 75th percentile value of 4.2 ppt.
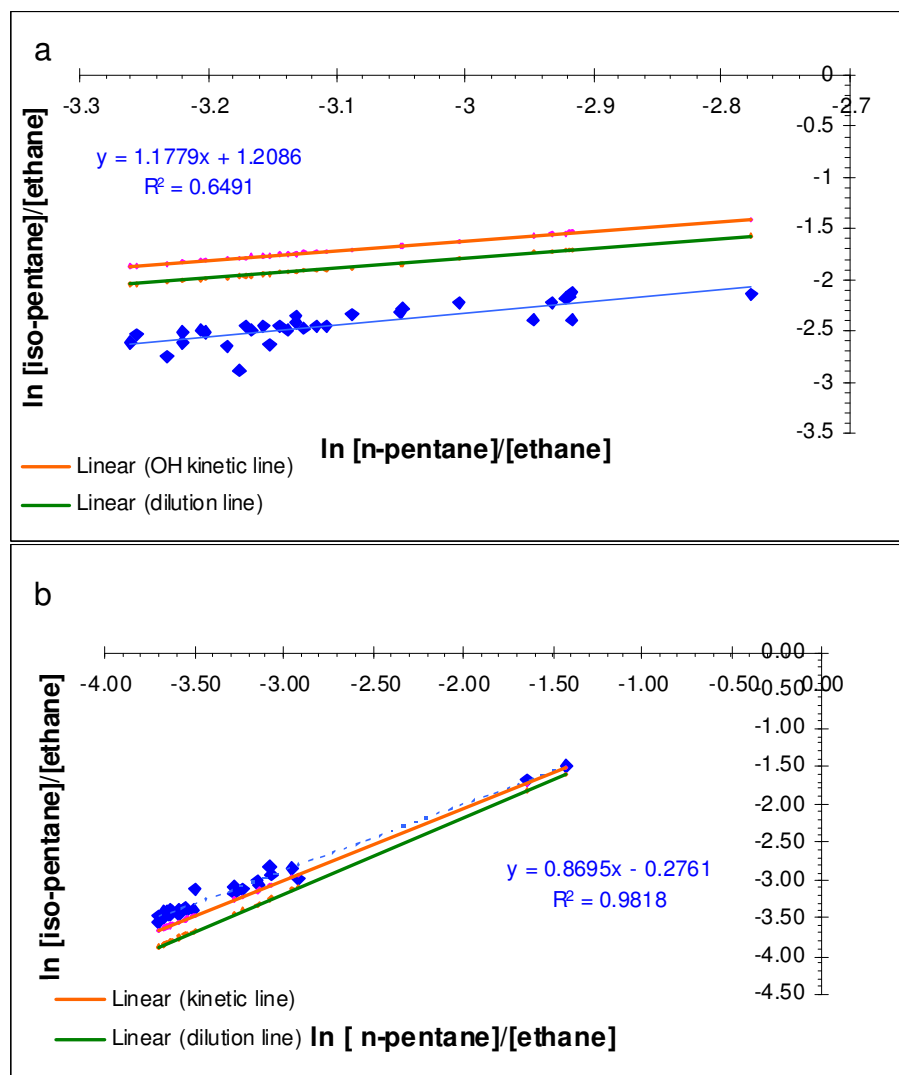
Figure 3.12: Plot of ln [*iso*-pentane]/[ethane] *versus* ln [*n*-pentane]/[ethane] comparing winter dusk B568 (a) and winter dawn B567 (b) flight data. A slope of 1.17, greater than the kinetic OH slope (0.94) for winter dusk data suggests the presence of NO_3 in accordance with the period covered before and after sunset. The observed slope of 0.86 for winter dawn data is less than theoretical kinetic slope (0.94) and suggestive of OH chemistry impact. Using the intercept value, the emission ratio ([*iso*-pentane]^0/[*n*-pentane]^0) comes out to be 3.3 and 0.76 for B568 and B567 flights respectively.

There are two things that become clear from this analysis of dusk and dawn flights compared in different seasons. First, the pentane isomer changes are only very small and do not necessarily correlate directly with expected air mass exposure to radicals. Whilst there is some evidence that the dominant oxidant is controlled by the day and night time fractions for each flight, there is

inconsistency in the behaviour at dawn. Whilst the instantaneous radical exposure over the flight B567 is skewed towards OH, one would intuitively expect the integrated effect of a full night time of processing by NO_3 to be shown in the ratios at dawn. This is not the case. Secondly, that small deviations from the OH kinetic line become visible in log-log plots when *in situ* measurements of NO_3 were around 10 ppt and this provides some guideline to the 'detection limit' of the indirect ratio method.

Clearly flight B567 is one worthy of further consideration since there is an inconsistency in the apparent dominance of OH influence in comparison to direct NO_3 measurement values, when one considers that the air mass has just been exposed to a full night of NO_3 reactions. This highlights the problem of comparing ratios which reflect a very integrated exposure to a particular radical and the *in situ* measurements which are instantaneous. In this case it is possible that fresh mixing on new emissions at dawn completely overwhelms any NO_3 signal.

Given that for these dawn and dusk flights the changes in ratio are so small, it is worth examining the uncertainties associated with the derivations, for example in the measurement or rate constant data. For example, one could consider that perhaps the rate constants were reversed, in other words *iso*-pentane being destroyed by OH at a slightly faster rate than *n*-pentane. Alternatively a false signal could be generated by a measurement problem with an unknown peak co-eluting with *iso*-pentane and then being quickly destroyed by OH resulting the reduction in peak area of *iso*-pentane. When this is tested, by comparing daytime flight data (**Figure 3.13**a) and nighttime data (**Figure 3.13**b) and by plotting two different isomer pairs (assuming that benzene/toluene is exclusively processed by OH and pentane isomer pair by NO_3) then a clear picture emerges which removes the possibility of rate constant and measurement issues generating false OH-driven NO_3 signal.
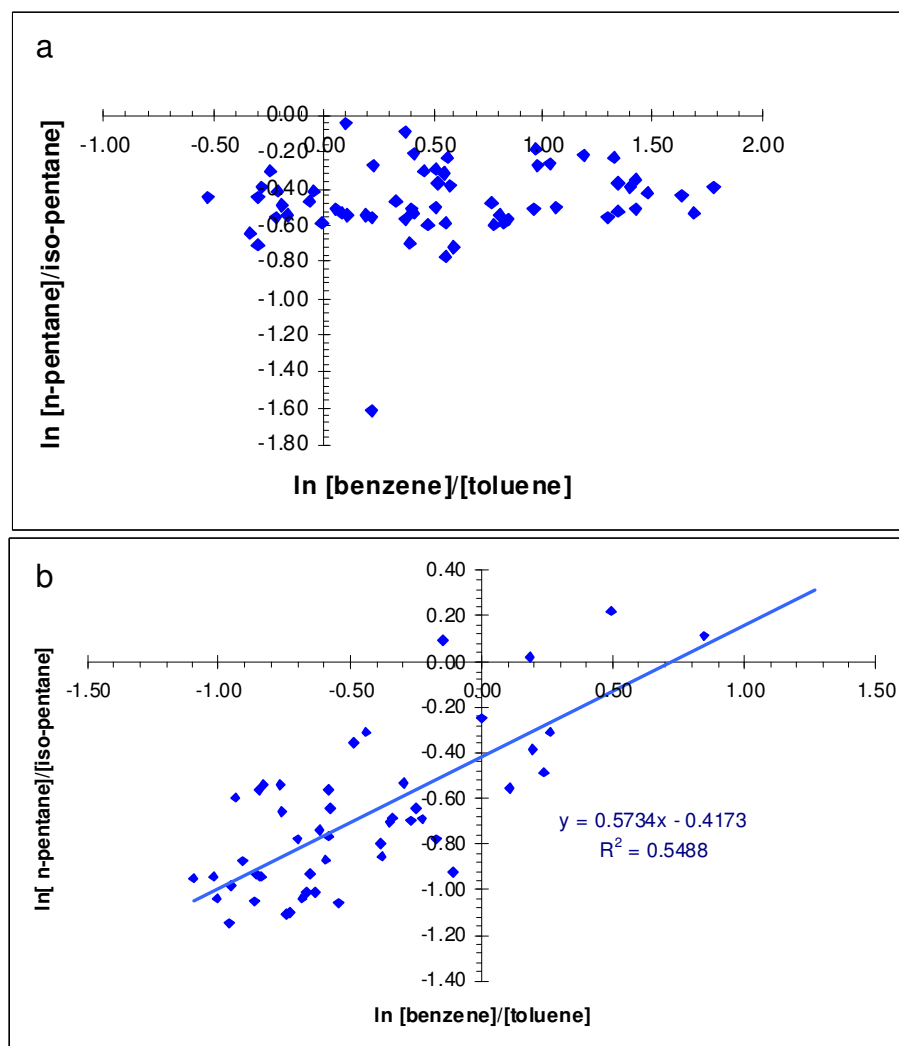
Figure 3.13: Plot of ln [*n*-pentane]/[*iso*-pentane] *versus* ln [benzene]/[toluene] for comparison between (a) autumn day (September 2010) B550 (b) and summer (July 2010) B535 night flight data. The [*n*-pentane]/[*iso*-pentane] ratio increases horizontally during day time as toluene is removed at a much faster rate by OH in comparison to benzene, whilst *n*-pentane and *iso*-pentane rate constants are similar with OH resulting an almost constant ratio range vertically. However, the nighttime data illustrates the involvement of both oxidants (benzene/toluene mainly by OH and *n*-pentane/*iso*-pentane mainly by NO_3) in processing the two different resulting a reasonable correlation.

As toluene is removed at a much faster rate by OH in comparison to benzene so this ratio is increased horizontally on the plot during day time, whilst n-pentane and iso-pentane rate constants with OH are similar resulting an almost constant

ratio range vertically. However, the nighttime data illustrate the involvement of both oxidants ([benzene]/[toluene] mainly by OH and [n-pentane]/[iso-pentane] mainly by NO_3) in processing the two different pairs.

Overall therefore it is clear that observing a clear signal in NO_3 in winter night-time data is not straightforward. Often the data show only a very limited range of ratios in hydrocarbon implying a homogeneous composition with limited differences between air masses. A useful flight to examine is in fact the first test flight B494 made in month of December 2009. This did not have *in situ* NO_3 measurements, but was one of the few winter flights to show a good correlation between ln [*iso*-pentane]/[ethane] *versus* ln [*n*-pentane]/[ethane] (**Figure 3.14**) over a reasonable wide range of air masses.
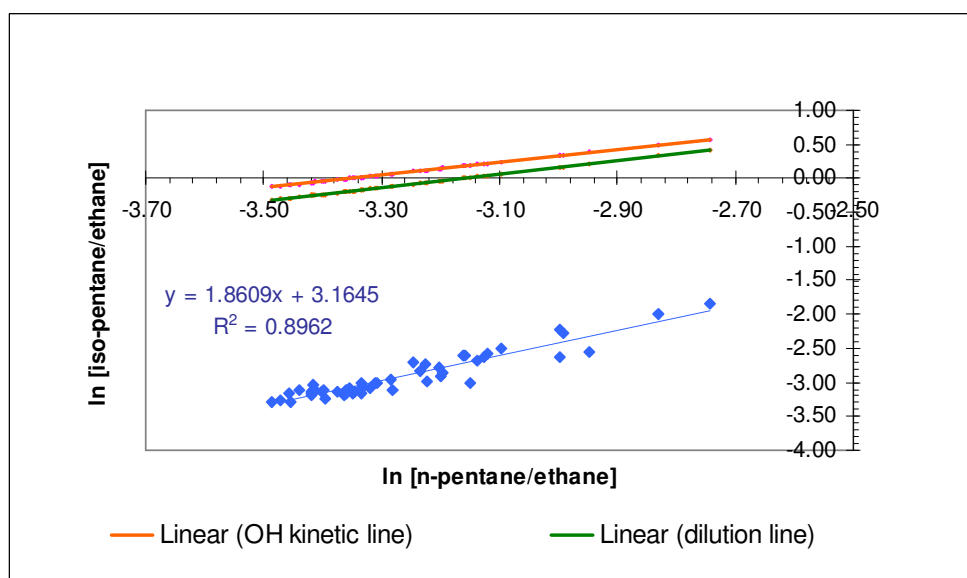
Figure 3.14: Plot of ln [*iso*-pentane]/[ethane] *versus* ln [*n*-pentane]/[ethane] for first test flight B494 (December 2009) flight data. The observed slope of 1.86 is very close to the theoretical NO_3-kinetic slope (1.85) implying the dominance of NO_3-initiated chemistry over mixing. Using the intercept value, the emission ratio ([*iso*-pentane]^0/[*n*-pentane]^0) comes out to be 22.2 for this flight. This value is much higher than reported values of estimated emissions of VOCs by species and by source in National Atmospheric Emissions Inventory 2006 speciation.

The most interesting feature of this plot is that the observed slope (1.86) is nearly the same as calculated kinetic slope (1.85) implying the high influence of NO_3 processing on data points as compared to mixing. The photochemical line represents the case when loss due to chemistry is prominent than mixing. Moreover, this is the only night flight data in which such a strong correlation (R^2 value =0.86) (as shown in **Figure 3.15**) between ln [*n*-pentane]/ [*iso*-pentane] *versus* ln [benzene]/ [toluene] has been observed. Frustrating during this first test flight, the direct NO_3 measurement instrument was not installed.
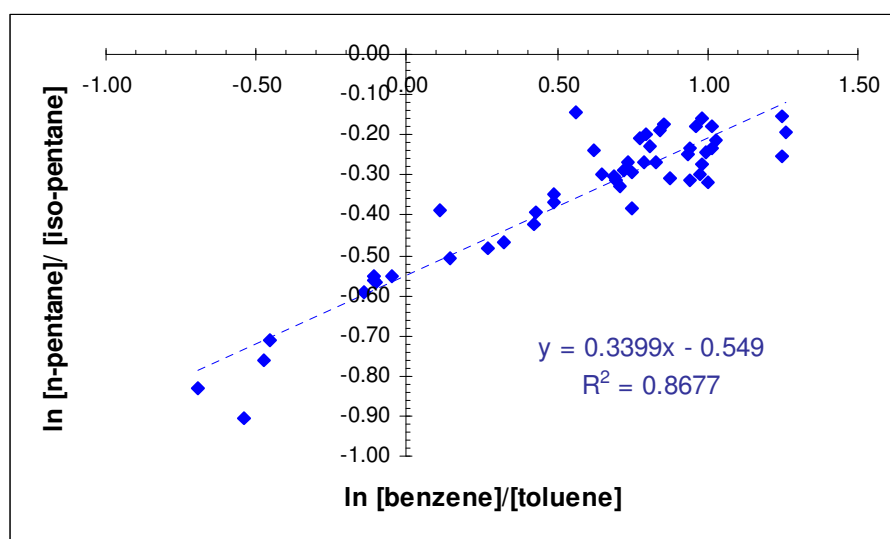
Figure 3.15: Plot of ln [*n*-pentane]/[*iso*-pentane] *versus* ln [benzene]/[toluene] for test night B494 flight data. An excellent correlation between two different pairs suggests the rate at which benzene/toluene is being changed by both oxidants (mainly by OH and negligibly by NO_3) is almost similar to the rate at which pentane isomer is being processed by both oxidants (chiefly NO_3 radical and to a lesser extent by OH).

3.3.3 Hydrocarbon pairs other than pentane isomers and their behaviour

Up to this point, the pentane isomer pair has formed the central focus of the chapter in providing evidence of the NO_3 radical in nighttime data. Given that other hydrocarbons also have differences in the NO_3 rate constant it may be informative to compare other isomer pairs' behaviour against benzene/toluene pair. Eligible pairs that matched the selection criteria of having the same

reactivity towards OH but different with respect to NO_3 are: *n*-butane/*iso*-butane, *n*- hexane/2+3- methylpentane, and *n*-heptane/ethylbenzene (see **Table 3.1**).

The reason for taking 2-methylpentane and 3-methylpentane together as a denominator with the hexane isomer pair is that these peaks appear together on the PLOT column. Their reactivities with respect to NO_3 differ by less than 20% (whilst both have similar rate constants towards OH). From a calculation point of view, the average of rate constants of 2-methylpentane and 3-methylpentane with NO_3 (2.0×10^{-16} cm^3 $molecule^{-1}$ s^{-1}) has been used.

As far as the heptane isomer pair is concerned, the selection of ethylbenzene does fulfil the requirements to form a pair with *n*-heptane; however, the ideal candidate is its branched-chain isomer analogue, 2,2-dimethylbutane, which was not observed in our system.

The pairs higher than C_7 show a difference in reactivity towards both oxidants, and could not be categorised as suitable pairs for demonstrating the presence of oxidants involved. For example, *n*-octane reacts with both OH and NO_3 at almost double the rate of (2,2,4-trimethylpentane or *iso*-octane). Similarly, the isomers of xylenes and trimethylbenzene show differences in rate constants with respect to both oxidants; both types of compounds failed to fall under the category of suitable pairs. Given this kinetic limitation in finding suitable higher hydrocarbon reacting pairs, the chemical analysis of whole air samples was limited to species as large as xylenes to save time and allow processing of as many samples as collected. GCxGC measurements do however provide information on the measurements of larger semivolatile VOCs.

Turning now to the comparison of selected isomer pairs with the benzene/toluene pair, three different plots of ln [*n*-butane]/[*iso*-butane], ln [*n*-hexane]/[2+3-

methylpentane] and ln [*n*-heptane]/[ethylbenzene] were plotted against ln [benzene]/[toluene] for same summer night flight B542. A plot of ln [*n*-pentane]/[*iso*-pentane] *versus* ln [benzene]/[toluene] from same flight has been put together with these plots for ease of comparison.

Starting the comparison with the butane isomer pair, **Figure 3.16** illustrates the pattern of butane isomer pair at night which is contrary to the expected behaviour. In terms of reactivity differences, *iso*-butane reacts with the NO_3 radical at almost double the rate of *n*-butane, but here the pattern exhibited by the butane isomer pair is in agreement with OH chemistry alone.
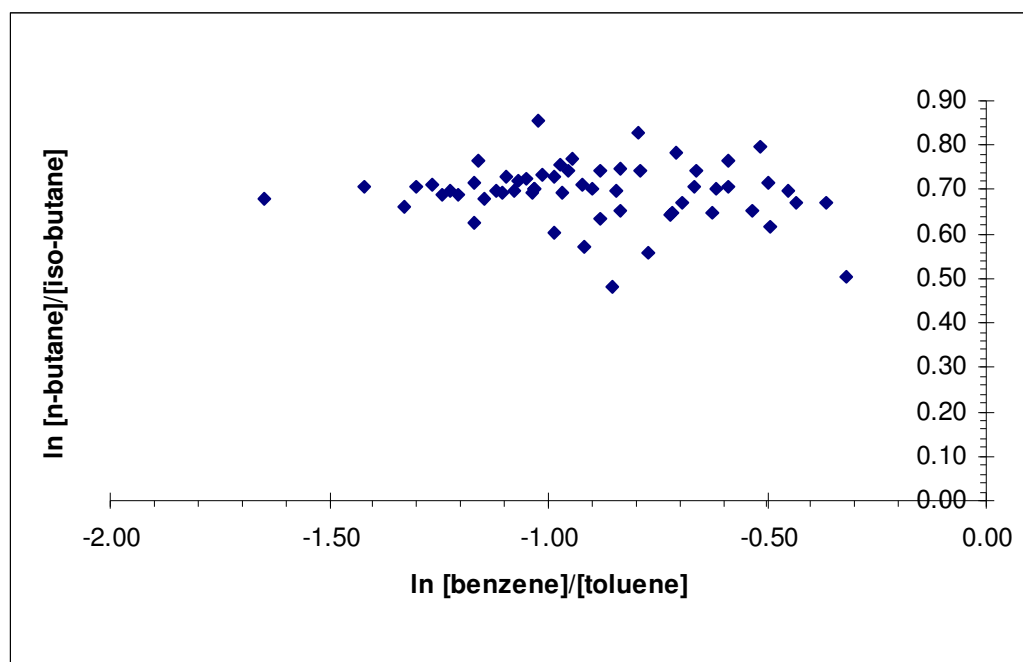
Figure 3.16: Plot of ln [*n*-butane]/ [*iso*-butane] *versus* ln [benzene]/ [toluene] for the summer night flight B542 flight data. The ratio for [benzene]/[toluene] is increasing as air gets processed in agreement with high reactivity of toluene than benzene with respect to OH radical. However, [*n*-butane]/[*iso*-butane] ratio is constant within a very limited range of 0.6-0.7 due to same reactivity with respect to OH.

The ratio for benzene/toluene is increasing as air gets processed in agreement with higher reactivity of toluene than benzene with respect to OH radical.

However, [*n*-butane]/[*iso*-butane] ratio is constant within a very limited range of 0.6-0.7 due to same reactivity with respect to OH. This pattern is similar to pentane isomer pair *versus* benzene/toluene pair demonstrated during day time.

Interestingly, the [*n*-butane]/[*iso*-butane] ratio when plotted (**Figure 3.17**) with acetylene showed a constant value at 2.0 over a reasonable range of more processed (50 pptv acetylene) to less processed air (280 pptv acetylene). The data points lying both sides of this constant range were fewer in number. More than 95% data appear to be influenced by OH chemistry.
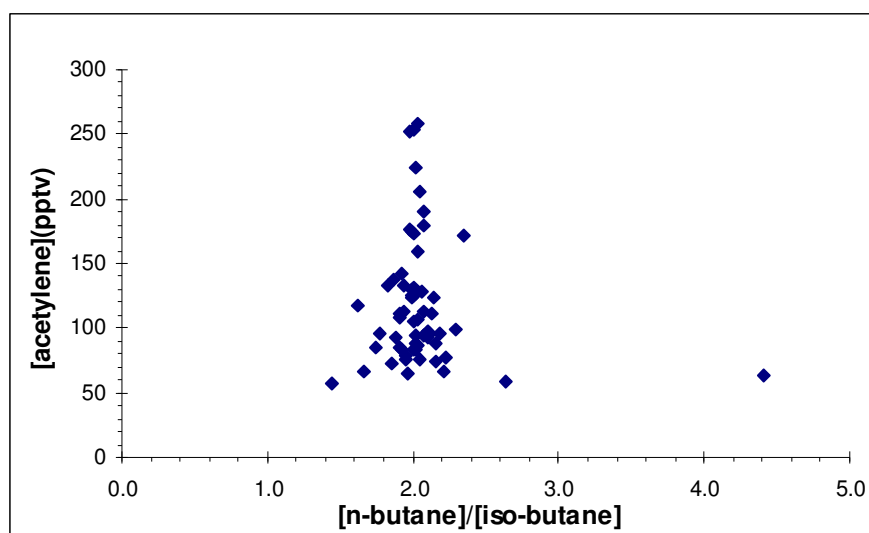
Figure 3.17: Variation of *n*-butane to *iso*-butane ratio with [acetylene] for summer night flight B542. The ratio *n*-butane to *iso*-butane shows a constant value at 2.0 over a reasonable range of more processed (50 pptv acetylene) to less processed air (280 pptv) acetylene More than 95% data appear to be influenced with OH chemistry.

The behaviour of the butane isomer pair was similar to that shown in **Figure 3.17** in all flight data at night. This is clearly a major inconsistency in deriving an NO_3 signal. However, Penkett et al. observed two types of behaviour, one similar to this study in which only a few data points lie to both sides of a constant ratio and the other behaviour showed the tendency of increasing ratio in cleaner air in agreement with NO_3 chemistry (Penkett et al., 2007).

If we closely examine Penkett et al. data in a seasonal study of NMHCs over the North Atlantic for *n*-butane and *iso*-butane, then the ratios calculated for both compounds by using winter background /London plume are the same (*n*-butane=0.07 and *iso*-butane=0.07) in contrast to other isomer pairs which showed systematic low values for *iso*-isomers (Penkett et al., 1993). This point suggests that the ratios derived by this method are in agreement with their respective rate constants with OH. However, for same study the free troposphere winter/free troposphere summer ratio (w/s) differ substantially as compared to their predicted reactivity differences. In this observation the *iso*-butane w/s ratio was 4.1 as compared to n-butane w/s ratio 16.2. This observation was not in agreement with their respective rate constants with OH and required the presence of another oxidant which reacts with *iso*-butane at faster rate than *n*-butane.

As far as the butane isomer behaviour in this study and above mentioned studies is concerned, there are three situations: first, in the current study data sets, the butane isomer when plotted with acetylene behaves by showing a constant ratio with few data points lying to both sides of the constant range, secondly, in the Penkett et al. study in addition to a similar behaviour to our dataset, a clear trend of increasing ratio is observed in agreement with NO_3 chemistry for the Rorvik (Sweden) winter sector, a site around North Sea (Penkett et al., 2007); thirdly free tropospheric seasonal variation of NMHCs over North Atlantic study (Penkett et al., 1993) winter/ summer value for iso-butane required the presence of NO_3 whereas free troposphere winter/urban plume for *n*-butane and *iso*-butane was in accordance with OH chemistry.

There is clearly therefore an inconsistency in butane ratios seen in this experiment, which do not indicate NO_3 processing. If we calculate the lifetime of the *n*-butane/*iso*-butane ratio with respect to average NO_3 levels (24.1 ppt) observed during this flight (B542) then it is 342.5 days as compared to 260 days for the pentane isomer and 214 days for the hexane isomer. As the alkane chain

length increases from butane to hexane, the rate constants with both oxidants increase and thus the lifetime of the ratio decreases.

When a plot of ln [*n*-pentane]/*[iso*-pentane] *versus* ln [benzene]/[toluene] for B542 is created (shown in **Figure 3.18**b) then a reasonable correlation (R^2 value 0.34) suggests the rate at which benzene/toluene is being changed by both oxidants (mainly by OH and negligibly by NO_3) is almost similar to the rate at which pentane isomer is being processed by both oxidants (chiefly NO_3 radical and to a lesser extent by OH). In other words, to observe a good correlation between two different pairs, the lifetime of the benzene/toluene ratio should be similar to the lifetime of the *n*-pentane/*iso*-pentane with respect to both oxidants.

By using the same lifetime or same decay rate concept (equation 3.8) for both isomer pairs, the $[NO_3]/[OH]$ ratio can be worked out by using rate constants(shown in **Table 3.3**) from (Atkinson and Arey, 2003) and substituting in to equations 3.9 and.3.10.

$$\tau_{\frac{benzene}{toluene}} = \tau_{\frac{\text{n-pentane}}{\text{iso-pentane}}} \qquad\qquad 3.8$$

$$\tau_{\frac{benzene}{toluene}} = \frac{1}{(k_{\text{ben-OH}} - k_{\text{tol-OH}})[OH] + (k_{\text{ben-NO}_3} - k_{tol-NO_3})[NO3]} \qquad 3.9$$

$$\tau_{\frac{\text{n-pentane}}{\text{iso-pentane}}} = \frac{1}{(k_{\text{n-pen-NO}_3} - k_{\text{i-pen-NO}_3})[NO3] + (k_{\text{n-pen-OH}} - k_{\text{i-pen-OH}})[OH]} \quad 3.10$$

$$\frac{[NO_3]}{[OH]} = \frac{(k_{\text{ben-OH}} - k_{tol-OH}) - (k_{n-pent-OH} - k_{i-pent-OH})}{(k_{\text{n-pent-NO}_3} - k_{\text{i-pent-NO}_3}) - (k_{\text{ben-NO}_3} - k_{tol-NO_3})} \qquad 3.11$$

The increasing $[NO_3]/[OH]$ ratio from hexane to butane pairs in **Table 3.3** shows that, for an equal value of OH (1 x 10^4 molecule cm^{-3}), a high concentration of NO_3 is required for the butane isomer case for it to correlate well with the benzene/toluene pair.

Table 3.3: NO_3 to OH ratio for butane isomer pair, pentane isomer pair and hexane isomer pair.

Ratio	*n*-butane isomer pair	*n*-pentane isomer pair	*n*-hexane isomer pair
$\dfrac{[NO_3]}{[OH]}$	2.31×10^5	1.31×10^5	0.88×10^5
$[NO_3]$ ppt	93.4	53.2	35.8

The assumption of OH concentration used in above calculation is based on the observed NO_3 mixing ratio; by assuming the observed average NO_3 mixing ratio (24.1 ppt) during flight B542, and using rate constants of *n*-pentane and *iso*-pentane with NO_3 in equation 3.12, would give the lifetime of *n*-pentane/*iso*-pentane ratio (mixing ratio is converted into number density unit as discussed in section 1.1.1). Setting this value equal to benzene/toluene lifetime in equation 3.13 gives a rough estimate of OH concentration.

$$\frac{\tau_{\text{n-pentane}}}{\text{iso-pentane}} = \frac{1}{(k_{\text{n-pentane-NO}_3} - k_{\text{iso-pentane-NO}_3})[NO_3]} \qquad 3.12$$

$$\frac{\tau_{\text{benzene}}}{\text{toluene}} = \frac{1}{(k_{\text{benzene-OH}} - k_{\text{toluene-OH}})[OH]} \qquad 3.13$$

The value of calculated OH concentration for this flight comes out to be 1 x 10^4 molecule cm^{-3} which seems to be reasonable night-time levels; Moreover the comparison of calculated OH concentration with measured OH concentration (FAGE instrument) also supports the derived OH levels by above method as the FAGE instrument during this flight was working below its detection limit (6.5 x 10^5 molecule cm^{-3}). By substituting an OH concentration 1 x 10^4 molecule cm^{-3} and using this value for the NO_3 to OH ratio for all pairs for same flight B542, the highest mixing ratio of NO_3 (93.4 ppt) is required in case of butane to compare well with benzene/toluene pair, as compared to the pentane and hexane isomer pair as shown in **Table 3.3**: NO_3 to OH ratio for butane isomer pair, pentane isomer pair and hexane isomer pair.**Table 3.3**. In other words the hexane isomer pair, due to its high reactivity, should be most efficient in displaying NO_3

evidence at lowest concentration and the butane isomer the least. During this flight, the range of NO_3 mixing ratios observed was 4.7-53.5 ppt with a upper 75th percentile value of 31.8 ppt. The observed NO_3 mixing ratios are quite low as compared to calculated NO_3 mixing ratios (93.4 ppt) needed for the butane isomer pair to compare well against a benzene/toluene isomer pairing and show evidence of the NO_3 radical. No flights encountered average NO_3 levels higher than 80 ppt; it would be interesting to see the behaviour of butane isomer pair at such a high mixing ratios since the implication would be that at this level the ratio would respond.

Comparing the hexane isomers against benzene/toluene for flight B542 and the pentane isomers *versus* benzene/toluene, the R^2 value is same in both plots but the slope is greater in the case of the pentane isomer. By using average NO_3 mixing ratio 24.1 ppt, the lifetime of hexane isomer would be calculated as 214 days as compared to 259 days for pentane isomer. As it can be seen from **Figure 3.18** that hexane isomer pair does indeed correlate well with benzene/toluene pair providing supporting evidence to that of pentane isomers.

It was interesting therefore to compare the hexane isomer pair for all night flights where there was evidence of NO_3 inferred by the pentane isomer pair. Clear signals similar to flight B542 were observed in the test flights with good correlation between two different pairs (R^2 0.65 and slope 0.36, not shown here) However, comparing the same pair for B535 flight, there seems to be no correlation between ln [*n*-hexane]/[2+3-methylpentane] and ln [benzene]/[toluene] pairs in **Figure 3.19**.

181
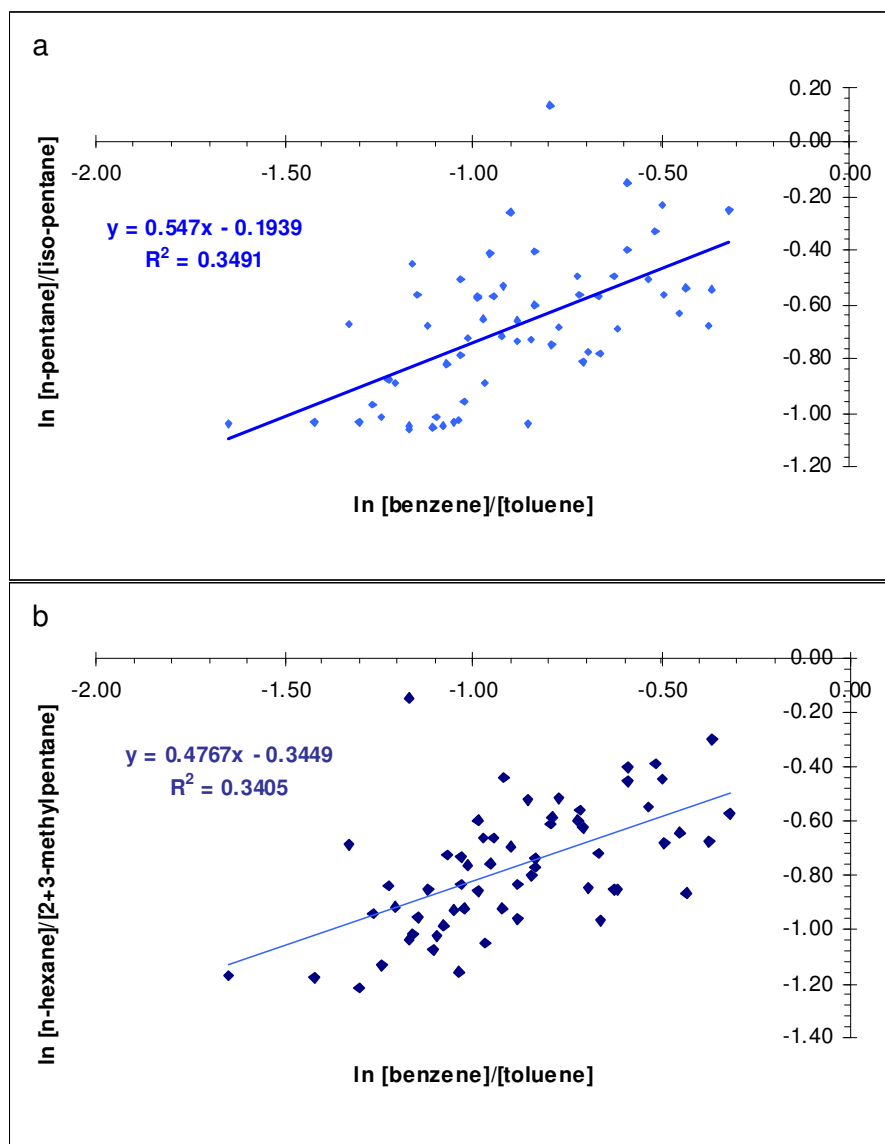
Figure 3.18: Plot of (a) ln [*n*-pentane]/[*iso*-pentane] *versus* ln [benzene]/[toluene] for summer night B542 flight data compared with (b) plot of ln [*n*-hexane]/[2+3-methylpentane] *versus* ln [benzene]/[toluene] for summer night B542 flight data. Both isomer pairs are reasonably correlated with benzene/toluene pair supporting the evidence of NO_3 radical.
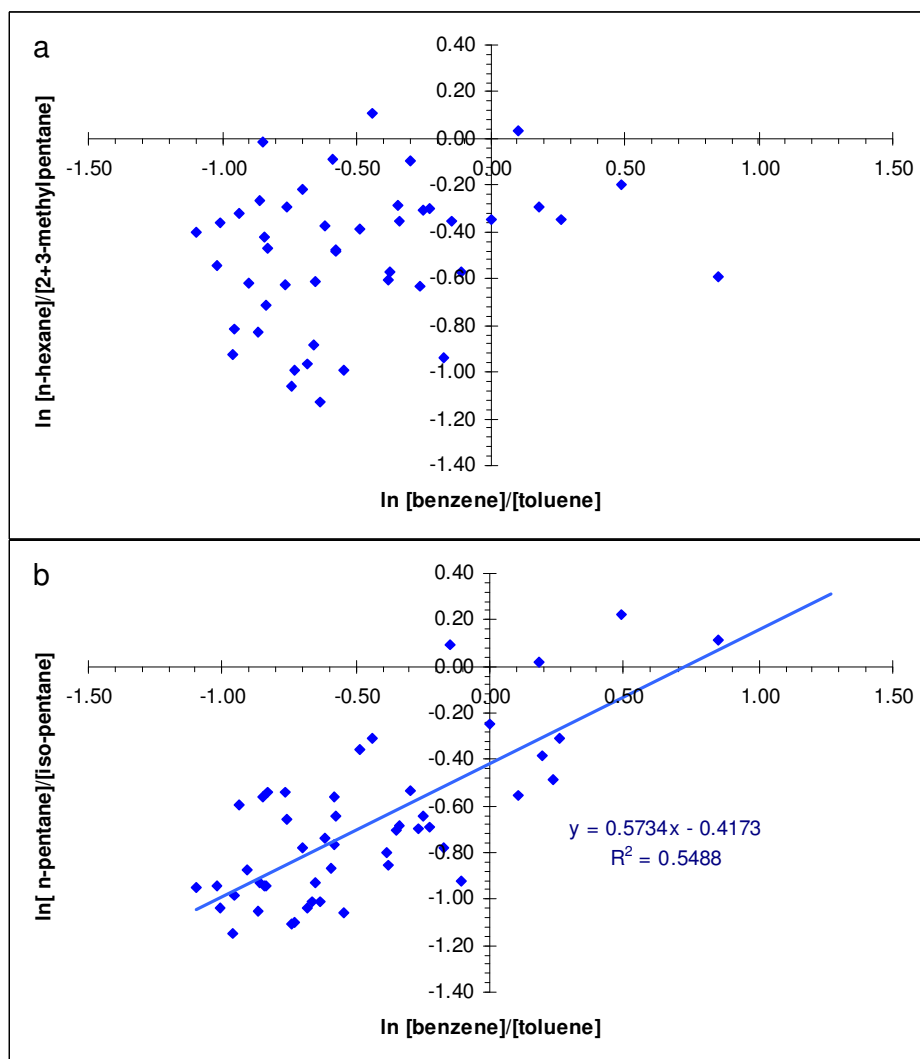
Figure 3.19 Plot of (a) ln [*n*-hexane]/[2+3-methylpentane] *versus* ln [benzene]/[toluene] for summer night B535 flight data compared with plot of (b) ln [*n*-pentane]/[*iso*-pentane] *versus* ln [benzene]/[toluene] for summer night B535 flight data (b). The hexane isomer pair is not correlated with benzene/toluene pair whilst pentane isomer pair displays a reasonable correlation with [benzene]/[toluene] pair for same flight data. It implies the importance of [NO$_3$]/[OH] ratio in controlling either strong or weak correlations with [benzene]/[toluene] pair and displaying NO$_3$ evidence.

The main difference between flight B535 and B542 is that the observed NO$_3$ mixing ratios were higher during B542 (4.7-53.5 ppt with a 75th percentile value of 31.8 ppt) in comparison with B535 (4.1-40.5 ppt with a 75th percentile value of 26.5 ppt). Using the same OH levels, the hexane pair needs 35.8 ppt NO$_3$ to display NO$_3$ evidence on the basis of the [NO$_3$]/ [OH] ratio. However, the flight

B535 saw only 4 data points above this limit out of 49 data points in comparison with 14 data points for B542 flight. This reason seems sufficient to explain the absence of hexane isomer correlation with benzene/toluene pair for flight B535. However, the pentane isomer pair, despite the criteria of requiring 52 ppt, which was not seen at all during this flight, correlated well with benzene/toluene pair. The reason for this is not clear but it may be related to the value of $[NO_3]/[OH]$ ratio in controlling either strong or weak correlations with benzene/toluene pair and displaying NO_3 evidence.

Ultimately there is a rather limited dataset collected here, but it does indicate that hexane isomers show a similar NO_3 signal in air masses where high NO_3 has been seen *in situ*, and this supports evidence of NO_3 derived from the pentane isomers. A lack of observed NO_3 signal from butane isomers may potentially be rationalised by its slower reaction rates, giving it a lower sensitivity to NO_3-induced changes.

Finally, the correlation of the heptane isomer pair with [benzene]/[toluene] pair as illustrated in **Figure 3.20** is very poor for flight B542, which had shown strong signals with both pentane and hexane pairs. For these species however absolute mixing ratios are rather low and this adds scatter into the data.

Overall, on the basis of comparison of three selected different pairs, it can be concluded that the pentane isomer pair shows the most consistent behaviour, switching its ratio from day to night, and dusk to dawn throughout different parts of the day. Its particular NO_3 lifetime coupled to high measurement sensitivity makes it a unique pair in diagnosing the presence of oxidant involved during processing.
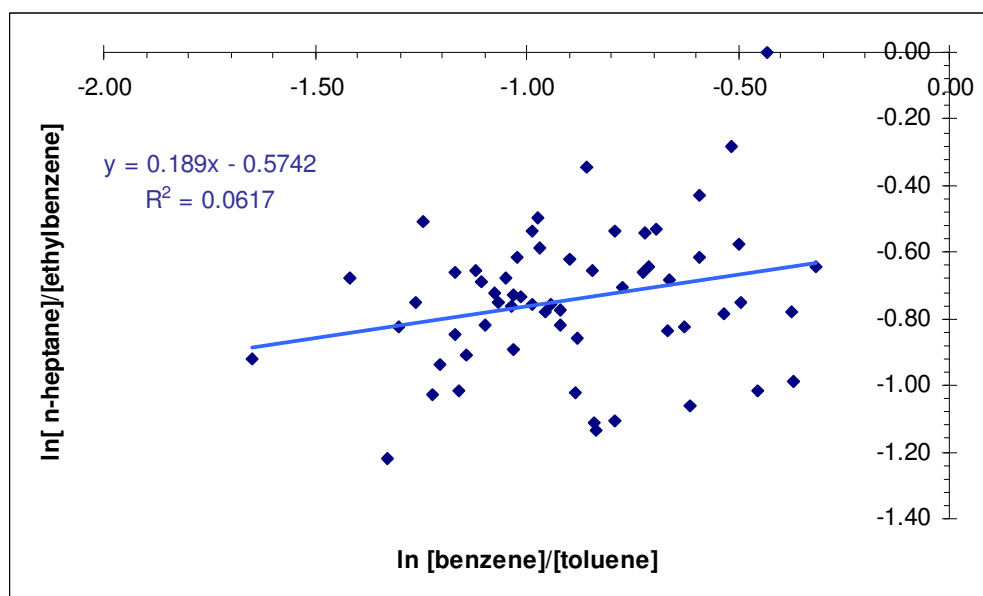
Figure 3.20: Plot of ln [*n*-heptane]/[ethylbenzene] *versus* ln [benzene]/[toluene] for summer night B542 flight data. The correlation of the heptane isomer pair with benzene/toluene pair is poor whilst for the same flight which had shown strong signals with both pentane and hexane pairs showed strong signals of NO_3 evidence. The inconsistent behaviour can not be explained on the basis of $[NO_3]/[OH]$ ratio argument, although may be related to the lower absolute mixing ratios which add scatter to the ratio calculations.

3.4 Summary

A hydrocarbon ratio approach has been used during summer, autumn and winter phases of RONOCO field campaign period between December 09 and January 11 to diagnose the changing pattern of log-log plots associated with the presence of different oxidants during day, night, dusk and dawn.

A linear log-log relationship has been used by plotting ln [*iso*-pentane]/[ethane] *versus* ln [*n*-pentane]/[ethane] throughout various phases of the day. The behaviour of the pentane isomer pair has been found often to be different between day and night. The observed slopes generally have been greater than predicted OH-kinetic slopes for night-time data giving a clear indication of deviation from OH chemistry and the influence of NO_3 chemistry. A good

agreement between observed and OH-kinetic slopes for daytime flight data is supportive of the dominance of OH chemistry during the day.

During winter night flights made in month of January 2011, the impact of high background mixing ratios and mixing was clear in our data, exhibiting slopes on occasion less (0.73) than the theoretical kinetic slope (0.94) although each flight was highly variable: a winter night flight made in month of December 09 showed a striking feature of observed slope (1.86) similar to calculated kinetic NO_3 slope (1.85) implying the dominance of processing rather than mixing.

Only small differences were seen in the derived NO_3 between dusk and dawn flights although on all these flight NO_3 was seen *in situ* to be rather low, and a signal in hydrocarbon ratios perhaps not expected.

When the pentane isomer pair was plotted against the [benzene]/[toluene] pair, which is exclusively processed by OH, then a good correlation was found for night data and no correlation with daytime data. During daylight hours both isomer pairs are processed by OH so data are horizontally aligned whilst during night both pairs are processed by different oxidants (pentane isomer pair mainly by NO_3 and [benzene]/[toluene] pair mainly by OH) illustrating a reasonable correlation. Such an analysis eliminates the possibility of an OH-driven artefact NO_3 signal generated by uncertainty in either the OH rate constants or a hidden or co-eluting hydrocarbon.

A reasonably good correlation between these two pairs of species indicated that the decay rate of both pairs was almost the same, or in other words the lifetime of both ratios ($\tau_{n\text{-pentane/iso-pentane}} = \tau_{benzene/toluene}$) are almost the same with respect to both oxidants OH and NO_3. On the basis of the same lifetime concept for two well correlated pairs, an [NO_3]/[OH] ratio was derived for [*n*-butane]/[*iso*-butane], [*n*-pentane]/[*iso*-pentane] and [*n*-hexane]/[2+3-methylpentane].

Using the same OH levels of 1 x 10^4 molecule cm^{-3} (calculated on the basis of observed NO_3 concentration), the highest mixing ratio of NO_3 (93.4 ppt) is required for butane isomers to perform well with the [benzene]/[toluene] pair, in comparison to faster reacting hexane and pentane. In principle the pentane and hexane isomer pairs should be more sensitive to indicating the presence of NO_3

186

and this may explain why butane isomers in many studies do not show NO_3-driven changes in ratio.

During both phases of the campaign, the observed NO_3 levels were less than 80 ppt (75th percentile) during whole air sampling period, which means that the required mixing ratio of nitrate (93 ppt) for a butane isomer pair to show NO_3 evidence was not met. This suggests the reason for not seeing evidence of NO_3 presence from log-log butane plots despite the differences in reactivity of butane isomer pair towards NO_3.

As far as the hexane isomer pair is concerned, it was correlated with [benzene]/[toluene] pair but not for all night flights in which NO_3 evidence was demonstrated by pentane isomer pair. The inconsistent behaviour can not be explained on the basis of $[NO_3]/[OH]$ ratio argument, although may be related to the lower absolute concentrations which adds scatter to the ratio calculations. For the higher hydrocarbons, there is also increasing risk of co-elution which may influence ratios.

The correlation of the heptane isomer pair with [benzene]/[toluene] for night flight data was very poor suggestive of involvement of OH in processing both pairs.

Overall it can be concluded that generally consistent behaviour of hexane and pentane isomers could be seen and that the derived NO_3 from this changing ratio was greatest when *in situ* measurements were at their highest. A lack of response in butane could be rationalised by it slower reaction rate.

Chapter 4:

The influence of nitrate radicals on the variability-lifetime relationship and loss rate of VOCs in the UK urban boundary layer

4.1 Introduction

4.1.1 Experimental goals and hydrocarbon measurements

The purpose of this supplementary chapter using data from the ROle of Nightime chemistry in controlling the Oxidizing Capacity of the AtmOsphere (RONOCO) field campaign dataset is to extend the discussion, and by applying another useful application of the variability-lifetime relationship to examine the influence of the NO_3 radicals on hydrocarbon variability trends. The themes that were touched upon in the previous chapter were focused on the utility of the ratio approach in diagnosing the presence of NO_3 radicals through the changing patterns of hydrocarbons in different seasons and different periods of the day and also to examine the competency and consistency of branched isomer pairs, other than the pentane isomer pair, in identifying the presence of NO_3 radicals. A wealth of data acquired in different seasons and different phases of the day during the RONOCO campaign presents us with a unique opportunity to test the robustness of variability-lifetime approach in investigating the impact of NO_3 radical on the variability patterns of hydrocarbons. To the best of our knowledge, these variability trends have not been explored before by comparing between day and night data sets with reference to the presence of NO_3 radicals.

In addition to comparing variability trends between summer and winter, and day and night in section 4.3.2, the hydrocarbon ratio approach has been used to compare the oxidation rates of two different pairs of hydrocarbons with different oxidants to derive the best estimate of the NO_3 to OH ratio. This has been compared to direct measurements made during the RONOCO flights and to a database on hydrocarbons collected from sites surrounding the North Sea during the European Union Hydrocarbons Across the North Sea Atmosphere (EU HANSA) project in section 4.3.3. Finally the VOC oxidation rates have been compared for alkanes, alkenes, aromatics and oxygenates with respect to the two

key night time oxidants, the NO_3 radical and O_3, in section 4.3.4. The key objectives of the present chapter are:

(a) To examine the atmospheric variability of C_2 –C_8 VOCs in summer and winter seasons, and compare the trends for branched chain isomers between day and night dataset with reference to the presence of NO_3 radicals.

(b) To compare the inferred $[NO_3]/[OH]$ ratio with the direct measurements and also with the historical HANSA data set.

(c) To investigate the impact of NO_3 at night on the loss of anthropogenic VOCs in the UK urban boundary layer.

4.2 Data Coverage

The hydrocarbon data presented here have been collected from 8 night flights in summer months (B534 to B539, B541 and B542) with approximately 395 whole air samples and 3 night flights (B564, B565 and B566) in winter months with roughly 175 whole air samples, and one winter night test flight B494 with almost 60 whole air samples. Here, summer and autumn have been classified as data captured in July 2010 and September 2010 respectively, while the winter data were collected in December 2009 (test flight B494) and January 2011. Data from day, dusk and dawn flights have also been used in this chapter for a comparative study. Two daytime flights, one in autumn (B550) and one in winter (B571); five dusk flights one in summer (B540), one in autumn (B549) and three in winter (B568 to B570) and two dawn flights one in autumn (B551) and one in winter (B567) were made during this field campaign. The experimental details are described in detail in the previous chapter. All data used here are from samples collected within the boundary layer and the sampling locations are shown in **Figure 4.1**.
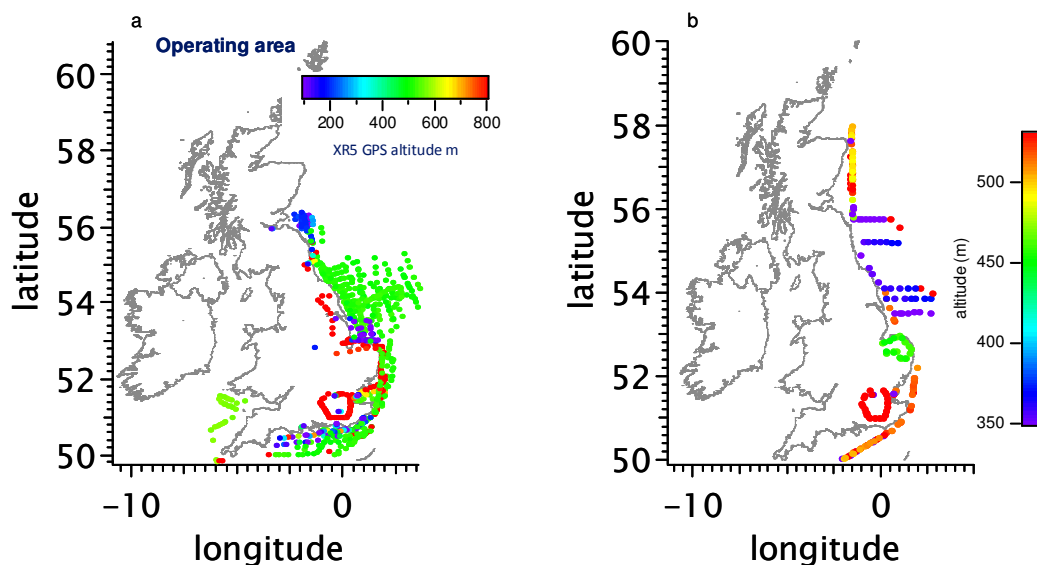
Figure 4.1: Map of UK showing sampling locations for (a) summer night and dusk flights (B534-B542) made in July 2010 and winter night, day, dusk and dawn flights (B564-B571) in January 2011; (b) one winter test flight B494 made in December 2009 and three autumn flights (B549, B550 and B551) in September 2010 during the RONOCO aircraft field campaign.

4.3 Results and discussion

4.3.1 VOC mixing ratios and statistical distributions

In order to assess the quality of a large hydrocarbon data set and the distribution patterns, the cumulative frequency distribution plots for summer and winter seasons have been plotted for selected compounds as shown in **Figure 4.2**. There is a clear distinction in the distribution patterns of data between winter and summer months. The *y* axis on this plot represents the actual frequency of a data point or in other words the fraction of data that are at or below the selected mixing ratio on the *x* axis. The frequency equal to 0.50 on the *y* axis corresponds to the median mixing ratio on the *x* axis. To check whether data are normally distributed or not, the mixing ratio corresponding to 50% distribution should be equal to the mean mixing ratio for each compound in a dataset. The mean and median mixing ratios for summer and winter months are presented in **Table 4.1**.
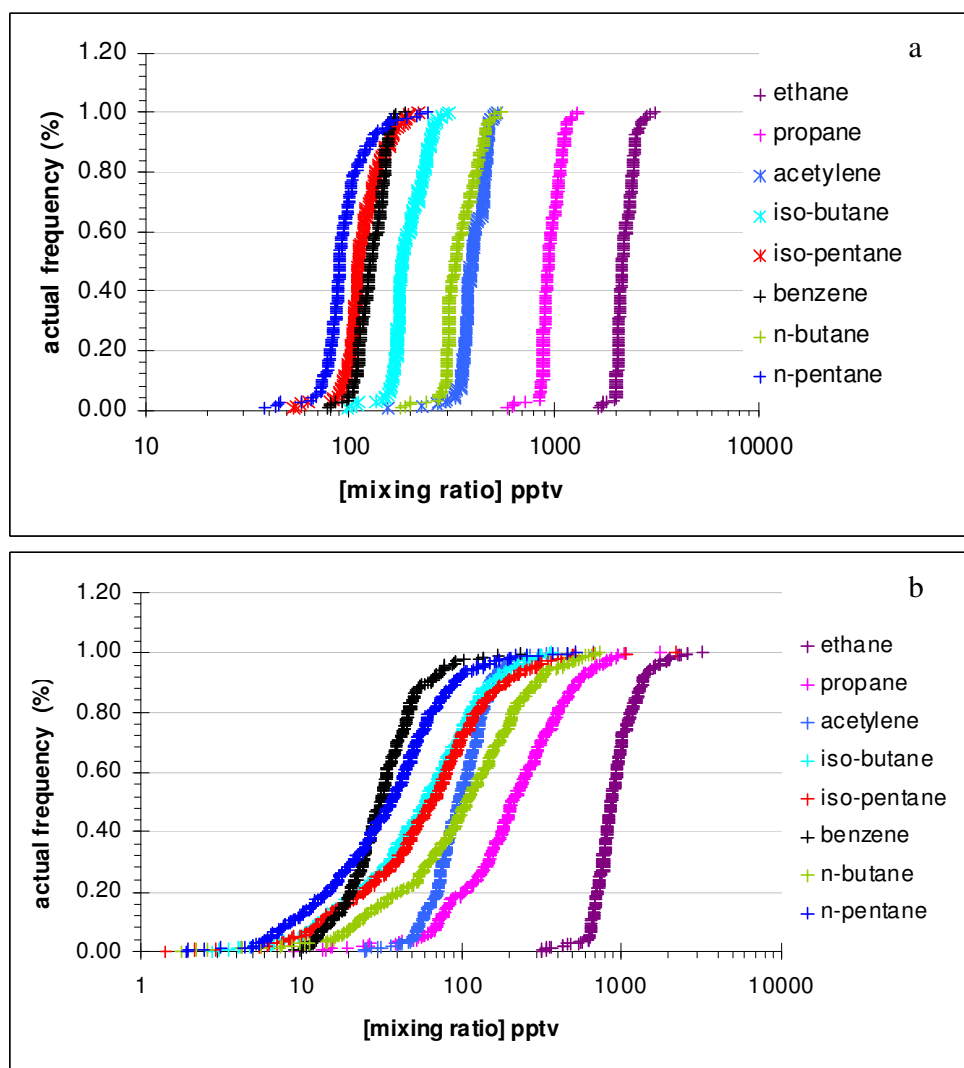
Figure 4.2: Cumulative frequency distributions of selected trace gases measured in the nighttime boundary layer above the UK during (a) winter (January 2011) and (b) summer phases (July 2010) of the RONOCO campaign.

It is clear from **Table 4.1** that mean mixing ratios for all selected compounds in both seasons are higher than the median mixing ratios; however the difference between mean and median for summer months are more significant compared to winter months. The mean mixing ratios for winter months are up to 2.5% higher than median for less reactive species for example ethane, acetylene, propane and benzene whilst the differences up to 7% are observed for reactive species. The differences between mean and median for summer season are up to 10% for ethane and acetylene and 30% for reactive species, except *iso*-pentane for which the difference is more than 45%.

Table 4.1: Comparison of mean and median mixing ratios (pptv) measured in the night time boundary layer above the UK during winter (January 2011) and summer (July 2010) phases of the RONOCO campaign.

Species	Winter (January 2011)		Summer (July 2010)	
	Mean mixing ratio (pptv)	Median mixing ratio (pptv)	Mean mixing ratio (pptv)	Median mixing ratio (pptv)
ethane	2231	2167	965	877
acetylene	405	395	107	97
propane	968	938	273	210
benzene	129	126	38	32
iso-butane	195	182	77	60
n-butane	351	330	144	109
iso-pentane	119	110	97	66
n-pentane	96	89	48	37

The higher values of mean mixing ratios in a dataset for all selected compounds in both seasons points to few data points with substantially elevated mixing ratios. This is also clear from the plot in **Figure 4.2** for summer data in which the elevated mixing ratios are observed at the high end of the mixing ratio range, and due to these data points the mean is shifted towards a high value, skewing the distribution with the increase in reactivity. To deal with these high value data points which are responsible for the skewed distribution, transformation on a natural log scale shifts these from the extreme right to towards left and gives more symmetrical shape to the distribution than without log transformation. Therefore the dataset in both seasons are regarded as log-normally distributed.

Another interesting feature of these plots is the range of mixing ratios, which increases with an increase in species reactivity to OH. Overall, the mixing ratio range is wider for the summer data than for winter in accordance with the concept of higher variability in a summer month dataset. The most reactive species in both plots is *iso*-pentane and its mixing ratio range in summer covers three orders of magnitude in comparison with that of the ethane displaying a range of roughly one order of magnitude. The variability of the hydrocarbons for

different seasons and different period of day will be discussed in more detail in the next section.

4.3.2 Variability-lifetime relationship

4.3.2.1   Variability comparison: summer *versus* winter data

This section takes advantage of the large hydrocarbon dataset by comparing all summer night data with all winter night data to observe the influence of NO_3 on variability trends. **Figure 4.3** illustrates a double logarithm plot for the variation of standard deviation of natural logarithm of C_2 to C_8 alkanes, C_2 to C_4 unsaturates, selected oxygenates and CO at their estimated photochemical lifetime in summer and winter data sets. The CO measurements were provided by FAAM and the rest of the species were measured by the dual channel GC-FID system.

The comparison of variability plots between winter and summer data clearly shows the differences in variability-lifetime relationship suggesting a varying degree of influences of mixing and chemistry between summer and winter months. Overall the standard deviation of ln[X] values for each species in winter is less than that of in summer as presented in **Table 4.2**. The winter dataset has a more coherent trend ($R^2 = 0.83$) than summer data ($R^2 = 0.43$) over a wide range of hydrocarbon reactivity, displaying an increase in variability as reactivity increases from ethane to octane.
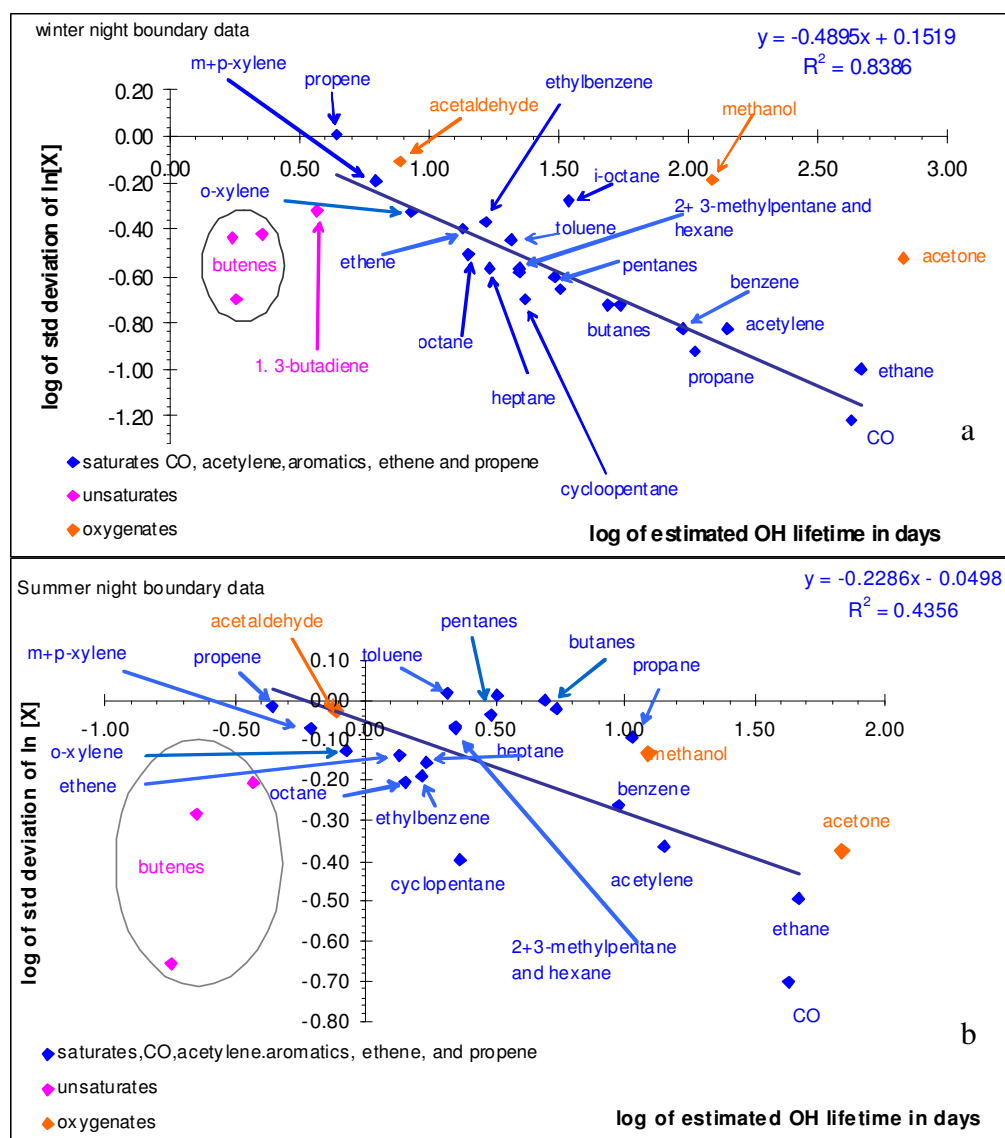
Figure 4.3: A plot of log of standard deviation of ln[X] against log of estimated lifetime (in days) for the entire RONOCO dataset for (a) winter, January 2011 and (b) summer, July 2010 campaign. Lifetimes were calculated using OH = 1×10^6 molecule cm^{-3} for summer and 1×10^5 molecule cm^{-3} in winter taking rate constants at 298 K (Atkinson and Arey, 2003). CO was measured in-flight and was averaged during whole air sampling times. The rest of the species were measured by GC-FID.

Although these observations are from the boundary layer, a good fit to winter data suggests that the influence of local sources is small as compared to summer data; the high background mixing ratios in winter for all species are less affected by local emissions as compared to the lower summer background mixing ratios, which are comparatively more susceptible to local emissions. The points

corresponding to *iso*-octane, propene, oxygenates and butenes for winter data in **Figure 4.3**a show noticeable deviations from the trend line. Despite the fact that the OH lifetime of *iso*-octane is 3 times longer than that of the *n*-octane, its variability is a factor of two higher than *n*-octane for the winter dataset, as presented in **Table 4.2**. Owing to the lack of measurements for *iso*-octane in summer, it is difficult to compare this feature between summer and winter months. The occurrence of *iso*-octane above the trend line suggests that there is an additional removal process in play. Generally the branched chain isomers, for example *iso*-butane, *iso*-pentane, 2 and 3-methylpentane, react faster with NO_3 in comparison with their straight chain analogues; however, it is *n*-octane which reacts faster, almost double, with the NO_3 radical than *iso*-octane as shown in **Table 3.1.**

The unusual observation of *iso*-octane either indicates involvement of a different source or inaccuracies in the reported rate constants. If we closely observe the variability difference for this isomer pair between day and night data then it is clear from the data presented in **Table 4.3** that the variability of *n*-octane is higher for day data than *iso*-octane justifying the higher reactivity of *n*-octane towards OH than *iso*-octane, as is obvious from rate constants given in **Table 3.1.** This gives us confidence in the octane isomer pair's OH rate constants used for the lifetime calculation. When taking the entire nighttime winter dataset, the variability of *iso*-octane is higher than *n*-octane, as can be seen from **Table 4.2**. This is in line with general intuition that the branched iso-octane should react faster with night time oxidant NO_3 radical than *n*-octane. However, from the literature, the rate constant of *n*-octane with NO_3 is reported to be almost double that of *iso*-octane as presented in **Table 3.1**.

Table 4.2: Comparison of Sln[X] values between summer, (July 2010) and winter, (January 2011) night data. Lifetimes were calculated using OH = 1×10^6 molecule cm^{-3} for summer and 1×10^5 molecule cm^{-3} in winter using rate constants at 298 K (Atkinson and Arey, 2003). The asterisk symbol (*) is for 2,2,4-trimethylpentane. NR denotes no data available.

Species	Summer (July 2010)		Winter (January 2011)	
	Sln[X]	Estimated lifetime (days)	Sln[X]	Estimated lifetime (days)
ethane	0.32	46.67	0.10	466.7
CO	0.20	42.87	0.06	428.67
acetylene	0.43	14.11	0.15	141.15
propane	0.81	10.62	0.12	106.18
iso-butane	0.95	5.46	0.19	54.59
n-butane	1.00	4.90	0.19	49.04
iso-octane*	NR	3.47	0.53	34.65
iso-pentane	1.03	3.22	0.22	32.15
n-pentane	0.92	3.05	0.25	30.46
cyclopentane	0.40	2.33	0.20	23.29
2+3-methylpentane	0.86	2.23	0.27	22.26
n-hexane	0.85	2.23	0.26	22.26
heptane	0.70	1.71	0.27	17.12
n-octane	0.63	1.43	0.31	14.27
ethene	0.73	1.36	0.40	13.58
propene	0.97	0.44	1.02	4.40
1-butene	0.62	0.37	0.48	3.69
iso-butene	0.52	0.23	0.38	2.25
trans-2-butene	0.22	0.18	0.20	1.81
1,3-butadiene		0.17	0.37	1.74
benzene	0.55	9.49	0.15	94.87
toluene	1.04	2.06	0.36	20.56
ethylbenzene	0.65	1.65	0.43	16.53
o-xylene	0.75	0.85	0.47	8.51
m+p-xylene	0.85	0.62	0.64	6.19
acetone	0.42	68.08	0.30	680.83
methanol	0.74	12.31	0.65	123.13
acetaldehyde	0.94	0.77	0.78	7.72

As shown in the hydrocarbon ratio plots with pentane isomers in the previous chapter, none of the winter flights showed the presence of NO_3 radical, although the direct measurements of NO_3 radical were reported at levels between 2 ppt and 20 ppt. On comparing the variability differences between other isomer pairs for the entire winter night dataset, it is clear that the differences between butane isomers are zero; whilst contrary to the expectations, it is *n*-pentane that exhibits higher variability by 14% and finally the branched isomer 2+3-methylpentane displays higher variability than its straight chain analogue by ~ 4%. Although there are differences and inconsistencies among isomer pairs in the winter dataset, the higher variability of the *iso*-octane in comparison with *n*-octane casts some doubt on their rate constants with respect to NO_3 radicals(**Table 4.5**), assuming that there is no instrumental artefact for this pair and the variability values are reliable.

Another feature of these plots is that the coherent pattern of lifetime-variability in the winter dataset gives us the opportunity to observe the differences between the trends of unsaturates and saturates. If ethene and propene variability lie along the same trend line that is defined by alkanes, acetylene and benzene then this fact can be used in determination of the OH concentration (Jobson et al., 1998). If we examine the data points corresponding to ethene, propene and butenes then it is clear from **Figure 4.3** that ethene falls on the trend line, whilst propene is above the trend line exhibiting higher variability. With respect to an OH concentration of 1×10^5 molecule cm^{-3} (a typical average OH mixing ratio for this time of year (Harrison et al., 2006)), the lifetime of ethene and propene is 13.6 and 4.4 days respectively. By including reaction with approximately 37 ppb O_3 and 9 ppt NO_3, roughly equal to the average mixing ratios measured for the winter months flights, the lifetime of ethene and propene is reduced to 5 and 0.8 days respectively. When these removal processes are factored in then propene falls on the trend line and ethene deviates slightly from trend line (not plotted). This improved agreement provides evidence that the observed variability for propene and ethene is consistent with a combined set of reactions with NO_3, O_3 and OH.

The low variablity of butenes and 1,3-butadiene can be interpreted in terms of local sources or contamination, where continuous supply of these chemicals is suppressing the trends. As these species are highly reactive, which means that their lifetime is short in comparison with mixing and transport scale times, making them more vulnerable to be influenced by local sources. Another reason for their suppressed variability could be instrumental or storage artefacts; however, in our case the stability tests performed at the interval of two weeks prove that these reactive species are stable within this time frame.

Another group of compounds which deviate from the general trend are oxygenates. Acetone and methanol lie on the parallel trend with a constant but higher offset in winter than summer dataset. On the reactivity scale, acetone is the least reactive whilst the most reactive compound is acetaldehyde. There is an increase in variability as we move from acetone through methanol to acetaldehyde; however, the variability of acetaldehyde is less than expected. It is important to note that there are known difficulties in the accurate measurement of acetaldehyde. Reaction with O_3 with heavy weight organic material in inlet lines is thought to produce acetaldehyde which could potentially lead to reporting higher acetaldehyde values resulting in less variability in the data shown here.

In order to make comparison for *b* values (the exponent *b* is the slope in the logarithmic correlation plot between log Sln[X] versus log of estimated OH lifetime in days (equation 1.92 in chapter 1) for different hydrocarbon species and is an indicator of mixing influences as discussed in (**section 1.2.8.2**) for the entire dataset between summer and winter months, **Figure 4.4** shows the comparison between summer and winter dataset for a plot between OH lifetime and variability for selected C_2 to C_5 compounds. There is a good correlation between OH lifetime and variability for both sets of data (R^2 =0.85 for summer and 0.88 for winter data) with slightly higher correlation for winter data. The variability differences between acetylene and propane are greater in summer than in winter; the reactivity of propane towards OH is roughly 25% greater than

acetylene; however, the observed variability of acetylene is higher than propane by 25% for winter data whilst for summer, the variability of propane is a factor of two high than acetylene. The *b* value ranges from 0.31 in winter to 0.44 in summer reflecting the greater influence of chemistry over mixing in summer. The calculated value of A (A is a fitting parameter and is an intercept in the logarithmic correlation plot between log Sln[X] versus log of estimated OH lifetime in days for different hydrocarbon species and is a measure of the spread in the range of air mass ages in the sampled data as discussed in (**section 1.2.8.2**) ranges from 0.67 in winter to 1.8 in summer comparable to a Harvard forest dataset (Goldstein et al., 1995b) reported by (Jobson et al., 1999) (A = 0.99) consisting of fresh continental air masses suggesting the smaller spread in the ages of the sampled air mass.
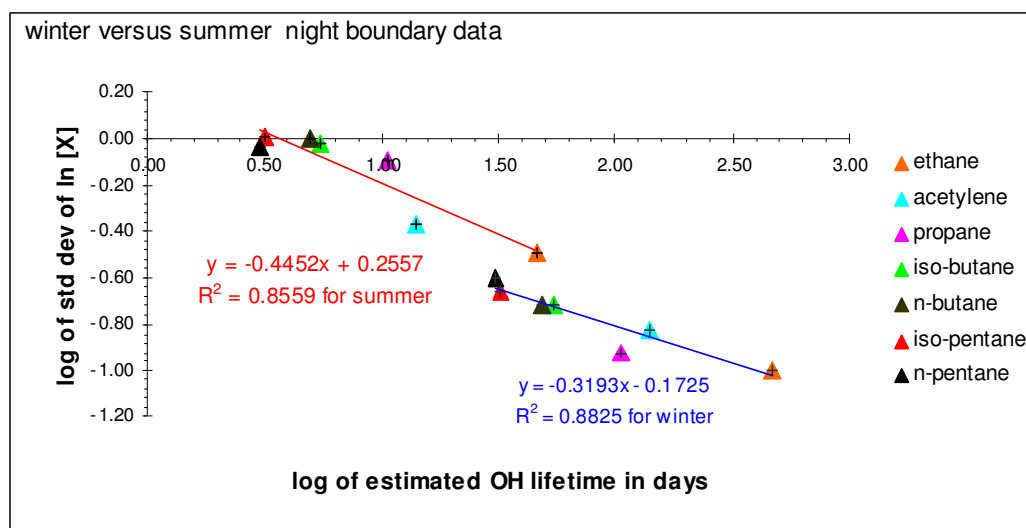
Figure 4.4: Comparison of log of standard deviation of the natural logarithm of selected hydrocarbons mixing ratios between summer, July 2010 and winter, January 2011 plotted against their logarithm of estimated seasonal OH lifetime. Lifetimes were calculated using OH = 1 x 10^6 molecule cm^{-3} for summer and 1 x 10^5 molecule cm^{-3} in winter using rate constants at 298 K (Atkinson and Arey, 2003).

The discussion up to this point has focussed on seasonal differences in the variability-lifetime relationship suggesting a varying degree of influence of mixing and chemistry between winter night and summer night datasets. A good correlation not only validates the measurement but also gives an indication that

the precision of the instrument involved in this study is better than the variability in the datasets (Williams et al., 2000). The purpose of introducing this approach for the RONOCO data set is to assess the influence of NO_3 radicals in affecting the variability-lifetime relationship among branched chain isomer pairs. This picture has emerged from a combined data set; nonetheless it is not difficult to detect the subtle variability differences between all winter night and all summer night flights. For the entire summer night dataset, the variability of *iso*-pentane is higher than *n*-pentane and for the entire winter night data *n*-pentane displays higher variability than *iso*-pentane as shown in **Table 4.2**.

As it was shown in the previous chapter there was no evidence of NO_3 presence through pentane isomers ratio plots during all three winter night flights; the observed slope (0.65 - 0.73) of ln[*iso*-pentane]/[ethane] v*ersus* ln[*n*-pentane]/[ethane] was less than the OH-kinetic slope (0.94). However, the influence of NO_3 was apparent from similar double logarithm plots for the few summer night flights. The good correlation in the entire winter data (**Figure 4.3**) suggests a negligible influence of NO_3 chemistry when compared to the summer data plot. For summer the larger scatter in the data set suggests the greater influence of the NO_3 radical. In the broader sense, the two approaches, hydrocarbon ratio and lifetime-variability, agree very well when compared between summer night and winter night data especially with reference to the pentane isomer pair. At this stage one question that needs to be asked is "can we clearly see differences in the changing pattern of the variability–lifetime relationship of branched chain isomer pairs between day and night?" similar to the hydrocarbon ratio approach adopted in the previous chapter for differentiating day data from night data. The next section attempts to address this question.

4.3.2.2 Variability comparison: day *versus* night data

To distinguish variability trends for branched chain isomer pairs between day and night, a typical night flight and a day flight were selected for comparison. The criteria for choosing a typical night flight was a good agreement between observed slope and NO_3-chemistry kinetic slope in a plot of ln[*iso*-pentane]/[ethane] *versus* ln[*n*-pentane]/[ethane]. On this basis flight B494 from December 2009 was chosen, where the observed slope (1.86) and NO_3-chemistry kinetic slope (1.85) were in good agreement. In order to make a comparison between flights for the same season, the day flight B571 was also chosen from the winter month as it was the only day flight for the whole winter phase of the campaign, so there was no other alternative to choose the best one on the basis of closeness of observed slope to OH-chemistry kinetic slope criteria. A good agreement between observed slope (0.85) and the OH chemistry kinetic slope (0.94) for this flight data was indicative of active OH chemistry during daylight hours. The compounds included in day *versus* night comparison are shown in **Table 4.3**.

Table 4.3: comparison for Sln[X] values between winter night flight B494 made in December 2009 and winter day flight B571 made in January 2011.NR denotes no data available

Species	Night flight B494, December 2009	Day flight B571 January. 2011
	Sln[X]	Sln[X]
ethane	0.18	0.20
propane	0.19	0.24
iso-butane	0.40	0.34
n-butane	0.37	0.35
iso-pentane	0.50	0.52
n-pentane	0.34	0.60
2+3-methylpentane	0.54	0.55
n-hexane	0.37	0.59
iso-octane	NR	0.38
n-octane	NR	0.53

The criteria for including branched-chain compounds in the comparison plot is the same as used in previous chapters, - that is having the same reactivity towards OH radical but different reactivity with respect to the NO_3 radical. The eligible pairs that match the criteria are: [*n*-butane]/[*iso*-butane], [*n*-pentane]/[*iso*-pentane] and [2+3-methylpentane]/[hexane]. The standard deviation of the natural logarithm values of mixing ratios for these pairs for B494 night and B571 day flights are compared in **Table 4.3**. This table includes the octane isomer pair values that formed a part of the discussion in the previous section though this pair has not been included in plots as it does not fulfil the selection criteria. A comparison of variability between day and night data for selected compounds is illustrated in **Figure 4.5**.
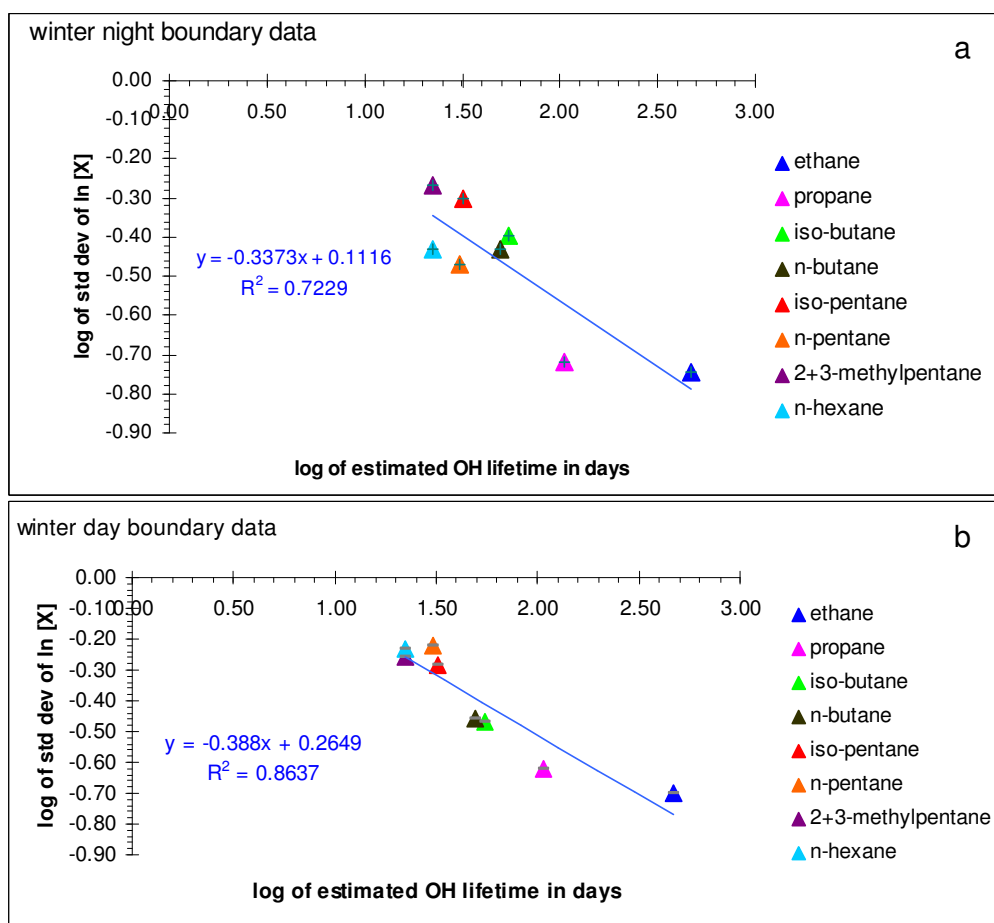
Figure 4.5: Comparison between (a) a typical night flight B494 and (b) a day flight B571 for the variability-lifetime relationship of selected branched chain isomer pairs. Lifetimes were calculated using OH = 1 x 10^6 molecule cm^{-3} for summer and 1 x 10^5 molecule cm^{-3} in winter using rate constants at 298 K (Atkinson and Arey, 2003). The value of *b* is independent of choice of OH concentration.

As it is apparent from the **Figure 4.5**, there is a slightly better correlation ($R^2 =$ 0.86) for the day data as compared to night data ($R^2 =$0.72). The most distinctive feature of these plots is that the observations corresponding to all the branched isomer pairs in the day plot are very close to the OH line, whilst these are offset in the night data as reactivity of compounds increases from *iso*-butane to 2+3-methylpentane with respect to the NO_3 radical. The reactivity of the straight chain compounds during daytime with respect to OH is higher by 5% for *n*-pentane and 11% for *n*-butane in comparison with their branched chain analogues, whilst the rate constants are identical for 2+3-methylpentane and *n*-hexane. However, the reactivity of branched-chain compounds with respect to NO_3 radical is almost a factor of 2 higher in comparison with their straight chain analogues.

Comparing the variability differences for day data it is clear that the difference is less than 3% for butane isomer pair, roughly 7% for 2+3- methylpentane isomer pair and finally 15% for pentane isomer pair with a higher variability displayed by all straight chain compounds. Whilst in the night plot these differences are 8% for butane isomer pair and 45% for pentane isomer pair and 47% for 2+3-methylpentane isomer pair with a higher variability exhibited by *iso*-isomers of all selected compounds. In fact, it is also clear from the plot that all *iso*-isomers are above the trend line passing through ethane and propane compounds that are used as reference compounds for reaction with OH alone. If the average mixing ratios of 30 ppt NO_3 (average mixing ratio for the summer month) of are included in this lifetime calculation then the i*so* species' variability behaviour matches the day data; e.g. the lifetime of *iso*-isomers is now reduced confirming that night time trends are influenced by the presence of NO_3 radical.

It can be concluded therefore that during daylight hours the variability of straight chain compounds is greater, whilst at night, the variability of branched-chain compounds is higher. However, night-time variability is not exactly that according to that predicted by their rate constants, but is reasonable. A note of

caution is that these results are from comparison of data from just one typical night and one day flight; to assess whether this a robust approach, further comparative tests, including a reasonable number of flights, need to be performed which at the moment is beyond the scope of this chapter.

4.3.2.3   Estimation of OH radical concentration

The mixing ratio of the NO_3 radical during day-time is considered almost negligible as its lifetime with respect to solar photolysis is less than 5 seconds; however, the levels of OH during night cannot be considered negligible despite the fact that its main route of formation is dependent on the solar radiation. The reason for non-zero levels of OH at night is the chemistry taking place between alkenes and O_3 and alkene and NO_3, which can significantly contribute to night-time OH production. The NO_3 radical is also known to initiate several VOC degradation reactions, often at faster rates, for example monoterpenes, DMS and phenols (Platt and Janssen, 1995). There is strong evidence for the presence of significant levels of peroxy radicals at night generated as a result of nighttime processing of hydrocarbons initiated by the NO_3 radical (Carslaw et al., 1997;Fleming et al., 2006). These peroxy radicals act as a chain carrier and can further initiate the formation of OH radical. Although the FAGE instrument was deployed aboard the aircraft during this campaign, the observed levels of OH concentration were below the instrument detection limit $(6.5 \times 10^5$ molecule cm^{-3}) most of the time.

One of the important applications of the large hydrocarbon dataset acquired during this campaign was to use these species to derive a nighttime OH radical concentration. Keeping this purpose in mind, few flight plans in both phases of the campaign were designed in such a way that urban plume spreading from London was intercepted downwind, to sample varying degree of processed air masses. Owing to the short lifetime of OH and hence challenges associated with real time measurements, several previous studies have taken advantage of VOC

measurements to infer the estimates of the OH radical. Blake et al (Blake et al., 1993) used VOC data collected during a plume development experiment tracking the same air mass from one location to another location with a time interval of 4.5 hours. The VOC data including alkanes, alkenes and aromatics were used to derive an average OH concentration using the differential decay method over several hours in the urban plume spreading from London. Other studies (Rivett et al., 2003;Khan et al., 2008;Khan et al., 2011) have used the variation of aromatic mixing ratios with respect to benzene, alkene decay and steady state approximation methods to calculate nighttime [OH] and [NO$_3$]. Since the demonstration of significant variability-lifetime relationships for a suite of VOCs in various studies (Jobson et al., 1998;Jobson et al., 1999), this approach has also been tested in deriving OH (Ehhalt et al., 1998;Williams et al., 2000;Williams et al., 2001;Karl et al., 2001) and NO$_3$ radical concentrations (Bartenbach et al., 2007).

In an attempt to derive the estimates of OH concentration from the present VOC dataset, two different approaches have been used. The choice of approach for winter data uses lifetime-variability as there is a significant coherent trend among wide range of reactive hydrocarbons as compared to summer dataset, whilst the hydrocarbon decay method has been used for summer month data. As the hydrocarbon decay method completely ignores the mixing effects, it is more appropriate to apply on summer data in the sense that a greater influence of chemistry over mixing has been observed in summer month data.

Starting with the variability *versus* lifetime relationship approach, it was suggested by Jobson et al (Jobson et al., 1998) that if the alkenes variability lies on the same trend defined by alkanes, acetylene and benzene then the levels of OH can be deduced provided that the O$_3$ concentration is known. The basic principle behind this is that for the species which react with both OH and O$_3$ and if the average concentration of O$_3$ is known, then by assuming varying OH concentration, a linear fit of varying degrees can be given to the data and the best

fit line, expressed by goodness of fit statistics, defines the average concentration of OH. Here we have adopted the approach used by Ehhalt et al (Ehhalt et al., 1998).

Figure 4.6 demonstrates the relationship between standard deviation of natural logarithm of mixing ratios of selected compounds and their OH rate constants. It is quite apparent from the figure that the increase in variability is in accordance with their rate constants. A linear fit is given to data points passing through alkanes, acetylene and aromatics; however observations corresponding to ethene and propene lie on the same trend but not included in the linear regression equation.
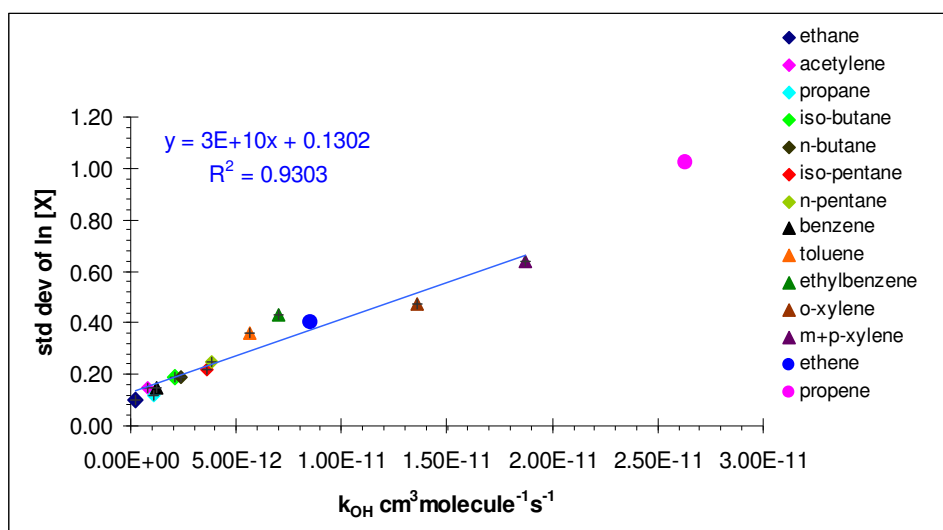
Figure 4.6: A plot of standard deviation of ln[X] for selected compounds *versus* their OH rate constants (Atkinson and Arey, 2003) for the entire winter night data set. The linear fit is given to alkanes, acetylene and aromatics. The linear regression equation has been used to derive 'fictitious' OH rate constants for ethene and propene by taking variability values from the plot**.**

This approach is based on the principle of including a trace gas whose lifetime is determined by more than one oxidant, for example alkenes which react with O_3 and OH during day and the reaction with NO_3 are also included for nighttime data. In that case if alkenes variability lies on the same trend line passing through

the compounds that are primarily removed by OH, for example alkanes, acetylene and benzene then using standard deviation of ln[X] values for alkenes in the linear regression equation that is exclusively derived for alkanes, acetylene and benzene will result in a false rate constant for alkenes that will be based on reaction with OH only. These 'fictitious' rate constants are then further corrected by including reaction with O_3 and OH during day and reaction with OH, NO_3 and O_3 at night.

Writing fictitious rate constants for ethene and propene:

$$k'_{\text{ethene-OH}} \cdot [OH] \quad = \quad k_{\text{ethene-OH}} \cdot [OH] + k_{\text{ethene}-O_3}[O_3] + k_{\text{ethene}-NO_3} \cdot [NO_3] \qquad 4.1$$

$$k'_{\text{propene-OH}} \cdot [OH] \quad = \quad k_{\text{propene-OH}} \cdot [OH] + k_{\text{propene}-O_3} \cdot [O_3] + k_{\text{propene}-NO_3} \cdot [NO_3] \quad 4.2$$

where $k'_{\text{ethene-OH}}$ and $k'_{\text{propene-OH}}$ are the fictitious rate constants of ethene and propene with OH radical respectively. $k_{\text{ethene-OH}}$, $k_{\text{propene-OH}}$, $k_{\text{ethene-O3}}$ and $k_{\text{propene-O3}}$, $k_{\text{ethene-NO3}}$ and $k_{\text{propene-NO3}}$ are actual rate constants for ethene and propene with OH radical, O_3 and NO_3 radical respectively. [OH] is the average concentration of OH radical to be determined and $[O_3]$ and $[NO_3]$ are the average concentration of observed O_3 and NO_3.

Solving the regression equation as shown in the **Figure 4.6** by using variability values for *y* equal to 0.40 for ethene and 1.02 for propene, the fictitious rate constants for ethene and propene are 8.99 x 10^{-12} cm^3 molecule^{-1} s^{-1} and 2.96 x 10^{-11} cm^3 molecule^{-1} s^{-1}. Then putting derived fictitious rate constants along with 37 ppb O_3 and 9.5 ppt NO_3 (these values are converted into molecule cm^{-3} according to unit conversions discussed in **section 1.1.1**), and laboratory rate constants (Atkinson and Arey, 2003), in equations 4.1 and 4.2, the average OH concentration comes out to be 3.2 x10^6 molecule cm^{-3} and 3.4 x 10^6

molecule cm^{-3} from ethene and propene respectively. These levels present the average concentration of OH that has affected the air mass between the emission point until the time of measurement. On comparing these concentration levels with the inferred OH levels for UK in previous published literature, the nighttime concentration is in the range of 10^4 to 10^5 molecule cm^{-3} for an urban background site located at Bristol, England (Rivett et al., 2003) and 10^5 to 10^6 for UK urban surface environments using the decay method and steady state approximation methods (Khan et al., 2011). The range of OH levels derived for present work is in-line with those derived from UK surface sites.

Turning now to the hydrocarbon decay method, the flight B535 made in summer 2010 over North Sea was chosen. The schematic diagram of flight track and canister samples identified as in plume at four locations A, B, C and D are shown in **Figure 4.7**.
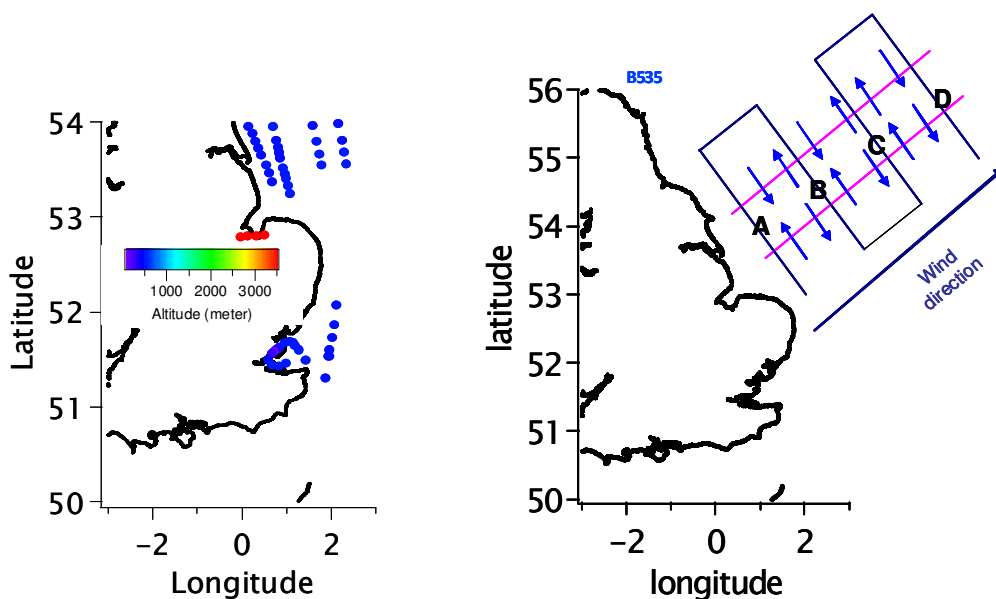
Figure 4.7: Schematic representation of the flight B535 track made in summer 2010 in UK map (right panel) alongside the actual sample filling locations (left panel). The whole air samples were collected along the North-South transects intercepting London plume downwind at Humberside. The whole air samples collected in plume are identified at A, B, C and D locations. The distance between first and second transect is 20.6 miles, second and third is 49 miles and third and fourth is 25 miles and the average wind speed is 7.7 m sec^{-1}.The blue arrows in left panel are representative of peripheral mixing.

The schematic is a simplified version of the actual flight path flown as shown in the left hand side of the figure. The samples were collected along North-South (N-S) transects to intercept downwind London plume at Humberside.

It can be seen from the hydrocarbon mixing ratios in **Figure 4.8** that as the plume proceeds downwind from London (interceptions of plume labelled as A, B, C and D), the mixing ratios of hydrocarbons decline. At the same time this figure draws attention towards significant and varying background mixing ratios of all species. Nonetheless, it is useful to apply the decay method by ignoring background mixing ratios and assuming that chemical removal accounts for most of the observed decline. The distance between point A and B is 20 miles and the wind speed is 7.7 m sec^{-1}; using these values, the time for an air mass to travel from location A to B is 1.18 hr which is suitable for using a more reactive species, for example propene, in equation 4.3. This equation also considers O_3 and NO_3 reactions in addition to OH. The average mixing ratio of O_3 and NO_3 observed during this flight was 28 ppb and 9 ppt respectively.
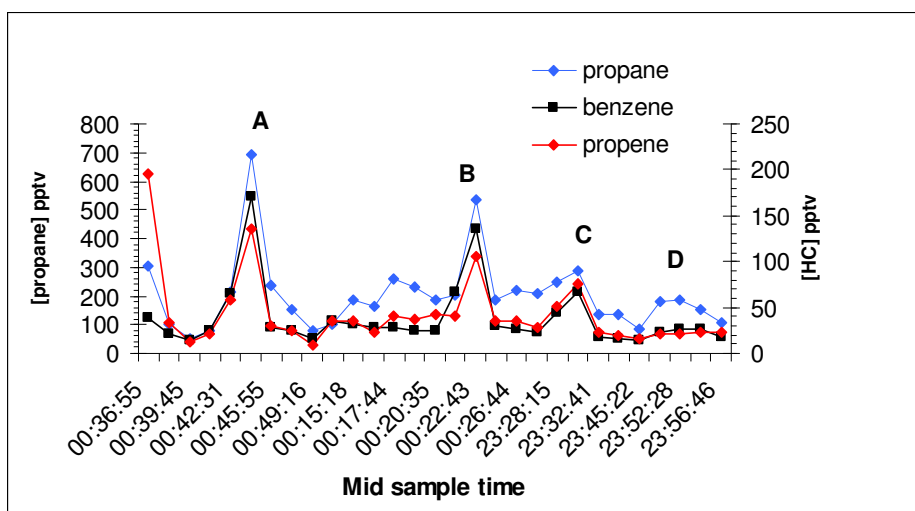
Figure 4.8: The mixing ratio of propane, benzene and propene along the transects downwind of London plume at Humberside measured for flight B535, July 2010 with four sample filling locations A, B, C, and D identified in the plume.

Applying an exponential decay equation on propene:

$$[\text{prop}]_B \quad = \quad [\text{prop}]_A \times \exp - (k_{\text{prop}-OH}[OH] + k_{\text{prop}-O_3}[O_3] + k_{\text{prop}-NO_3}[NO_3]).t \quad 4.3$$

where [Prop]$_B$ and [Prop]$_A$ are the mixing ratios of propene at time $t = t$ and $t = 0$ respectively. $k_{\text{prop-OH}}$, $k_{\text{prop-O3}}$ and $k_{\text{prop-NO3}}$ are the rate constants of propene with OH, O$_3$ and NO$_3$ in cm^3 molecule^{-1} s^{-1} respectively. [OH] is the concentration of hydroxyl radical in molecule cm^{-3} to be determined. [O$_3$] and [NO$_3$] are the concentrations of ozone and nitrate in molecule cm^{-3}. t is the time difference between sampling location A and B.

Writing the same expression for a less reactive species, for example acetylene, and assuming the negligible chemical loss within the time difference between A and B points to cancel out the dilution effects.

$$[\text{acetylene}]_B \quad = \quad [\text{acetylene}]_A \exp(-k_{\text{acetylene}-OH}[OH]t) \quad 4.4$$

where [acetylene]$_B$ and [acetylene]$_A$ are the mixing ratios of acetylene at time $t = t$ and $t = 0$ respectively. k$_{\text{acetylene-OH}}$ is the rate constant of acetylene with OH in cm^3 molecule^{-1} s^{-1}.

Dividing equation 4.3 by equation 4.4 to cancel out the dilution effects this gives the following final expression:

$$\ln \frac{[\text{prop}]_B}{[\text{acet}]_B} \quad = \quad \ln \frac{[\text{prop}]_A}{[\text{acet}]_A} + \{(k_{\text{acet}-OH} - k_{\text{prop}-OH})[OH] - k_{\text{prop}-O_3}[O_3] - k_{\text{prop}-NO_3}[NO_3]\}.t \quad 4.5$$

where [prop] and [acet] represents mixing ratios of propene and acetylene respectively.

Using measured propene mixing ratios at point B and point A from observations, the laboratory rate constants at 298 K (Atkinson and Arey, 2003) and measured concentration of O$_3$ and NO$_3$, the average OH concentration comes out to be 2 x10^6 molecule cm^{-3}. Comparing these derived OH levels with the measured OH

during the Tropospheric ORganic CHemistry (TORCH) summer campaign (Emmerson et al., 2007), inferred values in published literature for UK urban surface sites (Khan et al., 2011) and urban background site for summer season, Bristol, England (Rivett et al., 2003), the range is up to 8.5×10^5, 1×10^5 -1×10^6 molecule cm^{-3} and 1×10^4 -1×10^5 molecule cm^{-3}, respectively.

It was interesting to compare the OH concentration derived by propene with the other hydrocarbons for example propane and benzene. Surprisingly, using propane and benzene gives internally consistent OH concentrations that are two orders of magnitude higher than when propene is used. The inconsistencies among values derived by different compounds has also been observed in previous studies, for example (Blake et al., 1993) compared alkene-derived OH with aromatic derived OH, the values derived from aromatics are a factor of 1.5 to 2 higher than that of alkene-derived OH concentration. McKeen (McKeen et al., 1990) has also discussed the implications of decay methods adopted to derive OH by monitoring the decay of reactive compounds with respect to relatively inert species along the plume trajectory. This paper tests the assumption of lower OH estimates with the increase in reactivity with simple flow and a three dimensional mesoscale model.

To expect a good comparison between derived and direct measurement is unreasonable as the derived value gives the average concentration of OH that has affected the air mass since emission until measurement point whilst an instantaneous value gives the concentration of OH at that time; nevertheless the comparison between derived methods for different studies gives an insight into utility of the hydrocarbon decay method in the sense to what extent the assumption of the separating transport and mixing effects with photochemistry is reasonable.

4.3.3 Estimates of the [NO$_3$]/[OH] ratio

This section takes advantage of reactivity differences of [benzene]/[toluene] and [*n*-pentane]/[*iso*-pentane] pairs towards OH and NO$_3$ radical in deriving estimates of [NO$_3$]/[OH] ratio. **Figure 4.9** illustrates the logarithmic relationship between two pairs for winter night B494, summer night B535, winter dusk B568 and autumn dawn B551 flights along with the day flight data B550 for ease of comparison.
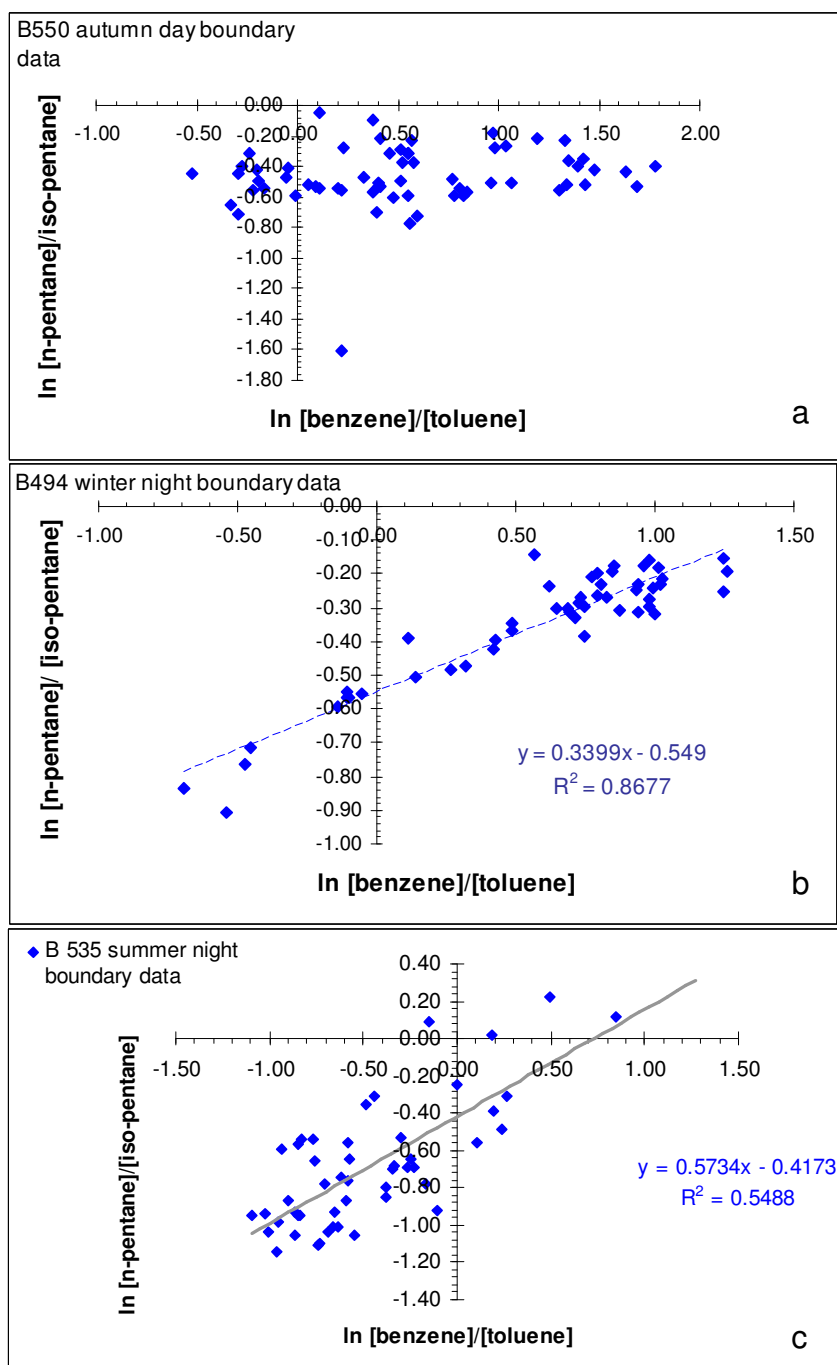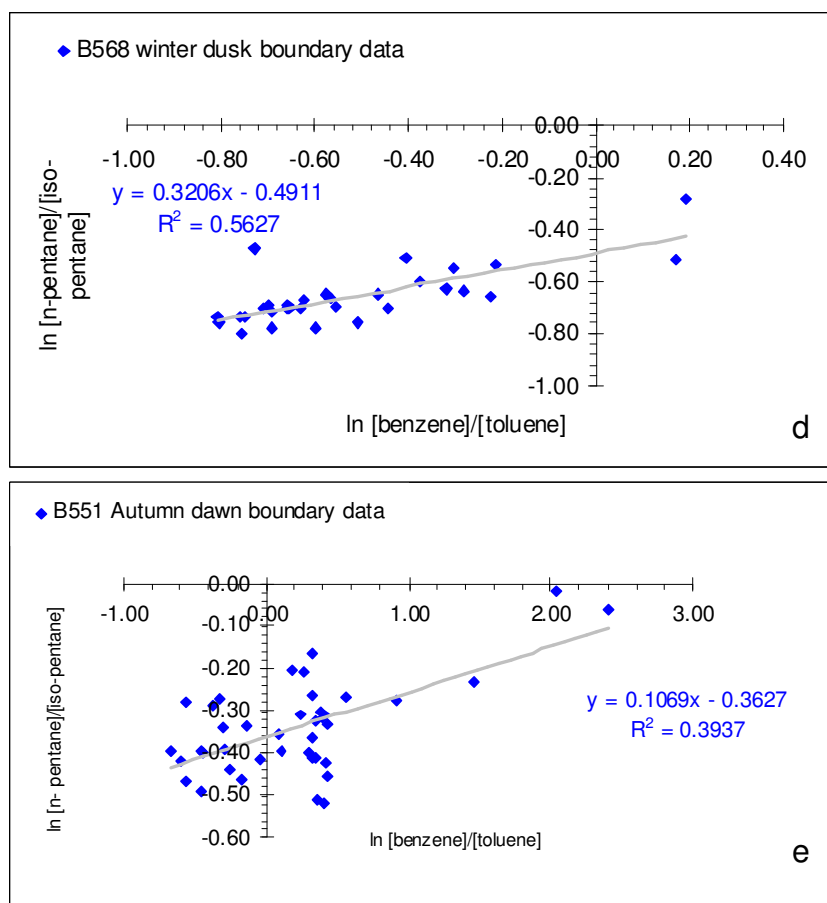
Figure 4.9: Plots of ln[*n*-pentane]/[*iso*-pentane] *versus* ln [benzene]/[toluene] for (a) B550 autumn day flight. (b) B494 winter test night flight (c) B535 summer night flight (d) B568 winter dusk and (e) B551 autumn dawn.

Comparison between day and selected night flight data for logarithm ratios of [*n*-pentane]/[*iso*-pentane] *versus* [benzene]/[toluene] clearly reveals the presence of NO_3 radicals as an additional oxidant during nighttime. During daylight hours both pairs are processed by OH radical and due to almost similar reactivity of pentane isomer pair towards OH, the ratios are nearly constant along the vertical axis of the plot whilst the higher reactivity of toluene, almost 5 times than benzene, leads to the increase in ratios as we move along the horizontal axis from left to right.

The presence of NO_3 radicals during the night shapes this correlation in such a way that depending on the extent of influence of NO_3 on ratios, a moderate ($R^2 =$

0.39) to excellent correlation ($R^2 = 0.86$) has been observed in different seasons. The slope of these plots is the difference between coordinates of 2 points and defines the change in ratios during sampling time along the trend line as we move from left to right.

$$m = \left[\frac{\ln\left[\frac{n-pentane}{iso-pentane}\right]_{t_1} - \ln\left[\frac{n-pentane}{iso-pentane}\right]_{t_2}}{\ln\left[\frac{benzene}{toluene}\right]_{t_1} - \ln\left[\frac{benzene}{toluene}\right]_{t_2}} \right] \quad 4.6$$

where *m* is the slope of plots (**Figure 4.9**) between ln[*n*-pentane]/[*iso*-pentane] *versus* ln [benzene]/[toluene] and t_1 and t_2 represents different processing times. t_1 indicates the coordinates at extreme right exhibiting high ratios due to the rapid removal of reactive denominator species and hence relatively processed air masses and t_2 shows the coordinates at extreme left demonstrating lower values of ratios suggesting comparatively fresh air masses and in a certain condition these can be considered equal to emission ratios which means that t_2 can be substituted by t_0.

Hence substituting t_0 for t_2 and t for t_1, the slope can be rewritten as:

$$m = \left[\frac{\ln\left[\frac{n-pentane}{iso-pentane}\right]_{t} - \ln\left[\frac{n-pentane}{iso-pentane}\right]_{t_0}}{\ln\left[\frac{benzene}{toluene}\right]_{t} - \ln\left[\frac{benzene}{toluene}\right]_{t_0}} \right] \quad 4.7$$

In previous sections using the lifetime-variability relationship, the influence of mixing on data was clearly observed through the *b* values in summer and winter data, yet this aspect is entirely ignored while deriving ratio $[NO_3]/[OH]$ on the basis of an exponential decay as in equation 4.8.

$$[X]_t = [X]_0 \exp(-L_x.t) \quad 4.8$$

where $[X]_t$ and $[X]_0$ are the mixing ratios of hydrocarbons at sampling time t and initial time t_0 respectively. L_X is the chemical loss term and in the context of night-time observations, this term includes the rate constants of a particular species with both oxidants OH and NO_3. t is the difference between emission and sampling time.

Including rate constants with both oxidants this equation can be rewritten as:

$$[X]_t \quad = \quad [X]_0 \exp{-(k_{x-OH}[OH] + k_{x-NO_3}[NO_3])t} \qquad 4.9$$

where $k_{x\text{-}OH}$ and $k_{x\text{-}NO3}$ are the rate constant of particular hydrocarbon species X with OH and NO_3 respectively.

Applying this equation on [benzene]/[toluene] and [*n*-pentane]/[*iso*-pentane] pairs

$$\ln\frac{[B]_t}{[T]_t} \quad = \quad \ln\frac{[B]_0}{[T]_0} + (k_{T-OH} - k_{B-OH})[OH]t + (k_{T-NO_3} - k_{B-NO_3})[NO_3]t \qquad 4.10$$

$$\ln\frac{[nP]_t}{[iP]_t} \quad = \quad \ln\frac{[nP]_0}{[iP]_0} + (k_{iP-OH} - k_{nP-OH})[OH]t + (k_{iP-NO_3} - k_{nP-NO_3})[NO_3]t \quad 4.11$$

where $[B]_t$ $[T]_t$ $[nP]_t$ $[iP]_t$ are the mixing ratios of benzene, toluene, *n*-pentane and *iso*-pentane at time t, respectively, and $[B]_0$ $[T]_0$ $[nP]_0$ $[iP]_0$ are the mixing ratios of benzene, toluene, *n*-pentane and *iso*-pentane at time t_0, respectively.

Substituting equations 4.10 and 4.11 in equation 4.7 and rearranging produces the final expression:

$$\frac{[NO_3]}{[OH]} \quad = \quad \frac{m \times (k_{T-OH} - k_{B-OH}) - (k_{iP-OH} - k_{nP-OH})}{(k_{iP-NO_3} - k_{nP-NO_3}) - m \times (k_{T-NO_3} - k_{B-NO_3})} \qquad 4.12$$

Table 4.4 compares the slopes from selected flights between the RONOCO and the HANSA datasets. The European Union Hydrocarbons Across the North Sea Atmosphere (EU HANSA) project was designed to collect an extensive hydocarbon database in addition to ozone and NOx in mid 1990s. A group of

measurement sites (Birkenes, Norway; Rörvik, Sweden; Kollumerwaard, the Netherlands; and Weybourne, UK) across Europe surrounding the North Sea was used.

Table 4.4: Comparison of NO_3 to OH ratio between the RONOCO and the HANSA datasets for selected flights: winter test night flight B494 (December 2009), summer night B535 (July 2010), autumn dawn B551 (September 2010) and winter dusk B568 (January 2011).

	RONOCO dataset			HANSA dataset	
	Slope (R^2)	$[NO_3]/[OH]$		Slope (R^2)	$[NO_3]/[OH]$
Winter night B494	0.34 (0.86)	2.24×10^4	Autumn and winter	0.37 (0.44)	2.53×10^4
Summer night B535	0.57 (0.54)	4.97×10^4	Summer	0.31 (0.27)	1.96×10^4
Autumn dawn B551	0.10 (0.39)	3.4×10^3	Spring	0.33 (0.47)	2.05×10^4
Winter dusk B568	0.32 (0.56)	2.05×10^4	All data	0.31 (0.32)	1.96×10^4

As it can be seen from the comparison, the higher the slope the greater the value of the ratios. It is apparent from this table that there is an excellent correlation ($R^2 = 0.86$) between two different pairs for winter test flight B494 with a slope of 0.34. An excellent correlation indicates almost the same processing rate of the pairs but with a different oxidant or in other words there is an equal impact of NO_3 and OH on ratios. The slope ranges from 0.10 ($R^2 = 0.39$) for autumn dawn to 0.57 ($R^2 = 0.54$) for summer night data with a reasonable correlation. The highest value of slope for summer night flight reflects the greater impact of NO_3 on data points as compared to OH; whilst for autumn dawn B551 flight, the lowest value of the slope (0.10) suggests less impact of NO_3 on data points compared with OH.

While explaining these observations logically, the effect of mixing is completely ignored; however, in reality the slope is a mixture of chemistry and mixing effects. The observed NO_3 levels alongside the values of slope would have provided better evidence of comparing the impact of chemistry over mixing, but, unfortunately NO_3 was not measured for all flights. Nonetheless, the comparison of observed NO_3 for two flights supports the view of a reasonable positive correlation between the NO_3 level and slope; the range of NO_3 for B535 during WAS times is from 4.2 to 41 ppt and the slope of the double log plot is 0.57 as shown in **Figure 4.9**. Whilst for winter dusk B568 flight, the observed NO_3 levels are between 2 and 8 ppt and the slope of the ratio plot is 0.32. The instrument was not installed for the rest of the flights so it is not possible to compare the observed NO_3 levels with the slope. It can be said conclusively that, although this equation does not take mixing into account, the utility of this equation to compare the impact of oxidants on air masses cannot be ignored.

Turning now to the comparison of the slope and derived ratios with the HANSA dataset, it is clear that in the HANSA dataset the slope is almost the same during all seasons with slight variations (0.31 - 0.37) and with a reasonable correlation (R^2 = 0.27 - 0.47), whilst the range of slopes in RONOCO dataset is much wider (0.10 - 0.57) with a moderate to excellent correlation. Using slope values for the HANSA dataset, the $[NO_3]$ to $[OH]$ ratio ranges from 1.96 x 10^4 to 2.54 x10^4 whilst for the present study, the range is relatively wide 3.4 x10^3 to 4.97 x10^4. The most contrasting feature of this comparison is that for the present study the inferred ratio is at a maximum for the summer flight B535 data and minimum for autumn dawn B551 whilst for the HANSA dataset the ratio is highest for autumn and winter data and minimum for summer data.

To further utilize this equation in deriving the absolute concentration of OH radicals, using the instantaneous NO_3 mixing ratio between 4 and 40 ppt for summer flight B535 and between 2 and 8 ppt for winter dusk B568 during WAS times (these mixing ratios are converted into number density units according to

equation 1.9 discussed in **section 1.1.1**) gives the range of OH of 2 x 10^3 to 2 x 10^4 and 2.4 x 10^3 to 9.6 x 10^3 respectively.

4.3.4 VOC oxidation rates

This section presents a comparison of VOC loss rates between summer and winter flight data with respect to two key night time oxidants, O_3 and NO_3 radical. During this campaign, a wide variety of anthropogenic C_2–C_8 VOCs, many of which are considered to be highly reactive towards the NO_3 radical, were measured. It has been conclusively shown in previous studies that reaction with biogenic compounds during the night is a more effective direct sink for NO_3 radicals compared to anthropogenic VOCs (Warneke et al., 2004;Ambrose et al., 2007). However, the results based on the industrial emissions in Houston, Texas consisting of highly reactive anthropogenic VOCs, mainly alkenes, indicated that 30-54% of VOCs were lost by NO_3 in comparison with 10-50% by isoprene (Brown et al., 2011). Hence depending on the emissions sources, be it from forested or industrial areas, the fraction of VOCs left for the next day will mainly consist of slower reacting anthropogenic VOCs, provided that there is an abundance of NO_x during the previous night.

The purpose of this section is to identify the seasonal differences, especially for highly reactive alkene compounds, with respect to the NO_3 radical and O_3 in addition to the comparison of total VOC loss rates due to the NO_3 radical and O_3. **Figure 4.10** demonstrates the relationship between VOC oxidation rate and NO_3 production rate for summer and winter flight data. The following expressions (Brown et al., 2011) have been used to calculate the loss rates of VOC species presented in **Table 4.5**. The VOC loss rate is the sum of the rate constants for reaction with a particular oxidant multiplied by the concentration of selected VOC and oxidant concentration:

$$\frac{-d[VOC]_{NO_3}}{dt} \quad = \quad \sum k_{VOC_{i-NO_3}} \times [VOC_i] \times [NO_3] \qquad 4.13$$

$$\frac{-d[VOC]_{O_3}}{dt} \quad = \quad \sum k_{VOC_{i-O_3}} \times [VOC_i] \times [O_3] \qquad 4.14$$

where $-d[VOC]_{NO3}/dt$ and $-d[VOC]_{O3}/dt$ are the VOC loss rates with respect to NO_3 and O_3, $k_{VOC-NO3}$ and k_{VOC-O3} are rate constants of particular VOC with NO_3 and O_3 respectively. The quantities in square brackets around VOC, NO_3 and O_3 indicate the concentration in molecule cm^{-3}. (the conversion from mixing ratio to number density unit has been done according to equations used in **section 1.1.1.**) The ancillary measurements were averaged between the WAS times.

The mixing ratio of NO_3 is in the range of 4 - 40 ppt with a mean of 23 ppt and 7-19 ppt with a mean of 13 ppt for flight B535 in summer and flight B565 in winter respectively. The range of O_3 mixing ratio in both seasons is more or less similar covering 20-40 ppb with a mean of 28 ppb for B535 in summer and 36 ppb for B565 in winter. The rate constants used for calculation are presented in **Table 4.5**. The NO_3 production rate is calculated by using the rate constants between NO_2 and O_3 reaction and concentration of O_3 and NO_2 from observations according to equation 1.21 discussed in chapter 1. The NO_3 production rate is in the range of 2.0×10^5 - 4.0×10^6 molecule $cm^{-3} s^{-1}$ for these selected flights data, whilst for whole campaign, the range is slightly wider covering 3.8×10^5 - 2.0×10^7 molecule $cm^{-3} s^{-1}$ and of 4.7×10^4 – 3.6×10^6 molecule $cm^{-3} s^{-1}$ in summer and winter respectively. However, the VOC oxidation rate with NO_3 is in the range of 10^4 -10^5 molecule $cm^{-3} s^{-1}$ in both seasons. A comparison between the magnitude of the two rates for selected summer and winter flight data indicates that the average NO_3 production rate is 0.2 ppbv hr^{-1} for both seasons whilst the VOC oxidation rate is 0.02 ppbv hr^{-1} and 0.006 ppbv hr^{-1} for B535 in summer and B565 in winter respectively indicating a wide difference between the magnitudes of two rates. This shows that the suite of anthropogenic organic compounds measured during this campaign are of limited importance in explaining the loss of the NO_3 radical in each season.

Table 4.5: A list of measured VOCs and the rate constants used in calculation. The rate constants are reported from (Atkinson and Arey, 2003) except where noted otherwise.: a from Brown et al 2001, b is average rate constant and c is from Geyer et al 2001.

Species	$O_3 (10^{17} \times k$ (298K) $cm^3 molecule^{-1}s^{-1}$	$NO_3\ k$ (298K) $cm^3 molecule^{-1}s^{-1}$
ethane	$<1 \times 10^{-6}$	$<1 \times 10^{-17}$
propane	$<1 \times 10^{-6}$	$<7 \times 10^{-17}$
n-butane	$<1 \times 10^{-6}$	4.59×10^{-17}
iso-butane	$<1 \times 10^{-6}$	1.06×10^{-16}
n-pentane	$<1 \times 10^{-6}$	8.7×10^{-17}
iso-pentane	$<1 \times 10^{-6}$	1.62×10^{-16}
cyclopentane	$<1 \times 10^{-6}$	[a]0.014×10^{-14}
2+3-methylpentane	$<1 \times 10^{-6}$	[b]2.0×10^{-16}
n-hexane	$<1 \times 10^{-6}$	1.1×10^{-16}
n-heptane	$<1 \times 10^{-6}$	1.5×10^{-16}
n-octane	$<1 \times 10^{-6}$	1.9×10^{-16}
2,2,4-trimethylpentane	$<1 \times 10^{-6}$	9×10^{-17}
ethene	0.159	2.05×10^{-16}
propene	1.01	9.49×10^{-15}
trans-2-butene	19.0	3.90×10^{-13}
cis-2-butene	12.5	3.52×10^{-13}
1-butene	0.964	1.35×10^{-14}
iso-butene	1.13	3.44×10^{-13}
1,3-butadiene	0.63	1.0×10^{-13}
trans-2-pentene	16	[a]39×10^{-14}
1-pentene	1.06	1.5×10^{-14}
acetylene	[c]7.8×10^{-4}	[c]5.1×10^{-17}
isoprene	1.27	7.0×10^{-13}
benzene	$<1 \times 10^{-3}$	$<3 \times 10^{-17}$
toluene	$<1 \times 10^{-3}$	7.0×10^{-17}
ethylbenzene	$<1 \times 10^{-3}$	$<6 \times 10^{-16}$
m+p-xylene	$<1 \times 10^{-3}$	[b]3.8×10^{-16}
o-xylene	$<1 \times 10^{-3}$	4.1×10^{-16}
methanol	$<1 \times 10^{-3}$	1.3×10^{-16}
acetone	$<1 \times 10^{-3}$	$<3 \times 10^{-17}$

Figure 4.10: Plot of VOC loss rate (molecule/cm^3 sec) for (a) summer B535 and (b) winter B565 flights data against NO$_3$ production rate P$_{NO3}$ (molecule/cm^3 sec). The magnitude of VOC oxidation rate is much smaller (0.02 ppbv hr^{-1} for B535 in summer and 0.006 ppbv hr^{-1} for B565 in winter) as compared to the NO$_3$ production rate 0.2 ppbv hr^{-1} in both seasons. There is no correlation between these two rates indicating the negligible impact of VOCs measured during this campaign on the overall the NO$_3$ loss rate.

According to a simple box model that considers the NO$_3$ production and a first-order NO$_3$ loss, the NO$_3$ production rate should be directly proportional to the NO$_3$ concentration (Heintz et al., 1996). As it can be seen from **Figure 4.11**, there is no correlation between the NO$_3$ concentration and the NO$_3$ production rate indicating that there are no substantial direct sinks for the NO$_3$ radical. The similar independence between the two quantities, the NO$_3$ concentration and the NO$_3$ production rate, was also observed in a dataset from a rural site in the Baltic Sea despite an appreciable loading of dimethylsulphide (DMS) (because the

presence of DMS serves as a substantial sink for NO_3) during the summer period (Heintz et al., 1996).

A large fraction of reactive VOCs including monoterpenes, aldehydes, reduced sulphur compounds, furans, oxygenate aromatics and polycyclic aromatic hydrocarbons do not form a part of the measured suite of VOCs. However, let us consider for a moment the present case with low loadings of biogenic hydrocarbons and other reactive unmeasured compounds, or in other words negligible sinks for NO_3, then according to equation 1.54 discussed in chapter 1, there should be an inverse relationship between the steady state nitrate lifetime and NO_2.
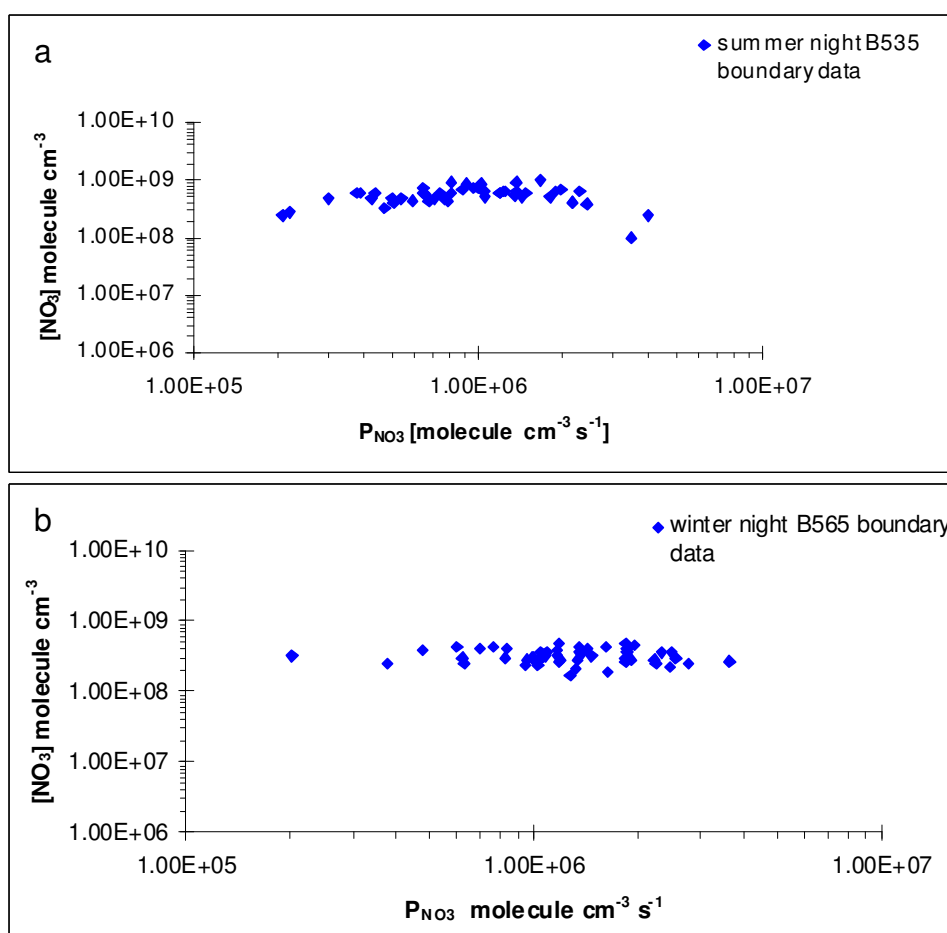
Figure 4.11: NO_3 radical concentration (molecule cm^{-3}) as a function of NO_3 production rate (molecule cm^{-3} sec^{-1}); the NO_3 concentration is independent of the NO_3 production rate implying the negligible impacts of direct sinks for the NO_3 radical.

As it can be seen from the **Figure 4.12** the steady state NO_3 lifetime is inversely proportional to the mixing ratio of NO_2 indicating that either the nature of the NO_3 sink is indirect or the sinks for N_2O_5 are significant.
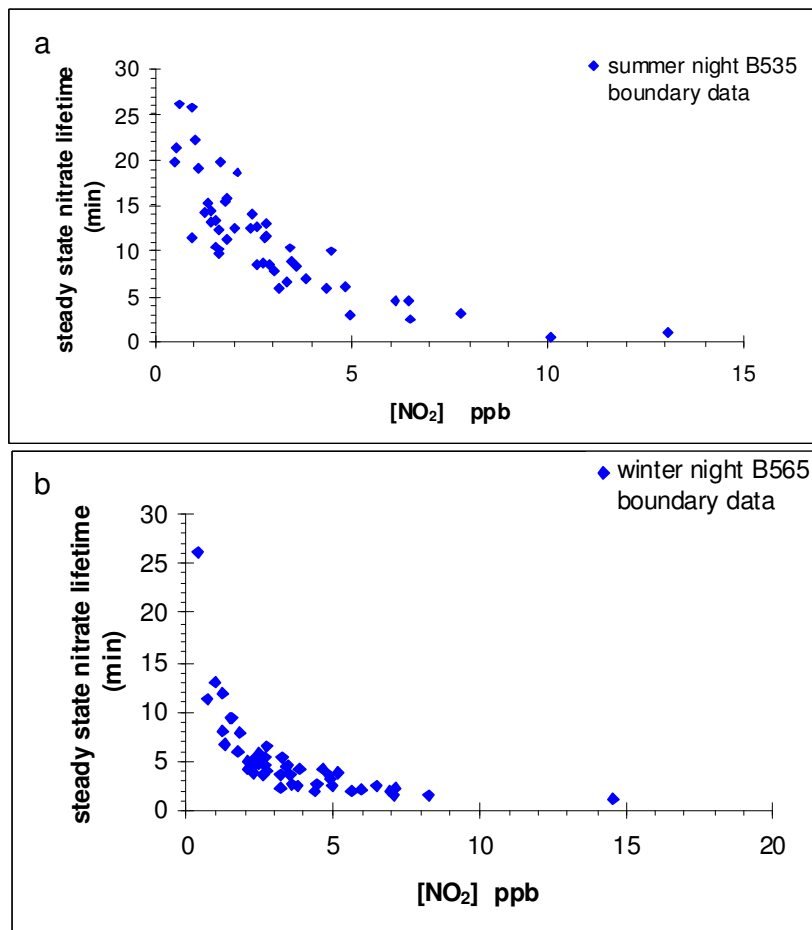
Figure 4.12: Steady state lifetime of the nitrate radical as a function of the NO_2 concentration for (a) summer B535 and (b) winter B565 flights data. For both seasons, an inverse correlation seems to be reflecting the importance of an indirect loss mechanism for the NO_3 radical.

This inverse correlation seems to be further supporting a view which neglects the direct sinks of NO_3; however, Brown et al (Brown et al., 2003) showed that this kind of anticorrelation can also arise from a system where the sinks for N_2O_5 are negligible or there is a lack of steady state in NO_3 and N_2O_5 and there is a large and variable concentration of NO_2 which could be due to mixing of different air masses. In the present data set the range of NO_2 mixing ratio is 0.53 - 13 ppb with a variability of 82% and 0.41-14.59 ppb with a variability of 67% for

summer B535 and winter B565 flight data, respectively, has been observed. It is clear that in present dataset the variability of NO_2 mixing ratio is significant.

If steady state is valid then a plot of inverse steady state lifetime of NO_3 against the product of K_{eq} (T) [NO_2] (Brown et al., 2003) should give a straight line (**Figure 4.13**) according to equation 1.56 as discussed in chapter 1. This equation is a result of an assumption of non-negligible sinks for both NO_3 and N_2O_5. It can be seen from **Figure 4.13** that for winter data an excellent correlation is observed between the inverse of steady state lifetime and the product of K_{eq} (T) [NO_2]. However, in the summer data, the impact of one data point on the gradient and R^2 value is apparent. The slope k_y^{-1} and intercept k_x^{-1} of this plot also gives information on the N_2O_5 and NO_3 sinks respectively.
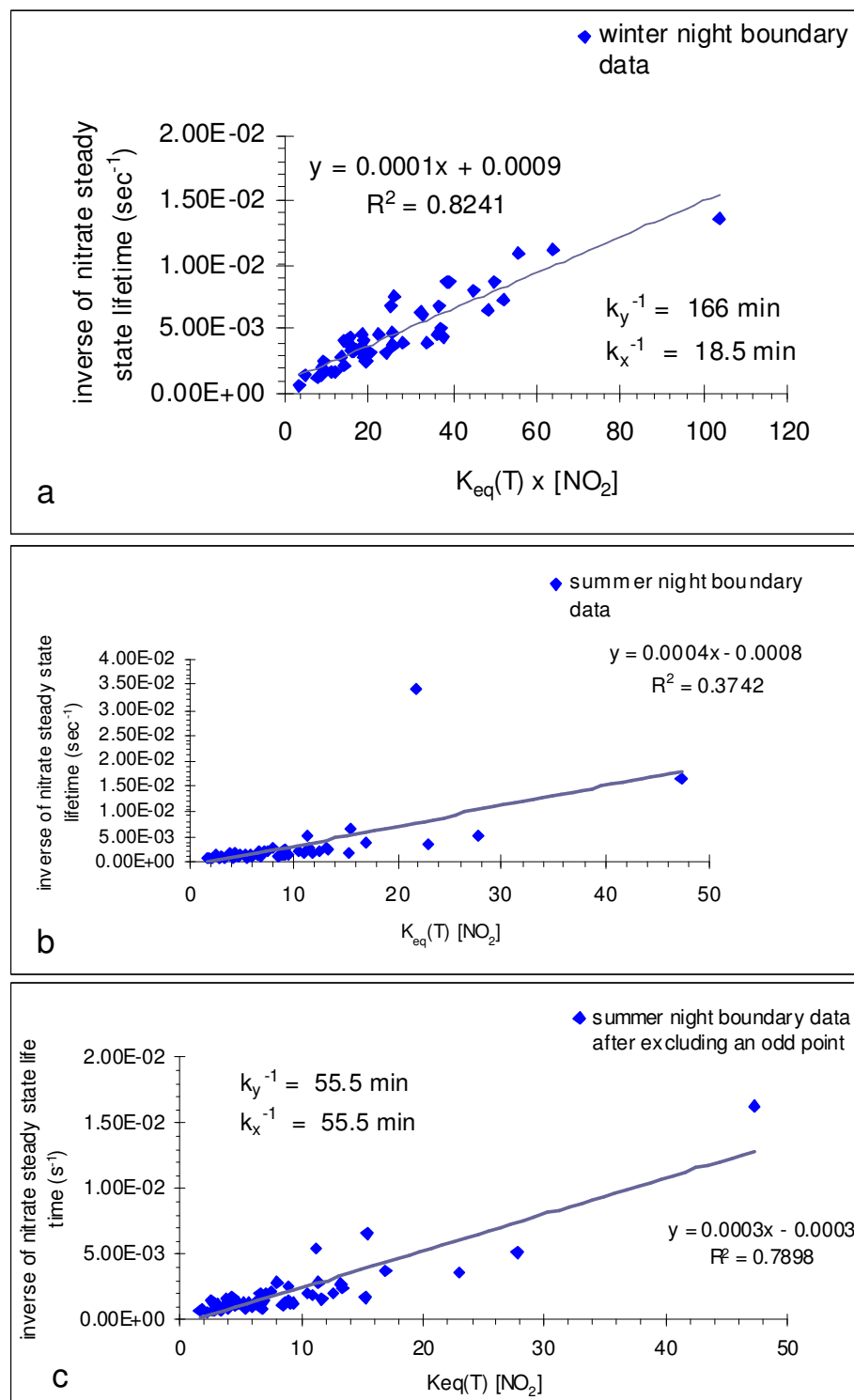
Figure 4.13: Inverse steady state NO_3 lifetime *versus* the product of $K_{eq}(T)$ $[NO_2]$ for (a) winter B565, (b) summer B535 flights data, and (c) summer B535 flight data after excluding an odd data point. An excellent correlation is apparent for winter (R^2 =0.82) as compared to summer (R^2 = 0.37). The slope k_x^{-1} =18.5 min and intercept k_y^{-1} = 166 min of the trend line passing through the data points for winter data gives the strength of NO_3 and N_2O_5 sinks.

To further compare the average relative contribution of NO_3 and O_3 towards VOC loss rates, the pie charts are presented in the following **Figure 4.14** for both seasons.
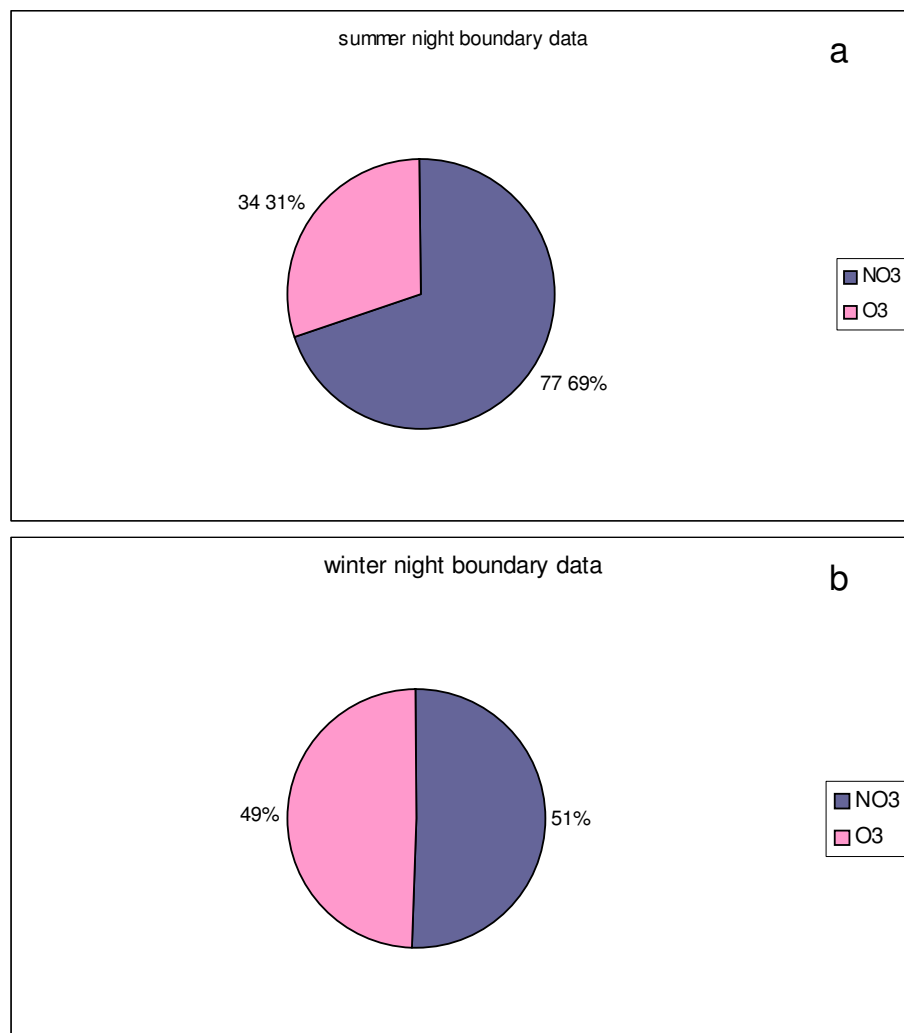
Figure 4.14: Comparison of the average instantaneous fraction of VOC oxidation due to nitrate (blue-grey) and ozone (pink) for (a) summer B535 and (b) winter B565 flights data. The VOC compounds used for loss rate calculations are reported in **Table 4.5**. The contribution of the NO_3 radical is relatively higher to VOC loss rate in comparison with O_3 in summer whilst both oxidants more or less play an equal role to VOC loss rate in winter.

It is clear that in summer the contribution of the NO_3 radical is more than double than that of O_3 whilst the equal participation of both oxidants to VOC loss rate is seen in winter.

Figure 4.15 further partitions the contribution of individual classes oxidised by NO_3 for the summer flight B535 and the winter flight B565. It is apparent that alkenes are the major fraction of VOCs (96% in winter and 82% in summer) in both seasons, followed by isoprene (14%) in summer season, oxidised by the NO_3 radical. Similar results are produced when partitioning is done with respect to O_3 (not shown here).
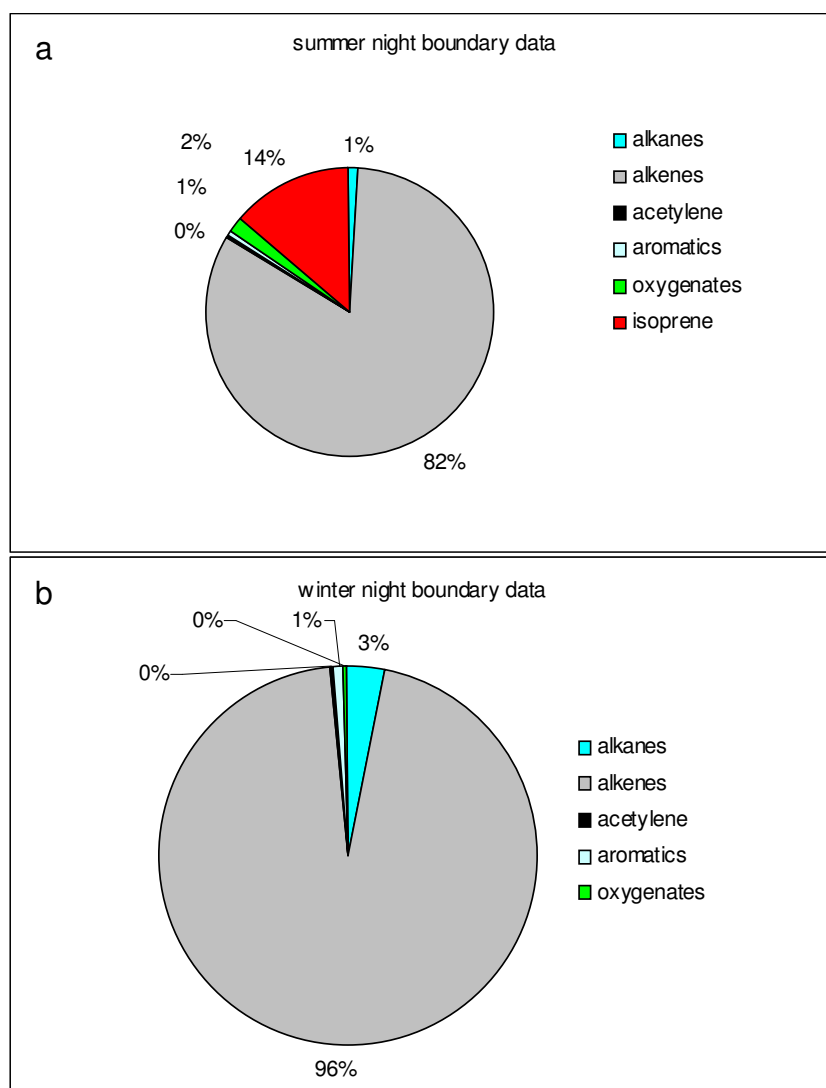
Figure 4.15: Relative contributions of anthropogenic VOCs towards NO_3 loss for (a) the summer B535 flight data and (b) winter B565 flight data. Alkenes are the largest fraction of VOCs lost by the NO_3 radicals in both seasons followed by the biogenic isoprene in summer month.

It was interesting to compare the contribution of NO_3 and O_3 towards alkene losses between summer and winter seasons (**Figure 4.16**). The rate constants of alkenes with O_3 are of the order of 10^{-17}-10^{-19} cm^3 molecule^{-1} s^{-1} whilst with NO_3 they are of the order of 10^{-13}-10^{-16} cm^3 molecule^{-1} s^{-1}. It is obvious that the contribution of the NO_3 radical to alkene loss rates is more than double for summer flight B535 data whilst the both oxidants play an equal role to VOC oxidation for B565 flight data in winter season with slightly higher importance of O_3 in comparison with the NO_3 radical.
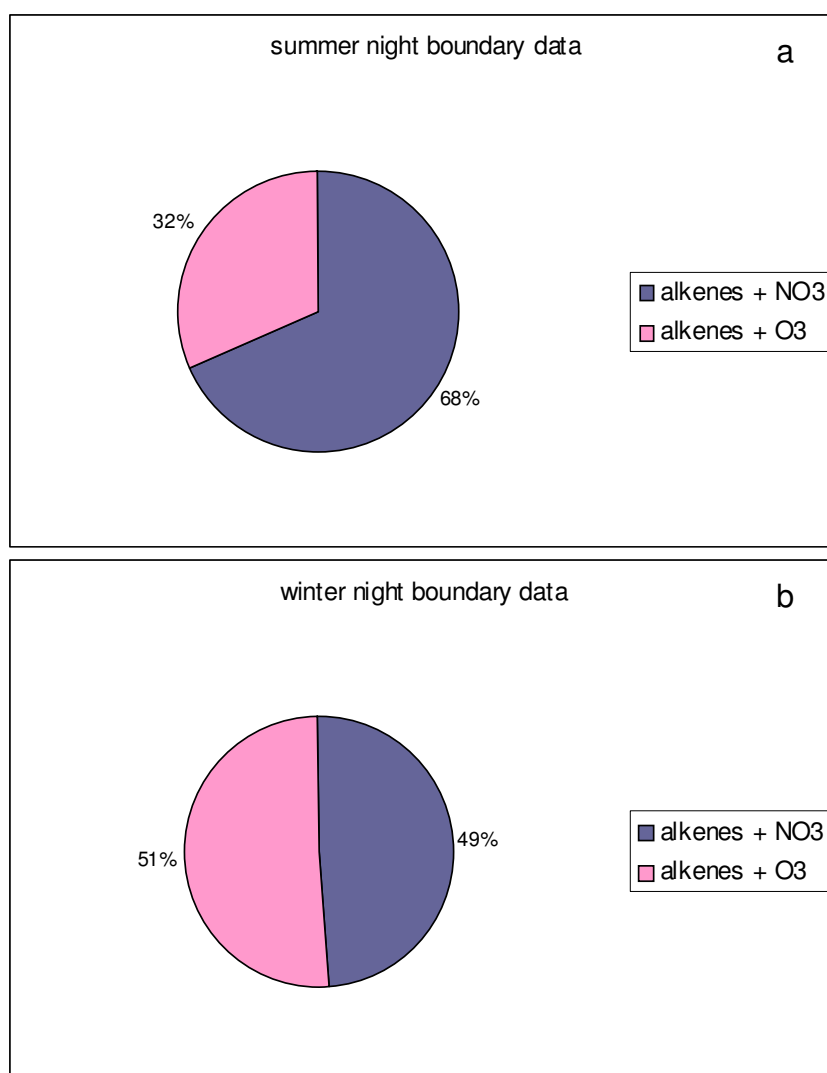
Figure 4.16: Comparison of relative contributions of the NO_3 radical (blue-grey) and O_3 (pink) to the alkenes oxidation for (a) summer B535 and (b) winter B565 flight data. The contribution of NO_3 is more than double than that of O_3 to alkenes oxidation for summer whilst in winter there is roughly an equal involvement of both oxidants with slightly higher impact of O_3 in comparison with NO_3.

4.4 Summary

The variability-lifetime relationship has been used to examine the influence of NO_3 radicals on hydrocarbon variability trends for the entire summer and winter datasets acquired during the RONOCO field campaign. A comparison between the complete summer and winter dataset suggests a varying degree of influence of mixing and chemistry. An excellent correlation for the entire winter dataset between the variability and the lifetime of a wide variety of hydrocarbons not only validates the measurement but also gives us confidence in the precision of the instrument involved in this study which is better than the atmospheric variability in the datasets.

One of the interesting facts about all winter night flights is that using the hydrocarbon ratio approach and pentane isomer pair log –log plots (see previous chapter), there was no evidence of the NO_3 radical; however, the mixing ratio of NO_3 was observed in the range of 2-20 ppt in winter season during WAS times. This led to the application of the variability-lifetime approach to compare the entire winter dataset with the entire summer dataset to assess the influence of NO_3 radical on branched chain isomers. For the entire summer night dataset, the variability of *iso*-pentane is higher than *n*-pentane suggesting an influence of NO_3 radical, whilst *n*-pentane displays higher variability than *iso*-pentane for the entire winter night data implying the negligible influence of NO_3 radical. In the broader sense, the two approaches agree very well when comparing between summer night and winter night data with reference to the pentane isomer pair. The variability differences between *n*-octane and *iso*-octane during night flights do not agree with the reported rate constants and this observation casts a possible doubt on the rate constant data.

Moving from branched isomer pairs to a more reactive group of alkenes for the winter dataset, propene displays higher variability than expected from OH alone and does not fall on the predicted trend line. By including an average NO_3

mixing ratio of 9 ppt and O_3 mixing ratio of 37 ppb, the propene observation falls on the trend line due to reduced lifetime, which suggests that the variablity of propene could be driven by NO_3 and O_3. This implies that in winter the highly reactive alkenes are more sensitive than branched-chain compounds in getting a NO_3 signal.

A comparison between a typical winter test night flight data and a winter day flight clearly shows the influence of OH chemistry during day and the NO_3 chemistry at night with respect to [*n*-butane]/[*iso*-butane], [*n*-pentane]/[*iso*-pentane] and [2+3-methylpentane]/[hexane] pairs. The variability of straight-chain compounds during daylight hours is greater in accordance with the higher rate constants of straight chain compounds with respect to the OH radical than that of the branched-chain compounds; whilst at night, the variability of branched-chain compounds is higher in accordance with the higher reactivity of branched chain isomers with respect to NO_3 radical than that of the straight-chain compounds. To further test the robustness of approach in identifying the presence of different oxidants during different phases of the day, further comparative tests, by including a reasonable number of flights, should be planned for future work.

Two different approaches have been used in different seasons to derive an OH concentration. The lifetime-variablity approach has been used to deduce the average OH concentration for entire winter dataset. The average OH concentration levels for entire winter dataset using this approach were 3.2×10^6 molecule cm^{-3} and 3.4×10^6 molecule cm^{-3}, derived from ethene and propene respectively. These levels present the average OH concentration which has affected the air mass since the emission point until the time of measurement.

The alternative hydrocarbon decay method has been used on the summer dataset. Using measured propene mixing ratios near source and at time t, the average OH concentration comes out to be 2×10^6 molecule cm^{-3}. There are inconsistencies in

OH concentration when propane and benzene species are used. On comparing these concentration levels with the previous studies with nighttime OH levels for UK urban surface measurements (1×10^5 -1 $\times 10^6$ molecule cm^{-3}), the levels here are higher. Although these derived concentration levels seem to be much higher than instantaneous nighttime OH concentration levels, the comparison between derived and the direct measurement is unreasonable as the derived value gives an average concentration of OH that has affected the air mass since emission until measurement point, whilst an instantaneous value gives the concentration of OH at that time; nevertheless the comparison between derived methods for different studies gives an insight into the difficulty in utilizing these methods in the sense to what extent the assumption of the separating transport and mixing effects with photochemistry is reasonable.

The reactivity differences of [benzene]/[toluene] and [*n*-pentane]/[*iso*-pentane] pairs towards OH and NO_3 radical has been used in deriving estimates of [NO_3]/[OH] ratio. An excellent correlation (R^2 = 86) with a reasonable slope (0.34) for winter test flight indicates an equal impact of OH and the NO_3 radical whilst the reasonable correlation (R^2 = 0.54) with a higher slope (0.57) suggests the greater impact of NO_3 on summer flight data. The data from 2 flights supports the view of a reasonable positive correlation between the observed NO_3 level and slope of the two hydrocarbon pair log-log plot. This further confirms that although this equation does not take mixing into account, the utility of this equation to compare the impact of oxidants on air masses cannot be ignored.

On comparing the slope of plot between ln [n pentane]/[iso-pentane] *versus* ln [benzene]/[toluene] from the present work with the HANSA dataset, it is clear that in HANSA dataset the slope is almost the same during all seasons with slight variations (0.31-0.37) and with a reasonable correlation (R^2 = 0.27 - 0.47); whilst the range of slope in the RONOCO dataset is much wider (0.10 - 0.57) with a moderate to good correlation. Using slope values for the HANSA dataset, the [NO_3] to [OH] ratio ranges from 1.96 x 10^4 to 2.54 x10^4 whilst for the present

study, the range is slightly wide 3.4×10^3 - 4.97×10^4. The most contrasting feature of this comparison is that for the present study the inferred ratio is at a maximum for summer flight B535 data and minimum for autumn dawn B551 whilst for HANSA dataset the ratio is highest for autumn and winter data and minimum for summer data. This equation has further been utilized in deriving an absolute concentration of OH radical, using the instantaneous NO_3 between 4 and 40 ppt for summer flight B535 and between 2 and 8pptv for winter dusk B568 during WAS sampling times gives the range of OH as 2×10^3 to 2×10^4 molecule cm^{-3} and $2\ 4 \times 10^3$ to 9.6×10^3 molecule cm^{-3} respectively. The direct measurements of OH by FAGE instrument during this campaign were most of the time below the detection limit so comparison cannot be made directly.

A comparison between the magnitude of the NO_3 production rate and the VOC oxidation rate for selected summer and winter flight data indicate that the average NO_3 production rate is 0.2 ppbv hr^{-1} for both seasons whilst the VOC oxidation rate is 0.02 ppbv hr^{-1} and 0.006 ppbv hr^{-1} for summer and winter data, respectively, indicating a wide difference between the magnitudes of the two processes. This shows that the suite of anthropogenic organic compounds measured during this campaign is of less importance in explaining the loss of the NO_3 radical in both seasons. Moreover, the NO_3 concentration is independent of the NO_3 production rate for both seasons implying negligible direct sinks for the NO_3 radical. An inverse correlation between the steady state NO_3 lifetime and NO_2 mixing ratio for both seasons seems to be reflecting the importance of an indirect loss mechanism for the NO_3 radical.

The average relative contribution of NO_3 and O_3 towards VOC loss rates, indicate that in summer the contribution of the NO_3 radical is more than double than that of O_3 whilst an equal participation of both oxidants to VOC loss rate is seen in winter. On further partitioning the relative contribution of individual classes it is clear that alkenes are the major fraction (82%) of measured suite of VOCs during this campaign followed by isoprene (14%) that are oxidised by the

NO_3 radical. Similar results are produced when partitioning is done with respect to O_3. To further identify the seasonal differences of alkenes with respect to two key nighttime oxidants, a comparison between a summer and winter flight data indicate that the contribution of the NO_3 radical (68%) to alkene loss rates is more than double for summer data in comparison with O_3 (32%) whilst the both oxidants play an equal role to oxidation of alkenes for winter data with slightly higher importance of O_3 (51%) in comparison with the NO_3 radical (49%).

Chapter 5:

A two-year study of C_2-C_8 Volatile Organic Compounds (VOCs) in the free troposphere above the UK

5.1 Introduction

5.1.1 VOC measurements in the free troposphere

The importance of volatile organic compounds (VOCs) as one of the precursor substances for O_3 formation was first recognized by Haagen-Smit and co-workers in 1950s (Haggen-Smit, 1952). Since then numerous research papers have focused their attention towards the various environmental issues linked to VOCs to better understand their sources and emission rates (Russo et al., 2010), oxidation chemistry (Helmig et al., 2008;Goldan et al., 2000), vertical, latitudinal and temporal distribution (Ehhalt et al., 1985;Rudolph and Ehhalt, 1981;Singh and Salas, 1982;Blake et al., 2003;Purvis et al., 2005) and seasonal variations at remote locations (Swanson et al., 2003;Sharma et al., 2000;Greenberg et al., 1996), oceanic sites (Singh and Salas, 1982;Broadgate et al., 1997) coastal sites (Hov and Schmidbauer, 1992), marine and mountain sites (Laurila and Hakola, 1996;Hakola et al., 2006), Canadian boreal forest (Young et al., 1997), rural locations (Bottenheim and Shepherd, 1995), lower polar troposphere (Gautrois et al., 2003), midlatitude Northern Hemisphere (NH) free troposphere sites (Lightman et al., 1990;Penkett et al., 1993;Goldstein et al., 1995a;Grant et al., 2011), Antarctic troposphere (Rudolph et al., 1989) surface air (Gnauk and Rolle, 1998) and continental background atmosphere (Klemp et al., 1997).

As a result of human activities and emissions from vegetation, a wide variety of reactive organic compounds are present at mixing ratios below few parts per trillion to tens of parts per billion. Despite their low mixing ratios, their significance in altering the composition of the present-day atmosphere is well known. Once these compounds are emitted into the atmospheric boundary layer, their chemical degradation, photolysis rate, dry and wet deposition controls the lifetime of a given species and this in turn affects their spatial distribution. The lifetime of VOCs is primarily controlled by the OH radical, with resulting VOC lifetimes varying over time-scales from a few hours to many days.

The atmospheric boundary layer height is between a few hundred meters in winter to roughly 2 km in mid summer. Mostly short-lived compounds are confined within this turbulent layer and are oxidized quickly near the source area leading to the O_3 formation downwind. The less well mixed free troposphere is separated from the boundary layer by the temperature inversion zone. This zone acts as a barrier to the mixing of air between well-mixed boundary layer and free troposphere layer above. Nevertheless, longer-lived VOC species can detrain into the free troposphere and undergo further photo-oxidation processes which also ultimately lead to O_3 formation.

In winter, due to more limited photochemical activity and hence reduced OH radical concentrations, slower reacting compounds can accumulate in both the boundary layer and free troposphere and have the potential to be transported far from their source regions. This reaches a maximum mixing ratio in January-February in the NH. With the onset of spring and hence increased photochemical activity, VOCs start declining, and this is thought to result in the seasonal spring formation of O_3 in clean areas (Monks, 2000). In addition to O_3 formation, oxygenated volatile organic compounds (oVOCs) can also be produced as intermediate products during the organic degradation process. The low vapour pressure and higher water solubility of these compounds as compared to their precursors may favour partition into particle phase leading to the formation of secondary organic aerosols (SOA). The subsequent role of SOAs in modifying the radiative balance of the atmosphere is an entire research field in itself.

Another important species in the remote background troposphere is Peroxyacetyl nitrate (PAN), formed mainly *via* the oxidation of acetaldehyde. This acts as an excellent indicator of tropospheric photochemistry (Penkett and Brice, 1986) and since PAN is relatively stable in cold temperatures, it acts as a reservoir for reactive nitrogen during long-range transport. At ground level it has adverse effects on plants and as an eye irritant in smog conditions.

Free tropospheric air therefore contains a mix of longer-lived compounds advected by large-scale winds, together with shorter-lived more reactive gases which may have been ventilated by small scale meteorology phenomena such as convective events from the polluted boundary layer to free troposphere (Purvis et al., 2003). The emission patterns from a variety of sources, different removal rates together with transport mechanism and meteorological events complicate their distribution with respect to space and time. The complex mixture containing alkanes, alkenes, aromatics and various intermediate oxidized products such as acetaldehyde, formaldehyde, acetone, and methanol define the chemical signature of a particular region. The rate at which all compounds are removed, primarily by OH radical from the atmosphere is a measure of the oxidising capacity of the atmosphere. Changing mixing ratios of organic trace gases has the potential therefore to affect the concentration of the OH radicals and hence the oxidising power of the atmosphere.

In the free troposphere, CO, a by-product of VOC photo-oxidation, serves as one of the major fuels for the formation of O_3, in addition to CH_4 and the collective VOCs. The product of the concentration of compound and its reaction rate with OH radical determine the OH reactivity of a particular compound. On this OH reactivity scale, CO ranks higher than non-methane hydrocarbons (NMHCs) due to its relatively high concentration and thus can be considered to be the most important species, on a global scale, in limiting the concentration of OH in the background troposphere. However, the contribution of NMHCs to the formation of O_3 in clean areas, despite their low concentration, becomes appreciable due to its faster reaction with OH than that of CH_4 (Rudolph and Ehhalt, 1981). A healthy and desirable level of O_3 is necessary to play its role as an oxidant and a precursor of OH radical; however, its increasing concentration trends in background NH by up to 10 μg m^{-3} over the last 20-30 years (Air quality expert group, 2009) has potential for plant and crop damage and an impact on human health. It is now well established that increased O_3 in the upper troposphere acts as a greenhouse gas.

VOC observations in the free troposphere are of interest, particularly for light and saturated hydrocarbons which have significant reactivity in comparison with more abundant species such as CH_4 and CO. They have sufficiently long atmospheric lifetimes to enable us to sometimes trace air mass origins over long distances and probe the processes at various timescales using hydrocarbon ratios, as discussed in chapter 3. An excellent correlation between ln [butane]/[ethane] *versus* ln [propane]/[ethane] from a wide variety of air masses from urban centres through marine environment to remote free troposphere locations is a good demonstration of the chemical evolution of free troposphere ratios from their typical urban ratios (Parrish et al., 1992). Likewise, the background measurement of ethane, the second most abundant organic trace gas in the atmosphere, has served as an excellent tool to understand seasonal and geographical distribution and global model validation (Rudolph, 1995). Long-term seasonal patterns of ethane are not only associated with the general seasonal trends of OH but small changes in the amplitude of the seasonal cycle may act as an indicator of the oxidising potential of the atmosphere (GAW Report No 171, 2006). In addition to the ratio techniques, the analysis of long-term free troposphere hydrocarbon data sets combined with the measurement of the distribution of VOCs and their variability acts as a unique tool in assessing the relative importance of three processes, namely emissions, transport and chemical losses.

5.1.2 Aims of this study

Given the importance of free tropospheric VOC measurements, a number of observatories at high elevation have been established under the World Meteorological Organization Global Atmospheric Watch (WMO/GAW) VOC network. Mainly deploying gas chromatography techniques, VOC data are collected as part of a systematic and long-term measurement programme to better understand the spatial and temporal global VOC distribution and capture important aspects of VOC chemistry in the free troposphere. High altitude observatories often have complex local meteorology and the only means to ensure a data set is truly representative of the regional free troposphere, are

routine and systematic observations from research aircraft. This is a logistically challenging task. So far two aircraft studies have been reported in the literature on UK free tropospheric VOC measurements for the period between December 1982 and March 1986 (Lightman et al., 1990) and January 1987 and April 1990 (Penkett et al., 1993); since then, the true free troposphere VOC measurement over the UK from mobile platforms are lacking.

The FAAM BAe 146-301 aircraft, a facility provided by the UK Met office and Natural Environment Research Council (NERC) for the UK atmospheric research community, has a ceiling altitude of 35000 feet and a maximum endurance of about 6 hours (indicated air speed around 200 kts or 100 ms^{-1}). It is typically involved in variety of different campaigns and UK detachments throughout year. In order to make use of aircraft whilst it was involved in other campaigns and science projects, it was planned to collect VOC data above the boundary layer on a routine basis, according to the flight schedule and the cooperation of the research groups involved in the various other science projects. The flight plans were based on the needs of each research project's specific objectives. Therefore, the present study is representative of random sampling of the atmosphere. This study not only reports true free tropospheric VOC measurements and their seasonal variations but provides a useful comparison with the baseline data from previous free troposphere studies (Lightman et al., 1990;Penkett et al., 1993) after a gap of approximately twenty years. This allows a comparison in terms of hydrocarbon composition, seasonal trends, source profile, and oxidation over a period when VOC have undergone major reductions in emissions, through reduced solvent usage and the introduction of catalytic convertors. The measurements were made during a study period between January 2009 and January 2011.

5.2   Experimental procedures

5.2.1 Sampling procedures and data coverage

Approximately 200 whole air samples were collected in an altitude range of 1100 m to 7000 m during 36 flights over the UK by deploying the Whole Air Sampling (WAS) system aboard the FAAM BAe 146-301 research aircraft between Jan 2009 and Jan 2011. **Figure 5.1** illustrates the sampling locations at varying altitudes over a UK map. The flights were scheduled from Cranfield airfield, located about 65 km north of London, throughout the study period during daytime except for the period July 2010 and Jan 2011 when these were operated during the night from the temporary base station at East Midland Airport, UK. The involvement of the research aircraft in various individual science projects allowed the collection of up to eight samples in evacuated 3 litre internal volume electro polished stainless steel canisters (Thames Restek) per flight before executing science for other projects.

The canisters were filled to a pressure of 40 psig (appr 3 bar) using an all-stainless steel assembly double headed bellows pump (Senior Aerospace, USA) at variable intervals between 30 to 45 seconds filling time depending on the pressure associated with a particular altitude. Filling at high pressure not only ensured the stability of the hydrocarbons in ambient air samples but also provided a usable volume of 9 litres for analysis. Thus depending on the speed and the ascent/descent rate of the aircraft, each sample represents an air mass sampled over a horizontal distance of 3 to 5 km or a vertical distance up to around 1 km. The frequency of ambient air samples collection was at least once in a month except when there was no flight planned during maintenance periods. A detailed description of WAS System and sample filling procedures are given in **section 2.3.2.2.**
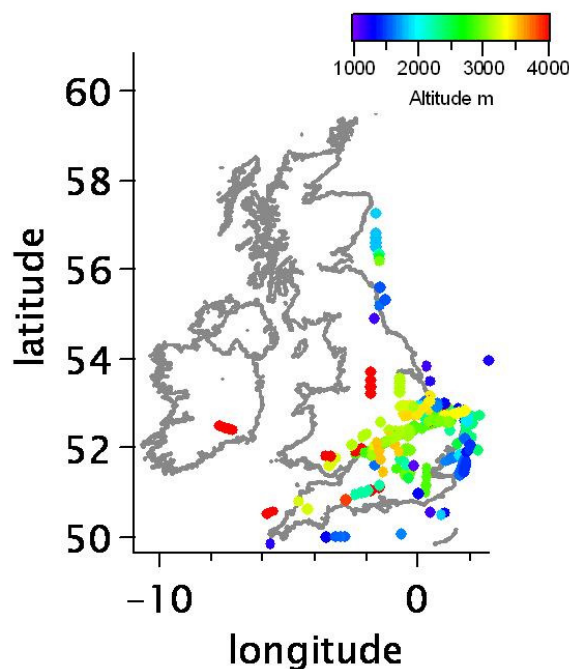
Figure 5.1: Map showing the sampling location and altitudes. The samples were collected at altitudes between 1100 m and 7000 m. The altitude range on a colour scale is adjusted to illustrate the variation among data points. This study includes data from altitudes higher than 2 km.

The core chemistry data (CO, O_3 and NO_x), 3-d wind components, wind speed, temperature, relative humidity and positional data were made available by FAAM.

5.2.2 Analysis

The whole air samples were analyzed generally within one week or at the most two weeks after sample collection. The stability of hydrocarbons in the canisters was tested during this time period and no contamination or growth problems were experienced as demonstrated in **section 2.3.2.2** The canisters were transported back to the University of York and analyzed by using a dual channel gas chromatograph (Perkin-Elmer) equipped with flame ionization detectors (GC-FID); an instrument provided and maintained by the Facility for Ground-based Atmospheric Measurements (FGAM) at York (FGAM-York) for the UK atmospheric science community. A more detailed description of the instrument is

given in (Hopkins et al., 2003;Hopkins et al., 2011). Here, the procedures involved during analysis are briefly described.

The samples were delivered into the measurement system in a fully automated way controlled by Lab view software (home-written software La Vespa, National Instruments). The transfer lines introducing samples to the instrument and other stainless steel tubing within the system were maintained at approximately 70 °C. The presence of moisture in the air sample made it necessary to use a glass finger immersed in an ethylene glycol and water mix (50:50), maintained at -30 °C as a water removal step. The preconcentration stage involved the use of a Peltier-plate cooled dual-bed charcoal trap consisting of Carboxen 1000 and Carbotrap B (Supelco) maintained at -20 °C during sampling time. The sample air was drawn through charcoal trap at a flow rate of 100 ml min^{-1} controlled by mass flow controller (MKS instrument 1000 sccm N$_2$) for 10 minutes thus trapping a litre of sample. The flows were continuously logged in order to monitor any drop in the sample flow rate with subsequent data marked with a flagging system.

Once the trapping step was complete, the 2-position 10-port valve (Valco) was switched to the inject position which allowed methane to flush away in a flow of helium carrier gas, whilst the trap was cold for another 3.5 minute. Following the methane elution from the system, all the analytes were thermally desorbed at a rapid rate (-20 to 325 °C in 18 seconds) in a flow of helium gas on to the two capillary columns housed in the GC oven in a split ratio of approximately 50:50. The separation of non-polar hydrocarbon compounds C$_2$ to C$_8$ was achieved on a Na$_2$SO$_4$ deactivated aluminium oxide porous layer open tubular (PLOT) column (50 m, 0.53 mm i.d., Varian Netherlands) and more polar compounds including oxygenates were separated on a LOWOX column (10 m, 0.53 mm i.d., Varian Netherland). The flow of carrier gas was maintained 20 ml min^{-1} (40 ml min^{-1} in total) through each column for 30 minute and then it was increased to 40 ml min^{-1} (80 ml min^{-1} in total) for rest of the run time to enable the heavier weight compounds elute from the system quickly and leaving no trace of these

compounds as an interference for subsequent runs. The GC oven was programmed by setting a starting temperature of 40 °C until the thermal desorption started at 16.5 minute and then temperature was raised at the rate of 13 °C min^{-1} up to 110 °C and finally the ramp rate was 8 °C min^{-1} until the final isothermal temperature 200 °C was reached where it remained up to the end of the run. The analytes eluting from both columns were analyzed by the independent flame ionization detectors (FID). Thus one complete GC run of an hour including sample acquisition, trapping and analysis forms a basic measurement cycle.

To minimise any memory effects of the GC system from previous samples and maintain the consistency of retention times similar to ambient air samples, humidified nitrogen (prepared by passing dry and purified nitrogen N 6.0 through the headspace of deionised water in a glass vessel) was used as a zeroing gas between samples and standards runs. The presence of a small peak of benzene (6 area unit) in blanks has been considered in quantification. The signal from the FID was output to a computer running Totalchrom software for peak integration. Each chromatogram was manually processed to ensure correct peak identification and assign a correct peak area. A typical free troposphere air sample, standard and zero gas chromatograms are shown in **Figure 5.2**. The detection limit for a 1000 ml sample was between 1 and 10 pptv for NMHCs and between 10 and 40 pptv for oxygenated VOCs.
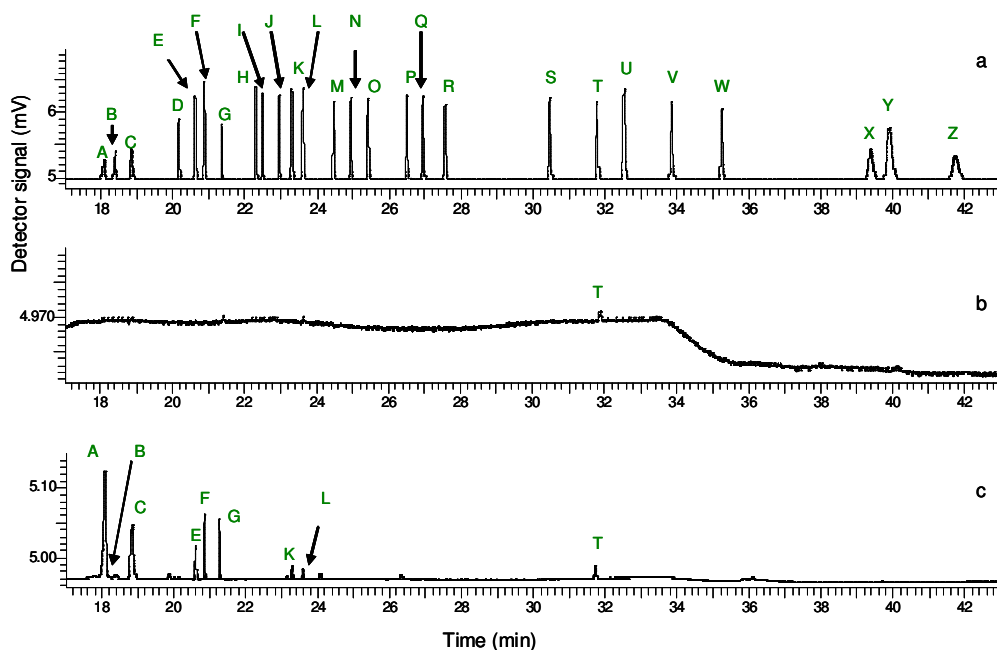
Figure 5.2: FID chromatogram of (a) NPL calibration standard (b) zero gas in an enlarged scale and (c) a typical free troposphere air sample in enlarged scale. The identification of peaks are as follows (A) ethane, (B) ethene, (C) propane, (D) propene, (E) *iso*-butane, (F) *n*-butane, (G) acetylene, (H) *trans*-2-butene, (I) 1-butene, (J) *cis*-2-butene, (K) *iso*-pentane, (L) *n*-pentane, (M) 1,3-butadiene, (N) *trans*-2-pentene, (O) 1-pentene, (P) 2-methylpentane, (Q) *n*-hexane, (R) isoprene, (S) *n*-heptane, (T) benzene, (U) 2,2,4-trimethylpentane, (V) *n*-octane, (W) toluene, (X) ethylbenzene, (Y) *m*-xylene, and (Z) *o*-xylene.

5.3   Results and discussion

5.3.1 Statistical distribution and variability trends

This section focuses on capturing some important features in terms of overall distribution and variability by looking at a general data overview, before going into more detailed discussion. As a preliminary assessment of the data, the cumulative frequency distribution plots for selected trace gases are compared in **Figure 5.3** for winter and summer months.
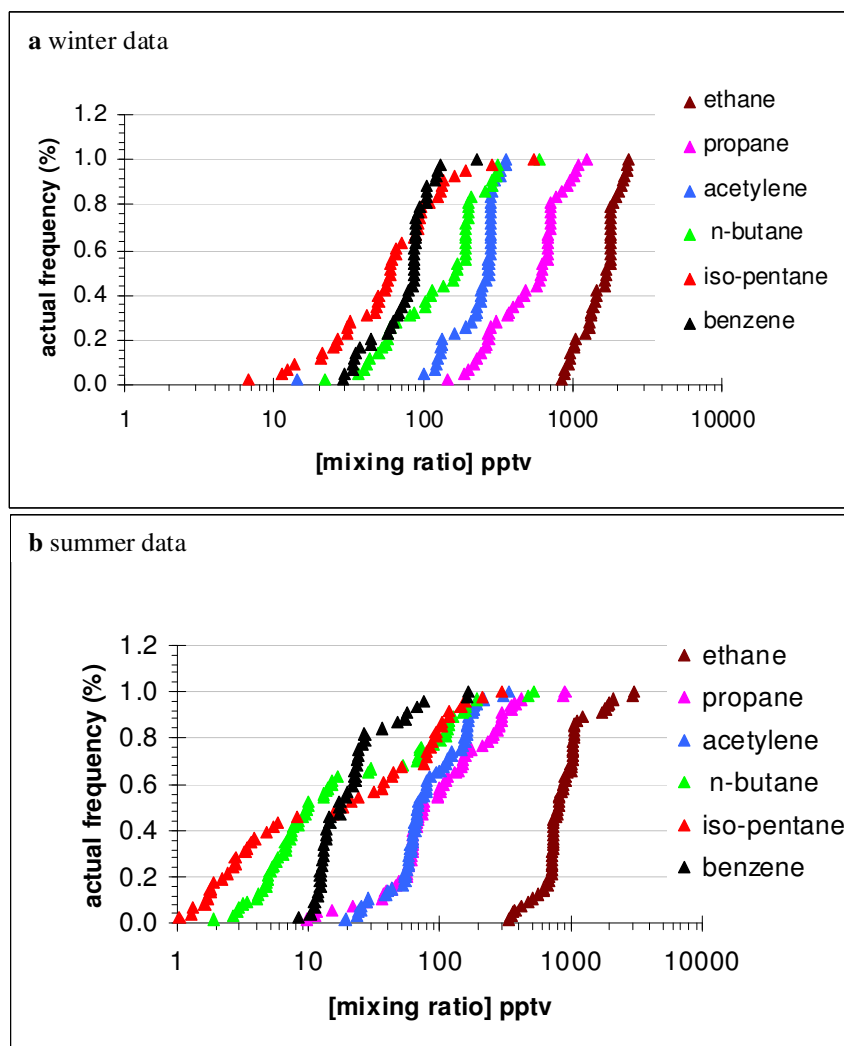
Figure 5.3: Cumulative frequency distributions of selected trace gases during (a) winter and (b) summer seasons measured for the UK free troposphere 2009-2011 study. The probability of a data point at or below any given mixing ratio for selected species is represented by actual frequency in % on *y* axis and mixing ratios on *x* axis are presented on log scale.

The data coverage for winter months is spread from January 09, February 09 and December 09 through February 10 and December 10 to January 11; whilst the observations for summer months are from June 09, July 10 and August 10 period. The cumulative distribution plots have been used in previous work (Jobson et al., 1998;Jobson et al., 1999;Williams et al., 2000;Helmig et al., 2008) to assess the overall hydrocarbon dataset for consistency, to identify the outliers and to demark different source distributions.

The actual frequency in percent on the *y* axis represents the probability of a data point at or below any selected mixing ratio on *x* axis. The mixing ratio corresponding to the value equal to 0.50 on *y* axis represents the median mixing ratio for each species. The median and mean mixing ratios are listed in **Table 5.1** for selected trace gases in increasing order of reactivity.

Table 5.1: Comparison of mean and median mixing ratios (pptv) for summer (June, July and August) and winter months (Dec, Jan and Feb) during the study period 2009-11.

	Winter		Summer	
	Mean mixing ratio (pptv)	Median mixing ratio (pptv)	Mean mixing ratio (pptv)	Median mixing ratio (pptv)
ethane	1583	1675	948	805
acetylene	238	275	96	68
propane	576	624	148	75
benzene	81	87	29	17
n-butane	162	168	54	10
iso-pentane	83	60	49	20

The decrease in absolute mixing ratio with increase in carbon number from ethane to *iso*-pentane reflects primarily the increased reactivity with respect to OH radical and secondarily the relative source strength and vapour pressure to some extent. In both seasons, the mixing ratio for propane is higher than acetylene; although on the OH reactivity scale, propane is slightly more reactive than acetylene. This observation is similar to the Harvard forest dataset (Goldstein et al., 1995b) re-examined by Jobson et al (Jobson et al., 1999) implying in our case the larger emission strength for propane across UK. This is further discussed in detail in section 5.3.3.2 in terms of relative impact of sources.

Benzene also displays a lower mixing ratio than *n*-butane and *iso*-pentane despite being less reactive than C$_4$ and C$_5$ species. This reflects the implementation of

stricter regulations to reduce benzene emissions within Europe (Dollard et al., 2007). These absolute mixing ratios are further compared with a North Atlantic free troposphere study in section 5.3.2 conducted some 20 years ago in UK between January 1987 and April 1989 (Penkett et al., 1993), a period before the implementation of exhaust gas catalyst and evaporative canister control technologies on petrol engined motor vehicles.

The median mixing ratios are slightly higher than the mean for the winter dataset whereas the mean mixing ratios are significantly higher than the median mixing ratio for summer data set for all selected species presented in **Table 5.1**. In the frequency distribution plot (**Figure 5.3**) for summer months, the measured mixing ratios are exceptionally high for every species at the high end of the mixing ratio range; these data points have been further explored and found to be influenced by nonurban sources and discussed in the section 5.3.3.1 at length. The winter data for all selected species are best described by a Gaussian probability distribution function except *iso*-pentane whilst for summer data, the mean is shifted towards the higher value due to a few elevated data points from the June month samples (flights B458, B459 and B460) skewing the distribution towards a higher value; therefore, transforming the summer data by taking a natural logarithm yields a dataset that is normally distributed.

Another feature of these plots is that as reactivity increases the variation in the range of mixing ratio increases. The mixing ratio range for *iso*-pentane varies by approximately two orders of magnitude (from 6 pptv to 544 pptv) for winter months whilst ethane mixing ratio for the same months varies by a factor of 3 (ranging from 835 pptv to 2344 pptv). Overall the summer data exhibit a significantly higher dynamic range in comparison with the winter dataset due to shorter OH-induced lifetimes. The plots for autumn and spring seasons are not representative of the variability in the present dataset as these seasons comprise not more than one or two months of data.

To further examine the variability trends, the deviation of each data point (natural log of mixing ratio values) with respect to the median mixing ratio in terms of standard deviation (Z scores = (mixing ratio – median mixing ratio)/standard deviation) *versus* natural log of mixing ratio has been plotted for selected hydrocarbons. Zero on the *y*-axis represents the median mixing ratio, therefore, ln [median mixing ratio] for each compound can be calculated by setting *y* = 0 in equations for regression lines as depicted in **Figure 5.4**.
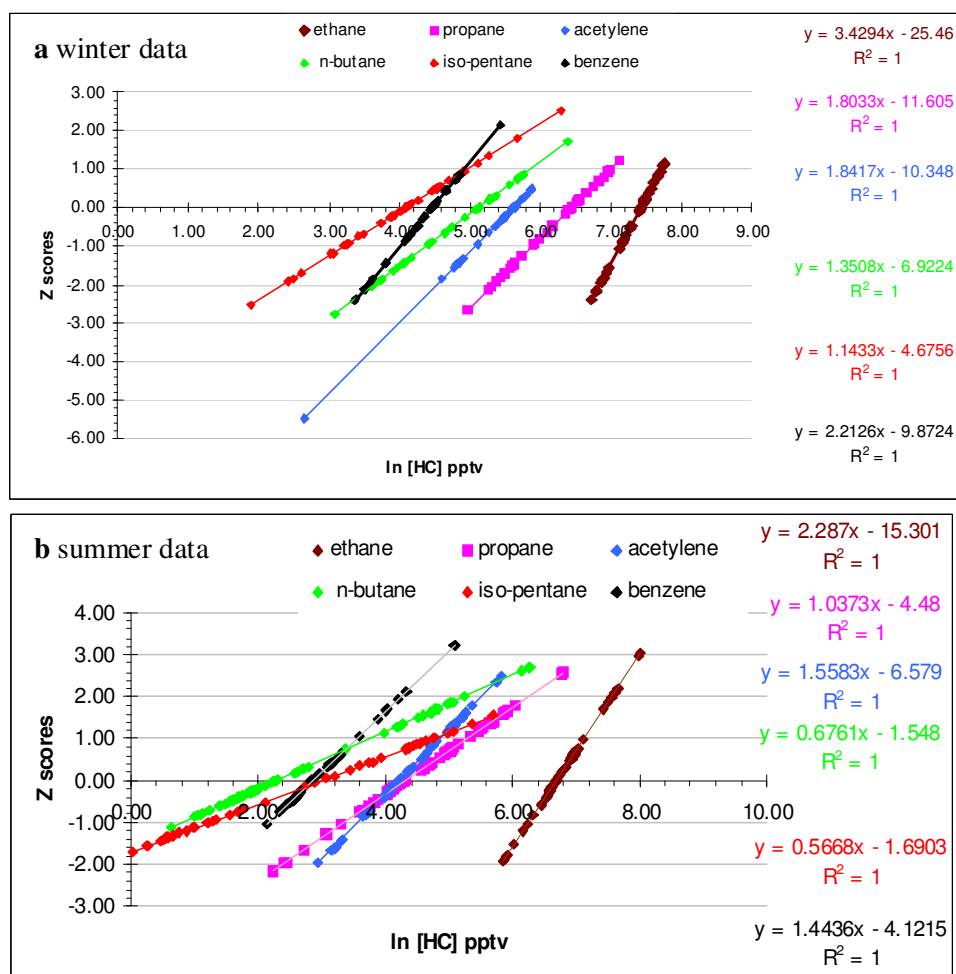
Figure 5.4: The deviation of natural log of each data point with respect to median mixing ratio (Z-scores) *versus* ln of mixing ratio for selected species for (a) winter data and (b) summer data. The ln [median mixing ratio] in pptv for any species can be calculated by setting *y* = 0 in regression equations.

The regression line slopes through data points for each species indicate the extent of variability. As reactivity increases from ethane to *iso*-pentane, the decreasing

value of each gradient implies an increase in the variability. The gradients are consistently lower for the summer month data indicating the higher variability resulting from the shorter seasonal lifetime due to chemistry, mixing effects and lower absolute mixing ratios.These gradients were compared with the lower free troposphere data from the Pico mountain observatory as shown in **Table 5.2** (Helmig et al., 2008); the gradients in this present study are, on the whole, lower than the Pico data though comparable. The slightly higher values of the gradients in Pico data can be interpreted as a result of reduced variability due to air masses sampled with only a small range of ages.

Table 5.2: Comparison of regression slopes for summer and winter months, derived from a plot of the Z scores *versus* natural log of median mixing ratio, between current work and Pico Mountain Observatory data set (Helmig et al., 2008). NR = not reported.

	Gradients for winter data		Gradients for summer data	
	This study	Helmig et al study	This study	Helmig et al study
ethane	3.4	4.5	2.3	2.7
propane	1.8	2.5	1.0	1.4
acetylene	1.8	NR	1.6	NR
n-butane	1.4	1.6	0.67	0.97
iso-pentane	1.1	1.2	0.56	0.77
benzene	2.2	NR	1.4	NR

To further examine the remoteness of the measurement locations from source and the relative importance of mixing and chemistry in the observed distribution, the standard deviation of the natural logarithm of the mixing ratio (Sln[X]) *versus* estimated OH lifetime in days for selected hydrocarbon species has been compared for summer and winter data as shown in **Figure 5.5**.
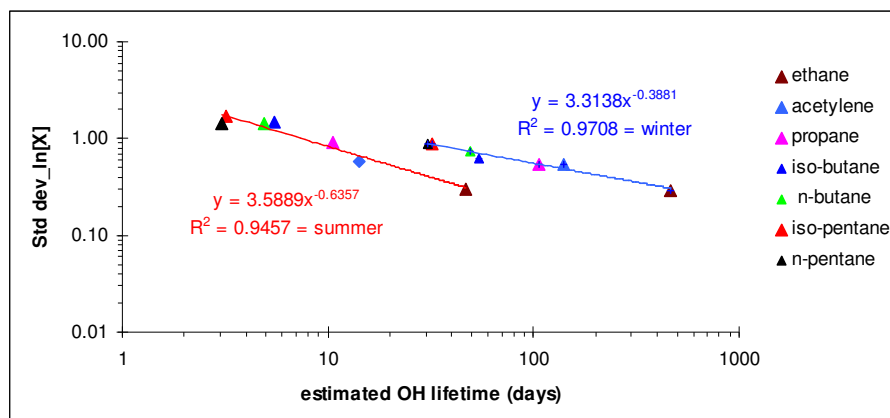
Figure 5.5: A plot of the standard deviation of the natural logarithm of mixing ratio (Sln[X]) *versus* estimated seasonal OH lifetime in days for summer and winter data measured during the free troposphere study. Lifetimes were calculated using an OH density OH = 1 x 10^5 molecule cm^{-3} in winter and 1 x 10^6 molecule cm^{-3} in summer using rate constants at a temperature 298 (Atkinson and Arey, 2003).

The relationship between lifetime and variability is given by the equation 1.91 (as discussed in chapter 1) provided that the distribution of sources and sinks is similar (Jobson et al., 1998). *A* is a proportionality constant and is a measure of the spread in range of air mass ages in the sampled data and the exponent *b* is an index of mixing influence on data. The value of *b* close to zero is indicative of no dependence on chemical lifetime whilst the value approaching one highlights a stronger dependency on lifetime. Here lifetime in days has been estimated by using an OH concentration of 1 x 10^5 molecule cm^{-3} in winter and 1 x 10^6 molecule cm^{-3} in summer. The chosen value of OH concentration does not affect the *b* value, though the value of A depends on the OH concentration used in data.

A good correlation between variability and the lifetime for different species in both seasons does indicate that the atmospheric variability is much greater than the variability caused by the instrumental noise (winter data exhibits a highly coherent trend (R^2= 0.97) but weaker dependence on lifetime by displaying a lower value of *b* (b= 0.38) in comparison with the *b* value for summer data (*b* = 0.63, R^2 = 0.94). A lower value of *b* for winter data is in agreement with the fact

that there is a stronger influence of mixing due to longer lifetime of hydrocarbons as a result of reduced OH concentration. A reasonable higher value of b for summer data suggests the influence of mixing and chemistry on the data.

The data from June month samples comprise of only one flight B457, as the rest of the three flights (B458-B560) data are influenced by nonurban sources (discussed in section 5.3.3.1) and have been excluded from variability-lifetime plots in order to avoid the misrepresentation of variability trends. However including these data points the slope representing the *b* value for summer period is 0.52. As stated earlier the value of A is dependent on the choice of OH concentration, nonetheless, it is interesting to compare these values with other datasets. The value of *A* for Pico observatory is from 1.4 in summer to 1.9 in winter seasons which is roughly half in comparison with values in present dataset (3.5 in summer and 3.3 in winter). The greater the value of *A*, the higher the standard deviation in 'age distribution' of air mass ages in a dataset. We can say that here a wider variety of air masses with different pollution ages have been sampled as compared to a limited range of air masses captured at Pico observatory.

By looking at the qualitative cumulative frequency distribution through semi-quantitative Z scores plots to quantitative lifetime variability relationship, the most important inferences up to this point are that there is a clear seasonal difference in the variability between winter and summer which is reflected by the gradients of Z score plots and the *b* values in the lifetime-variability relationship. The summer data exhibit more variability as a result of both mixing and processing influences than winter data. In addition to diagnosing the mixing influences (*b* value), these plots also have been useful in giving an idea of the range of air masses sampled (*A* value) and to evaluate the precision of the instrument compared to atmospheric variability.

252

5.3.2 NMHC mixing ratios and seasonal trends

5.3.2.1   General data overview

NMHC mixing ratios from January 2009 to January 2011 are presented in **Table 5.3** with monthly statistics for selected species. The hydrocarbon data presented here have been compiled by including observations at sampling altitudes higher than 2 km. The data coverage is well spread throughout the study period except April, May and October months. The observations from July 2010 and January 2011 represent nighttime mixing ratios. **Figure 5.6** on next page illustrates the monthly median mixing ratios, superimposed on raw data points, along with a sinusoidal fit to compare the seasonal variations for selected compounds.
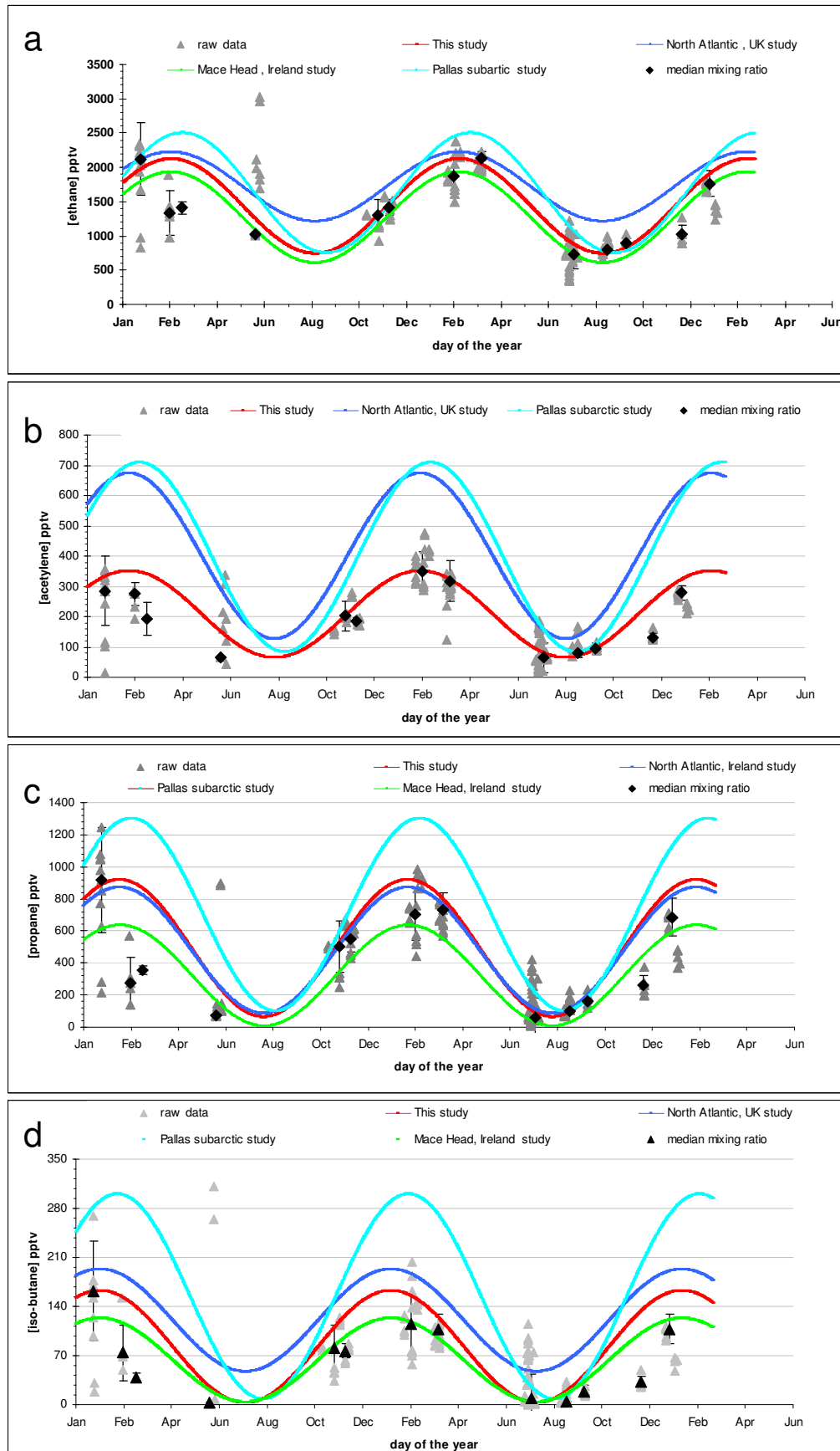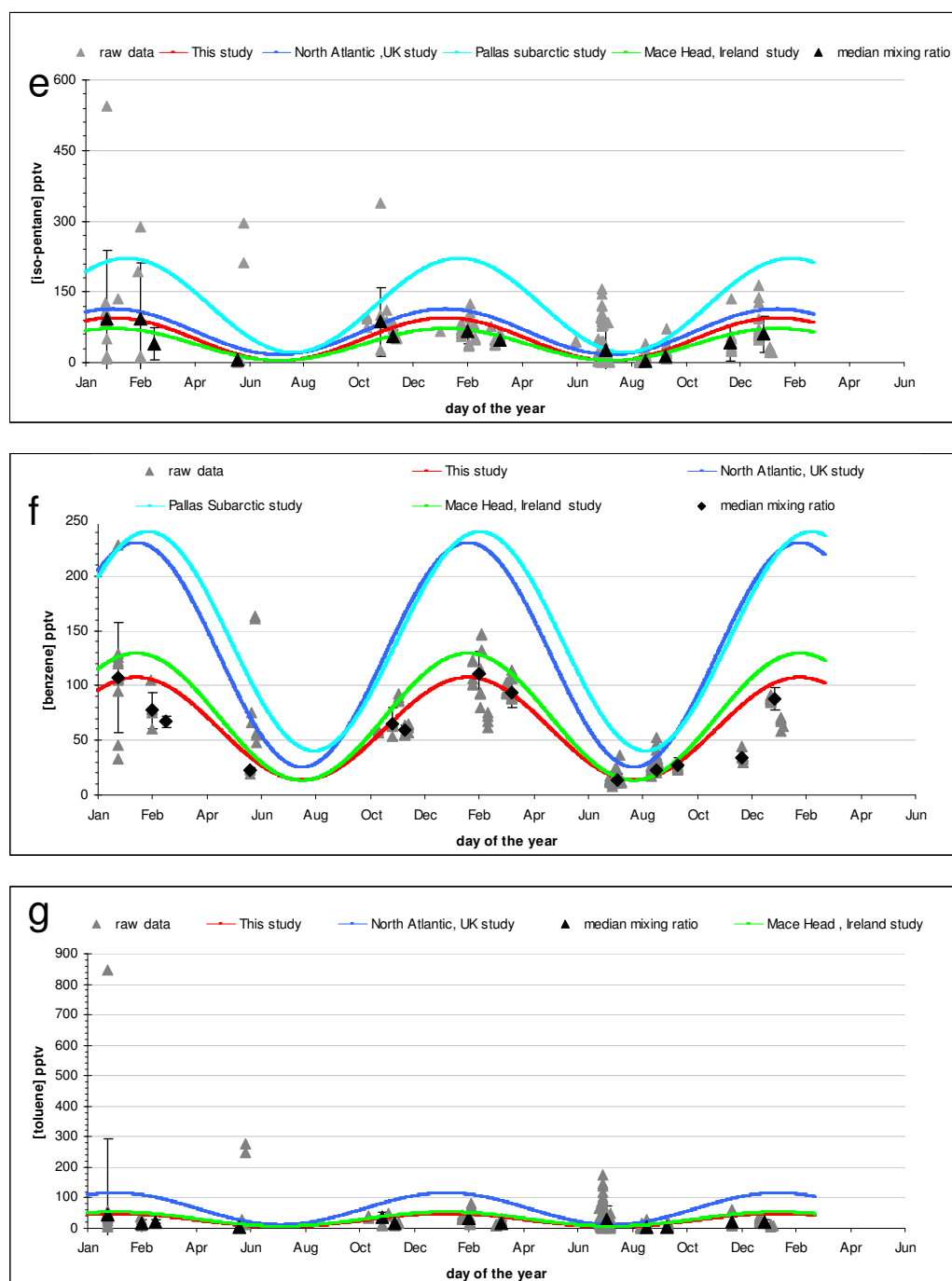
Figure 5.6: C₂-C₇ NMHC seasonal trends for (a) ethane, (b) acetylene, (c) propane, (d) *iso*-butane, (e) *iso*-pentane, (f) benzene, and (g) toluene over the two year study period from January 2009 to January 2011. The value of each error bar represents the one sigma standard deviation for each month data. The sinusoidal fit for the present study (red) is compared to the cycles for two mid latitude sites – (North Atlantic, UK aircraft study (Penkett et al., 1993); Mace Head station, Ireland (Grant et al., 2011)), and a higher latitude Pallas subarctic site (Hakola et al., 2006).The raw data denotes each month observations for the present study.

255

Table 5.3: C_2 to C_7 hydrocarbon mixing ratios (pptv) with monthly statistics for the period of Jan 2009 - Jan 2011. The mixing ratios against 0.05, 0.5 and 0.95 are quantiles. Std dev is the standard deviation, *n* is the number of samples * = The samples are from only B457 flight, see text for full details.

Species	Monthly statistics	Jan/09 (n = 11)	Feb/09 (n = 5)	Mar/09 (n = 4)	Jun*/09 (n = 4)	Nov/09 (n = 13)	Dec/09 (n = 8)	Feb/10 (n = 14)	Mar/10 (n = 21)	July/10 (n = 49)	Aug/10 (n = 5)	Sep/10 (n = 34)	Dec/10 (n = 7)	Jan/11 (n = 20)
ethane	0.05	910	1036	1312	1018	1048	1245	1574	1973	368	685	738	891	1324
ethane	Average	1902	1381	1405	1786	1330	1395	1911	2094	779	767	874	1016	1657
ethane	0.50	2119	1333	1410	1820	1305	1415	1871	2131	739	805	887	1022	1763
ethane	Std dev	529	327	85	732	219	117	266	98	216	63	71	133	183
ethane	0.95	2338	1790	1491	2991	1572	1516	2371	2223	1073	816	975	1215	1794
acetylene	0.05	57	202	141	53	148	171	293	237	24	71	83	124	222
acetylene	Average	246	252	195	150	215	184	361	319	86	84	98	135	266
acetylene	0.50	285	275	193	121	202	187	350	317	64	79	95	131	279
acetylene	Std dev	116	38	54	104	50	11	63	67	50	13	18	14	23
acetylene	0.95	355	282	253	325	275	196	471	421	172	99	129	157	286
propane	0.05	248	163	315	71	285	436	487	592	13	68	77	194	394
propane	Average	825	307	394	246	484	535	702	734	132	90	150	256	618
propane	0.50	918	273	356	108	504	551	704	732	63	98	161	259	686
propane	Std dev	329	160	29	320	159	81	160	107	116	19	45	61	117
propane	0.95	1164	519	375	891	661	616	963	916	351	110	210	346	707
iso-butane	0.05	24	54	35	2	41	61	66	83	2	3	3	25	61

iso-butane	Average	139	84	40	85	81	73	118	107	30	4	17	33	95
iso-butane	0.50	162	75	40	3	80	77	115	108	10	4	19	32	108
iso-butane	Std dev	71	40	5	140	34	10	43	21	33	1	9	8	21
iso-butane	0.95	222	137	45	297	122	86	191	147	90	6	28	45	111
n-butane	0.05	48	25	64	6	72	111	114	141	3	5	5	44	102
n-butane	Average	261	61	73	108	143	139	198	182	48	9	29	58	168
n-butane	0.50	291	43	76	12	146	147	195	179	11	9	34	57	195
n-butane	Std dev	151	46	8	208	56	22	68	39	56	4	14	14	40
n-butane	0.95	460	124	78	505	206	161	311	255	154	14	47	80	199
iso-pentane	0.05	9	12	29	27	55	50	35	38	2	1	1	25	21
iso-pentane	Average	119	120	53	171	104	62	68	48	45	2	16	52	65
iso-pentane	0.50	93	92	40	212	87	55	67	49	28	2	13	42	60
iso-pentane	Std dev	146	120	35	149	73	13	28	7	47	1	16	38	38
iso-pentane	0.95	336.13	270	95	287	203	81	113	59	124	4	40	114	138
n-pentane	0.05	12	8	15	26	17	29	24	32	2	1	1	9	18
n-pentane	Average	126	16	18	79	42	38	49	41	28	2	8	13	42
n-pentane	0.50	80	9	19	103	43	39	48	42	11	2	8	13	49
n-pentane	Std dev	215	12	3	54	20	7	22	7	31	1	6	4	11
n-pentane	0.95	429	33	22	117	66	46			53	94	3	18	19	51

benzene	0.05	39	63	60	21	56	55	88	68	11	18	23	29	63
benzene	Average	111	79	66	65	71	60	112	92	15	23	29	35	82
benzene	0.50	107	77	67	55	65	60	110	94	13	23	27	35	88
benzene	Std dev	50	16	5	52	15	5	21	14	6	4	7	5	10
benzene	0.95	179	99	70	162	91	65	147	110	25	27	43	43	90
toluene	0.05	8	10	19	3	10	11	15	8	2	2	1	10	8
toluene	Average	109	21	25	67	33	17	37	17	42	2	9	23	21
toluene	0.50	46	17	22	12	38	17	32	17	30	2	6	19	21
toluene	Std dev	246	12	8	112	15	4	21	8	44	0.59	8	17	9
toluene	0.95	452	36	34	266	48	22	77	29	134	3	21	51	34
ethene	0.05	103	366	263	25	41	32	55	10	14	27	37	46	29
ethene	Average	182	510	600	174	92	38	138	39	48	45	76	53	40
ethene	0.50	135	522	333	118	84	34	135	36	44	49	75	51	41
ethene	Std dev	104	117	587	182	45	7	67	23	27	13	34	7	8
ethene	0.95	379	634	1309	515	148	48	244	75	88	55	140	64	50
propene	0.05	20	51	44	12	4	4	9	4	4	4	4	11	3
propene	Average	35	58	67	36	7	5	15	7	14	5	7	14	5
propene	0.50	31	59	54	21	7	4	13	6	6	6	7	13	4
propene	Std dev	16	6	33	37	2	1	7	4	19	1	2	3	2
propene	0.95	61	64	106	107	10	5	28	12	70	6	10	19	9

The data points lying at both extremes give the highest spread to Jan 2009 month observations. The range of altitudes covered for this month observations is between 2 km and 7 km. The lowest mixing ratio data points correspond to the highest altitude.

Figure 5.7 represents a good correlation (R^2 = 0.96) between *iso*-butane and *n*-butane during the study period at varying altitudes. A range of mixing ratios is observed between altitudes of 2 and 4 km, whilst the range becomes narrow as altitude increases in the free troposphere. All samples from December 2010 months are also from altitudes between 6.7 km and 7.5 km explaining the lower mixing ratios than in corresponding month of 2009 year.
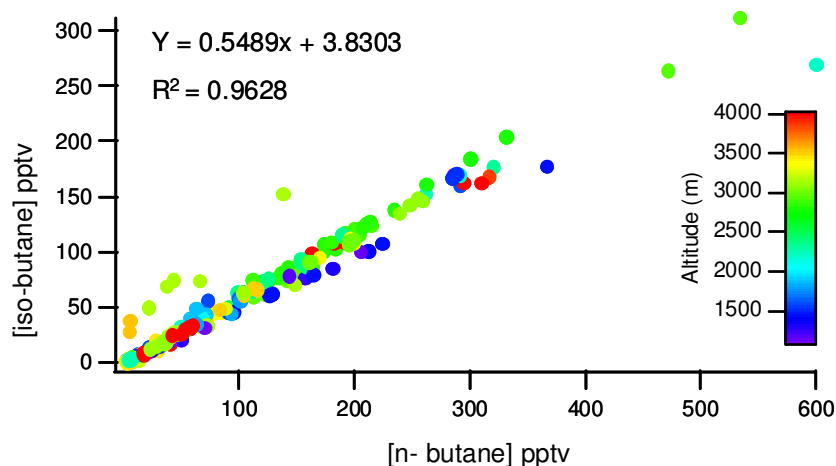
Figure 5.7: The mixing ratios of [*iso*-butane] *versus* that of [*n*-butane] for 2009-11 period. The points are coloured by the altitude of the observations according to the colour scale to the right of the graph.

As can be seen from **Figure 5.6**, a data point corresponding to a January month with an exceptionally high mixing ratio is present in each plot except in ethane and acetylene. The difference between normal data points and unusually high observations increases with the increase in the reactivity and this is clearly exhibited in the plot for toluene where the difference between normal and

259

unusually high mixing ratio data points is the greatest. The CO observation corresponding to this high mixing ratio is however not elevated at all and mixing ratio is same (120 ppb) corresponding to other data points and the same is true for acetylene observation. This rules out the possibility of local anthropogenic sources such as evaporation of fuels and air traffic contamination and indicates towards the contamination issues associated with the sampling stage.

The deviation in median mixing ratios from the sinusoidal fit for February 09 and March 09 are higher than respective months for 2010 year. The limited number of samples (n =5) captured in this month could be the reason of not truly representative of February month samples. Another noticeable point of these plots is the difference between January 2009 and January 2011 mixing ratios which increases with the increase in the species reactivity. As discussed previously, the present data set includes nighttime mixing ratios for July 2010 and January 2011 months. The nighttime mixing ratios for January 2011 observations present us with an opportunity to compare with daytime mixing ratios for January 2009. The ratio of day to night median mixing ratios is illustrated in **Figure 5.8**a for species having a wide range of reactivities. There is a gradual increase in ratio up to *iso*-pentane and then from toluene to propene this increase becomes more significant with the increase in reactivity.

For a better graphical presentation, the percentage difference between day and night mixing ratios for different species is shown in **Figure 5.8**b. It is apparent from the figure that as reactivity increases from ethane to propene, the difference between day and night time mixing ratios also increases. The difference between day and night mixing ratios differs by 2% for acetylene and up to 25% for ethane, propane and benzene whilst for reactive species this difference increases from 30% to 90% with decreasing lifetime. Two data sets, one from Harvard Forest in North America (Goldstein et al., 1995b) and other from the Black Forest in southwest Germany (Klemp et al., 1997) also include nighttime mixing ratios in their long-term datasets. However, the difference in day and night mean

mixing ratios in the hydrocarbon dataset from the Black Forest is less than 10% for ethane and propane and rises up to 25% for reactive species, which is much less than the differences in our dataset. The difference could be due to the differences in datasets based on random and systematic sampling.
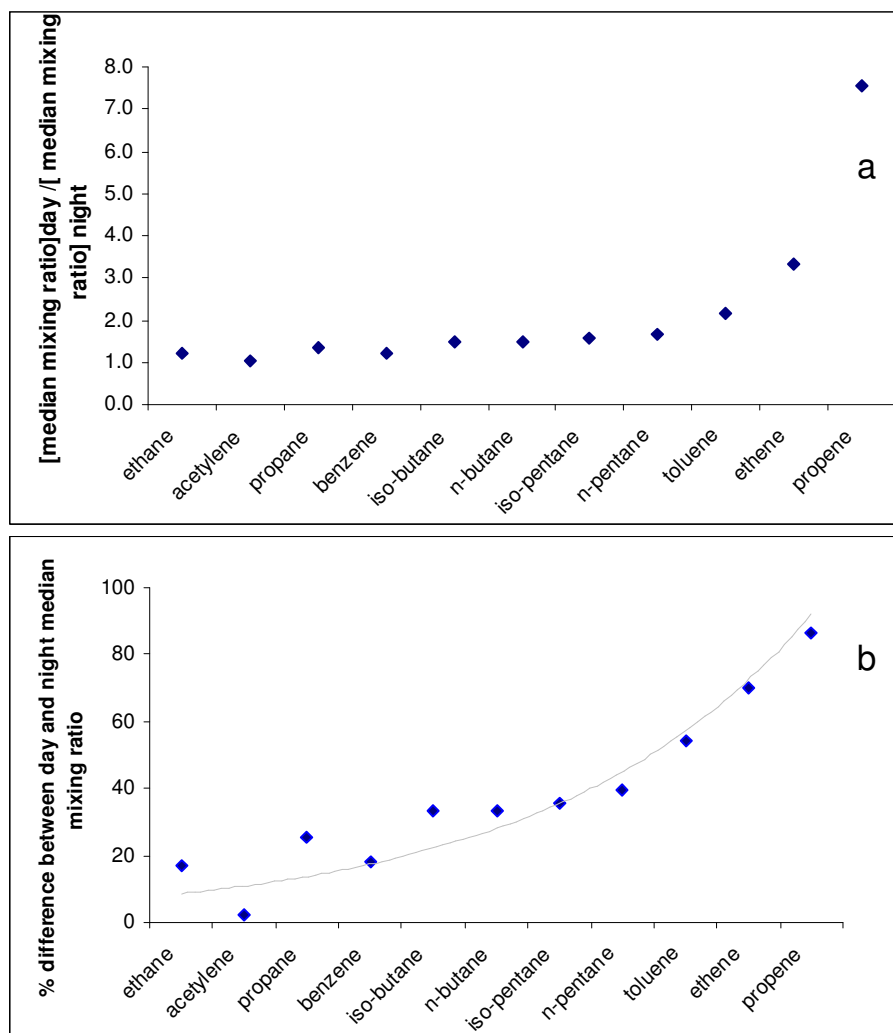
Figure 5.8 a) Day to night ratio of median mixing ratio for selected species. The observations corresponding to January 2009 is from daylight hours whilst January 2011 covers night time mixing ratios. b) Percentage difference between day and night median mixing ratios.

Coming to the general data overview for the summer months, it can be seen from **Figure 5.6** that the data exhibits higher variability, which is in agreement with the greater influence of chemistry due to increased photochemical activity during this season. The samples for June 2009 are from four flights B457, B458, B459

and B460. The difference in mixing ratios between B457 and the other three flights is a factor of 2.5 to 3 higher. These high mixing ratio data points were further investigated by using five days air mass back trajectories and found to be influenced by the North America continent. These data points form a part of the present data set; however, the median mixing ratios presented in **Table 5.3** is calculated by considering data only from the B457 flight, which can be considered to be a truly representative of June month free troposphere value.

5.3.2.2   Comparison with published literature

To compare the seasonal trends with published data, two UK studies from mid latitudes and one subarctic Pallas site from higher latitudes have been chosen. Using the dataset collected aboard a small Jetstream aircraft from January 1987 to April 1989 in the free troposphere over North Atlantic Ocean above the UK (Penkett et al., 1993) presents us with an opportunity to compare the hydrocarbon composition in UK free troposphere air in the present work after a gap of 20 years. Another dataset is from surface measurements at Mace Head, Ireland which is (53.20 °N, 9.54 °W) representative of Northern Hemispheric air (Grant et al., 2011). A final dataset for comparison is taken from the subarctic Pallas site (67 58 °N, 24.07°E) representative of higher latitude background station (Hakola et al., 2006).

Table 5.4 shows the comparison between winter maxima and summer minima for these sites. In order to select the winter maxima, the median mixing ratios for the winter months (December, January and February) are compiled and the highest value is chosen for all species to represent winter maxima, likewise the lowest median mixing ratio has been selected out of summer months median mixing ratios to represent summer minima. Data with mixing ratios below the detection limit are assigned a value half of the instrument's detection limit. This approach has recently been adopted by the Aerosols, Clouds, and Trace Gases Research Infrastructure Network (ACTRIS-VOC network). In the case of *n*-pentane

observations, for example, where only 4% of data were below the detection limit, a value of 0.5 pptv was assigned to values below the detection limit of 1 pptv.

Table 5.4: Comparison of winter maxima and summer minima mixing ratios reported for the different sites at mid Northern latitude and high Northern latitude. Summer is defined as June to August, and winter is defined as December to February except Pallas station where summer extends till September and winter till March. NR represents 'not reported'.

	This work UK free troposphere aircraft data		Mace Head Ireland station baseline data (53.20 °N, 9.54 °W)		North Atlantic UK aircraft data		Pallas station (67.58 °N, 24.07 °E)	
Species	winter	summer	winter	summer	winter	summer	winter	summer
ethane	2119	739	1928	604	2220	1210	2500	750
propane	918	63	635	6.5	870	85	1300	100
benzene	107	14	129	13	230	25	240	40
acetylene	350	64	NR	NR	673	126	NR	NR
n-butane	291	6.6	246	3.0	405	25	590	100
iso-butane	162	2.6	123	3.5	193	47	300	8
n-pentane	80	2..0	69	2.0	147	8	150	20
iso-pentane	93	2.0	71	3.0	112.3	15.5	220	20
toluene	46	2.3	52	4.7	115	10	NR	NR

The values for the winter maxima in benzene, acetylene and toluene are a factor of two higher in the North Atlantic, UK study than for the present work. On comparing the maxima between this study and Mace Head work, the winter maxima for Mace Head site is lower by up to 25% for all selected compounds presented in the table except for benzene and toluene for which the values are higher by 20% and 13% respectively. It seems to be suggestive of differences in measurement locations; the Mace Head site represents a clean background location with baseline data in contrast to the data from random sampling in the

present work. Comparison with the North Atlantic study reveals up to a 45% decrease in acetylene, benzene, toluene, butane and pentane over the entire seasonal cycle as compared to ethane and propane during the intervening twenty years. This decrease is due to implementation of three-way catalytic converters and canisters to control CO, VOC and NO_x since 1991 (Dollard et al., 2007). Comparing with the subarctic Pallas site, the winter maxima is a factor of 1.5 to 2 higher for all species than all other sites in comparison.

Large differences in values of the summer minima are observed for ethane between the North Atlantic study and other studies; the summer minima is a factor of approximately 1.5 to 2 higher in the older North Atlantic data than all other studies in comparison and it is reflected by the shallow amplitude of the ethane in the seasonal pattern of North Atlantic data in **Figure 5.6**. To a certain extent, these differences are attributed to the method of selecting winter maxima and summer minima in different studies. In the North Atlantic study, it is derived from fitting curves through the mixing ratio data plotted with respect to time, whilst the present work adopts a different method discussed at the start of this section. Another explanation for high value of summer minima seems to be lack of sample coverage in summer months in the North Atlantic work, a value representative of summer minima in the North Atlantic study is from only two flights made in month of July 1988 and August 1988 during the three year data set.

In the absence of a continuous data set for the current study, the day of maxima for hydrocarbons is estimated by sorting data for each compound in descending order and then the Julian day corresponding to the highest mixing ratio has been considered as an estimated time of winter maxima for all species. The ethane and acetylene winter maxima appeared in the last week of February whilst propane and benzene in mid Febuary and for butanes, pentanes and toluene in the last week of January. This is in accordance with the work done by the previous study (Bottenheim and Shepherd, 1995) showing the relationship between the rate

coefficient of reaction with OH and the estimated number of days after the winter solstice for the occurrence of a maximum. The time delay is larger for ethane and acetylene as compared to the more reactive species like butanes, pentanes and toluene implying the need of higher OH concentration for ethane and acetylene to respond to the source strength. A seasonal fit defined by the formula y = a sin b (day + c) + d is given to ethane, propane, acetylene, benzene, *iso*-butane, *iso*-pentane and toluene as demonstrated in **Figure 5.6**; where a is the amplitude, b is 2π/period and the period is 365 days, c is the phase shift and d is the vertical shift. **Table 5.5** compares the three characteristic features of the seasonal cycle (amplitude, phase shift and vertical shift) of the current work with other studies.

Hydrocarbon species having a sufficiently long atmospheric residence time clearly show a seasonal change in their mixing ratio by exhibiting maximum mixing ratio in Jan-Feb and minimum in July-August months. The seasonal cycle is more pronounced for less reactive species like ethane, acetylene, and benzene in comparison with more reactive species like propane, butane, pentane and toluene. The amplitude is defined as half of the difference between winter maxima and summer minima value; it is apparent from **Table 5.5** that as reactivity increases from ethane to toluene the amplitude of seasonal cycle for all studies in comparison also decreases except propane and benzene. Although the reactivity of propane towards OH is higher than acetylene by roughly 30%; the amplitude of propane in the seasonal plot is approximately a factor of 3.5 higher than acetylene in the current work whilst by a factor of 1.5 in North Atlantic work suggesting a large seasonally dependant emission strength of propane across the UK and this feature was also apparent from the cumulative distribution plots. This is not unreasonable given that natural gas forms the largest source of propane emissions in the UK and the use (and leakage) of this peak in winter.

Table 5.5: Comparison of amplitude (a), phase shift (c) and vertical shift (d) in a seasonal fit given to data expressed by equation y = a sin b (day + c) + d between present work and other studies. The other studies include North Atlantic UK free tropospheric aircraft study (Penkett et al., 1993), the Mace Head atmospheric research station, west coast of Ireland (Grant et al., 2011) and Pallas, a subarctic higher latitude site (Hakola et al., 2006). NR signifies no measurement reported for particular compound.

Species	This study			North Atlantic,UK			Mace Head, Ireland UK			Pallas, Arctic site		
	a	c	d	a	c	d	a	c	d	a	c	d
ethane	690	31	1429	505	31	1715	662	31	1266	875	16	1625
acetylene	143	39	207	273	39	399	NR	NR	NR	NR	NR	NR
propane	427	46	490	392	46	477	314	46	321	600	31	700
*iso-*butane	80	61	82	73	61	120	60	61	63	146	39	154
*iso-*pentane	46	61	48	48	61	63	34	61	37	100	46	120
benzene	47	49	60	102	49	127	58	49	71	100	36	140
toluene	22	61	24	53	61	62	24	61	28	NR	NR	NR

Likewise the reactivity differences between propane and benzene are not more than 25% with benzene showing higher reactivity towards OH; nonetheless the amplitude of benzene is relatively low in all studies in comparison suggesting the implementation of stricter policies to control the emissions of benzene across the the UK. Overall the amplitude of the seasonal cycles for the older North Atlantic study are much higher for acetylene, benzene and toluene in comparison with the present work and the Mace Head dataset, implying a significant decrease in mixing ratios of hydrocarbons across UK during the last twenty years. All selected hydrocarbon compounds from higher latitude subarctic Pallas site (67.58 °N, 24.07 °E) exhibit the highest amplitudes of all the studies resulting from the lower levels of OH at these high latitude.

Another feature of the seasonal plot is the vertical shift, which is defined as half of the sum of the winter maxima and summer minima for a selected species.

These values are the best estimates of annual average for all selected compounds in UK free troposphere. Finally, the phase of the seasonal cycle for each compound is defined by the temporal occurrence of the maximum and minimum, which in turn depends on the reactivity of the particular compound towards OH. The least reactive compounds, for example ethane, exhibit maxima in late winter as compared to the more reactive compounds, for example toluene, which occur in mid winter. In a full complete seasonal cycle, the period of 365 is equivalent to 2π and the maxima corresponding to $\pi/2$ is equivalent to 91 days. In order to get the value of phase shift, the Julian day corresponding to the maxima is subtracted from a constant value of 91. It is clear from the **Table 5.5** that as reactivity of a compound with OH increases, the value of phase shift also increases due to an earlier occurrence of the winter maxima. Occurrence of the maxima is almost the same in this current work, the North Atlantic and Mace Head data illustrating that all three cycles are in phase. The delay in the winter maxima in the Arctic seasonal cycle is observed due to the almost negligible photochemical activity during the extended winter of the polar region.

5.3.3 Hydrocarbon ratios as atmospheric tracers

To this point the absolute mixing ratios of hydrocarbon species have been discussed to highlight the distribution and seasonal variability in a dataset on a monthly basis. This section attempts to use hydrocarbon ratios to investigate i) unusually high concentration samples in the month of June collected from flights B458, B459 and B460, ii) the extent of photochemical processing in different seasons and links with O_3 variability, iii) the relative impact of sources on the composition of UK free troposphere air, iv) the source profile variation especially for benzene, acetylene, and toluene over the intervening twenty years.

5.3.3.1 Nonurban sources and background ratios

Once entered into the atmosphere**,** the mixing ratio of trace gas X decreases exponentially by chemical loss and dilution process according to equation 1.59

discussed in section 1.2.8.1. To examine the extent of the aging process, ratios of suitable pairs are plotted in a double logarithm plot. The natural logarithm plot of [*n*-butane]/[ethane] *versus* [propane]/[ethane] has been used in previous studies (Rudolph and Johnen, 1990;Parrish et al., 1992;Greenberg et al., 1996;Swanson et al., 2003;Parrish et al., 2004;Helmig et al., 2008) to investigate the effects of mixing and aging on the composition of a given air parcel. Here these plots have been plotted for winter and summer seasons to compare the influence of photochemical processing and mixing in different seasons as shown in **Figure 5.9**.

The correlation between ratios for the winter season is tight ($R^2 = 0.96$) in comparison with summer seasons ($R^2 = 0.84$). The range of ratios in the winter season is limited and larger values of logarithm ratios (ln [propane]/[ethane] higher than -2.5) implies a lesser degree of photochemical processing, whilst the wide range of ratios and smaller values of logarithmic ratios (ln [propane]/[ethane] lower than -2.5) in the summer season are as a result of greater extent of processing. This is also supported by the regression slope for winter data (slope = 1.66), which is slightly less than that of summer data (slope = 1.74). Overall in both seasons the data fall between two theoretical limits represented by the dilution and the photochemical lines suggesting the contribution of two processes during aging.
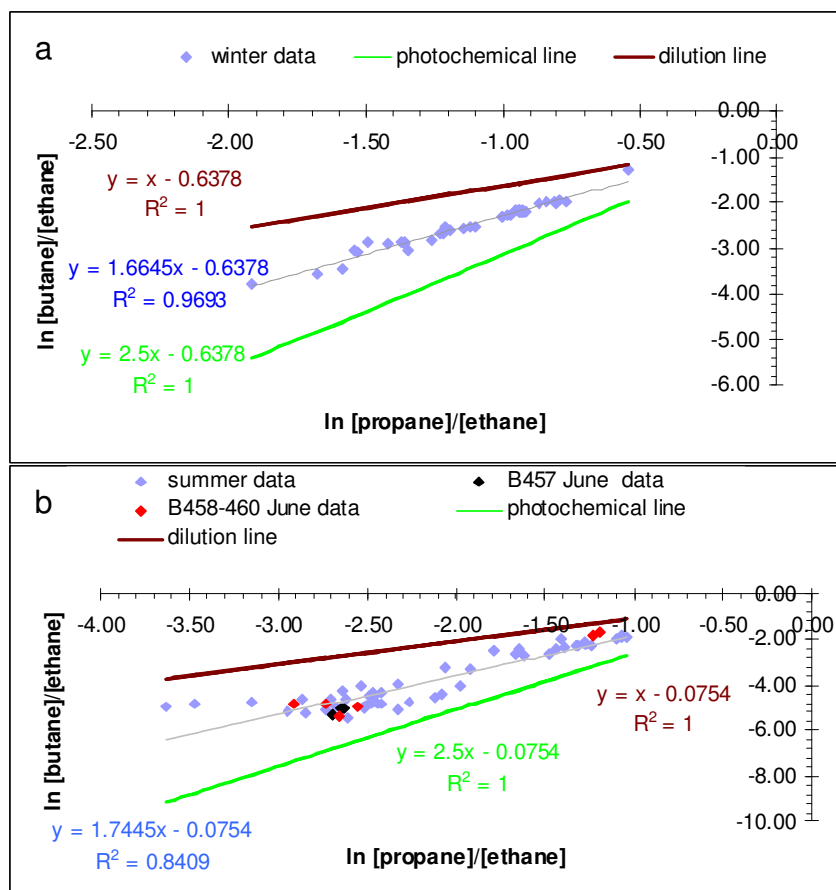
Figure 5.9: The relationship between the natural logarithms of [*n*-butane]/[ethane] and [propane]/[ethane] for (a) winter and (b) summer seasons. The linear regression line is fitted to the data in both plots. The theoretical dilution line and theoretical photochemical lines (OH chemistry) are also plotted to compare the occurrence of observations between these two limits. The intercept for these lines are the same as that of the observed data on the basis of a common emission ratios principle. The samples from June 2009 months are separated in two groups and shown in different colours– data from B457 and unusually high mixing ratio data points from flight B458, B459 and B460 flights.

As it can be seen from **Figure 5.10**, when all data are taken into account for double logarithms plot between ln [*n*-butane]/[ethane] and ln [propane]/[ethane] then a reasonably good correlation ($R^2 = 0.82$) exists and the slope equal to 1.46 is in accordance with the previous work (Parrish et al., 1992) (slope = 1.47).
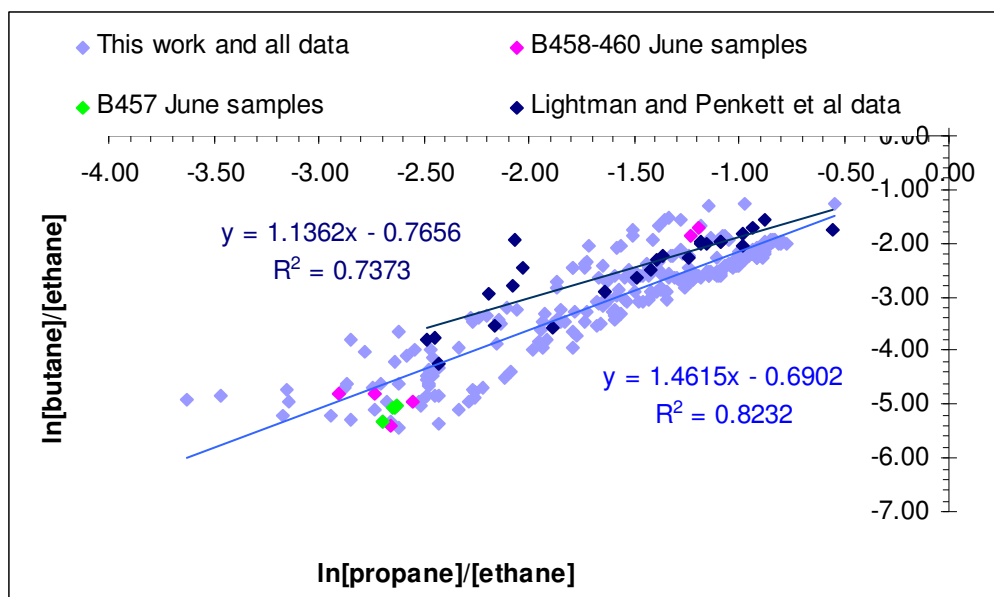
Figure 5.10: Correlation of the natural logarithm of ln [*n*-butane]/[ethane] and ln [propane]/[ethane] for all samples collected during the study period. The samples from the month of June are separated on the basis of unusual high mixing ratios from flight B458, B459 and B460 as compared to normal mixing ratio from flight B457. Also included the data from previous two studies – UK free tropospheric aircraft study between 1982 and 1986 (Lightman et al., 1990) and North Atlantic UK free troposphere aircraft study between 1987 and 1989 (Penkett et al., 1993) to compare the aging pattern with the present work. Regression slopes for the combined (Lightman et al., 1990;Penkett et al., 1993) that is between 1982-1989 study is 1.13 and for the present work is 1.46.

The plot in the Parrish et al. study (Parrish et al., 1992) (Fig 1.9 chapter 1) compiles data from a wide variety of air masses from urban through to rural continent and marine data from both Pacific and Atlantic Oceans to the free troposphere environment. The most striking feature of the plot in the Parrish et al. work is an excellent correlation (R^2 = 0.95) between logs of the two hydrocarbon ratios for a wide variety of air masses, though the disagreement between the observed slope (1.46) and kinetic slope (2.5) has been a debatable topic. McKeen and Liu (McKeen and Liu, 1993) gave an explanation for the deviation from the kinetic slope by using a meso-scale model, indicating that the slope is a result of photochemistry, mixing and dilution processes rather than considering only photochemistry.

Coming back to the plot in Parrish et al work, the good agreement among a wide range of ratios led the authors to conclude that light alkanes from all different environments mainly come from anthropogenic sources and with relatively uniform emission ratios. However, the list compiled by (Swanson et al., 2003) for source emission ratios normalized with respect to ethane for different source signatures for light alkanes points out that there is a significant variation in emission ratios between urban and non urban sources. When these different emissions ratios (urban emissions, biomass burning and gas/venting leakage from oil production and natural gas emissions) ratios were overlaid on a ln [*n*-butane]/[ethane] *versus* ln [propane]/[ethane] plot then urban emissions and gas leakage emissions lie at the upper right corner whilst biomass burning and natural gas emissions lie in the lower left corner. Therefore, a data point lying to the lower left could be aged anthropogenic emissions or fresh emissions from a source particularly rich in ethane explaining low ratios and consequently smaller slope. This point highlighted the importance of the influence of air masses with different source signatures in addition to those dilution processes that could be responsible for the observed deviation from the kinetic slope.

Up to this point it is clear that data points from different source signatures on ln [propane]/[ethane] *versus* ln [*n*-butane]/[ethane] plot are indistinguishable from urban anthropogenic emissions. This is further illustrated in **Figure 5.9**b (summer plot) and **Figure 5.10** (all data) that includes exceptionally high mixing ratio June samples from three flights (B458, B459 and B460) along with normal June samples from a single flight (B457). These abnormally high mixing ratio data points do fall on the trend line and appear to be indistinguishable from aged urban emissions. The data (alkanes) from flight B458, B459 and B460 are a factor of 2.5 to 3 high in comparison with that of flight B457 as shown in **Table 5.6**. To investigate this, five-day back trajectories were used: data from flight B457 were found to be originated from the North Atlantic Ocean whilst B458-460 flight data seemed to be influenced from North America continent as presented in **Figure 5.11**.

Table 5.6: The mixing ratio for selected light alkanes from four flights made in the month of June. The mixing ratios from flight B458 to B460 are of 1.5 to 2 times higher in comparison with that of flight B457. The number of samples is represented by *n*.

Flight	Date (n)	ethane pptv	propane pptv	acetylene pptv	*n*-butane pptv	*iso-*butane pptv
B457	16/06/2009	1008	68	67	5	2
	(4)	1037	73	64	7	3
		1055	76	66	7	2
		1027	74	67	7	2
B458	18/06/2009	1994	130	161	16	-
	(2)	2117	149	216	9	-
B459	22/06/2009	3021	882	311	471	264
	(2)	2962	901	338	533	311
B460	23/06/2009	1906	149	193	13	-
	(3)	1820	100	43	15	7
		1700	108	121	-	
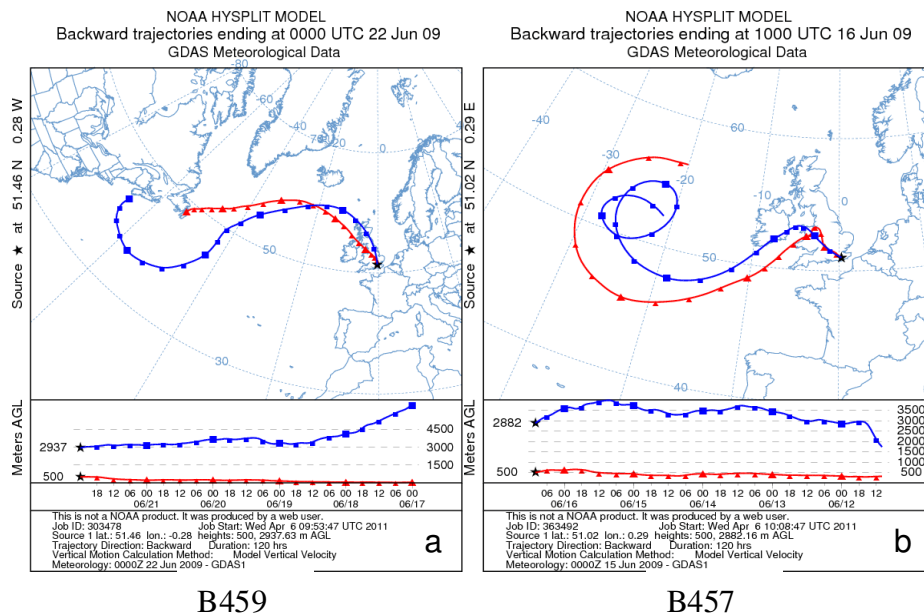
Figure 5.11: Five-day back trajectories run with NOAA HYSPLIT model for data from (a) B459 and (b) B457 flights.

Parrish et al (Parrish et al., 2004) showed the importance of using log-transformed data *versus* linear scale data to examine the source specific variability and photochemical removal, and also the use of propane as a robust photochemical processing indicator in addition to the ln [propane] to [ethane] ratio. When ln [propane]/[ethane] is plotted *versus* the [propane] mixing ratio on a logarithm scale, then these June month samples influenced by North America are identified as outliers as shown in **Figure 5.12** and fall above the trend line, exhibiting a different aging pattern in comparison with the other data points; these odd data points correspond to higher propane concentrations than normal June month samples data points, indicating the fresh non urban emissions rather than aged urban emissions.
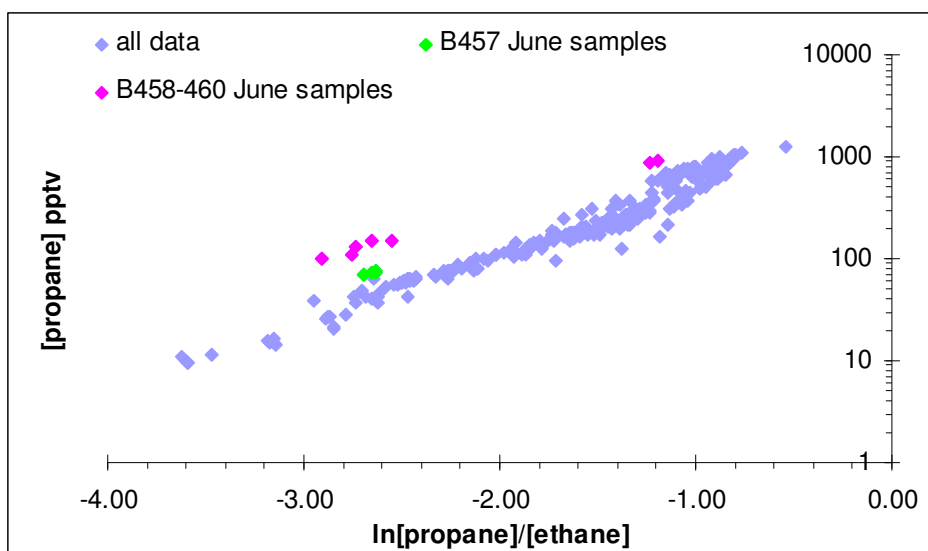
Figure 5.12: The mixing ratio of propane on a logarithmic scale plotted against the natural logarithm of [propane]/[ethane] plotted for data covering study period from January 09 to January 11. The unusually high mixing ratio data from flight B458 to 460 flights clearly stand out from usual mixing ratio data from B457 flight.

It was interesting to compare the aging pattern with the previous two aircraft studies (Lightman et al., 1990;Penkett et al., 1993) conducted over the UK between 1982 and 1989 as shown in **Figure 5.10**. In both data sets the ratios are well correlated suggesting that the aging pattern of hydrocarbons has remained constant over the intervening twenty years, although there is a significant difference in slopes of the linear regressions (slope from combined two aircraft

studies = 1.13 and slope from present work =1.46) which can be attributed to the effects of dilutions and mixing with air masses with hydrocarbons of different ages and perhaps the influence of air masses with different source signatures.

5.3.3.2 Hydrocarbon ratios and impact of various sources

Despite the fact that propane is only slightly more reactive (30%) than acetylene towards OH radical, the mixing ratio for propane in both seasons is a factor of 2 higher than acetylene suggesting larger emission strength of propane across UK. Likewise the reactivity differences between propane and benzene are less than 20% however, the mixing ratio of propane is a factor of 5 higher in both seasons. To investigate the relative impact of various sources on the chemical composition of air masses observed in UK free troposphere air, the correlation plots between propane and acetylene, propane and benzene, benzene and acetylene have been used as shown in **Figure 5.13**.

A good correlation exists (R^2 = 0.80-0.83) between propane and benzene, propane and acetylene and benzene and acetylene. The slopes are equal to 2.3 and 6.83 for [propane]/[acetylene] and [propane]/[benzene] correlation plots respectively, are greater than 1, suggesting the impact of natural gas relative to incomplete combustion as a source of propane throughout the study period (PORG report, 1997). However, the [benzene]/[acetylene] correlation slope is less than 1 (0.31) indicating the vehicular emissions as a primary source. These ratios are in accordance with the ratios observed at the University of New Hampshire AIRMAP , an atmospheric observing station at Thompson Farm in Durham, New Hampshire (Russo et al., 2010).
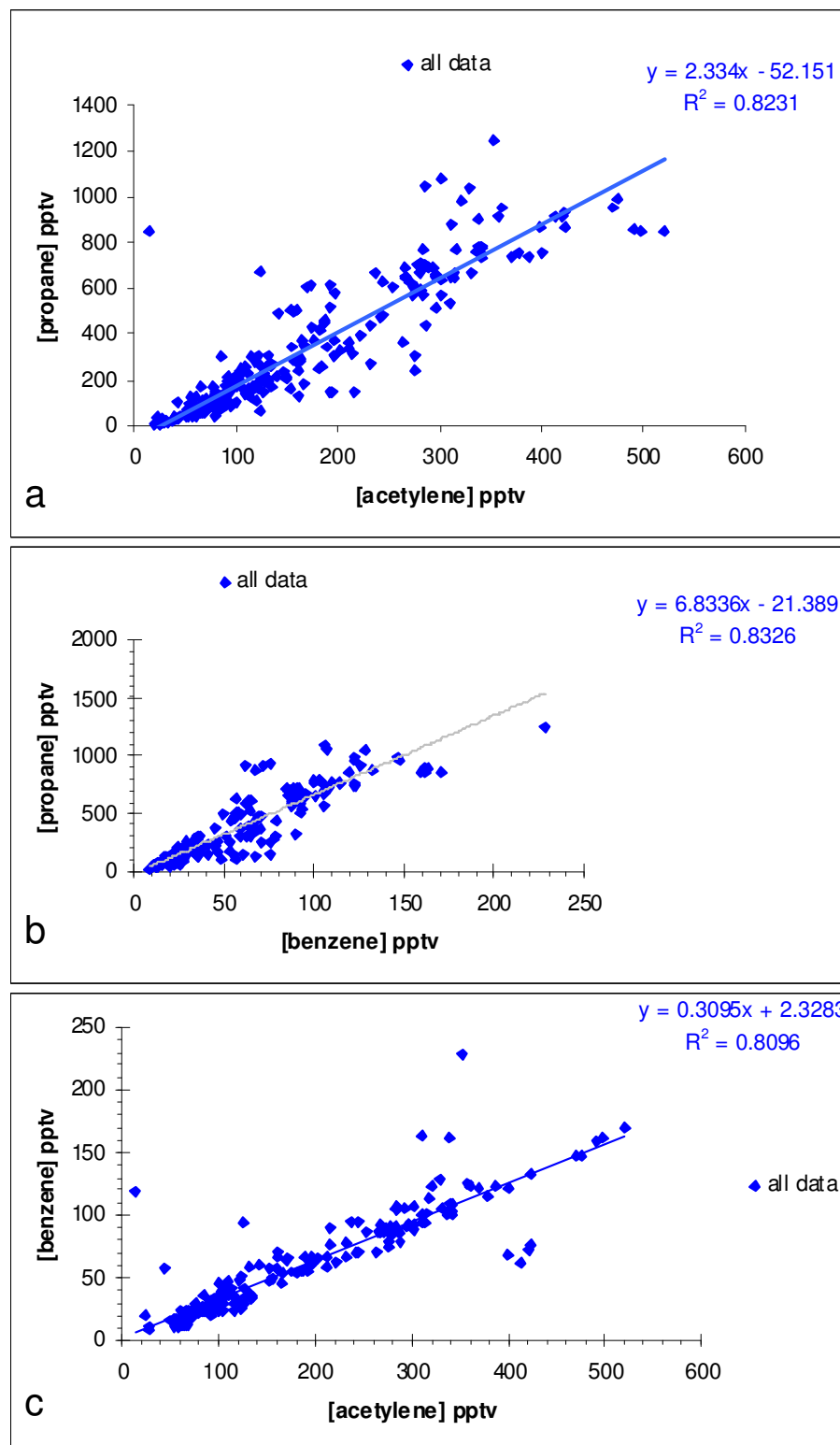
Figure 5.13: Correlation between (a) propane and acetylene, (b) propane and benzene, and (c) benzene and acetylene over the two year study period January 2009-January 2011.

The [acetylene]/[propane] ratio has been used to compare region-wide emissions in previous studies (Goldan et al., 2000;Russo et al., 2010), because both compounds have different sources, whilst the rate of atmospheric oxidation of both species with respect to OH varies by less than 30%. This makes pair suitable for gaining information on the relative impact of various sources in a region. Acetylene mainly comes from exhaust emissions and propane from natural gas and LPG. Despite their likely differing sources, a good correlation between these two species suggests a common geographic source region for these compounds. The evolution of the ratio is due to the combined effects of photochemical removal, mixing and dilution during transport. For simplicity, if we assume that this ratio has evolved mainly due to reactivity differences with respect to OH during transport and then applying an exponential decay equation to both species as presented below:

$$\ln \frac{[\text{propane}]}{[\text{propane}]_0} = -k_{\text{propane}}[OH]t \qquad 5.1$$

$$\ln \frac{[\text{acetylene}]}{[\text{acetylene}]_0} = -k_{\text{acetylene}}[OH]t \qquad 5.2$$

where [propane] and [acetylene] are the mixing ratios at time t and [propane]$_o$ and [acetylene]$_o$ are initial mixing ratios. k_{propane} and $k_{\text{acetylene}}$ are bimolecular rate constants with OH for propane and acetylene respectively and [OH] is the concentration averaged over time t. By subtracting equation 5.2 from 5.1 we get ratios of the two compounds.

$$\ln \frac{[\text{propane}]}{[\text{acetylene}]} = \ln \frac{[\text{propane}]_0}{[\text{acetylene}]_0} - (k_{\text{propane}} - k_{\text{acetylene}})[OH]t \qquad 5.3$$

And finally substituting [OH]t from 5.1 into 5.3, we get following expression:

$$\ln \frac{[\text{propane}]}{[\text{acetylene}]} = m \times \ln[\text{propane}] + C \qquad 5.4$$

where slope m and intercept C are as follows

$$m \quad = \quad \left(\frac{k_{propane} - k_{acetylene}}{k_{propane}} \right)$$

$$C \quad = \quad \ln \frac{[propane]_0}{[acetylene]_0} - \frac{k_{propane} - k_{acetylene}}{k_{propane}} \ln[propane]_0$$

By using the laboratory rate constants, the theoretical slope can be calculated. The term C gives information on the initial mixing ratio or in other words, emission ratio or source profile. Plotting ln [propane]/[acetylene] *versus* ln [propane] according to equation 5.4 should give a straight line as shown in **Figure 5.14** .
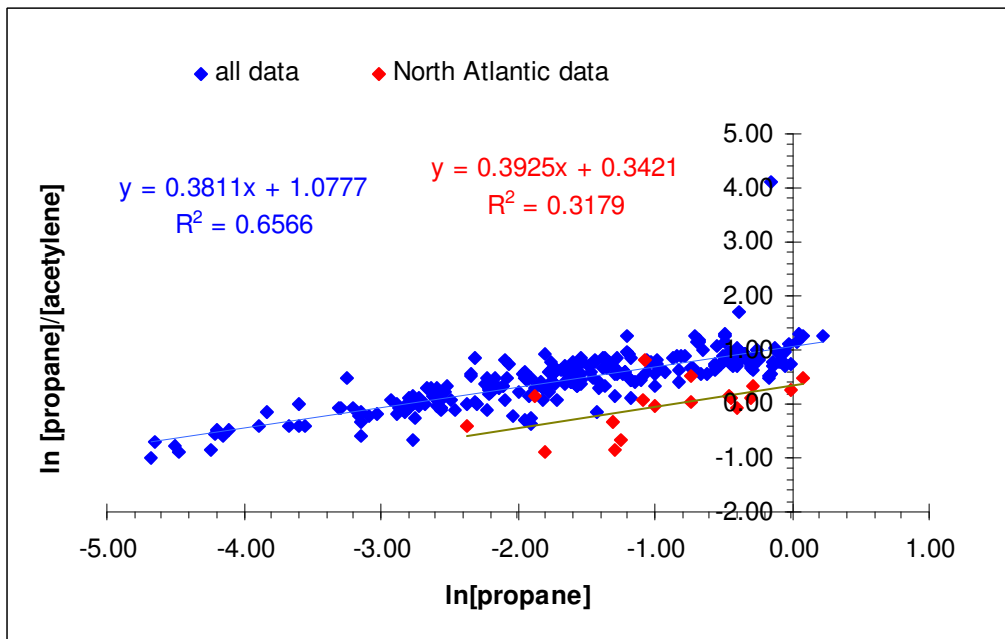
Figure 5.14: Correlation plot of ln [propane]/[acetylene] *versus* ln [propane] for two measurements (1) UK free troposphere study (blue) period 2009-11 (2) North Atlantic data (red) 1987-1989 period (Penkett et al., 1993).

Figure 5.14 also includes the data from the North Atlantic study period January 1987-April 1989 in order to compare the source profile between the North Atlantic and the present work. It is obvious from the figure that in both studies

the slope, which is related to the ratio of their kinetic rate constants with OH, is nearly the same (present work = 0.38 and North Atlantic work = 0.39) giving confidence that the same processing patterns are affecting both studies. The rate constants are taken from (Atkinson and Arey, 2003).

As far as the comparison for the intercept is concerned, then the intercept in present work is higher (1.07) than the North Atlantic study (0.34). The intercept of the regression line gives information on the initial mixing ratios of both species according to equation 5.4. The higher intercept (1.07) in our study supports decreased levels of acetylene emissions (relative to propane) as compared to the North Atlantic study period twenty years ago. This ratio analysis has further supported the differences between the median mixing ratios for acetylene between the two studies as discussed in section 5.3.2.2.

A similar approach was applied to the toluene and benzene pair (**Figure 5.15**) to compare the source profile with the North Atlantic study. In contrast with the propane and acetylene pair, benzene and toluene share similar sources and the reactivity differences for both species with respect to OH differ by a factor of 5 making this pair suitable for estimating average age of air masses. The purpose of adding the North Atlantic data in this plot was to compare again the intercept and see the differences in source profile; however, there is a lack of correlation in North Atlantic data indicative of sources other than vehicular emissions.
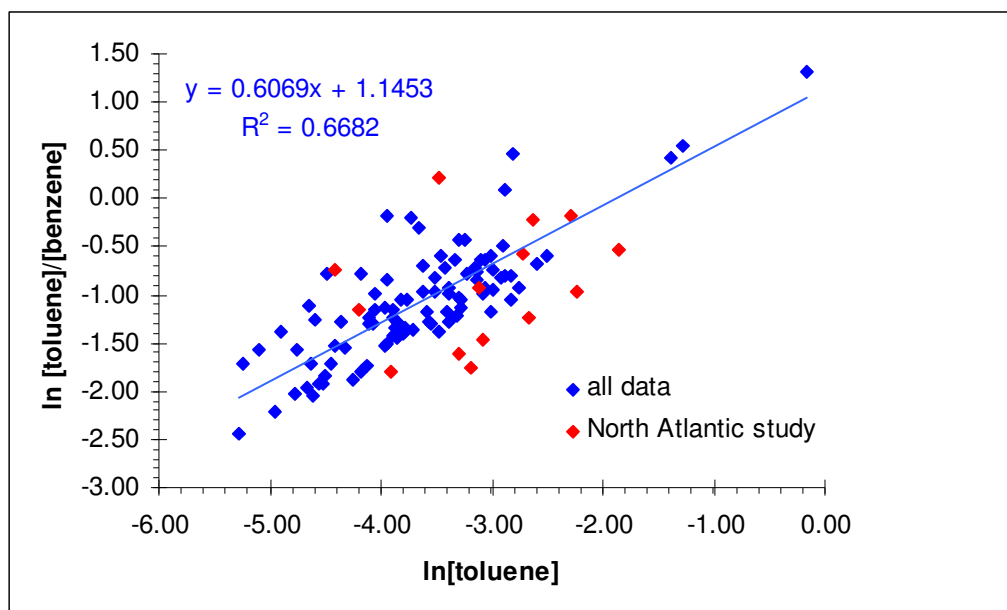
Figure 5.15: Correlation plot of ln [toluene]/[benzene] *versus* ln [toluene] for two measurements (1) UK free troposphere study period (blue) 2009-11 (2) North Atlantic data (red) 1987-1989 period (Penkett et al., 1993).

5.3.3.3   Relationship between O$_3$ and aging of hydrocarbons

The oxidation of a wide variety of reduced carbon species in the troposphere proceeds *via* a complex series of reactions and, depending upon the concentration of NO$_x$ in the free troposphere, either O$_3$ is produced or destroyed. The simultaneous measurement of O$_3$ also helped us to assess the relationship between hydrocarbon aging and O$_3$ throughout the study period. The one Hz O$_3$ measurements were averaged over the sampling time for the hydrocarbons. The natural logarithm of propane to ethane ratio has been used with a reasonable confidence in previous studies as a marker of aged and fresh air (Helmig et al., 2008) and used to examine the changing photochemical environment by observing O$_3$ dependence on ratios (Parrish et al., 2004). **Figure 5.16** shows the variation of O$_3$ as a function of ln [propane]/[ethane] throughout the study period. A large variability in O$_3$ has been observed in the summer month data in comparison with any other months. The range of O$_3$ mixing ratio observed during July month was 14 - 90 ppb. Here, it is again necessary to mention that July 2010 samples for the present study represent mixing ratios from the

nighttime free troposphere. Broadly interpreting the correlation between O_3 and an aging marker, it is apparent that aged air has less O_3 than relatively fresh air masses.
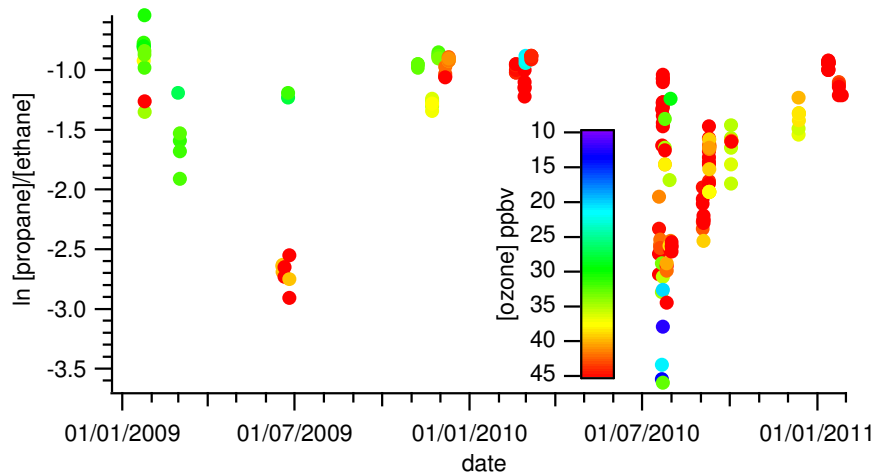
Figure 5.16: Variation of ln [propane/ethane] *versus* O_3 for whole study period (January 2009-January 2011). The actual range of O_3 mixing ratio varied from 14-90 ppb during summer months. The range on the colour scale is adjusted to see variation in data.

In order to get the finer details of this relationship for summer period, **Figure 5.17** illustrates O_3 in relation to the natural logarithm of [propane]/[ethane] for the period from July 16, 2010 to July 20, 2010 from flights B534 to 537 in addition to the rest of the study period. The variation in O_3 mixing ratio with ln [propane]/[ethane] for other seasons is not significant suggesting no dependence of O_3 mixing ratios on ratios, whilst for the summer season, there exists a positive correlation implying that the more processed air masses have lower mixing ratios of O_3 as compared to the relatively less processed air masses and this behaviour seems to be interpreted in terms of overall net photochemical O_3 destruction taking place during the period in July month. The net O_3 destruction during summer and spring months has also been observed during transport of air masses over the central North Atlantic to Pico observatory (Helmig et al., 2008). At this point there were two questions to further ask

280

relating to the ozone dependence on ratios for summer months: (1) how is CO related to ozone during same period? and (2) what was the concentration of NO_x during this month?
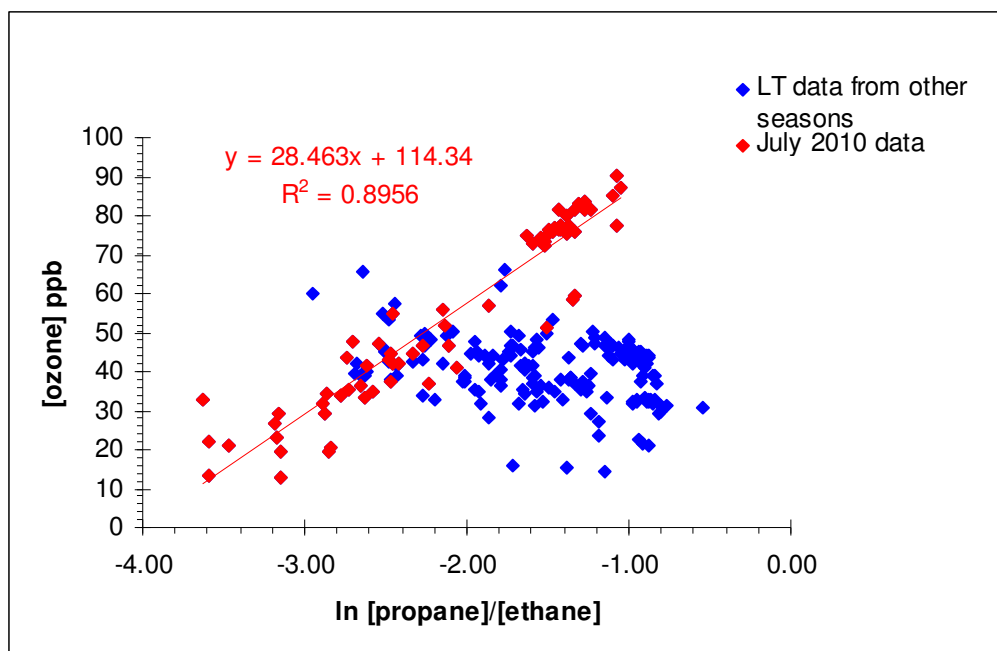
Figure 5.17: Comparison of correlation of ozone levels with ln [propane] to [ethane] ratios for summer month data covering a period of July 16, 2010 to July 20, 2010 from flights B534 to 537 (red) with data for rest of the study period (blue).

Coming to the first question, an excellent correlation ($R^2 = 0.96$) between CO and O_3 during the same period in **Figure 5.18** is consistent with the behaviour of ln [propane] /[ethane] *versus* O_3 relationship. Air masses with elevated CO have high ozone mixing ratio implying that as aging processes proceed the O_3 is being destroyed or heavily diluted with low O_3 mixing ratio in background air.
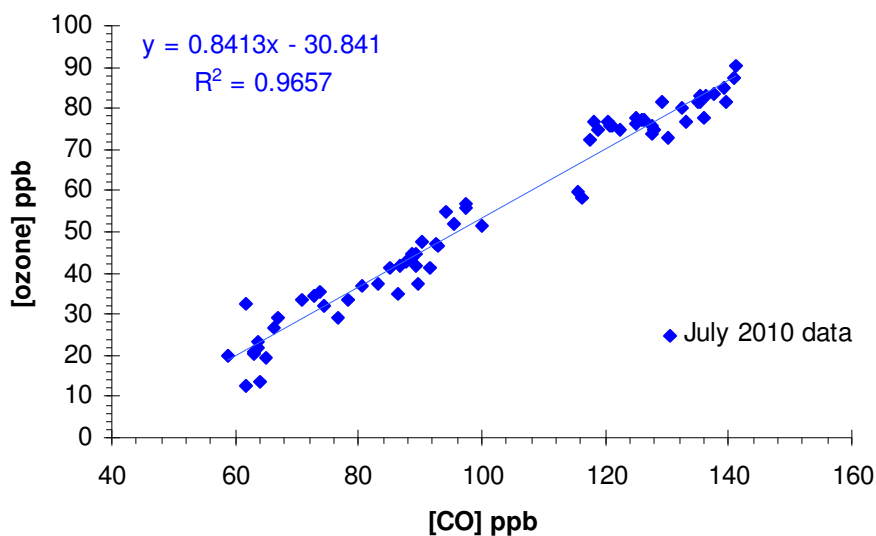
Figure 5.18: Correlation of O_3 with CO during summer month covering a period of July 16, 2010 to July 20, 2010 from B534 to B537 flights for present study.

The assessment of local concentration of NO is critical in determining whether the atmosphere in a particular region is a either a source or a sink of O_3 (Seinfeld and Pandis, 1998). The rough assessment of local concentration of NO can be done by considering the fate of HO_2 radical. In the hydrocarbon oxidation system, the HO_2 radical reacts with NO and oxidises NO to NO_2 which further photolysis to give O_3. The rate of O_3 production is similar to the rate of this reaction in which HO_2 oxidises NO to NO_2 as given in equation 5.5. There is a competing reaction of HO_2 radicals with O_3 which is responsible for the destruction of O_3 (equation 5.6). Thus the ratio of the rates of these two reactions decides whether O_3 is being produced or lost (Seinfeld and Pandis, 1998).

$$HO_2 + NO \qquad \xrightarrow{k_{HO_2+NO}} \qquad NO_2 + OH \qquad\qquad 5.5$$

$$HO_2 + O_3 \qquad \xrightarrow{k_{HO_2+O_3}} \qquad OH + 2O_2 \qquad\qquad 5.6$$
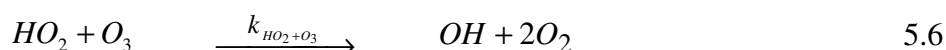
where k_{HO2+NO} and k_{HO2+O3} are the rate constants of HO_2 with NO and O_3 respectively.

$$\frac{R_{HO_2+O_3}}{R_{HO_2+NO}} = \frac{k_{HO_2+O_3}[O_3]}{k_{HO_2+NO}[NO]} \qquad 5.7$$

where R_{HO2+O3} and R_{HO2+NO} are the rate of reactions of HO_2 with O_3 and NO respectively.

For a given level of ozone, the concentration of NO at which this ratio (R_{HO2+O3}/R_{HO2+NO} is unity is called the *breakeven concentration of NO or compensation point;* below which O_3 is consumed and above which O_3 is produced. At 298 K the ratio of the two rate coefficient is

$$\frac{k_{HO_2+O_3}}{k_{HO_2+NO}} = 2.3 \times 10^{-4} \qquad 5.8$$

In our case this breakeven concentration corresponds to mixing ratio of NO = 3-20 ppt for a 14-90 ppb of ozone for July data and measured NO is much less than this implying the dominance of $HO_2 + O_3$ reaction over $HO_2 + NO$ and causing net O_3 destruction.

A strong positive correlation exists between CO and O_3 and with the concentration of NO_x below the breakeven concentration. This suggests that low O_3 levels in air that has been heavily processed (as shown by hydrocarbon data) are due to chemical losses of O_3. However, it cannot be denied that there are potentially other effects, for example the mixing of polluted air with clean Atlantic marine air over long aging periods could also be responsible for O_3 destruction. It was interesting to compare the O_3 dependence on ratios with the older North Atlantic study; however the lack of data points in summer months forces us to examine this relationship for all data. In this case an anticorrelation is observed between O_3 and ln [propane]/[ethane] for all data implying the dominance of net O_3 production as aging proceeds.
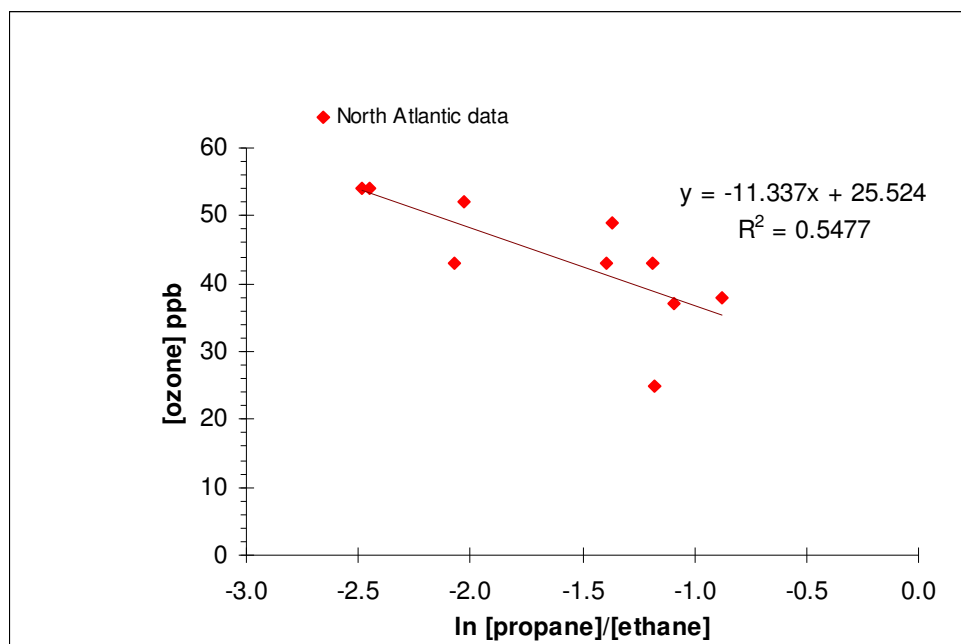
Figure 5.19: Correlation of ozone levels with the natural logarithm of [propane] to [ethane] ratios for the entire data set of North Atlantic study covering period from January 1987 to April 1989 (Penkett et al., 1993).

5.4 Summary

A dataset from a two-year study of C_2-C_8 hydrocarbons in UK free troposphere clearly shows the seasonal behaviour of hydrocarbons in the background atmosphere, with maxima in mixing ratios in Jan-Feb and minima in July-Aug, in line with the seasonal abundance of OH radicals. The seasonal cycles are more pronounced for the less reactive species like ethane, acetylene and benzene when compared with the reactive species such as propane, butanes, pentanes and toluene. A comparison of this work with a North Atlantic aircraft study conducted in the free troposphere over the North Atlantic Ocean UK twenty years ago shows that the amplitude of the seasonal cycle has declined by a factor of approximately two for acetylene, benzene and toluene. Smaller declines were seen in the amplitude of the season cycle of more reactive species such as butanes and pentanes, when compared to those seen twenty years ago. This decrease in amplitude of the cycle in mixing ratios can be rationalised by consideration of the implementation of three-way catalytic converters and

canisters to control CO, VOCs and NO$_x$ since 1991, a control policy that has very substantially reduced emissions in North America and Europe.

A good correlation was seen between the observed atmospheric variability and kinetic lifetime for a range of different species. This was seen in winter and summer seasons and was always greater than the variability caused by the measurement uncertainty. A variability-lifetime analysis for C$_2$ – C$_5$ compounds clearly indicated a seasonal difference with a higher inter-species correlation yet weaker dependence on lifetime (b = 0.38) for winter data, in comparison with a greater dependence on lifetime (b = 0.60) for summer data, suggesting a greater influence of OH chemistry over mixing in summer season.

The hydrocarbon ratio approach to data analysis has clearly highlighted the importance of influence of air masses with different source signatures on certain June samples and this has led us to conclude that the composition of the UK free troposphere is dominated by a mix of anthropogenic source emissions and non urban sources such as biomass burning. A plot of ln [*n*-butane]/[ethane] *versus* [propane]/[ethane] has been used to compare between the current work and a combined dataset from UK free troposphere aircraft study (Lightman et al and Penkett et al). In both datasets the ratios are well correlated suggesting that the aging pattern/behaviour of hydrocarbons has remained constant over the intervening twenty years, although there are a significant difference in slopes of the linear regressions (1.13 for the combined two aircraft studies and 1.46 from present work) which can be attributed to the effects of dilution and mixing with air masses with hydrocarbons of different ages and perhaps the influence of air masses with different source signatures.

The high absolute mixing ratio of propane and consequently high amplitude of propane's seasonal cycle (as compared to acetylene) clearly indicates that there is proportionately high emission strength of propane across the UK. Furthermore, the correlation plots between propane and acetylene, propane and benzene, benzene and acetylene have been used to investigate the relative impact of

various sources on the chemical composition of air masses observed in UK free troposphere air. The ratio analysis has clearly indicated the impact of natural gas relative to the incomplete combustion as a source of propane throughout the study period. The emissions of benzene and acetylene mainly come from tailpipe vehicular emissions. A plot of ln [propane]/[acetylene] *versus* ln [propane] has been used compare the source profile variation between current work and the North Atlantic work from twenty years ago; the higher intercept (1.07) in the present study supports emissions predictions that acetylene has declined as a fraction of urban emissions as compared to the early 1990s. The slope of this plot is similar in both cases indicating the same aging patterns holds for both studies and time periods.

The relationship between ln [propane]/[ethane] with O$_3$ suggests there is a connection between aging processes and O$_3$ for summer data. The variation in O$_3$ mixing ratio with ln [propane/ethane] for other seasons is not significant suggesting no particular connection between O$_3$ and hydrocarbon ratios. For summer seasons there exists a positive correlation implying that the more processed air masses have lower levels of O$_3$ as compared to relatively less processed air masses and this behaviour may be interpreted in terms of overall net photochemical O$_3$ destruction taking place during the period in July month. For this study a good correlation between CO and O$_3$ exists with NO$_x$ concentrations typically below the compensation point, supportive of a general chemical O$_3$ loss in summer as hydrocarbons decline through OH reaction. A similar analysis of the complete data set from the 1990s North Atlantic work (seasonal data not available) indicated an anticorrelation between ozone and ln [propane]/[ethane] for the North Atlantic work implying the dominance of net O$_3$ production as aging proceeds. This would again be indicative of a general decline in O$_3$ precursors in the free troposphere over the Atlantic / UK between this study period and twenty years ago.

Chapter 6:

The influence of biomass burning on the global distribution of selected non-methane organic compounds

This chapter is derived from observations and analysis made during the course of this PhD, but also includes input from a variety of other collaborators who are acknowledged in the text. The chapter distils the combined work published in: 'The influence of boreal forest fires on the global distribution of non-methane hydrocarbons.' A.C.Lewis, M.J.Evans, J.R.Hopkins, S.Punjabi, K.A.Read, S.Andrews, S.J.Moller, L.J.Carpenter, J.D.Lee, A.R.Rickard, P.I.Palmer, and M.Parrington. *Atmos. Chem. Phys. Discuss.*, 12, 23433-23469, 2012. This is now accepted for ACP.

6.1 Introduction

Non-methane organic compounds are a class of trace compound found throughout the troposphere and include non-methane hydrocarbons (NMHCs) and oxygenated volatile organic compounds (oVOCs). NMHCs are released from a wide range of biogenic and anthropogenic sources. Most individual NMHCs have a mix of sources, with isoprene (the largest global emission by mass) being the prime exception with emissions almost exclusively from terrestrial vegetation. Incomplete combustion is generally the largest individual anthropogenic source of NMHCs, including petrol and diesel engines, static power generation and the burning of wood and coal for heating and cooking (AQEG, 2009 for the UK, Badol et al., 2008 for France, Morino et al. 2011 for Japan).

Biomass burning has long been recognised as a major source of trace gases to the atmosphere, of relevance to this study, being the work of (Crutzen et al., 1979) first estimating the emission of carbon monoxide (and other gases) from biomass burning. The co-emission of hydrocarbons species along with CO has been reported extensively and the correlation with CO used to derive emission ratios for many species (Crutzen and Andreae, 1990). Vegetation burning occurs globally from the tropics in South America, Africa, SE Asia and Australia through to the boreal forests of North America and Siberia. A summary of emissions for many trace species including hydrocarbons is reported in (Andreae and Merlet, 2001) As a class of compound NMHCs have wide range of atmospheric lifetimes, from a few minutes to several months, which together with their disparate regional sources, control their global distributions (Atkinson, 1994).

Long-term automated measurements of NMHCs are currently skewed in number towards urban and sub-urban locations, reflecting the important role of NMHCs in controlling urban air quality. In urban locations the sources of most NMHCs

tend to be overwhelmingly anthropogenic and in many locations have shown downwards trends of the order 1-5% per year (von Schneidemesser et al., 2010), dependant on species, arising from the effective introduction of vehicle emissions control technologies and a reduction in industrial and domestic solvent usage. Global data on emissions, disaggregated by sector, geography, time and hydrocarbon species, does not currently exist. However at a national level, using the UK as an example, exhaust emissions and solvent usage have decreased to around 1/4 and 1/3 respectively of the emissions in 1990 (see for example http://naei.defra.gov.uk/). Trends in developing countries are more difficult to estimate given a lack of observations. It may be a reasonable assumption that catalytic controls may not have as effectively penetrated vehicle fleets in these locations and growth in traffic volume may outweigh control measures. It is potentially reasonable however to assume that there has not been an increase in benzene use as a solvent since it has been replaced effectively by other less harmful solvents. Observations of NMHCs in the background atmosphere are confined largely to process studies and short-term research missions. A substantial literature exists on the subject, e.g., 'Volatile Organic Compounds In The Atmosphere' (Koppmann, 2007).

There is an increase in the number of long-term (> 5 years) background measurements (typically hundreds of km from urban sources) of NMHCs in the troposphere, using flask samples (Pozzer et al., 2010) and from *in situ* observations (Plass-Dulmer et al., 2002;Read et al., 2009;Simpson et al., 2012). Recognizing the importance of addressing the limited extent of the measurement relative to other atmospheric species, the World Meteorological Organization now has a specific long-term monitoring activity for VOCs as part of the Global Atmosphere Watch programme (WMO-GAW) (Helmig et al., 2009). NMHCs including ethane, propane, acetylene, butane and pentane form part of the target suite of compounds (GAW Report No 171, 2006) in this network. Observations of NMHCs in remote terrestrial or oceanic environments are less easy to categorize in terms of contributing sources than comparable urban measurements, requiring a more detailed analysis of other variables such as

trajectory origins, source receptor modelling and use of chemical transport models. It is possible for many NMHCs that the observation of a given species will arise because of the combined releases of anthropogenic and natural emissions, followed by transport and degradation. Extracting value and information from long-term trends in background NMHCs requires therefore a robust understanding of the various contributing sources in background, non-urbanized environments.

The measurements reported in this thesis were made as part of the research project - Quantifying the impact of BOReal forest fires on Tropospheric oxidants over the Atlantic using Aircraft and Satellites (BORTAS). Boreal forests, defined as high latitude 50 – 70 °N forests, account for roughly one third of total global forested area (Kasischke and Stocks, 2000), and their fires emit many more species in addition to NMHCs. CO_2, CO and CH_4 are the largest emissions by mass with CH_3OH and HCHO the most dominant organic compounds (see most recently for Canadian boreal fires (Simpson et al., 2011)). Of the NMHCs, ethane, benzene, ethene and propene have been seen in many studies including in laboratory combustion experiments, relatively close to source, and many days downwind. These and many other hydrocarbon emissions are summarised in (Andreae and Merlet, 2001;Simpson et al., 2011) report an exceptionally comprehensive catalogue of different species released by boreal fires, including NMHCs, halocarbons, oxygenated species and organic nitrates, and particular attention is paid in comparison to this study since it provides very good overlap in terms of chemical speciation and was made in the same geographic region. Laboratory evaluation of organic emissions include those reported in (Christian et al., 2003;Christian et al., 2004;Yokelson et al., 2008;Warneke et al., 2011), in the near field by (Yokelson et al., 2007;Yokelson et al., 2009;Jost et al., 2003;Sinha et al., 2003), and in long range transport by (Holzinger et al., 2005;de Gouw et al., 2006;Duck et al., 2007;Yuan et al., 2010).

Whilst tropical biomass burning dominates total emissions, boreal fires account for around 9% of all fire carbon emissions (van der Werf et al., 2010) and can have major impacts on the global atmosphere. Perturbation to the global growth rate in CO, CH_4 and C_2H_6 have been attributed to single regional boreal burning events (Kasischke et al., 2005;Yurganov et al., 2005). The areal extent of burned biomass is related to regional temperature and rainfall, and there is evidence that in Canada the forest area burned has increased since the 1970s (Girardin, 2007). Published model predictions of boreal fires all show significant increases with higher temperature associated with future climate scenarios, leading to greatly increased emissions in all those species released in the burning process (Flannigan et al., 2005;Kasischke and Turetsky, 2006;Soja et al., 2007;Marlon et al., 2008;Amiro et al., 2009;Wotton et al., 2010).

Boreal forest fires have a strong influence on air quality in mid latitudes in the Northern hemisphere. Due to convection and pyroconvection of plumes they can inject trace gases and aerosols into the upper troposphere and occasionally lower stratosphere where long-range transport can widely distribute the emissions (Fromm et al., 2000;Jost et al., 2004). Canadian forest fire signatures in NMHCs have been seen frequently at the Pico observatory on the opposite side of the Atlantic Ocean (Val Martin et al., 2010). Measurements from several different aircraft over the central and Eastern North Atlantic have shown elevations in species such as ethene and benzene of between 100 and 1000 times over the typical marine background concentration (Lewis et al., 2007;Fehsenfeld et al., 2006). The photochemical impact of biomass plumes over the North Atlantic ocean remains somewhat uncertain however, with literature disagreement as to whether or not they contribute significantly to more general tropospheric O_3 production e.g. (Jaffe and Wigder, 2012). This wider atmospheric chemistry challenge provides the motivation for the BORTAS study, of which this dataset forms one part.

6.2 Aims

This study aims to quantify the release of 29 different NMHC species from boreal forest fires, a major emission source to the mid and high latitudes of the Northern hemisphere. This information is combined with a global 3-D chemical transport model (CTM) and a global fire map to produce a geographically resolved estimate of the boreal and other biomass burning fraction of NMHCs in the troposphere to show the influence of biomass burning on the global distributions of benzene, toluene, ethene and propene (species which are controlled for air quality purposes, sometimes used as indicative tracers of anthropogenic activity). Using the observationally derived emission ratios and the GEOS-Chem CTM, this study attempts to show that biomass burning can be the largest fractional contributor to observed benzene, toluene, ethene and propene levels in many global locations. The contributions of overall NMHC abundance from biomass burning and anthropogenic sources are placed in context with the locations of the 28 global status stations that form WMO-GAW, providing an assessment of how NMHCs at these locations are likely to be influenced by future changes to biomass burning activity or anthropogenic emissions.

6.3 Experimental

The observational programme for this campaign was conducted from Halifax International airport, Canada (W 063° 30' / N 44° 52') between 12th July 2010 and 2nd August 2010. This comprised a series of 15 different sorties, each comprising either one or two flights in a day and of duration between 3 and 8 hours flying time. The data represents a total observing period of approximately 79 flight hours covering around 28,000 km in sample tracks. See (Palmer et al., 2012) for further details of this campaign. In addition to measurements made from Halifax, the dataset also includes observations made during the trans-Atlantic crossing from/to the United Kingdom *via* the Azores. The flights have Facility for Airborne Atmospheric Measurement (FAAM) catalogue numbers

from B618 to B632 and all data in this paper are publically accessible at www.badc.nerc.ac.uk/data/bortas. Figure 6.1 shows the flight tracks and sample points of all whole air samples included in this paper. Acetylene is used as a representative tracer for both biomass burning emission and anthropogenic pollution in this plot, with substantial elevations visible on many flights.

VOCs were sampled using the Whole Air Sampling (WAS) system fitted to the FAAM 146 research aircraft. The WAS system consists of sixty-four silica passivated stainless steel canisters of three litre internal volume (Thames Restek, Saunderton UK) fitted in packs of 8, 9 and 15 canisters to the rear lower cargo hold of the aircraft. Each pack of canisters was connected to a 5/8 inch diameter stainless steel sample line connected, in turn, to an all-stainless steel assembly double-headed three phase 400 Hz metal bellows pump (Senior Aerospace, USA). The pump drew air from the port-side aircraft sampling manifold and pressurized air in to individual canisters to a maximum pressure of 3.25 bar (giving a useable sample volume for analysis of up to 9 L).

Air samples were analysed on location in Halifax within 48 hours of collection using a dual channel gas chromatograph with two flame ionization detectors (Hopkins et al., 2011). One litre samples of air were withdrawn from the sample canisters and dried using a glass condensation finger held at –30 °C. Samples were pre-concentrated onto a dual-bed carbon adsorbent trap, consisting of Carboxen 1000 and Carbotrap B (Supelco), held at –23 °C and then heated to 325 °C at 16 °C s^{-1} and transferred to the GC columns in a stream of helium. The eluent was split in a fixed ratio between an aluminium oxide (Al_2O_3, $NaSO_4$ deactivated) porous layer open tubular PLOT column (50 m, 0.53 mm i.d.) for analysis of NMHCs and a LOWOX column (10 m, 0.53 mm i.d.) in series for analysis of polar oVOCs. This split was determined experimentally from the relative sizes of benzene peaks on both columns and in this experiment was in a ratio 54:46. Both columns were supplied by Varian, Netherlands.

Peak identification and calibration were made by reference to a part per billion level certified gas standard (National Physical Laboratory, ozone precursors mixture, cylinder number: D64 1613) for NMHCs. This standard and instrument has in turn been evaluated as part of the WMO GAW programme and was within target operating limits. A relative response method was used for the calibration of oVOCs in the field, with reference to propane. The response values of oxygenated volatile organic compounds (oVOC) relative to propane were derived from laboratory calibration using ppm gas standard dilution and permeation methods. Detection limits were in the range 1 – 9 ppt and 10 – 40 ppt for NMHCs and oVOCs respectively. The detection limit for ethene was 2 ppt with a precision of 1% and accuracy of 5% for mixing ratios greater than 100 ppt. The detection limit for propene, benzene and toluene were 1 ppt with 1% and accuracy of 5% for mixing ratios greater than 100 ppt.
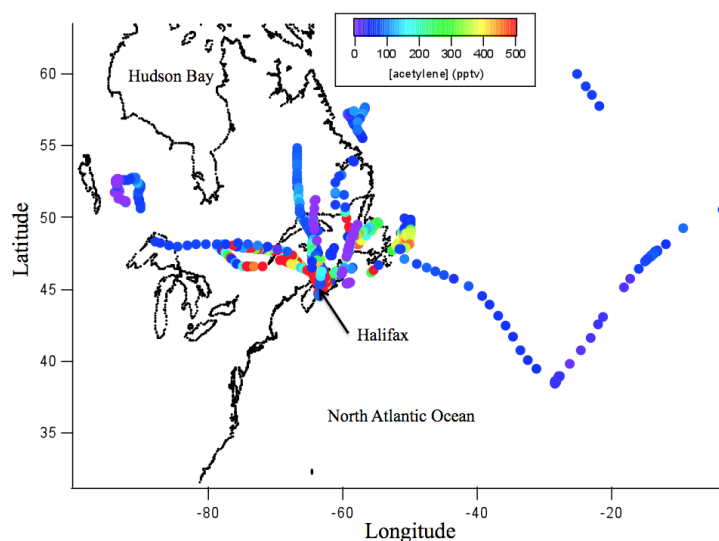
Figure 6.1: FAAM BAe 146-301 flight tracks during August 2012, overlaid with sample locations for whole air samples. The points are coloured by acetylene mixing ratio.

6.4   Results and discussion

6.4.1 Summary of non-methane hydrocarbon mixing ratios and emissions

To determine the relative emissions of NMHCs from biomass burning in comparison to sources it is necessary to identify case studies where the overwhelming contributor to NMHC abundance is from a burning event. This approach is needed so that any calculated emission ratio based on the behaviour of NMHC against CO is not influenced by, for example, non-combustion emissions of the NMHC. It is not attempted to derive emission strength for any other source, other than biomass burning.   The published emission values for non-biomass burning sources are drawn on in the later model activities. There are two major means of achieving a filtering for biomass burning data. The first is to make a case-by-case examination of data and assign data as being either 'in' or 'out' of a biomass burning plume. This works well where plumes are very distinct. The other means is to assign a threshold or filter for certain tracers of biomass burning and thus categorize all data above the filter threshold as having the attributes of a biomass burning plume.

In this study, the latter approach has been used since on many occasions plume edges were indistinct, and the averaging whole air samples smoothed across plume boundaries. The NMHCs and CO in this study have been categorized into three classes: i) observations made in background air, as defined by CO <200 ppb; ii) observations made in clearly identifiable biomass burning plumes (CO >200 ppb, plume confirmed by presence of furan and furfural by in flight GC-MS) and iii) observations made in anthropogenic plumes (CO >200 ppb, no biomass burning tracers by GC-MS). Classifications (i) and (ii) are summarised in **Table 6.1**, along with the highest plume mixing ratios for all observed NMHCs.

In practice, the very high NMHC and CO values in biomass burning plumes dominate the slopes obtained from subsequent NMHC – CO plots, and changing the thresholds, for example to 175, 150 or 125 ppb CO has no significant impact on the slopes obtained.

A common approach is to examine the emissions of various NMHCs as a function of co-measured CO, to derive an emission ratio (ER). This strictly refers to the ratio of the emissions at the point of release. All measurements made here were some distance downwind of the fire source and so chemical loss from the atmosphere must be appreciated. The primary loss from the plume of NMHC is likely to be through OH reaction; however, in the absence of OH measurements, it is difficult to make adjustments for transport losses.

A range of plumes of different ages are encountered in this study, from plume encounters directly over fires to several days downwind. The assessment of general plume ages has been made based on forecast trajectories used for flight planning purposes. It is not attempted for this study to place precise ages on plumes, although a range of techniques, based on transport and chemical clocks have been reported previously. However, in this study general plume age does not appear to substantially change the slope obtained of any given NMHC against CO. When flights are taken individually the slopes obtained are all very similar to the slope obtained when all the biomass burning plume data is used in concert. This is a somewhat surprising observation suggesting that losses of more reactive species such as alkenes are not high during transport. Overall therefore we estimate emission ratios for a range of species of differing reactivities in **Table 6.1** without correction for plume age, but would highlight that there are increased uncertainties associated with more reactive hydrocarbons for the reasons outlined above.

Table 6.1: Measurement statistics from the observations made during the BORTAS campaign. Any values observed below the limit of detection (LOD) have been assigned a value of half the LOD to enable a background value to be calculated. Median averages have been reported for the background mixing ratios in order to reduce the effect of a small number of samples with higher than expected VOC mixing ratios (likely corresponding to localised emissions from an unknown source) which would otherwise yield unrepresentatively high background values

Species	LOD (pptv)	Background median (pptv)	Plume average (pptv)	Plume maximum (pptv)	ER to CO (pptv/ppbv)	ER to CO (pptv/ppbv) Simpson et al.
CO		97.72 ppb	380.52 ppb	1049.03 ppb	-	-
ethane	9	773	2236	5721	5.13 ± 0.35	4.6 ± 0.9
propane	3	103	517	1355	1.26 ± 0.10	1.3 ± 0.3
iso-butane	1	6	37	85	0.077 ± 0.02	0.09 ± 0.02
n-butane	1	18	116	307	0.30 ± 0.04	0.32 ± 0.05
cyclopentane	1	8	10	16	0.007 ± 0.004	
iso-pentane	1	4	19	41	0.034 ± 0.01	0.07 ± 0.02
n-pentane	1	5	42	128	0.13 ± 0.021	0.14 ± 0.02
2,3-methylpentane	2	1	8	24	0.021 ± 0.007	0.05 ± 0.01
n-hexane	1	1	18	60	0.063 ± 0.01	0.08 ± 0.01
n- heptane	1	0.50	13	45	0.041 ± 0.008	0.06 ± 0.01

2,2,4-trimethylpentane	1	0.50	10	33	0.027 ± 0.01	
n-octane	2	1	11	101	0.028 ± 0.03	
ethene	7	49	1848	6663	6.9 ± 0.72	7.3 ± 0.1
propene	3	12	205	1475	1.19 ± 0.29	2.3 ± 0.1
propadiene	3	1.5	18	62	0.070 ± 0.02	
trans-2-butene	1	4	4	12	-	0.09 ± 0.01
1-butene	1	5	35	246	0.20 ± 0.06	0.34 ± 0.01
iso-butene	1	5	15	111	0.074 ± 0.04	0.03 ± 0.02
cis-2-butene	1	0.50	2	2	-	0.07 ± 0.004
1,3-butadiene	1	0.50	83	398	0.39 ± 0.07	0.32 ± 0.02
trans-2 pentene	1	0.50	6	21	0.019 ± 0.01	
1-pentene	1	0.50	14	75	0.064 ± 0.02	
isoprene	1	0.50	112	820	-	0.27 ± 0.05
acetylene	3	80	767	2046	2.07 ± 0.31	2.1 ± 0.9
benzene	2	27	424	1383	1.40 ± 0.11	1.70 ± 0.3
toluene	2	6	187	653	0.69 ± 0.09	0.67 ± 0.16
ethyl benzene	3	1.50	33	98	0.10 ± 0.03	0.058 ± 0.02
m+p-xylene	3	1.50	420	161	0.17 ± 0.04	0.14 ± 0.01

o-xylene	3	1.50	24	82	0.078 ± 0.03	0.064 ± 0.003
methacrolein	3	2	160	754	0.8 ± 1.1	0.15 ± 0.01
methanol	40	1556	4423	10335	8.9 ± 3.2	9.6 ± 1.9
acetone	9	1476	2550	4584	3.5 ± 0.8	1.6 ± 0.4

The emission ratios in **Table 6.1** are derived by subtracting a concentration value indicative of the background environment from the NMHC and CO data using a filter at 200 ppb CO to identify biomass burning. This is of course somewhat subjective, since all air masses encountered will have some degree of contribution to NMHCs and CO from biomass burning. Subtracting the background data from plume data gives the emissions ratio defined as:

$$
ER_{NMHC/CO} \quad = \quad \frac{[NMHC]_{plume} - [NMHC]_{bkgd}}{[CO]_{plume} - [CO]_{bkgd}} \qquad 6.1
$$

The uncertainty values for our emission ratios (**Table 6.1**) are a combination of slope (from the R-squared value), the measurement uncertainty for observations of CO (assumed to be 5%) and the compound specific uncertainties for the measurement of NMHCs. Within the stated uncertainties there is in general a very high degree of agreement between this study and the recent work of Simpson et al (Simpson et al., 2011) that was undertaken in a similar geographical region and using an aircraft platform. The values obtained for benzene, toluene, ethene and propene all fall within the reported ranges in the review article of (Andreae and Merlet, 2001). Some additional NMHCs are reported here which were not reported in the (Simpson et al., 2011) study; these new ERs are in line with similarly structured compounds reported previously. Notable outliers include propene, which is observed in this work to have an ER around half that reported in Simpson et al (Simpson et al., 2011) , and one third that reported in Akagi et al (Akagi et al., 2011) for boreal fires. Methacrolein in this study had an ER around five times higher than Simpson et al (Simpson et al., 2011). Whilst isoprene was elevated within biomass burning plumes in this study, it was not correlated to CO to a statistically significant ($R^2 < 0.15$) degree and so we do not assign an ER, unlike Simpson et al (Simpson et al., 2011). Its presence within the plume may be rationalized, however, through either close proximity vegetation releases , heat induced distillation of BVOCs of from emissions from peat combustion (Christian et al., 2003).

In **Figure 6.2**, the background data, biomass plume data and distinct plumes of anthropogenic emissions are summarized graphically for a range of alkane species. Each alkane is slightly different in terms of behaviour, but in general terms the majority of data points sit on a common slope, with a smaller number of outliers showing high alkane without enhancement in CO. These outliers may be assigned as being from a non-combustion source.
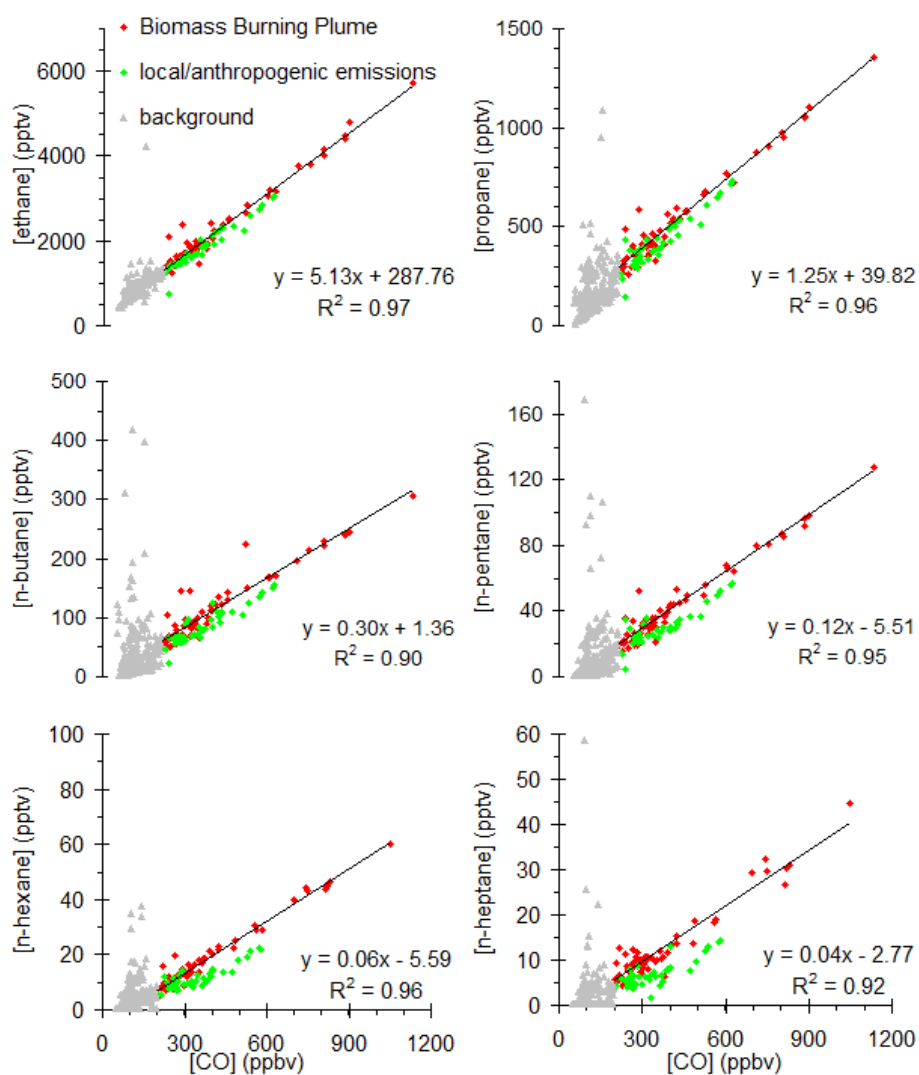
Figure 6.2: Selected plots of alkanes *versus* CO. Grey triangle assigned as background air, red diamonds assigned as biomass plumes and green diamonds assigned as anthropogenic plumes.

The use of a CO threshold value and a secondary mass spectroscopic marker means these non-combustion data points do not influence the calculated biomass burning slopes. **Figure 6.3** shows the relationships between a range of alkenes and CO.
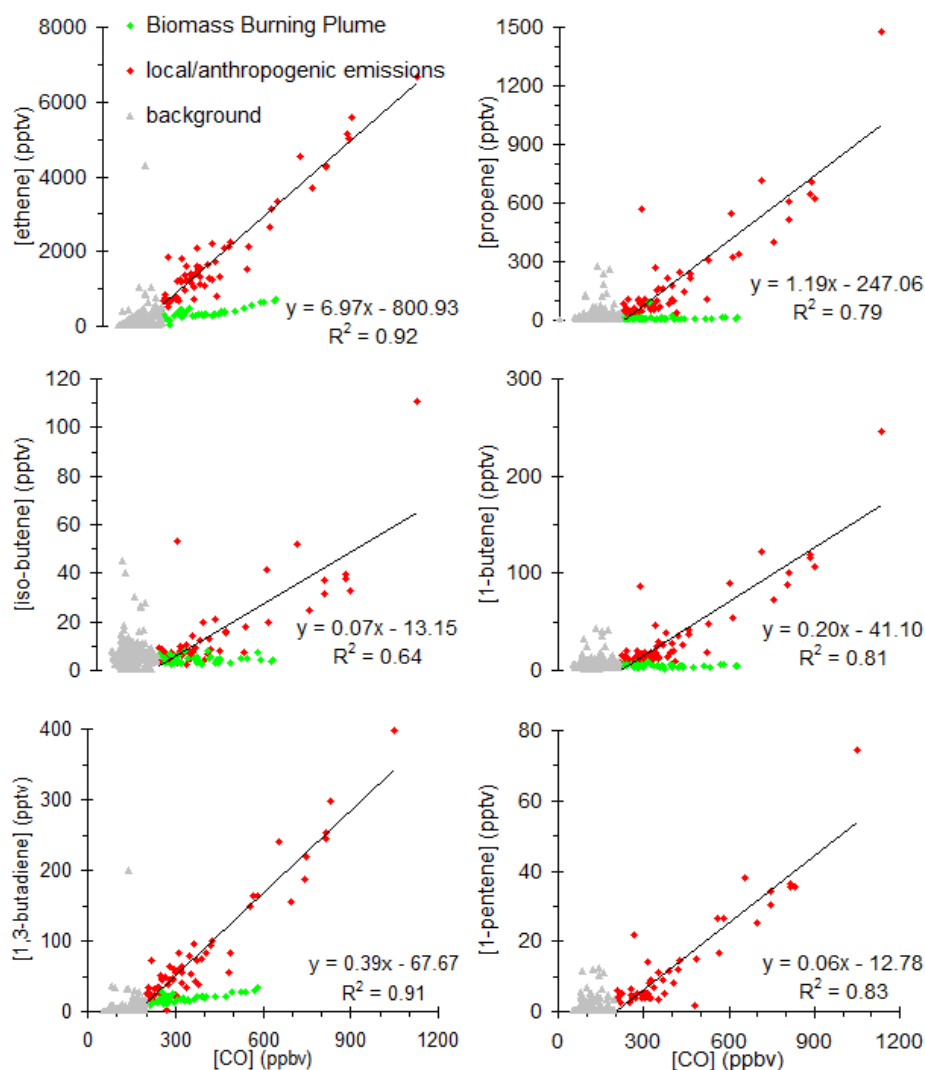
Figure 6.3: Selected plots of alkenes *versus* CO. Grey triangle assigned as background air, red diamonds assigned as biomass plumes and green diamonds assigned as anthropogenic plumes.

Here the differences between elevation caused by anthropogenic emissions and those caused by biomass burning are relatively clear, and in all cases are correlated to CO (but with different slopes), since the primarily alkene source is

also combustion. Somewhat surprisingly even for very short-lived NHMCs, in biomass burning plumes sampled some days downwind, the mixing ratios remained high and are in contrast to the anthropogenic plumes, where CO is significantly elevated, but the reactive alkenes are largely depleted. This mirrors observations in Lewis et al (Lewis et al., 2007) of plumes far out in the North Atlantic where ethene, for example, remained at mixing ratios >1000 ppt more than four days from emission.

Figure 6.4 shows the relationships between selected aromatic and oxygenated species and CO.
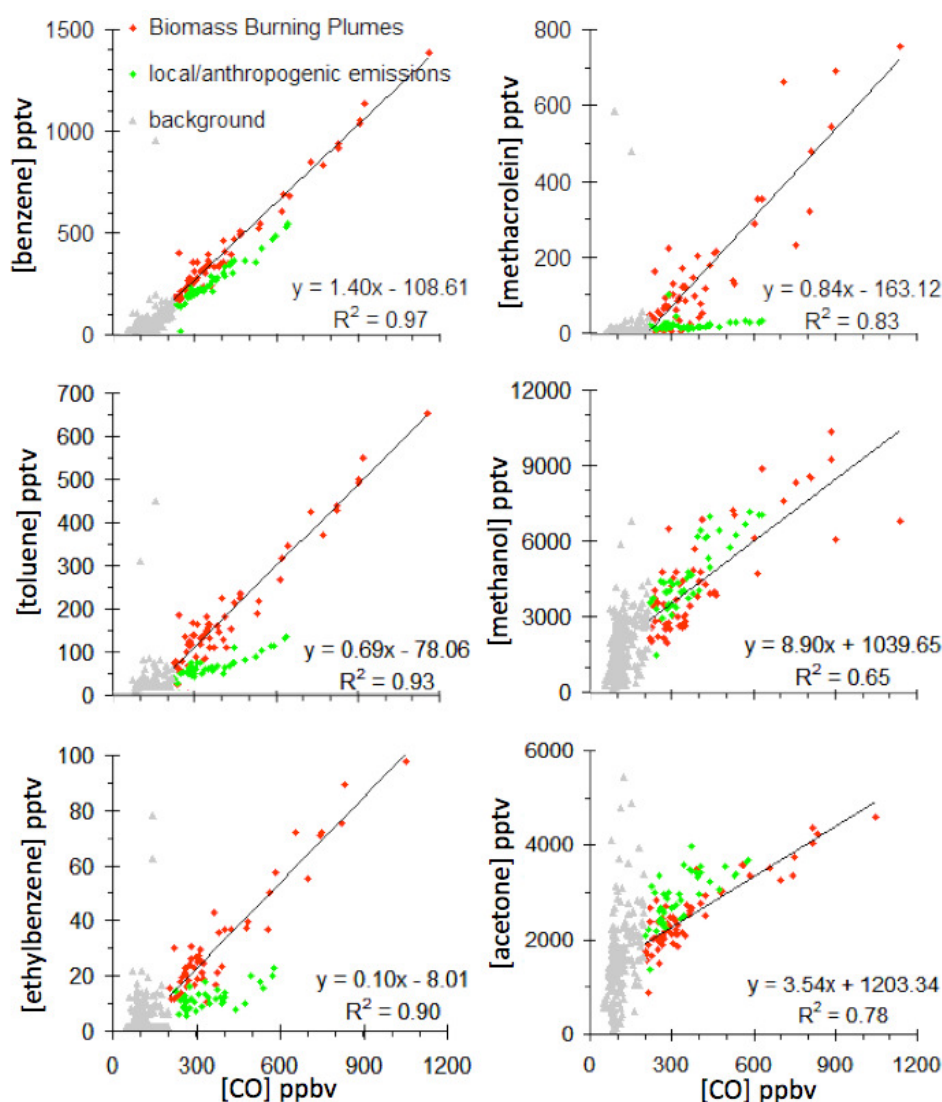
Figure 6.4: Selected plots of aromatics and oxygenates *versus* CO. Grey triangles assigned as background air, red diamonds assigned as biomass plumes and green diamonds assigned as anthropogenic plumes.

For toluene and methacrolein, again there are substantial differences in the slopes for anthropogenic and biomass plumes. A very small number of elevated benzene data points are observed without elevation in CO suggesting a localised non-combustion source in the region.

It is possible to provide a relative assessment of emissions scaled to the amount of biomass fuel burnt, referred to as an emission factor (EF). This essentially relates NMHC emissions to CO_2 rather than CO *via* an estimated value associated to the mass fraction of carbon in the biomass fuel. This scaling is not made here since CO_2 data for this experiment are much less complete than for CO, although when made for selected flights it shows a similarly good agreement with (Simpson et al., 2011) as the ER.

6.4.2 Model analysis and global impacts

The airborne observations made over Canada show strong correlations between the concentrations of individual NMHCs and CO in plumes from both biomass burning and fossil fuel burning origins. To explore the individual contributions from the distinct source types a 'tagged tracer' simulation of benzene, toluene, propene and ethene has been performed within the GEOS-Chem global model (version 9.1.2 http:// www.geos-chem.org/) (Bey et al., 2001;van der Werf et al., 2010) in which individual model tracers represent contributions of benzene, for example, emitted from a particular source and geographical region.

The model runs described here were conducted by Prof Mat Evans at the University of York, using measurement data generated in the course of this PhD.

These species are chosen in particular for study since they are often (if erroneously) considered in atmospheric chemistry as anthropogenic tracers, rather than from natural emissions. The substantial emissions from biomass burning are potentially of growing significance in those locations (particularly in developed countries) where such species are on downward emission trajectories, a result of control technologies, reformulation of gasoline composition and reduced solvent usage. In those locations with rapidly growing vehicle fleets in developing countries, it remains an open question as to whether benzene is on an increasing or decreasing trajectory.

The model NMHC tracers are adapted in a flexible way to simulate both tagged anthropogenic (the sum of combustion and non-combustion sources) and biomass burning sources. For simplicity any other biogenic source (e.g. direct leaf-level emissions of toluene or ocean source of alkenes) is ignored. The NMHC species as extra tracers are included in the full-chemistry model simulation. The emissions are simulated (the rate of the emission being described below), transport by the large-scale meteorology fields, and also by convection and boundary layer mixing. The NMHC species do not directly interact with the chemistry scheme but are subject to oxidation by the time-dependent oxidant fields of OH, O_3, and NO_3. The oxidation of these compounds is not considered in the stratosphere, which is a reasonable approximation given atmospheric lifetimes of 7 days or less and only modest convective outflow levels encountered during the experiments.

The purpose of the modelling is to apply the emissions ratios derived in this study and upscale the distribution of observed NMHCs on a global and annual timescale and to evaluate the model at remote surface sites, rather than to attempt along-flight-track simulations to match observations. A simple approach has been taken in using a single ER for certain hydrocarbon species for the biomass burning source since that captures much of the global behaviour of the hydrocarbon relative to CO. Ideally however a more detailed biomass burning

inventory that encapsulated the many different sources and fuels types would be used, but this would require far greater model sophistication in terms of input emissions and would require a source specific disaggregation of CO. Given the good to excellent agreement in ER between this study, and Simpson et al (Simpson et al., 2011) experiments conducted in different years, we consider that representative meteorology from any given year would be a reasonable approximation to simulate annual global hydrocarbon distributions from boreal biomass burning. The model is run for the year 2009 twice with the first year being considered as model spin-up. This year is chosen as GFED3 [Global Fire Emission Database] (van der Werf et al., 2010) emissions of CO are available for this year. Other fire emissions inventories exist, for example the NCAR model of (Wiedinmyer et al., 2011), and it must be acknowledged that differences between inventories naturally add to the uncertainty in any CO derived estimate of hydrocarbon distribution. A comparison of global inventories by Stroppiana et al (Stroppiana et al., 2010) would suggest that the biomass burning emission value of 350 Tg yr^{-1} from this study is consistent with the NCAR (FINN) model but towards the lower end of the range given in this analysis, suggesting our hydrocarbons from biomass burning are conservatively estimated.

Table 6.2 describes the emission rates of these target compounds released in the model. The RETRO emissions ('Reanalysis of the tropospheric chemical composition of the last 40 years' project) (Schultz et al., 2007) for 2000 are used for the anthropogenic sources, made up of ten sectors including various combustion sources, industrial emissions, waste treatment, agriculture and solvent emissions. Whilst more up to date anthropogenic data inventories exist at national levels, this database has the correct combinations of NMHC species, geographic and temporal disaggregation for the study here, and is well integrated with the GEOS-Chem model. Changes in emissions over recent years have occurred however, most notably for benzene, and the impacts of this on our conclusions are discussed later.

Table 6.2: Emissions and derived lifetimes of the simulated species. *bb is used for biomass burning

Compound	Emission Type	Emission source	Emission ($Tg\ yr^{-1}$)	Lifetime (days)
benzene	Biomass	CObb * 0.0014	1.77	7.42
	Anthropogenic	RETRO 2000	3.48	10.95
toluene	Biomass	CObb * 0.00069	1.11	1.55
	Anthropogenic	RETRO 2000	6.13	2.73
ethene	Biomass	CObb * 0.0069	0.85	1.15
	Anthropogenic	RETRO 2000	6.47	1.19
propene	Biomass	CObb * 0.0019	2.04	0.28
	Anthropogenic	RETRO 2000	2.74	0.30
CO	Biomass	CObb	272	

The biomass burning sources are scaled to the GFED3 CO emissions used in the model. The biomass burning emissions of the hydrocarbons uses the GFED3 CO emissions scaled by the ratios derived in section for the BORTAS data. We use a single value for the emission ratio of hydrocarbons from biomass burning and apply this to both boreal and tropical forest fires. Literature reviews of emissions indicate that whilst some species are very dependant on location and type of fuel, many hydrocarbon emissions (and indeed CO on a per dry mass burnt basis) are similar across extratropical and tropical forests. Using the summary values from Andrea and Merlet (Andreae and Merlet, 2001), the ER of benzene in tropical forests is estimated at around 1.65 ± 0.10 ppt per ppb CO, as compared to our boreal value of 1.40 ± 0.11. A similarly close agreement is found for ethene, propene and toluene – for example our boreal estimate for toluene is 0.69 ± 0.09 ppt per ppb CO, *versus* the tropical literature range of 0.73 ± 0.8. We consider therefore that the use of a single ER for all biomass burning emissions is sufficient to represent both regions in the model and that compared to uncertainty

in the overall size of CO biomass burning emissions and anthropogenic benzene, this is likely to be a minor factor.

Recent work suggests that smouldering fires can consume a substantial amount of organic material but may be poorly represented in emissions estimates (see for example (Bertschi et al., 2003;Hyde et al., 2011;Turetsky et al., 2011). It is clear that if our hydrocarbon ER was derived solely from near to source or fresh fire emissions then we would not capture this source in our data. However, the scale of the aircraft observations, covering 28000 km of sample tracks and from 500ft to 30000ft would suggest that all type of burning emissions are represented in our data. We do not observe any substantial deviation in hydrocarbon to CO slopes for biomass influenced air suggesting that the smoldering emission is captured in our ratio. There is a wider issue of whether smoldering CO is then captured appropriately by GFED3 but that is beyond this paper. The implication is that our estimates of influence may be under-estimates if the smoldering source is not captured and is significant.

The overall total estimates of global benzene and toluene emissions are comparable to previous studies (Henze et al., 2008). However, the estimates for the biomass burning source specifically, are somewhat lower than in (Henze et al., 2008); this arises due to different values for the emission ratio. For comparison, (Henze et al., 2008) used 3.4 $Tg(C_6H_6)$ yr^{-1} for the anthropogenic emission and 2.7 $Tg(C_6H_6)$ yr^{-1} for the biomass burning, we have used 3.5 $Tg(C_6H_6)$ yr^{-1} for anthropogenic emission and 1.8 $Tg(C_6H_6)$ yr^{-1} for the biomass burning source.

Lifetimes of individual hydrocarbons are derived as being the reciprocal of the annual globally integrated loss rate of the compound divided by the annual mean burden. For these simulations the global mean tropospheric OH concentration

was calculated to be 1.12 x 10^6 molecule cm^{-3}, which is broadly consistent with the available observational constraints (Krol et al., 1998).

6.4.3 Evaluation of the model against data

To evaluate the general performance of the global model in simulating global background hydrocarbon distributions from all sources it is compared against some remote NMHC measurements made as part of the WMO Global Atmosphere Watch (GAW) programme. The number of measurement stations for which this type of continuous data exists is very small – perhaps only 3-5 at any one time. More comprehensive geographic coverage is achieved for alkanes and acetylene from flask networks, but not the target species in this study. **Figure 6.5** shows observations of the concentration of benzene (monthly means, derived from hourly data) at the Cape Verde Atmospheric Observatory in the tropical mid-Atlantic and a comparison with the model simulation under a range of emission levels. The benzene measurements have been filtered to any local contamination or sources, such that the dataset represents a good measure of tropical North Atlantic open ocean variability. The grey bars represent the standard deviation variability. Again acknowledgement is given to the previous work of Dr Katie Read and Prof. Lucy Carpenter in helping to generate the benzene dataset used here.

Using baseline RETRO emission data for the nominal year 2000 reproduces the annual cycle of surface NMHC concentrations, but has a large positive bias. A better model agreement is attained between the concentration data only after the anthropogenic emissions are reduced by two thirds. There is some justification for allowing a significant reduction in anthropogenic benzene over the past decade, with many developed countries having very substantially reduced emissions following reformulation of gasoline content, the introduction of catalytic converters and the elimination of benzene as a solvent. Although sector specific data is limited for benzene sources, if one considers emissions from the

UK to be a reasonable proxy for Europe and other developed regions then solvent and production processes emission of benzene had by 2009 fallen to around 1/3 the levels of 1990. Road transport emissions are estimated to have fallen to appropriately 1/4 the 1990 value by 2009. This is not of course to say that atmospheric concentrations have shown that same level of reduction, but studies have shown a sustained reduction of around 20% a year during periods of emission control tightening (Dollard et al., 2007). It is emphasized here that it is not suggested the model proves that RETRO should be adjusted by a multiplier of 0.33, but rather than this is the level of change that is required to make an observation match with our model.
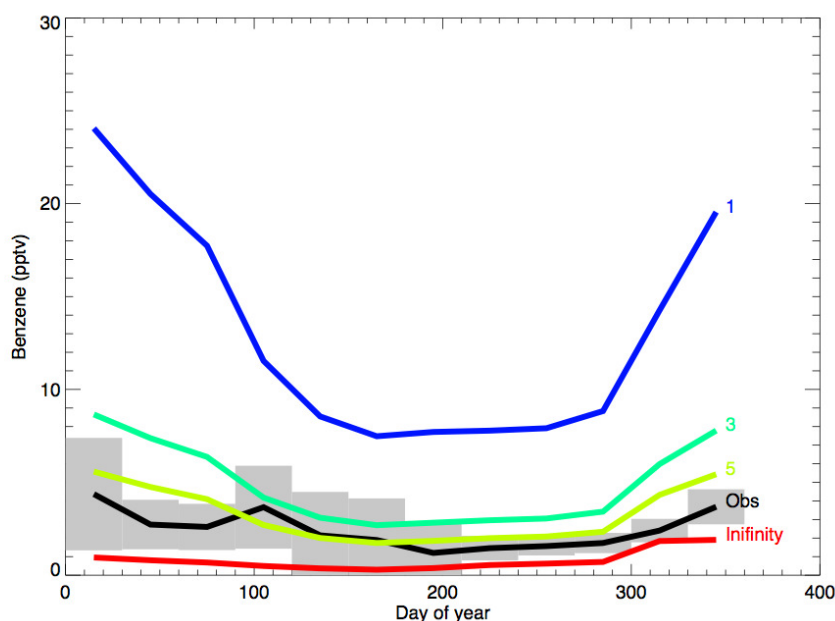
Figure 6.5: Comparison of GEOS-Chem model estimate for benzene and observations made at the Cape Verde GAW Observatory. Bars indicate ranges of monthly data and the black line the observed average. The blue line indicates the model estimate using biomass burning and RETRO emissions inputs. The two green lines show the estimated benzene by reducing benzene levels in RETRO. The red line show the model when no anthropogenic emissions are included.

It is considered therefore that the model shows suitable agreement to allow us to proceed in so far as it reasonably captures the annual variability seen in measurement and order of magnitude concentrations. Moving forward, in this

study it is continued to work with the RETRO database as is, but in a number of cases and figures highlight how biomass to anthropogenic contributions would be affected if a 2/3 reduction in anthropogenic benzene was applied.

6.4.4 Estimating global distribution of benzene, toluene, ethane and propene from biomass burning and anthropogenic emissions

Figure 6.6 shows the global annual mean mixing ratio of biomass burning benzene, and anthropogenic benzene estimated by the GEOS-Chem model, using the CO:benzene ratio from this work together with the GFED III CO emissions and the standard RETRO database for the year 2000 for the anthropogenic emissions. There are rather few long-term observations of benzene with which to compare to our model, and most in the literature refer to urban locations, many of which are roadside. It is not therefore appropriate to try to compare the outputs of a global scale model such as GEOS-Chem with such urban observations since the observations can be dominated by influences below the grid scale of the model. In very general terms however the order of magnitude comparison in benzene is reasonable when compared for example to (Baker et al., 2008) and (Dollard et al., 2007). In these papers, urban benzene from observations networks is reported for US and UK cities, typically at values in the range 150-450 ppt, in order of magnitude agreement with that predicted from our model.

Figure 6.6. highlights that for most locations the air quality or human health impact of these biomass burning emissions is generally very small, –benzene released from this source contributes typically a few parts per trillion. The same is true for toluene, ethane and propene (not shown). Exceptions are locations in Arctic regions where the estimated mixing ratios of benzene from biomass burning in our model year reach in to the ppb range. This study only attempts to model a single year of biomass burning emissions, and it should be appreciated that significant inter-annual variability in both intensity and location of burning

exists (eg Simpson et al., 2006) and this of course changes the extent to which locations may be impacted by this source. Future work may want to examine how variability in burning impacts on the global hydrocarbon distribution and this is of course something that may ultimately be inferred *via* a network of background GAW observations.
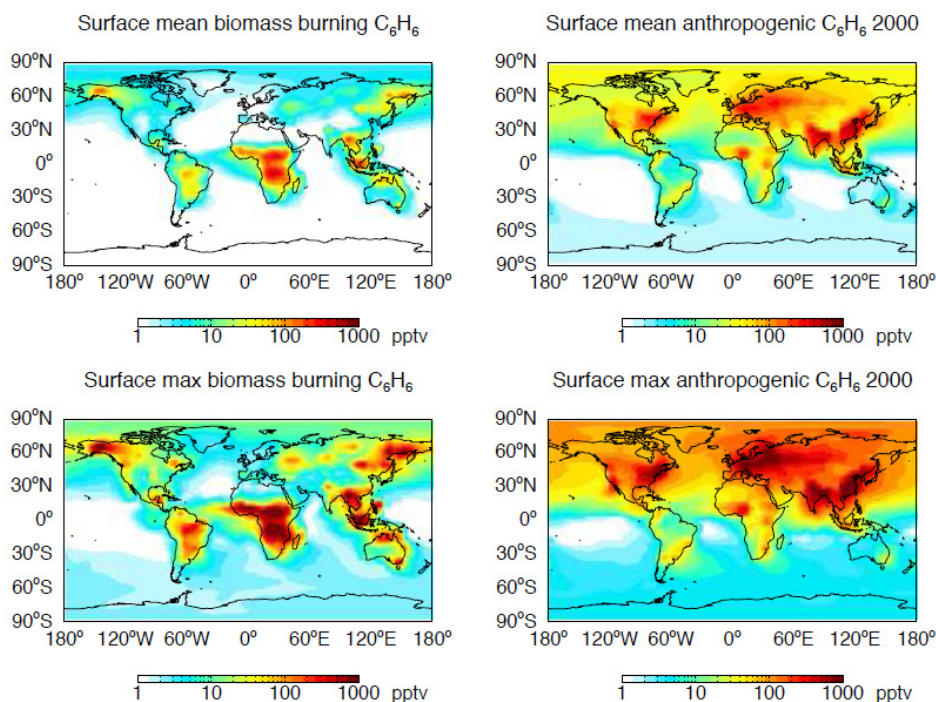
Figure 6.6:. Top row: model estimate of the annual surface mean mixing ratio of benzene resulting from biomass burning emissions (left) and from anthropogenic emissions (right) using the standard RETRO 2000 scenario. Second row of plots shows the monthly maximum surface mixing ratio from these two sources.

The biomass burning impacts on hydrocarbons are therefore perhaps most important to consider when attempting to evaluate trends, transport processes and longer-term behaviour in background locations. Conversely, background observations of such hydrocarbon in background locations may provide a new constraint on the size and distribution of global emissions. Values indicated by the model over Africa (in the hundreds of ppt and greater occasion), fall with the

range of concentrations seen for example by Sinha et al (Sinha et al., 2003) in biomass burning from Southern.

6.4.4.1   Biomass *versus* anthropogenic sources of benzene, toluene, ethane and propene

The tagged tracers in the GEOS-Chem model are then used in **Figure 6.7** to show the surface ratio of i) the mean of the monthly mean ratio of simulated biomass burning tagged hydrocarbon to total hydrocarbon (biomass burning tracer + anthropogenic tracer) and ii) the maximum of the same ratio observed in any of the individual twelve months in the year. The plots illustrate (with warm colours) those regions that on a mean annual basis have significant *fractional* biomass burning input to the observed NMHC, and also when influence can become important for shorter, monthly, periods.

Figure 6.7 (and **Figure 6.8** for benzene) shows extensive geographic regions where the abundance of all four hydrocarbons is heavily impacted by biomass burning. This is particularly the case in the Southern hemisphere, where tropical biomass burning provides a large source and fossil fuel burning from anthropogenic is lower. Here, our model indicates that biomass burning constitutes the largest source to the lower atmosphere. It should be remembered of course that this is a ratio of two abundances – the absolute abundance of NMHCs in many of these remote Southern hemisphere locations is very low, approaching the typical GC detection limits of around 1 ppt.

Over the northern industrial belt (North America, Europe, Asia) the annual mean ratios indicate that benzene, toluene, ethene and propene are generally dominated by the anthropogenic source. It is worth noting however that regions of the US and Canada have, even on a mean basis, a non-trivial fraction of benzene associated with biomass burning sources. One might expect this fraction to grow

in significance as vehicle emissions control further act to reduce anthropogenic emissions. Whilst health exposure limits for benzene vary widely internationally – from no limits in certain US states to 5 μg m^{-3} in Europe, and where controlled, they move generally only in a downwards direction; eg in Europe from 10 μg m^{-3} in the 2000 Second Daughter Directive 2000/69/EC to 5 μg m-3 in the 2008 Directive 2008/50/EC. The model simulations highlight that ultimately pragmatic approaches are needed in setting reasonable and achievable lower limits for benzene in the atmosphere given the apparent large and widespread source from biomass burning.
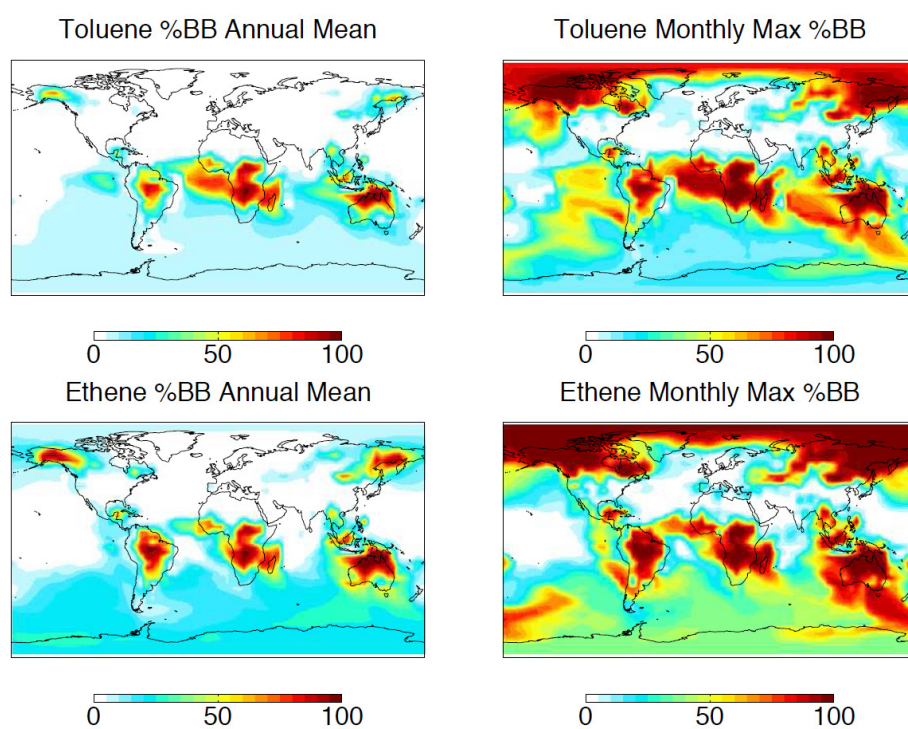
Figure 6.7: Fractional contribution to the total toluene (top) and ethene (bottom) from biomass burning. Left hand plots show annual mean contributions and right hand plots the monthly maximum fraction from biomass burning.
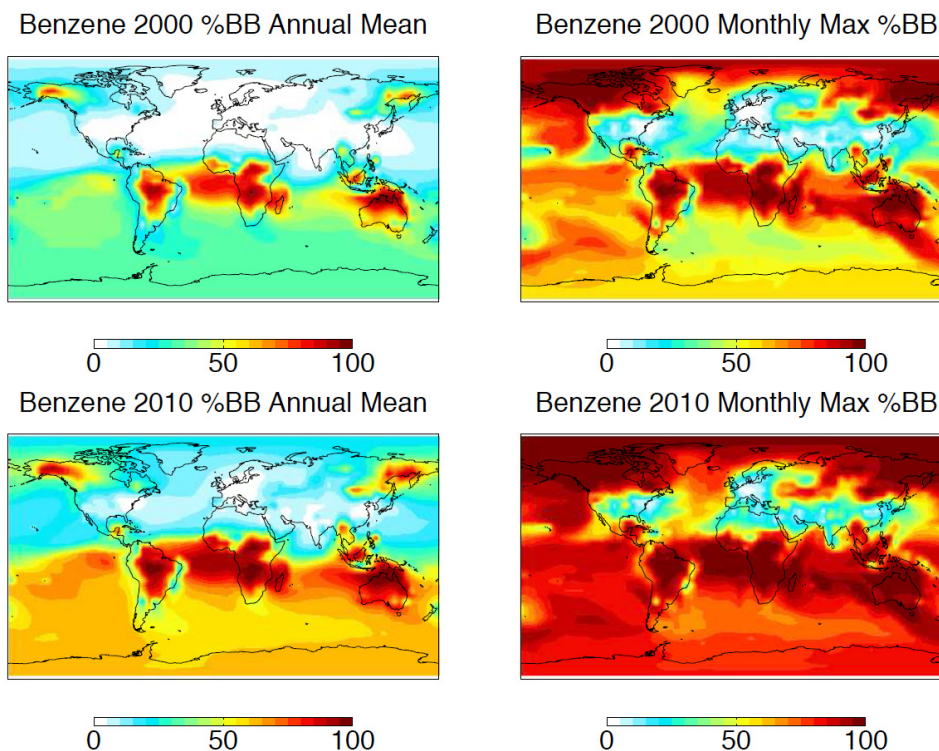
Figure 6.8: Fractional contribution to benzene from biomass burning as an annual mean (left top) and as the monthly maximum (top right). Left bottom plot shows how this fractional contribution is enhanced if a reduced 0.33 * RETRO anthropogenic emissions for benzene is implemented in line with the fit to Figure 3 based on Cape Verde observations for the year 2010.

The figure also shows the maximum monthly mean percentage, which indicates that for many regions biomass burning can, for shorter periods, make up the dominant source of the hydrocarbon observed. The feature is most striking for benzene, not unsurprising given it has the longest lifetime, but this is also the case for shorter-lived hydrocarbons as well. For fast reacting hydrocarbons such as propene the concentrations in remote areas, particularly over the oceans, become very low and this leads to numerical issues in the model. Areas where the mixing ratios approach the numerical resolution of the model (<0.01 ppt) are indicated in white.

As identified earlier it appears that the RETRO database may over estimate the present day amount of anthropogenic benzene (and to a lesser extent other NMHCs) released, when comparison is made with a very remote background GAW observatory. The resolution of the model used for this study is not appropriate to allow it to be sensibly compared to urban observations. Literature reports suggest that ambient urban concentrations have fallen significantly over the past 15 years, in some locations at rates of 20% per annum. Our comparison earlier of remote background benzene data with the model suggested that a two-thirds reduction in RETRO 2000 emissions would bring model and measurement in to reasonable agreement on a global scale.

This study is severely limited by the lack of appropriate background observations and it is very uncertain whether this is globally an appropriate figure to apply. The work reported here does, however, provide an indication of the general impacts of a reduction of this scale, as is shown in **Figure 6.8**. By reducing the anthropogenic emissions of benzene such that they agree better with real observations from 2010 at Cape Verde, the relative impact of the biomass burning contribution grows significantly (plots marked 2010). In broad terms it can be concluded from these simulations that for much of the planet the observed abundance of benzene, toluene, ethene and propene can be significantly influenced by a proportion of emissions from biomass burning, and that continued reductions in anthropogenic hydrocarbons will enhance this impact. The effects are largely realised in the background environment and away from localised urban anthropogenic sources.

6.4.4.2   Impacts on background measurement stations

Whilst sporadic research grade measurements of hydrocarbons have been made throughout the background troposphere, and some long-term records do exist, most routine and long-term observations continue to be focused on urban centres, reflecting air quality drivers. However, there are increasing efforts now made to

establish trends in the background atmosphere through the WMO Global Atmosphere Watch programme. GAW covers a wide range of parameters relating to atmospheric composition, and is considered the atmospheric chemistry component of the Global Climate Observing System (GCOS). Details can be found at www.wmo.int/gaw. Reactive gases form a subset of species to be observed including surface ozone (O_3), carbon monoxide (CO), volatile organic compounds (VOCs), oxidised nitrogen compounds (NOx, NOy), and sulphur dioxide (SO_2). GAW comprises several hundred observing sites, classified as 'contributing', 'regional' and 'global' depending on the scope of the measurement programme at each location (**Figure 6.9** and **Table 6.3**).

Figure 6.9: Locations of the WMO GAW Global observatories.

Table 6.3. List of the 28 GAW Global stations with three letter code names and locations.

Station name (Country)	CODE	Latitude	Longitude
Assekrem /Tamanrasset (Algeria)	TAM	23.26667	5.63333
Cape Verde Atmospheric Observatory (Cape Verde)	CVO	16.848	-24.871
Amsterdam Island (France)	AMS	-37.7983	77.5378
Mt. Kenya (Kenya)	KEN	-0.0622	37.2972
Cape Point (South Africa)	CPP	-34.35348	18.48968
Izaña (Tenerife, Spain)	IZA	28.309	-16.4994
Cape Grim (Australia)	CPG	-40.68222	144.6883
Mt. Waliguan (China)	WAL	36.2875	100.8963
Bukit Kototabang (Indonesia)	BUK	-0.20194	100.3181
Minamitorishima (Japan)	MIN	24.2852	153.9813
Danum Valley (Malaysia)	DAN	4.98139	117.8436
Nepal Climate Observatory - Pyramid (Nepal)	NEP	27.9578	86.8149
Lauder (New Zealand)	LAU	-45.038	169.684
Mauna Loa (United States)	MLO	19.53623	-155.5762
Samoa (United States)	SAM	-14.24747	-170.5645
Ushuaia (Argentina)	USH	-54.84846	-68.31069
Arembepe (Brazil)	ARE	-12.76667	-38.16667
Alert (Canada)	ALE	82.45	-62.51667
Barrow (United States)	BAR	71.32301	-156.6115
Trinidad Head (USA)	TRI	41.0541	-124.151
Pallas/Sodankylä (Finland)	PAL	67.97361	24.11583
Zugspitze/ Hohenpeissenberg (Germany)	ZUG	47.4165	10.9796
Mace Head (Ireland)	MAC	53.32583	-9.89945
Monte Cimone (Italy)	MON	44.16667	10.68333
Zeppelin Mountain (Norway)	ZEP	78.92358	11.92366
Jungfraujoch (Switzerland)	JFJ	46.54749	7.98509
Neumayer (Antarctica)	NEU	-70.666	-8.266
Halley (Antarctica)	HAL		
South Pole (Antarctica)	SPO	-89.99695	-24.8

We consider it useful to examine the major NMHC source influences on the primary global measurement stations in that network, accepting that at present only a small number make continuous NMHC measurements. A focus here is on the 28 global GAW stations that make the most comprehensive range of measurements. The names and locations of the global stations are shown in **Table 6.3** and in **Figure 6.9**.

Using output from the GEOS-Chem model an annual time series is simulated for benzene (biomass burning derived and total) for four 'clean' background surface GAW sites from around the world. For this we continue to use the standard RETRO emissions. **Figure 6.10** shows for four selected GAW locations, the simulated total benzene at each site, the benzene derived from biomass burning, and a separate plot showing the fractional contributions. Should our calculated 2/3 reduction is applied in anthropogenic emissions then that naturally these plots are shifted substantially to show increasing biomass burning influence and this is refleted in later **Table 6.4**. At present none of these sites has online measurements year round. Those sites in reasonable proximity to biomass burning sources, (e.g. Barrow, Alaska and Bukit Kototabang, Indonesia) are subject to significant impacts with modelled benzene events of ~500 pptv due almost entirely due to burning. Very remote GAW sites (e.g. Samoa, Halley) show very low absolute concentrations but show a significant fraction of that coming from biomass burning. Taking Barrow as a test case, the implied CO mixing ratios during the burning maximum would be of the order 600-800 ppb. Publically available data on the NOAA ESRL website indicates peak CO values in 2009, derived from flask samples, as 678 ppb, in good agreement with the model.
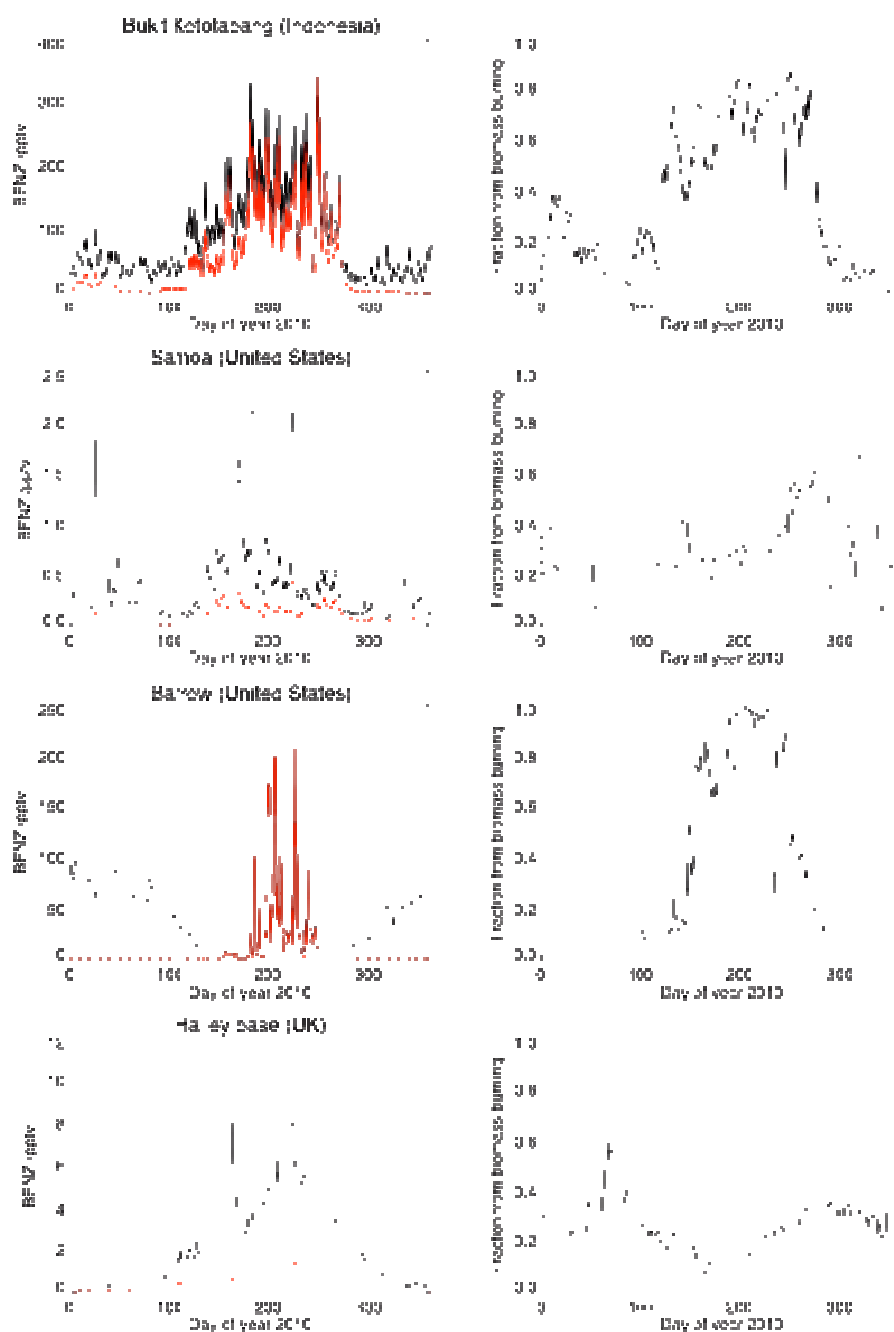
Figure 6.10: Model estimates of the biomass burning inputs to benzene at four GAW observatories currently without NMHC on line measurements. From top: Bukit Kototabang, Indonesia; Samoa, Pacific; Halley, Antarctica; Barrow, Arctic. Left figures show estimated mixing ratios (black) and biomass contribution (red). Right hand figures show % biomass contribution.

Table 6.4: GEOS-Chem model estimated fraction of annual benzene associated with biomass burning, given as the annual mean and as the monthly maximum. The anthropogenic emissions used are that of RETRO and 0.33 x RETRO.

Biomass burning / anthropogenic benzene fraction	Annual Mean	Annual Mean (RETRO * 0.33)	Monthly Maximum	Monthly Maximum (RETRO * 0.33)
0.0 – 0.2	TAM CVO KEN IZA WAL MIN DAN NEP MLO ARE TRI PAL ZUG MAC MON JUN HLF	IZA WAL NEP PAL ZUG MAC MON JUN HLF	NEP ZUG MON JUN	ZUG MON JUN
0.2 – 0.4	AMS CPP CPG LAU SAM USH ALE BAR ZEP NEU SPO HAL	TAM CVO KEN MIN DAN MLO ARE ALE TRI ZEP	IZA	NEP
0.4 – 0.6	BUK	CPP CPG LAU USH BAR	TAM CVO WAL ARE	
0.6 – 0.8		AMS BUK SAM NEU SPO HAL	KEN CPP MIN DAN SAM TRI PAL MAC NEU SPO HAL HLF	TAM IZA WAL ARE
0.8 - 1			AMS CPG BUK LAU MLO USH ALE BAR ZEP	CVO AMS KEN CPP CPG BUK MIN DAN LAU MLO SAM USH ALE BAR TRI PAL MAC ZEP NEU SPO HAL HLF

Taking all the global GAW locations from **Table 6.3**, It is then placed into categories based on the annual mean fraction of likely experienced benzene that is from biomass and the maximum monthly fraction of benzene that is from biomass burning. The categories are for fraction values 0-20%, 20-40%, 40-60%, 60-80% and 80-100%. Using the standard RETRO emission values for benzene the majority of GAW Global stations on a mean annual basis are in the lowest 0-

20% impact category and all but one station covered by that and the 20-40% category. An analysis of monthly maximum impact however is rather different, indicating that benzene at the majority of stations can be dominated on occasion by biomass burning sources.

As discussed previously, the likely anthropogenic emissions and very likely lower than expressed in RETRO and so we include separate rows that show how the stations would partition if a 66.7% anthropogenic reduction in benzene was implemented in the model. In this case on an annual mean basis a significant number of stations would be in the 40-60 and 60-80% biomass burning benzene category, and the majority in the highest category when considered on a monthly maximum basis. Uncertainty here is dominated by the emissions term (factor of 2), rather than by meteorology or chemistry (OH term uncertain to around 20%). Given this uncertainty in the correct reduction in benzene emissions to include in the model, the reality is likely to lie somewhere between these two scenarios in **Table 6.4**.

6.4.5 Conclusions

An extensive set of airborne measurements of NMHCs have been made in boreal forest fire plumes over Canada. The data expands on the global dataset adding some new emission estimates for certain hydrocarbon species and providing confirmatory measurements to some species previously published. The generally very good agreement between emissions derived from different aircraft studies by different groups in the same region and this provides significant confidence in making extrapolations from these estimates in models. The wider comparison of the ERs obtained here with earlier studies from other geographic regions indicates that many hydrocarbon ERs do not vary substantially between tropical and extra-tropical burning, although some sources such as smouldering may not be fully represented. Using the GEOS-Chem CTM the relative contributions of anthropogenic and biomass burning emissions to the background abundance of benzene, toluene, ethene and propene is examined. These species are chosen in

particular since are often controlled in an air quality context and are species with generally declining urban concentrations in developed economies. The tagged model showed that in most of the Southern hemisphere a significant fraction of observed benzene at any given location is from biomass burning, and that biomass burning as a major contributor to the global hydrocarbon abundance extends at times to the Northern hemisphere also. The largest source of uncertainty in the model arise from the emission estimates rather than chemistry or meteorology, however even varying the emissions by a factor of 3 (moving from the 2000 RETRO base emissions to a 2/3 value in line with observations) does not change this general conclusion. It is only over heavily industrialized regions that these hydrocarbon distributions are dominated by the anthropogenic source. The lack of appropriate background monitoring sites to compare our modelling to is a major limitation. The expansion of the GAW network should help in this regard. The behaviour of benzene is particularly interesting here since it is a heavily regulated pollutant that is often considered in terms of toxicology as having no safe lower limit ((Duarte-Davidson et al., 2001). The study here shows that pragmatic air quality targets are needed for benzene given that regional and transboundary biomass burning sources can make up a significant fraction of the benzene experienced globally.

Very limited experimental data exist for the long-term trends in hydrocarbons in the background atmosphere; however, comparison of model against benzene in the tropical Atlantic shows that the annual cycle can be reasonably captured, although suggesting that the model emissions database is over estimating anthropogenic emissions. When the model is used to estimate the contribution of biomass burning to the hydrocarbons experienced at GAW Global stations the picture is mixed. At some locations such as Barrow and Alert high absolute and fractional biomass contributions are suggested from model simulations, up to several hundred ppt of benzene for example, whilst in some tropical and polar regions the absolute amounts are predicted to be low, (single figure ppt mixing ratios) but with a significant fraction (20-60%) from biomass burning. An assessment is made of the likely biomass burning input to all 28 GAW Global

stations as a hopefully useful precursor exercise prior to the practical extension to the GAW-VOC measurement programme.

Chapter 7:
Summary and conclusions

Summary and conclusions

A dual channel GC-FID instrument has been used to make extensive observations of VOCs in the atmosphere from an aircraft platform. The analytical methods deployed have been evaluated and tested in comparison with other instrumentation.

Observations of VOCs have been made above Canada to observe the emissions from forest fires which found that the effects of forest fire emissions were persistent throughout the globe and in some regions (often far away from the source regions) were found to be the dominant source for some VOCs. Observations were also made above the UK during a seasonal study of VOCs in the free troposphere where comparison with previous studies showed a decrease in mixing ratios of a number of VOCs including benzene which is likely due to the effectiveness of control strategies for emissions of VOCs. In a separate study, observations were also made above the UK at different times of day and hydrocarbon ratios were used to study the effect of the NO_3 radical on the VOC observations.

The hydrocarbon ratio approach has been utilized in the interpretation of the VOC data analyzed in this thesis. Seasonal variation in hydrocarbon mixing ratios and measurements based on kinetic and model studies have shown that ratios of a reactive hydrocarbon to a relatively inert hydrocarbon can be approximated to be entirely determined by OH chemistry. The ratio operation nullifies the effects of differing degrees of dilution among air parcels provided that the background mixing ratio is negligible. These assumptions and simplifications make ratio treatment much simpler by viewing a given hydrocarbon ratio in an air parcel decreasing from the ratio of initial emissions according to first order decay kinetics. Therefore, the logarithm of an appropriately properly chosen ratio provides an approximate, linear measure of the degree of photochemical processing that has affected that air parcel.

326

In this thesis the pentane isomer pair (*n-* and *iso*) has been particularly useful when diagnosing the presence of different oxidants during day, night, dusk and dawn. In the winter night flight data, the demonstration of the absence of the NO_3 radical by pentane *n-* and *iso-* isomer pair is supported by the lifetime-variability analysis and this gives a confidence in using the pentane isomer pair as a sensitive indicator to differentiate the presence of different oxidants between day and night provided that the nitrate levels are present above the detection limit (10 ppt) of the ratioing treatment. To further test the robustness of the variability-lifetime approach in identifying the presence of different oxidants during different phases of the day, further comparative tests, by including a reasonable number of flights, are planned for future work.

The behaviour of butane isomer pair ($n - iso$) in comparison with pentane isomer pair, in demonstrating the absence of nitrate radical, has led to the conclusion that its slow reacting rate makes it less suitable for this application. Further analysis on the butane isomer pair also suggests that in presence of higher concentrations of NO_3 radical, it could be responsive. To further test the behaviour of butane isomer pair, the observations from an environment with high concentration of NO_3 is needed for future work. Although propene gives indication of presence of NO_3 radical in winter flights in the variability-lifetime analysis, it has not been used in the ratioing operation; hence, for future work the compounds that are more sensitive to NO_3 radical, for example propene, and isomers of trimethylbenzene can be tested for diagnosing radical presence.

In summary, it can be concluded that despite the complicated effects of non-zero background mixing ratio and atmospheric mixing, the ratio treatment on data included in this thesis has been still useful as a tracer for net atmospheric processing, diagnosing radical presence, tracing the influence of air masses with different source signature, evaluating the impact of various sources on chemical signature of a particular region, and to indirectly determine the radical concentration.

Abbreviations

AASE	Airborne Arctic Stratosphere Expedition
ABLE	Arctic Boundary Layer Expedition
Active SPME	Active Solid Phase Micro Extraction
ACTRIS	Aerosols, Clouds, and Trace Gases Research Infrastructure Network
AMMA	African Monsoon Multidisciplinary Analysis
AMOVOC	Airborne Measurements of Volatile Organic Compounds
AMS	Aerosols Mass Spectrometry
AR54	Apel Reimer 54 component gas standard
ASHOE	Airborne Southern Hemisphere Ozone Experiment
ASTM	American Society for Testing and Materials
BAe	British Aerospace
BBCEAS	Broadband Cavity Enhanced Absorption Spectroscopy
BL	Boundary Layer
BORTAS	BOReal forest fires on Tropospheric oxidants over the Atlantic using Aircraft and Satellites
BTV	Breakthrough volume
BVOCs	Biogenic Volatile Organic Compounds
CARIBIC	Civil Aircraft for the Regular Investigation of the atmosphere Based on an Instrument Container
CCN	Cloud Condensation Nuclei

CFCs	Chlorofluorocarbons
CH₃Br	Methyl bromide
CH₃I	Methyl Iodide
CH₃OH	Methyl alcohol
CH₄	Methane
CIMS	Chemical Ionization Mass Spectrometry
ClearfLo	Clean Air for London
CO	Carbon monoxide
COS	Carbonyl sulphide
CS₂	Carbon disulphide
CTMs	Chemical Transport Models
CVAO	Cape Verde Atmospheric Observatory
DMS	Dimethylsulphide
DOAS	Differential Optical Absorption Spectroscopy
ECD	Electron Capture Detector
ECN	Effective Carbon Number
EDGAR	Emission Databases for Global Atmospheric Research
EMEP	European Monitoring and Evaluation Programme
ER	Emission Ratio
EU HANSA	European Union Hydrocarbons Across the North Sea Atmosphere

FAAM	Facility for Airborne Atmospheric Measurements
FAGE	Fluorescence Assay by Gas Expansion
FGAM	Facility for Ground-based Atmospheric Measurements
FID	Flame Ionization Detector
FSL	Fused-silica-lined canisters
GAW	Global Atmospheric Watch
GC x GC	Two dimensional Gas Chromatography
GC-FID	Gas Chromatograph with Flame Ionisation Detectors
GCOS	Global Climate Observing System
GFED	Global Fire Emission Database
H₂S	Hydrogen sulphide
HANSA	Hydrocarbons Across the North Sea Atmosphere
HCHO	Formaldehyde
HETP	Height Equivalent to a Theoretical Plate
HID	Helium Ionisation Detector
HIRES	HIgh REsolution whole air Sampling system
HNO₃	Nitric acid
HONO	Nitrous acid
HYSPLIT	Hybrid single-particle Langrangian Integrated Trajectory
i.d.	Internal diameter
ITOP	International Transport for Ozone and Precursors

LIF	Laser Induced Fluorescence
MBL	Marine Boundary Layer
MDQ	Minimum Detectable Quantity
MFC	Mass Flow Controllers
MS	Mass Spectrometer
N_2O	Nitrous oxide
N_2O_5	Dinitrogen pentaoxide
NAMBLEX	North Atlantic Marine Boundary Layer Experiment
NBL	Nocturnal Boundary Layer
NCAR	National Centre for Atmospheric Research
NERC	Natural Environment Research Council
NH	Northern Hemisphere
NH_3	Ammonia
NH_4^+	Ammonium ion
NH_4NO_3	Ammonium nitrate
NIST	National Institute of Standards and Technology
NMHC	Non-Methane Hydrocarbons
NO	Nitric oxide
NO_2	Nitrogen dioxide
NO_3	Nitrate radical
NOAA	U.S National Oceanic and Atmospheric Administration

NO_x	$NO + NO_2$
NO_y	Total reactive nitrogen
NPD	Nitrogen Phosphorous Detector
NPL	UK National Physical Laboratory
$O\,(^1D)$	Excited singlet D oxygen atom
o.d.	Outer diameter
O_3	Ozone
OH	Hydroxyl radical
OP3	Oxidant and Particle Photochemical Processes above a South-East Asian Tropical Rain Forest
oVOCs	oxygenated Volatile Organic Compounds
PAN	Peroxyacetylnitrate
PBL	Planetary Boundary Layer
PCRF	Per Carbon Response Factors
PERCA	Peroxy Radical Chemical Amplifier
PID	Photo Ionization Detector
PLOT	Porous Layer Open Tubular Column
PORG	Photochemical Oxidant Review Group
ppbv	Parts per billion by volume
ppmv	Parts per million by volume
pptv	Parts per trillion by volume

PTR-MS	Proton Transfer Reaction Mass Spectrometry
R.F	Response factor
RETRO	Reanalysis of the tropospheric chemical composition of the last 40 years' project
RO$_2$	Peroxy radical
RONO$_2$	alkylnitrates
RONOCO	ROle of Nightime chemistry in controlling the Oxidizing Capacity of the AtmOsphere
SH	Southern Hemisphere
SO$_2$	Sulphur dioxide
SOAs	Secondary Organic Aerosols
SPADE	Stratospheric Photochemistry Aerosols and Dynamics Expedition
TCD	Thermal Conductivity Detector
TORCH	Tropospheric ORganic CHemistry
TRAC	Triggered Reterospective Air Collector
UK	United Kingdom
VOC	Volatile Organic Compounds
WAS	Whole Air Sampling System
WCC-VOC	World Calibration Centre for VOCs
WMO	World Meteorological Organization

References

Air quality expert group: Ozone in the United Kingdom, Department for Environment, Food and Rural Affairs, 2009.

Akagi, S. K., Yokelson, R. J., Wiedinmyer, C., Alvarado, M. J., Reid, J. S., Karl, T., Crounse, J. D., and Wennberg, P. O.: Emission factors for open and domestic biomass burning for use in atmospheric models, Atmos. Chem. Phys., 2011.

Aliwell, S. R., and Jones, R. L.: Measurements of tropospheric NO_3 at midlatitude, Journal of Geophysical Research-Atmospheres, 103, 5719-5727, 10.1029/97jd03119, 1998.

Allan, B. J., Carslaw, N., Coe, H., Burgess, R. A., and Plane, J. M. C.: Observations of the Nitrate Radical in the Marine Boundary Layer, J Atmos Chem, 33, 129-154, 10.1023/a:1005917203307, 1999.

Ambrose, J. L., Mao, H., Mayne, H. R., Stutz, J., Talbot, R., and Sive, B. C.: Nighttime nitrate radical chemistry at Appledore Island, Maine during the 2004 International Consortium for Atmospheric Research on Transport and Transformation, J. Geophys. Res., 112, D21302, 10.1029/2007jd008756, 2007.

Amiro, B. D., A Cantin, M D Flannigan, and Groot., W. J. D.: Future emissions from Canadian boreal forest fires., Canadian Journal of Forest Research 39, 383-395, 2009.

Andreae, M. O., and Crutzen, P. J.: Atmospheric Aerosols: Biogeochemical Sources and Role in Atmospheric Chemistry, Science, 276, 1052-1058, 10.1126/science.276.5315.1052, 1997.

Andreae, M. O., and Merlet, P.: Emission of trace gases and aerosols from biomass burning, Global Biogeochem. Cycles, 15, 955-966, 10.1029/2000gb001382, 2001.

Apel, E. C., Calvert, J. G., and Fehsenfeld, F. C.: The Nonmethane Hydrocarbon Intercomparison Experiment (NOMHICE): Tasks 1 and 2, J. Geophys. Res., 99, 16651-16664, 10.1029/94jd00086, 1994.

Aschmann, S. M., and Atkinson, R.: Rate Constants for the Gas-Phase Reactions of Alkanes with Cl Atoms at 296+/-2 K, International Journal of Chemical Kinetics, 27, 613-622, 1995.

Atkinson, R., and Aschmann, S. M.: Hydroxyl radical production from the gas-phase reactions of ozone with a series of alkenes under atmospheric conditions, Environ Sci Technol, 27, 1357-1363, 10.1021/es00044a010, 1993.

Atkinson, R.: Gas-phase tropospheric chemistry of organic compounds, , *J. Phys. ChemRef. D* 2, 216-234, 1994.

Atkinson, R., and Arey, J.: Atmospheric degradation of volatile organic compounds, Chemical Reviews, 103, 4605-4638, Doi 10.1021/Cr0206420, 2003.

Baker, A. K., Beyersdorf, A. J., Doezema, L. A., Katzenstein, A., Meinardi, S., Simpson, I. J., Blake, D. R., and Rowland, F. S.: Measurements of nonmethane hydrocarbons in 28 United States cities, Atmospheric Environment - ATMOS ENVIRON 42, 170-182, 2008.

Baker, A. K., Slemr, F., and Brenninkmeijer, C. A. M.: Analysis of non-methane hydrocarbons in air samples collected aboard the CARIBIC passenger aircraft, Atmos. Meas. Tech., 2010.

Bartenbach, S., Williams, J., Plass-Dülmer, C., Berresheim, H., and Lelieveld, J.: In-situ measurement of reactive hydrocarbons at Hohenpeissenberg with comprehensive two-dimensional gas chromatography (GCxGC-FID): use in estimating HO and NO_3, Atmos. Chem. Phys., 7, 1-14, 10.5194/acp-7-1-2007, 2007.

Bechara, J., Borbon, A., Jambert, C., and Perros, P. E.: New off-line aircraft instrumentation for non-methane hydrocarbon measurements, Anal Bioanal Chem, 392, 865-876, 10.1007/s00216-008-2330-3, 2008.

Bertschi, I., Yokelson, R. J., Ward, D. E., Babbitt, R. E., Susott, R. A., Goode, J. G., and Hao, W. M.: Trace gas and particle emissions from fires in large diameter and belowground biomass fuels, J. Geophys. Res., 108, 8472, 10.1029/2002jd002100, 2003.

Bey, I., Jacob, D. J., Yantosca, R. M., Logan, J. A., Field, B. D., Fiore, A. M., Li, Q., Liu, H. Y., Mickley, L. J., and Schultz, M. G.: Global modeling of tropospheric chemistry with assimilated meteorology: Model description and evaluation, J. Geophys. Res., 106, 23073-23095, 10.1029/2001jd000807, 2001.

Blake, N. J., Penkett, S. A., Clemitshaw, K. C., Anwyl, P., Lightman, P., Marsh, A. R. W., and Butcher, G.: Estimates of Atmospheric Hydroxyl Radical Concentrations from the Observed Decay of Many Reactive Hydrocarbons in Well-Defined Urban Plumes, Journal of Geophysical Research-Atmospheres, 98, 2851-2864, 1993.

Blake, N. J., and Blake, D. R.: TROPOSPHERIC COMPOSITION:VOCs:overview in: Encyclopedia of Atmospheric science, edited by: Holton, J. R., Pyle, J. A., and Curry, J. A., Academic Press, London,U.K, 2438-2445, 2002.

Blake, N. J., Blake, D. R., Sive, B. C., Katzenstein, A. S., Meinardi, S., Wingenter, O. W., Atlas, E. L., Flocke, F., Ridley, B. A., and Rowland, F. S.: The seasonal evolution of NMHCs and light alkyl nitrates at middle to high northern latitudes during TOPSE, Journal of Geophysical Research-Atmospheres, 108, 2003.

Bottenheim, J. W., and Shepherd, M. F.: C_2-C_6 hydrocarbon measurements at four rural locations across Canada, Atmos Environ, 29, 647-664, 1995.

Braithwaite, A., and Smith, F. J.: Chromatographic methods, Fourth ed., Chapman and Hall, 1985.

Brasseur, G. P., Orlando, J. J., Tyndall, G. S., and National Center for Atmospheric Research (U.S.): Atmospheric chemistry and global change, Topics in environmental chemistry, Oxford University Press, New York, xviii, 654 p. pp., 1999.

Broadgate, W. J., Liss, P. S., and Penkett, S. A.: Seasonal emissions of isoprene and other reactive hydrocarbon gases from the ocean, Geophys. Res. Lett., 24, 2675-2678, 10.1029/97gl02736, 1997.

Brown, S. S., Stark, H., and Ravishankara, A. R.: Applicability of the steady state approximation to the interpretation of atmospheric observations of NO_3 and N_2O_5, Journal of Geophysical Research-Atmospheres, 108, 2003.

Brown, S. S., Dubé, W. P., Peischl, J., Ryerson, T. B., Atlas, E., Warneke, C., de Gouw, J. A., te Lintel Hekkert, S., Brock, C. A., Flocke, F., Trainer, M., Parrish, D. D., Feshenfeld, F. C., and Ravishankara, A. R.: Budgets for nocturnal VOC oxidation by nitrate radicals aloft during the 2006 Texas Air Quality Study, Journal of Geophysical Research: Atmospheres, 116, n/a-n/a, 10.1029/2011jd016544, 2011.

Carslaw, N., Carpenter, L. J., Plane, J. M. C., Allan, B. J., Burgess, R. A., Clemitshaw, K. C., Coe, H., and Penkett, S. A.: Simultaneous observations of nitrate and peroxy radicals in the marine boundary layer, Journal of Geophysical Research: Atmospheres, 102, 18917-18933, 10.1029/97jd00399, 1997.

Christian, T. J., Kleiss, B., Yokelson, R. J., Holzinger, R., Crutzen, P. J., Hao, W. M., Saharjo, B. H., and Ward, D. E.: Comprehensive laboratory measurements of biomass-burning emissions: 1. Emissions from Indonesian, African, and other fuels, J. Geophys. Res., 108, 4719, 10.1029/2003jd003704, 2003.

Christian, T. J., Kleiss, B., Yokelson, R. J., Holzinger, R., Crutzen, P. J., Hao, W. M., Shirai, T., and Blake, D. R.: Comprehensive laboratory measurements of biomass-burning emissions: 2. First intercomparison of open-path FTIR, PTR-MS, and GC-MS/FID/ECD, J. Geophys. Res., 109, D02311, 10.1029/2003jd003874, 2004.

Crutzen, P. J., Heidt, L. E., Krasnec, J. P., Pollock, W. H., and Seiler, W.: Biomass burning as a source of atmospheric gases CO, H2, N2O, NO, CH3Cl and COS, Nature, 282, 253-256, 1979.

Crutzen, P. J., and Andreae, M. O.: Biomass Burning in the Tropics: Impact on Atmospheric Chemistry and Biogeochemical Cycles, Science, 250, 1669-1678, 10.1126/science.250.4988.1669, 1990.

de Gouw, J. A., Warneke, C., Stohl, A., Wollny, A. G., Brock, C. A., Cooper, O. R., Holloway, J. S., Trainer, M., Fehsenfeld, F. C., Atlas, E. L., Donnelly, S. G., Stroud, V., and Lueb, A.: Volatile organic compounds composition of merged and aged forest fire plumes from Alaska and western Canada, J. Geophys. Res., 111, D10303, 10.1029/2005jd006175, 2006.

Derwent, R. G., Hester, R. E., and Harrison, R. M.: Sources, distributions, and fates of VOCs in the atmosphere, in: Volatile Organic Compounds in the Atmosphere, The Royal Society of Chemistry, 1995.

Dettmer, K., Felix, U., Engewald, W., and Mohnke, M.: Application of a unique selective PLOT capillary column for the analysis of oxygenated compounds in ambient air, Chromatographia, 51, S221-S227, 10.1007/bf02492810, 2000.

Dettmer, K., and Engewald, W.: Ambient air analysis of volatile organic compounds using adsorptive enrichment, Chromatographia, 57, S339-S347, 10.1007/bf02492126, 2003.

Dewulf, J., Van Langenhove, H., and Wittmann, G.: Analysis of volatile organic compounds using gas chromatography, TrAC Trends in Analytical Chemistry, 21, 637-646, 2002.

Dietz, W. A.: Response factors for gas chromatography analyses, Journal of gas chromatography 5, 68-71, 1967.

Dillon, M. B., Lamanna, M. S., Schade, G. W., Goldstein, A. H., and Cohen, R. C.: Chemical evolution of the Sacramento urban plume: Transport and oxidation, Journal of Geophysical Research-Atmospheres, 107, 2002.

Dollard, G. J., Dumitrean, P., Telling, S., Dixon, J., and Derwent, R. G.: Observed trends in ambient concentrations of C_2-C_8 hydrocarbons in the United Kingdom over the period from 1993 to 2004, Atmos Environ, 41, 2559-2569, http://dx.doi.org/10.1016/j.atmosenv.2006.11.020, 2007.

Domingo, R. C.: Chromatography, in: Paint and Coating Testing Manual, Fifteen ed., edited by: Koleske, J. V., 2012.

Duarte-Davidson, R., Courage, C., Rushton, L., and Levy, L.: Benzene in the environment: an assessment of the potential risks to the health of the population, Occupational and Environmental Medicine, 58, 2-13, 10.1136/oem.58.1.2, 2001.

Duck, T. J., Firanski, B. J., Millet, D. B., Goldstein, A. H., Allan, J., Holzinger, R., Worsnop, D. R., White, A. B., Stohl, A., Dickinson, C. S., and van Donkelaar, A.: Transport of forest fire emissions from Alaska and the Yukon Territory to Nova Scotia during summer 2004, J. Geophys. Res., 112, D10S44, 10.1029/2006jd007716, 2007.

Ehhalt, D. H., Rudolph, J., Meixner, F., and Schmidt, U.: Measurements of selected C_2-C_5 hydrocarbons in the background troposphere: Vertical and latitudinal variations, J Atmos Chem, 3, 29-52, 10.1007/bf00049367, 1985.

Ehhalt, D. H., Rohrer, F., Wahner, A., Prather, M. J., and Blake, D. R.: On the use of hydrocarbons for the determination of tropospheric OH concentrations, Journal of Geophysical Research-Atmospheres, 103, 18981-18997, 1998.

Emmerson, K. M., Carslaw, N., Carslaw, D. C., Lee, J. D., McFiggans, G., Bloss, W. J., Gravestock, T., Heard, D. E., Hopkins, J., Ingham, T., Pilling, M. J., Smith, S. C., Jacob, M., and Monks, P. S.: Free radical modelling studies during the UK TORCH Campaign in Summer 2003, Atmos. Chem. Phys, 7, 167-181, 2007.

Trends in Atmospheric Carbon Dioxide: www.esrl.noaa.gov/gmd/ccgg/trends/, 2012.

Fehsenfeld, F. C., Ancellet, G., Bates, T. S., Goldstein, A. H., Hardesty, R. M., Honrath, R., Law, K. S., Lewis, A. C., Leaitch, R., McKeen, S., Meagher, J., Parrish, D. D., Pszenny, A. A. P., Russell, P. B., Schlager, H., Seinfeld, J., Talbot, R., and Zbinden, R.: International Consortium for Atmospheric Research on Transport and Transformation (ICARTT): North America to Europe-;Overview of the 2004 summer field study, J. Geophys. Res., 111, D23S01, 10.1029/2006jd007829, 2006.

Finlayson-Pitts, B. J., and Pitts, J. N.: Chemistry of the upper and lower atmosphere : theory, experiments and applications, Academic Press, San Diego, Calif. ; London, xxii, 969 p. pp., 2000.

Flannigan, M. D., Logan, K. A., Amiro, B. D., Skinner, W. R., and and Stocks, B. J.: Future area burned in Canada, *Clim. Change*, 72, 1-16, 2005.

Fleming, Z. L., Monks, P. S., Rickard, A. R., Bandy, B. J., Brough, N., Green, T. J., Reeves, C. E., and Penkett, S. A.: Seasonal dependence of peroxy radical concentrations at a Northern hemisphere marine boundary layer site during summer and winter: evidence for radical activity in winter, Atmos Chem Phys, 6, 5415-5433, 2006.

Fromm, M., Alfred, J., Hoppel, K., Hornstein, J., Bevilacqua, R., Shettle, E., Servranckx, R., Li, Z., and Stocks, B.: Observations of boreal forest fire smoke in the stratosphere by POAM III, SAGE II, and lidar in 1998, Geophys. Res. Lett., 27, 1407-1410, 10.1029/1999gl011200, 2000.

Gautrois, M., Brauers, T., Koppmann, R., Rohrer, F., Stein, O., and Rudolph, J.: Seasonal variability and trends of volatile organic compounds in the lower polar troposphere, Journal of Geophysical Research: Atmospheres, 108, n/a-n/a, 10.1029/2002jd002765, 2003.

GAW Report No 111: WMO-BMBF Workshop on VOC, 1995.

GAW Report No 171: A WMO/GAW Expert Workshop on Global Long-Term Measurements of Volatile Organic Compounds (VOCs), 2006.

Geyer, A., Alicke, B., Konrad, S., Schmitz, T., Stutz, J., and Platt, U.: Chemistry and oxidation capacity of the nitrate radical in the continental boundary layer near Berlin, J. Geophys. Res., 106, 8013-8025, 10.1029/2000jd900681, 2001.

Girardin, M. P.: Interannual to decadal changes in area burned in Canada from 1781 to 1982 and the relationship to Northern Hemisphere land temperatures, Global Ecology and Biogeography, 16, 557-566, 10.1111/j.1466-8238.2007.00321.x, 2007.

Gnauk, T., and Rolle, W.: A Three-year Study of Nonmethane Hydrocarbons in Surface Air over Saxony (Germany), J Atmos Chem, 30, 371-395, 10.1023/a:1006001020538, 1998.

Goldan, P. D., Parrish, D. D., Kuster, W. C., Trainer, M., McKeen, S. A., Holloway, J., Jobson, B. T., Sueper, D. T., and Fehsenfeld, F. C.: Airborne measurements of isoprene, CO, and anthropogenic hydrocarbons and their implications, Journal of Geophysical Research: Atmospheres, 105, 9091-9105, 10.1029/1999jd900429, 2000.

Goldstein, A. H., Daube, B. C., Munger, J. W., and Wofsy, S. C.: Automated in-situ monitoring of atmospheric non-methane hydrocarbon concentrations and gradients, J Atmos Chem, 21, 43-59, 10.1007/bf00712437, 1995a.

Goldstein, A. H., Wofsy, S. C., and Spivakovsky, C. M.: Seasonal variations of nonmethane hydrocarbons in rural New England: Constraints on OH concentrations in northern midlatitudes, J. Geophys. Res., 100, 21023-21033, 10.1029/95jd02034, 1995b.

Gong, Q., and Demerjian, K. L.: Measurement and analysis of C_2-C_{10} hydrocarbons at Whiteface Mountain, New York, Journal of Geophysical Research: Atmospheres, 102, 28059-28069, 10.1029/97jd02703, 1997.

Grant, A., Yates, E. L., Simmonds, P. G., Derwent, R. G., Manning, A. J., Young, D., Shallcross, D. E., and O'Doherty, S.: A five year record of high-frequency in situ measurements of non-methane hydrocarbons at Mace Head, Ireland, Atmos. Meas. Tech., 4, 955-964, 2011.

Greenberg, J. P., Zimmerman, P. R., Pollock, W. F., Lueb, R. A., and Heidt, L. E.: Diurnal variability of atmospheric methane, nonmethane hydrocarbons, and carbon monoxide at Mauna Loa, Journal of Geophysical Research: Atmospheres, 97, 10395-10413, 10.1029/91jd02295, 1992.

Greenberg, J. P., Helmig, D., and Zimmerman, P. R.: Seasonal measurements of nonmethane hydrocarbons and carbon monoxide at the Mauna Loa Observatory during the Mauna Loa Observatory Photochemistry Experiment 2, J. Geophys. Res., 101, 14581-14598, 10.1029/95jd01543, 1996.

Guenther, A., Hewitt, C. N., Erickson, D., Fall, R., Geron, C., Graedel, T., Harley, P., Klinger, L., Lerdau, M., McKay, W. A., Pierce, T., Scholes, B., Steinbrecher, R., Tallamraju, R., Taylor, J., and Zimmerman, P.: A global model of natural volatile organic compound emissions, J. Geophys. Res., 100, 8873-8892, 10.1029/94jd02950, 1995.

Haggen-Smit, A. J.: Chemistry and physiology of Los Angles smog, Ind.Eng.Chem., 44, 1342-1346, 1952.

Hakola, H., Heidi, H., and Laurila, T.: Ten years of light hydrocarbons (C_2-C_6) concentration measurements in background air in Finland, Atmos Environ, 40, 3621-3630, http://dx.doi.org/10.1016/j.atmosenv.2005.08.019, 2006.

Halliday, J., Hamilton, J., Rhodes, C., Lewis, A., Bartle, K., Homewood, P., Grenfell, R., Goody, B., Harling, A., and Brewer, P.: Lab-on-a-chip GC for environmental research, LC-GC Europe, 23, 2010.

Hamilton, J. F., and Lewis, A. C.: Chromatographic Methods, in: Analytical Techniques for Atmospheric Measurement, Blackwell Publishing, 361-405, 2007.

Harper, M.: Sorbent trapping of volatile organic compounds from air, J Chromatogr A, 885, 129-151, http://dx.doi.org/10.1016/S0021-9673(00)00363-0, 2000.

Harrison, R. M.: Pollution : causes, effects and control, 4th ed., Royal Society of Chemistry, Cambridge, xxiv, 579 p. pp., 2001.

Harrison, R. M., Yin, J., Tilling, R. M., Cai, X., Seakins, P. W., Hopkins, J. R., Lansley, D. L., Lewis, A. C., Hunter, M. C., Heard, D. E., Carpenter, L. J., Creasey, D. J., Lee, J. D., Pilling, M. J., Carslaw, N., Emmerson, K. M., Redington, A., Derwent, R. G., Ryall, D., Mills, G., and Penkett, S. A.: Measurement and modelling of air pollution and atmospheric chemistry in the U.K. West Midlands conurbation: Overview of the PUMA Consortium project, Sci Total Environ, 360, 5-25, http://dx.doi.org/10.1016/j.scitotenv.2005.08.053, 2006.

Heard, D. E.: Field Measurements of Atmospheric Composition, in: Analytical Techniques for Atmospheric Measurement, Blackwell Publishing, 1-71, 2007.

Heintz, F., Platt, U., Flentje, H., and Dubois, R.: Long-term observation of nitrate radicals at the Tor Station, Kap Arkona (Rügen), J. Geophys. Res., 101, 22891-22910, 10.1029/96jd01549, 1996.

Helmig, D.: Air analysis by gas chromatography, J Chromatogr A, 843, 129-146, http://dx.doi.org/10.1016/S0021-9673(99)00173-9, 1999.

Helmig, D., Tanner, D. M., Honrath, R. E., Owen, R. C., and Parrish, D. D.: Nonmethane hydrocarbons at Pico Mountain, Azores: 1. Oxidation chemistry in the North Atlantic region, Journal of Geophysical Research-Atmospheres, 113, 2008.

Helmig, D., Bottenheim, J., Galbally, I. E., Lewis, A., Milton, M. J. T., Penkett, S., Plass-Duelmer, C., Reimann, S., Tans, P., and Thiel, S.: Volatile Organic Compounds in the Global Atmosphere, Eos Trans. AGU, 90, 10.1029/2009eo520001, 2009.

Henze, D. K., Seinfeld, J. H., Ng, N. L., Kroll, J. H., Fu, T.-M., Jacob, D. J., and Heald, C. L.: Global modeling of secondary organic aerosol formation from aromatic hydrocarbons: high- vs. low-yield pathways, Atmos. Chem. Phys., 8, 2405-2420, 2008.

Holzinger, R., Williams, J., Salisbury, G., Klüpfel , T., de Reus, M., Traub, M., Crutzen, P. J., and Lelieveld, J.: Oxygenated compounds in aged biomass burning plumes over the Eastern Mediterranean: evidence for strong secondary production of methanol and acetone, Atmos. Chem. Phys., 5, 39-46, 2005.

Hopkins, J. R.: Analysis of Atmospheric Hydrocarbons in Urban,Rural and Remote Marine Boundary Layers, PhD thesis, Chemistry, University of Leeds, 2001.

Hopkins, J. R., Jones, I. D., Lewis, A. C., McQuaid, J. B., and Seakins, P. W.: Non-methane hydrocarbons in the Arctic boundary layer, Atmos Environ, 36, 3217-3229, 2002.

Hopkins, J. R., Lewis, A. C., and Read, K. A.: A two-column method for long-term monitoring of non-methane hydrocarbons (NMHCs) and oxygenated volatile organic compounds (o-VOCs), Journal of Environmental Monitoring, 5, 8-13, 10.1039/b202798d, 2003.

Hopkins, J. R., Jones, C. E., and Lewis, A. C.: A dual channel gas chromatograph for atmospheric analysis of volatile organic compounds including oxygenated and monoterpene compounds, Journal of Environmental Monitoring, 13, 2268-2276, Doi 10.1039/C1em10050e, 2011.

Hov, Ã. y., and Schmidbauer, N.: Atmospheric concentrations of nonmethane hydrocarbons at a North European coastal site, J Atmos Chem, 14, 515-526, 10.1007/bf00115255, 1992.

Hyde, J. C., Smith, A. M. S., Ottmar, R. D., Alvarado, E. C., and Morgan, P.: The combustion of sound and rotten coarse woody debris: a review, International Journal of Wildland Fire, 20, 163-174, http://dx.doi.org/10.1071/WF09113, 2011.

Intergovernmental Panel on Climate Change, Climate Change 2001: The Scientific basis, 2001.

IUPAC: Recommendation on Nomenclature for Chromatography, Pure Appl. Chem., 37, 447, 1974.

Jacobson, M. Z.: Atmospheric pollution : history, science, and regulation, Cambridge University Press, Cambridge, UK ; New York, xi, 399 p. pp., 2002.

Jaffe, D. A., and Wigder, N. L.: Ozone production from wildfires: A critical review, Atmos Environ, 51, 1-10, http://dx.doi.org/10.1016/j.atmosenv.2011.11.063, 2012.

Ji, Z., Majors, R. E., and Guthrie, E. J.: Porous layer open-tubular capillary columns: preparations, applications and future directions, J Chromatogr A, 842, 115-142, http://dx.doi.org/10.1016/S0021-9673(99)00126-0, 1999.

Jobson, B. T., Niki, H., Yokouchi, Y., Bottenheim, J., Hopper, F., and Leaitch, R.: Measurements of C_2-C_6 hydrocarbons during the Polar Sunrise1992 Experiment: Evidence for Cl atom and Br atom chemistry, J. Geophys. Res., 99, 25355-25368, 10.1029/94jd01243, 1994.

Jobson, B. T., Parrish, D. D., Goldan, P., Kuster, W., Fehsenfeld, F. C., Blake, D. R., Blake, N. J., and Niki, H.: Spatial and temporal variability of nonmethane hydrocarbon mixing ratios and their relation to photochemical lifetime, Journal of Geophysical Research-Atmospheres, 103, 13557-13567, 1998.

Jobson, B. T., McKeen, S. A., Parrish, D. D., Fehsenfeld, F. C., Blake, D. R., Goldstein, A. H., Schauffler, S. M., and Elkins, J. W.: Trace gas mixing ratio variability versus lifetime in the troposphere and stratosphere: Observations, Journal of Geophysical Research D: Atmospheres, 104, 16091-16113, 1999.

Jost, C., Trentmann, J., Sprung, D., Andreae, M. O., McQuaid, J. B., and Barjat, H.: Trace gas chemistry in a young biomass burning plume over Namibia: Observations and model simulations, Journal of Geophysical Research: Atmospheres, 108, n/a-n/a, 10.1029/2002jd002431, 2003.

Jost, H.-J., Drdla, K., Stohl, A., Pfister, L., Loewenstein, M., Lopez, J. P., Hudson, P. K., Murphy, D. M., Cziczo, D. J., Fromm, M., Bui, T. P., Dean-Day, J., Gerbig, C., Mahoney, M. J., Richard, E. C., Spichtinger, N., Pittman, J. V., Weinstock, E. M., Wilson, J. C., and Xueref, I.: In-situ observations of mid-latitude forest fire plumes deep in the stratosphere, Geophys. Res. Lett., 31, L11101, 10.1029/2003gl019253, 2004.

Junge, C. E.: Residence time and variability of tropospheric trace gases, Tellus, 26, 477-488, 10.1111/j.2153-3490.1974.tb01625.x, 1974.

Karl, T., Crutzen, P. J., Mandl, M., Staudinger, M., Guenther, A., Jordan, A., Fall, R., and Lindinger, W.: Variability-lifetime relationship of VOCs observed at the Sonnblick Observatory 1999-estimation of HO-densities, Atmos Environ, 35, 5287-5300, 2001.

Kasischke, E. S., and Stocks, B. J.: Introduction, in: Fire, Climate Change, and Carbon Cycling in the Boreal Forest, edited by: Kasischke, E. S., and Stocks, B. J., Ecological Studies, Springer New York, 2000.

Kasischke, E. S., Hyer, E. J., Novelli, P. C., Bruhwiler, L. P., French, N. H. F., Sukhinin, A. I., Hewson, J. H., and Stocks, B. J.: Influences of boreal fire emissions on Northern Hemisphere atmospheric carbon and carbon monoxide, Global Biogeochem. Cycles, 19, GB1012, 10.1029/2004gb002300, 2005.

Kasischke, E. S., and Turetsky, M. R.: Recent changes in the fire regime across the North American boreal region—Spatial and temporal patterns of burning across Canada and Alaska, Geophys. Res. Lett., 33, L09703, 10.1029/2006gl025677, 2006.

Khan, M. A. H., Ashfold, M. J., Nickless, G., Martin, D., Watson, L. A., Hamer, P. D., Wayne, R. P., Canosa-Mas, C. E., and Shallcross, D. E.: Night-time NO_3 and OH radical concentrations in the United Kingdom inferred from hydrocarbon measurements, Atmospheric Science Letters, 9, 140-146, 10.1002/asl.175, 2008.

Khan, M. A. H., Hoque, M. M. N., Alam, S. S., Ashfold, M. J., Nickless, G., and Shallcross, D. E.: Estimation and comparison of night-time OH levels in the UK urban atmosphere using two different analysis methods, Journal of Environmental Sciences, 23, 60-64, http://dx.doi.org/10.1016/S1001-0742(10)60373-7, 2011.

Klemp, D., Kley, D., Kramp, F., Buers, H. J., Pilwat, G., Flocke, F., Pätz, H. W., and Volz-Thomas, A.: Long-Term Measurements of Light Hydrocarbons (C_2-C_5) at Schauinsland (Black Forest), J Atmos Chem, 28, 135-171, 10.1023/a:1005878018619, 1997.

Kley, D.: Tropospheric Chemistry and Transport, Science, 276, 1043-1044, 10.1126/science.276.5315.1043, 1997.

Koppmann, R.: Volatile organic compounds in the atmosphere, 1st ed., Blackwell Pub., Oxford ; Ames, Iowa, xii, 500 p. pp., 2007.

Krol, M., van Leeuwen, P. J., and Lelieveld, J.: Global OH trend inferred from methylchloroform measurements, J. Geophys. Res., 103, 10697-10711, 10.1029/98jd00459, 1998.

Kumar, A., and Viden, I.: Volatile Organic Compounds: Sampling Methods and Their Worldwide Profile in Ambient Air, Environmental Monitoring and Assessment, 131, 301-321, 10.1007/s10661-006-9477-1, 2007.

Laurila, T., and Hakola, H.: Seasonal cycle of C_2-C_5 hydrocarbons over the Baltic Sea and Northern Finland, Atmos Environ, 30, 1597-1607, 1996.

Lewis, A. C., Bartle, K. D., Heard, D. E., McQuaid, J. B., Pilling, M. J., and Seakins, P. W.: *In situ*, gas chromatographic measurements of non-methane hydrocarbons and dimethylsulfide at a remote coastal location (Mace Head, Eire) July-August 1996, Journal of the Chemical Society, Faraday Transactions, 93, 1997.

Lewis, A. C., Evans, M. J., Methven, J., Watson, N., Lee, J. D., Hopkins, J. R., Purvis, R. M., Arnold, S. R., McQuaid, J. B., Whalley, L. K., Pilling, M. J., Heard, D. E., Monks, P. S., Parker, A. E., Reeves, C. E., Oram, D. E., Mills, G., Bandy, B. J., Stewart, D., Coe, H., Williams, P., and Crosier, J.: Chemical composition observed over the mid-Atlantic and the detection of pollution signatures far from source regions, J. Geophys. Res., 112, D10S39, 10.1029/2006jd007584, 2007.

Lewis, A. C., Evans, M. J., Hopkins, J. R., Punjabi, S., Read, K. A., Andrews, S., Moller, S. J., Carpenter, L. J., Lee, J. D., Rickard, A. R., Palmer, P. I., and Parrington, M.: The influence of boreal forest fires on the global distribution of non-methane hydrocarbons, Atmos. Chem. Phys. Discuss., 12, 23433-23469, 10.5194/acpd-12-23433-2012, 2012.

Lidster, R. T., Hamilton, J. F., and Lewis, A. C.: The application of two total transfer valve modulators for comprehensive two-dimensional gas chromatography of volatile organic compounds, Journal of Separation Science, 34, 812-821, 10.1002/jssc.201000710, 2011.

Lightman, P., Kallend, A. S., Marsh, A. R. W., Jones, B. M. R., and Penkett, S. A.: Seasonal variation of hydrocarbons in the free troposphere at mid-latitudes, Tellus B, 42, 408-422, 10.1034/j.1600-0889.1990.t01-4-00002.x, 1990.

Marlon, J. R., Bartlein, P. J., Carcaillet, C., Gavin, D. G., Harrison, S. P., Higuera, P. E., Joos, F., Power, M. J., and Prentice, I. C.: Climate and human influences on global biomass burning over the past two millennia, Nature Geosci, 1, 697-702, 2008.

Martinez, M., Perner, D., Hackenthal, E. M., Kulzer, S., and Schutz, L.: NO3 at Helgoland during the NORDEX campaign in October 1996, Journal of Geophysical Research-Atmospheres, 105, 22685-22695, 10.1029/2000jd900255, 2000.

McKeen, S. A., Trainer, M., Hsie, E. Y., Tallamraju, R. K., and Liu, S. C.: On the indirect determination of atmospheric OH radical concentrations from reactive hydrocarbon measurements, Journal of Geophysical Research: Atmospheres, 95, 7493-7500, 10.1029/JD095iD06p07493, 1990.

McKeen, S. A., and Liu, S. C.: Hydrocarbon ratios and photochemical history of air masses, Geophys. Res. Lett., 20, 2363-2366, 10.1029/93gl02527, 1993.

McKeen, S. A., Liu, S. C., Hsie, E. Y., Lin, X., Bradshaw, J. D., Smyth, S., Gregory, G. L., and Blake, D. R.: Hydrocarbon ratios during PEM-WEST A: A model perspective, Journal of Geophysical Research-Atmospheres, 101, 2087-2109, 1996.

McLaren, R., Salmon, R. A., Liggio, J., Hayden, K. L., Anlauf, K. G., and Leaitch, W. R.: Nighttime chemistry at a rural site in the Lower Fraser Valley,

Atmos Environ, 38, 5837-5848, http://dx.doi.org/10.1016/j.atmosenv.2004.03.074, 2004.

Miller, J. M.: Chromatography: Concepts and Contrasts, Wiley Interscience, New York, 1987.

Monks, P. S.: A review of the observations and origins of the spring ozone maximum, Atmos Environ, 34, 3545-3561, http://dx.doi.org/10.1016/S1352-2310(00)00129-1, 2000.

Monks, P. S.: Gas-phase radical chemistry in the troposphere, Chem Soc Rev, 34, 2005.

Nelson, P. F., and Quigley, S. M.: Nonmethane hydrocarbons in the atmosphere of Sydney, Australia, Environ Sci Technol, 16, 650-655, 10.1021/es00104a005, 1982.

Noxon, J. F., Norton, R. B., and Marovich, E.: NO3 in the troposphere, Geophys. Res. Lett., 7, 125-128, 10.1029/GL007i002p00125, 1980.

Palmer, P. I., Parrington, M., Lee, J. D., Lewis, A. C., Rickard, A. R., Bernath, P. F., Duck, T. J., Waugh, D. L., Tarasick, D. W., Andrews, S., Aruffo, E., Bailey, L. J., Barrett, E., Bauguitte, S. J.-B., Curry, K. R., Di Carlo, P., Chisholm, L., Dan, L., Forster, G., Franklin, J. E., Gibson, M. D., Griffin, D., Helmig, D., Hopkins, J. R., Hopper, J. T., Jenkin, M. E., Kindred, D., Kliever, J., Le Breton, M., Matthiesen, S., Maurice, M., Moller, S., Moore, D. P., Oram, D. E., O'Shea, S. J., Christopher Owen, R., Pagniello, C. M. L. S., Pawson, S., Percival, C. J., Pierce, J. R., Punjabi, S., Purvis, R. M., Remedios, J. J., Rotermund, K. M., Sakamoto, K. M., da Silva, A. M., Strawbridge, K. B., Strong, K., Taylor, J., Trigwell, R., Tereszchuk, K. A., Walker, K. A., Weaver, D., Whaley, C., and Young, J. C.: Quantifying the impact of BOReal forest fires on Tropospheric oxidants over the Atlantic using Aircraft and Satellites (BORTAS) experiment: design, execution and science overview, Atmos. Chem. & Phys. Discussion, 13, 4127-4181, 2012.

Parrish, D. D., Hahn, C. J., Williams, E. J., Norton, R. B., Fehsenfeld, F. C., Singh, H. B., Shetter, J. D., Gandrud, B. W., and Ridley, B. A.: Indications of photochemical histories of Pacific air masses from measurments of atmospheric trace species at Point Arena, California, Journal of Geophysical Research-Atmospheres, 97, 15883-15901, 1992.

Parrish, D. D., Dunlea, E. J., Atlas, E. L., Schauffler, S., Donnelly, S., Stroud, V., Goldstein, A. H., Millet, D. B., McKay, M., Jaffe, D. A., Price, H. U., Hess, P. G., Flocke, F., and Roberts, J. M.: Changes in the photochemical environment of the temperate North Pacific troposphere in response to increased Asian emissions, Journal of Geophysical Research-Atmospheres, 109, 2004.

Parrish, D. D., Stohl, A., Forster, C., Atlas, E. L., Blake, D. R., Goldan, P. D., Kuster, W. C., and de Gouw, J. A.: Effects of mixing on evolution of hydrocarbon ratios in the troposphere, Journal of Geophysical Research-Atmospheres, 112, 2007.

Penkett, S. A., and Brice, K. A.: The spring maximum in photo-oxidants in the Northern Hemisphere troposphere, Nature, 319, 655-657, 1986.

Penkett, S. A., Blake, N. J., Lightman, P., Marsh, A. R. W., Anwyl, P., and Butcher, G.: The Seasonal-Variation of Nonmethane Hydrocarbons in the Free Troposphere over the North-Atlantic Ocean - Possible Evidence for Extensive Reaction of Hydrocarbons with the Nitrate Radical, Journal of Geophysical Research-Atmospheres, 98, 2865-2885, 1993.

Penkett, S. A., Burgess, R. A., Coe, H., Coll, I., Hov, O., Lindskog, A., Schmidbauer, N., Solberg, S., Roemer, M., Thijsse, T., Beck, J., and Reeves, C. E.: Evidence for large average concentrations of the nitrate radical (NO_3) in Western Europe from the HANSA hydrocarbon database, Atmos Environ, 41, 3465-3478, 2007.

Plass-Dulmer, C., Michl, K., Ruf, R., and Berresheim, H.: C_2 -C_8 Hydrocarbon measurement and quality control procedures at the Global Atmosphere Watch

Observatory Hohenpeissenberg, J Chromatogr A, 953, 175-197, http://dx.doi.org/10.1016/S0021-9673(02)00128-0, 2002.

Platt, U., Perner, D., Winer, A. M., Harris, G. W., and Pitts, J. N., Jr.: Detection of NO_3 in the polluted troposphere by differential optical absorption, Geophys. Res. Lett., 7, 89-92, 10.1029/GL007i001p00089, 1980.

Platt, U., and Janssen, C.: Observation and role of the free radicals NO_3, ClO, BrO and IO in the troposphere, Faraday Discussions, 100, 175-198, 1995.

Platt, U., and Stutz, J.: Differential Optical Absorption Spectroscopy, Springer London, Limited, 2008.

Pollmann, J., Helmig, D., Hueber, J., Plass-Dülmer, C., and Tans, P.: Sampling, storage, and analysis of C_2-C_7 non-methane hydrocarbons from the US National Oceanic and Atmospheric Administration Cooperative Air Sampling Network glass flasks, J Chromatogr A, 1188, 75-87, http://dx.doi.org/10.1016/j.chroma.2008.02.059, 2008.

PORG report: Ozone in the United Kingdom, 1997.

Pozzer, A., Pollmann, J., Taraborrelli, D., Jöckel, P., Helmig, D., Tans, P., Hueber, J., and Lelieveld, J.: Observed and simulated global distribution and budget of atmospheric C2-C5 alkanes, Atmos. Chem. Phys., 10, 4403-4422, 2010.

Price, H. U., Jaffe, D. A., Cooper, O. R., and Doskey, P. V.: Photochemistry, ozone production, and dilution during long-range transport episodes from Eurasia to the northwest United States, Journal of Geophysical Research-Atmospheres, 109, 2004.

Purvis, R. M., Lewis, A. C., Carney, R. A., McQuaid, J. B., Arnold, S. R., Methven, J., Barjat, H., Dewey, K., Kent, J., Monks, P. S., Carpenter, L. J., Brough, N., Penkett, S. A., and Reeves, C. E.: Rapid uplift of nonmethane

hydrocarbons in a cold front over central Europe, J. Geophys. Res., 108, 4224, 10.1029/2002jd002521, 2003.

Purvis, R. M., McQuaid, J. B., Lewis, A. C., Hopkins, J. R., and Simmonds, P.: Horizontal and vertical profiles of ozone, carbon monoxide, non-methane hydrocarbons and dimethyl sulphide near the Mace Head observatory, Ireland, Atmos. Chem. Phys. Discuss., 5, 12505-12530, 2005.

Rauthe-Schoch, A., Weigelt, A., Hermann, M., Martinsson, B. G., Baker , A. K., Heue, K.-P., Brenninkmeijer, C. A. M., Zahn, A., Scharffe, D., Eckhardt, S., Stohl, A., and Van Velthoven, P. F. J.: CARIBIC aircraft measurements of Eyjafjallajokull volcanic clouds ¨in April/May 2010, Atmos Chem Phys, 2012.

Read, K. A., Lee, J. D., Lewis, A. C., Moller, S. J., Mendes, L., and Carpenter, L. J.: Intra-annual cycles of NMVOC in the tropical marine boundary layer and their use for interpreting seasonal variability in CO, Journal of Geophysical Research: Atmospheres, 114, n/a-n/a, 10.1029/2009jd011879, 2009.

Rivett, A. C., Martin, D., Gray, D. J., Price, C. S., Nickless, G., Simmonds, P. G., O'Doherty, S. J., Greally, B. R., Knights, A., and Shallcross, D. E.: The role of volatile organic compounds in the polluted urban atmosphere of Bristol, England, Atmos. Chem. Phys., 3, 1165-1176, 2003.

Rudolph, J., and Ehhalt, D. H.: Measurements of C_2–C_5 hydrocarbons over the North Atlantic, Journal of Geophysical Research: Oceans, 86, 11959-11964, 10.1029/JC086iC12p11959, 1981.

Rudolph, J., Khedim, A., and Wagenbach, D.: The seasonal variation of light nonmethane hydrocarbons in the Antarctic troposphere, Journal of Geophysical Research: Atmospheres, 94, 13039-13044, 10.1029/JD094iD10p13039, 1989.

Rudolph, J., and Johnen, F. J.: Measurements of Light Atmospheric Hydrocarbons over the Atlantic in Regions of Low Biological-Activity, Journal of Geophysical Research-Atmospheres, 95, 20583-20591, 1990.

Rudolph, J.: The tropospheric distribution and budget of ethane, Journal of Geophysical Research: Atmospheres, 100, 11369-11381, 10.1029/95jd00693, 1995.

Rudolph, J., Ramacher, B., PlassDulmer, C., Muller, K. P., and Koppmann, R.: The indirect determination of chlorine atom concentration in the troposphere from changes in the patterns of non-methane hydrocarbons, Tellus B, 49, 592-601, 1997.

Russo, R. S., Zhou, Y., White, M. L., Mao, H., Talbot, R., and Sive, B. C.: Multi-year (2004-2008) record of nonmethane hydrocarbons and halocarbons in New England: seasonal variations and regional sources, Atmos Chem Phys, 10, 4909-4929, DOI 10.5194/acp-10-4909-2010, 2010.

Schultz, M., Rast, S., van het Bolscher, M., Pulles, T., Brand, R., Pereira, J., Mota, B., Spessa, A., Dalsøren, S., van Nojie, T., and Szopa, S.: Emission data sets and methodologies for estimating emissions, RETRO project report D1-6, Hamburg, , 2007.

Seinfeld, J. H.: Urban Air Pollution: State of the Science, Science, 243, 745-752, 1989.

Seinfeld, J. H., and Pandis, S. N.: Atmospheric chemistry and physics : from air pollution to climate change, Wiley, New York, xxvii, 1326 p. pp., 1998.

Sharma, U. K., Kajii, Y., and Akimoto, H.: Seasonal variation of C_2-C_6 NMHCs at Happo, a remote site in Japan, Atmos Environ, 34, 4447-4458, 2000.

Shi, J., and Bernhard, M. J.: Kinetic studies of Cl-atom reactions with selected aromatic compounds using the photochemical reactor-FTIR spectroscopy technique, International Journal of Chemical Kinetics, 29, 349-358, 10.1002/(sici)1097-4601(1997)29:5<349::aid-kin5>3.0.co;2-u, 1997.

Simpson, I. J., Akagi, S. K., Barletta, B., Blake, N. J., Choi, Y., Diskin, G. S., Fried, A., Fuelberg, H. E., Meinardi, S., Rowland, F. S., Vay, S. A., Weinheimer,

A. J., Wennberg, P. O., Wiebring, P., Wisthaler, A., Yang, M., Yokelson, R. J., and Blake, D. R.: Boreal forest fire emissions in fresh Canadian smoke plumes: C1-C10 volatile organic compounds (VOCs), CO2, CO, NO2, NO, HCN and CH3CN, Atmos. Chem. Phys., 11, 6445, 2011.

Simpson, I. J., Sulbaek Andersen, M. P., Meinardi, S., Bruhwiler, L., Blake, N. J., Helmig, D., Rowland, F. S., and Blake, D. R.: Long-term decline of global atmospheric ethane concentrations and implications for methane, Nature, 488, 490-494, 2012.

Singh, H., and Kasting, J.: Chlorine-hydrocarbon photochemistry in the marine troposphere and lower stratosphere, J Atmos Chem, 7, 261-285, 1988.

Singh, H. B., and Salas, L. J.: Measurement of selected light hydrocarbons over the Pacific Ocean: Latitudinal and seasonal variations, Geophys. Res. Lett., 9, 842-845, 10.1029/GL009i008p00842, 1982.

Sinha, P., Hobbs, P. V., Yokelson, R. J., Bertschi, I. T., Blake, D. R., Simpson, I. J., Gao, S., Kirchstetter, T. W., and Novakov, T.: Emissions of trace gases and particles from savanna fires in southern Africa, Journal of Geophysical Research: Atmospheres, 108, n/a-n/a, 10.1029/2002jd002325, 2003.

Skoog, D. A.: Fundamentals of analytical chemistry, 8th ed., Thomson-Brooks/Cole, Belmont, CA, 1 v. (various pagings) pp., 2004.

Slemr, J., Slemr, F., D'Souza, H., and Partridge, R.: Study of the relative response factors of various gas chromatograph-flame ionisation detector systems for measurement of C_2-C_9 hydrocarbons in air, J Chromatogr A, 1061, 75-84, http://dx.doi.org/10.1016/j.chroma.2004.10.037, 2004.

Smyth, S., Bradshaw, J., Sandholm, S., Liu, S., McKeen, S., Gregory, G., Anderson, B., Talbot, R., Blake, D., Rowland, S., Browell, E., Fenn, M., Merrill, J., Bachmeier, S., Sachse, G., Collins, J., Thornton, D., Davis, D., and Singh, H.: Comparison of free tropospheric western Pacific air mass classification schemes

for the PEM-West A experiment, Journal of Geophysical Research-Atmospheres, 101, 1743-1762, 1996.

Soja, A. J., Tchebakova, N. M., French, N. H. F., Flannigan, M. D., Shugart, H. H., Stocks, B. J., Sukhinin, A. I., Parfenova, E. I., Chapin III, F. S., and Stackhouse Jr., P. W.: Climate-induced boreal forest change: Predictions versus current observations, , Global Planet. Change, , 56, 274-296, 2007.

Solomon, S., Smith, J. P., Sanders, R. W., Perliski, L., Miller, H. L., Mount, G. H., Keys, J. G., and Schmeltekopf, A. L.: Visible and near-ultraviolet spectroscopy at McMurdo Station, Antarctica: 8. Observations of nighttime NO_2 and NO_3 from April to October 1991, Journal of Geophysical Research: Atmospheres, 98, 993-1000, 10.1029/92jd02390, 1993.

Sternberg, J. C., Gallaway, W. S., and and Jones, D. T. L.: Chapter XVIII: The Mechanism of Response of Flame Ionization Detectors, in: Gas Chromatography, edited by: Brenner, N., Callen., and J. E., a. W., M. D., Academic Press, New York and London,, 231-267, 1962.

Stewart, R.: Environmental Science in the 21st Century-An online text book, Department of geosciences, Texas A&M university, 2009.

Stroppiana, D., Brivio, P. A., Grégoire, J.-M., Liousse, C., Guillaume, B., Granier, C., Mieville, A., Chin, M., and Pétron, G.: Comparison of global inventories of CO emissions from biomass burning derived from remotely sensed data, Atmos. Chem. Phys., 10, 12173-12189, 2010.

Swanson, A. L., Blake, N. J., Atlas, E., Flocke, F., Blake, D. R., and Rowland, F. S.: Seasonal variations of C_2-C_4 nonmethane hydrocarbons and C_1-C_4 alkyl nitrates at the Summit research station in Greenland, J. Geophys. Res., 108, 4065, 10.1029/2001jd001445, 2003.

Swell, P. A., and Clarke, B.: Chromatographic Separations, John Wiley & Sons, 1987.

Tanner, D., Helmig, D., Hueber, J., and Goldan, P.: Gas chromatography system for the automated, unattended, and cryogen-free monitoring of C_2 to C_6 non-methane hydrocarbons in the remote troposphere, J Chromatogr A, 1111, 76-88, http://dx.doi.org/10.1016/j.chroma.2006.01.100, 2006.

Turetsky, M. R., Kane, E. S., Harden, J. W., Ottmar, R. D., Manies, K. L., Hoy, E., and Kasischke, E. S.: Recent acceleration of biomass burning and carbon losses in Alaskan forests and peatlands, Nature Geosci, 4, 27-31, 2011.

Uno, I., Wakamatsu, S., Wadden, R. A., Konno, S., and Koshio, H.: Evaluation of hydrocarbon reactivity in urban air, Atmospheric Environment (1967), 19, 1283-1293, http://dx.doi.org/10.1016/0004-6981(85)90259-8, 1985.

Val Martin, M., Logan, J. A., Kahn, R. A., Leung, F.-Y., Nelson, D. L., and Diner, D. J.: Smoke injection heights from fires in North America: analysis of 5 years of satellite observations, Atmos. Chem. Phys., 10, 1491-1510, 2010.

van der Werf, G. R., Randerson, J. T., Giglio, L., Collatz, G. J., Mu, M., Kasibhatla, P. S., Morton, D. C., DeFries, R. S., Jin, Y., and van Leeuwen, T. T.: Global fire emissions and the contribution of deforestation, savanna, forest, agricultural, and peat fires (1997–2009), Atmos. Chem. Phys., 10, 11707-11735, 2010.

von Schneidemesser, E., Monks, P. S., and Plass-Duelmer, C.: Global comparison of VOC and CO observations in urban areas, Atmos Environ, 44, 5053-5064, http://dx.doi.org/10.1016/j.atmosenv.2010.09.010, 2010.

Vrekoussis, M., Kanakidou, M., Mihalopoulos, N., Crutzen, P. J., Lelieveld, J., Perner, D., Berresheim, H., and Baboukas, E.: Role of NO3 radical in oxidation processes in the eastern Mediterranean troposphere during the MINOS campaign, Atmos. Chem. Phys. Discuss., 3, 3135-3169, 10.5194/acpd-3-3135-2003, 2003.

Wang, D. K. W., and Austin, C. C.: Determination of complex mixtures of volatile organic compounds in ambient air: canister methodology, Anal Bioanal Chem, 386, 1099-1120, 10.1007/s00216-006-0466-6, 2006.

Warneke, C., de Gouw, J. A., Goldan, P. D., Kuster, W. C., Williams, E. J., Lerner, B. M., Jakoubek, R., Brown, S. S., Stark, H., Aldener, M., Ravishankara, A. R., Roberts, J. M., Marchewka, M., Bertman, S., Sueper, D. T., McKeen, S. A., Meagher, J. F., and Fehsenfeld, F. C.: Comparison of daytime and nighttime oxidation of biogenic and anthropogenic VOCs along the New England coast in summer during New England Air Quality Study 2002, J. Geophys. Res., 109, D10309, 10.1029/2003jd004424, 2004.

Warneke, C., Roberts, J. M., Veres, P., Gilman, J., Kuster, W. C., Burling, I., Yokelson, R., and de Gouw, J. A.: VOC identification and inter-comparison from laboratory biomass burning using PTR-MS and PIT-MS, International Journal of Mass Spectrometry, 303, 6-14, http://dx.doi.org/10.1016/j.ijms.2010.12.002, 2011.

Wayne, R. P., Barnes, I., Biggs, P., Burrows, J. P., Canosa-Mas, C. E., Hjorth, J., Le Bras, G., Moortgat, G. K., Perner, D., Poulet, G., Restelli, G., and Sidebottom, H.: The nitrate radical: Physics, chemistry, and the atmosphere, Atmospheric Environment. Part A. General Topics, 25, 1-203, 1991.

Wayne, R. P.: Chemistry of atmospheres : an introduction to the chemistry of the atmospheres of Earth, the planets, and their satellites, 3rd ed., Oxford University Press, Oxford ; New York, 2000.

Whalley, L. K., Lewis, A. C., McQuaid, J. B., Purvis, R. M., Lee, J. D., Stemmler, K., Zellweger, C., and Ridgeon, P.: Two high-speed, portable GC systems designed for the measurement of non-methane hydrocarbons and PAN: results from the Jungfraujoch High Altitude Observatory, J Environ Monit, 6, 234-241, 10.1039/b310022g, 2004.

Wiedinmyer, C., Akagi, S. K., Yokelson, R. J., Emmons, L. K., Al-Saadi, J. A., Orlando, J. J., and Soja, A. J.: The Fire INventory from NCAR (FINN): a high resolution global model to estimate the emissions from open burning, Geosci. Model Dev., 4, 625-641, 2011.

Williams, J., Fischer, H., Harris, G. W., Crutzen, P. J., Hoor, P., Hansel, A., Holzinger, R., Warneke, C., Lindinger, W., Scheeren, B., and Lelieveld, J.: Variability-lifetime relationship for organic trace gases: A novel aid to compound identification and estimation of HO concentrations, J. Geophys. Res., 105, 20473-20486, 10.1029/2000jd900203, 2000.

Wotton, B. M., Nock, C. A., and Flannigan, M. D.: Forest fire occurrence and climate change in Canada,, Int. J. Wildland Fire, 19, 253-271, 2010.

http://www.scientistsolutions.com/t12358-theoratical+plates.html, 2009.

Yokelson, R. J., Urbanski, S. P., Atlas, E. L., Toohey, D. W., Alvarado, E. C., Crounse, J. D., Wennberg, P. O., Fisher, M. E., Wold, C. E., Campos, T. L., Adachi, K., Buseck, P. R., and Hao, W. M.: Emissions from forest fires near Mexico City, Atmos. Chem. Phys., 7, 5569-5584, 2007.

Yokelson, R. J., Christian, T. J., Karl, T. G., and Guenther, A.: The tropical forest and fire emissions experiment: laboratory fire measurements and synthesis of campaign data, Atmos. Chem. Phys., 8, 3509-3527, 2008.

Yokelson, R. J., Crounse, J. D., DeCarlo, P. F., Karl, T., Urbanski, S., Atlas, E., Campos, T., Shinozuka, Y., Kapustin, V., Clarke, A. D., Weinheimer, A., Knapp, D. J., Montzka, D. D., Holloway, J., Weibring, P., Flocke, F., Zheng, W., Toohey, D., Wennberg, P. O., Wiedinmyer, C., Mauldin, L., Fried, A., Richter, D., Walega, J., Jimenez, J. L., Adachi, K., Buseck, P. R., Hall, S. R., and Shetter, R.: Emissions from biomass burning in the Yucatan, Atmos. Chem. Phys., 9, 5785-5812, 2009.

Young, V. L., Kieser, B. N., Chen, S. P., and Niki, H.: Seasonal trends and local influences on nonmethane hydrocarbon concentrations in the Canadian boreal forest, Journal of Geophysical Research: Atmospheres, 102, 5913-5918, 10.1029/96jd03375, 1997.

Yuan, B., Liu, Y., Shao, M., Lu, S., and Streets, D. G.: Biomass Burning Contributions to Ambient VOCs Species at a Receptor Site in the Pearl River Delta (PRD), China,, Environ. Sci. & Technol., 44, 2010.

Yurganov, L. N., Duchatelet, P., Dzhola, A. V., Edwards, D. P., Hase, F., Kramer, I., Mahieu, E., Mellqvist, J., Notholt, J., Novelli, P. C., Rockmann, A., Scheel, H. E., Schneider, M., Schulz, A., Strandberg, A., Sussmann, R., Tanimoto, H., Velazco, V., Drummond, J. R., and Gille, J. C.: Increased Northern Hemispheric carbon monoxide burden in the troposphere in 2002 and 2003 detected from the ground and from space, Atmos. Chem. Phys., 5, 563-571, 2005.